COMPOSITE PROTON EXCHANGE MEMBRANES FOR INTERMEDIATE TEMPERATURE FUEL CELLS

BY

MARISKA HATTENBERGER

A thesis submitted to the

University of Birmingham

For the degree of

DOCTOR OF PHILOSOPHY

Centre for Hydrogen and Fuel Cell Research

School of Chemical Engineering

University of Birmingham

June 2015

DECLARATION

I, Mariska Hattenberger, hereby declare that the work presented in this thesis is my own with no help of more than the cited literature and auxiliary means.

I also confirm that this work has not been submitted to another examination office, neither in content nor in shape.

_____

Signature: Mariska Hattenberger

Date: _____

ACKNOWLEDGMENTS

This thesis marks the culmination of my research carried out between January 2011 and December 2014 at the Centre for Hydrogen and Fuel Cell research in the School of Chemical Engineering at the University of Birmingham. The personal journey and work carried out during the four years would not have been possible without the help of many people who I would like to thank.

The late Dr. Waldemar Bujalski was a great inspiration to me and many other researchers in the Fuel Cell group. His enthusiasm, practical advice and positive outlook had a great effect on me and the possibility to complete the project.

I would like to thank my supervisors, Dr. Neil Rees, Dr. Surbhi Sharma and Dr. Valerie Self for their wise guidance and advice throughout, and for always being interested in discussing my work. Thanks also to the EPSRC for the funding of this PhD and to Tata Motors European Technical Centre for their financial assistance.

Dr. Shangfeng Du and Dr. Ramaiyan Kannan gave their time to discuss results and give practical advice. Huge thanks are in order to our technician Mr. Bob Sharpe for being able to fit, fix or modify anything that was presented to him. I would also like to say a special thanks to John Hooper and Lynn Draper who assisted with all administrative aspects of the PhD. Finally a collective thanks to everyone in G5 and G6 for making the working environment such a pleasant place.

My deepest thanks go to my family and friends, who have been there for me throughout. I would not have been able to do it without your support on so many levels. Thank you!

ABSTRACT

Intermediate temperature (IT) proton exchange membrane fuel cells (PEMFCs) offer a future that does not rely on the burning of fossil fuels, but dictate durable and high performance component materials. At operating conditions of 120 °C and 50 % relative humidity (RH), composite proton exchange membranes (PEMs) offer increased performance due to enhanced water uptake and retention resulting from the hydrophilic filler material.

This project aimed to relate measured data for composite PEMs with literature data on Nafion-graphene oxide (GO) PEMs. In order to achieve this, the membrane casting method was optimised and GO was synthesised in-house. A range of membranes were tested using a calibrated and optimised high temperature test stand. In-situ and ex-situ testing was carried out between 80 °C and 120 °C, and between 25 and 95 % RH.

In contrast with some published data, this study found inconsistent trends between water uptake, ion exchange capacity, membrane resistance and single cell performance. Overall it was found that recast and composite membranes had higher in-plane resistance than Nafion 212, but that composite membranes with low filler loading had comparable in-situ performance to the commercial membrane. Further single cell optimisation is likely to result in further advances for composite PEMs.

LIST OF PUBLICATIONS

1. El-Kharouf, A., A. Chandan, **M. Hattenberger** & B. G. Pollet (2012) Proton exchange membrane fuel cell degradation and testing: review. *Journal of the Energy Institute,* 85**,** 188-200.

2. **Hattenberger, M.**, S. Sharma, W. Bujalski, B. Pollet, V. Self & J. Richmond (2012) Novel Composite Proton Exchange Membrane Materials for Intermediate Temperature Fuel Cells. *Procedia Engineering,* 44**,** 858-860.

3. Chandan, A., **M. Hattenberger**, A. El-kharouf, S. Du, A. Dhir, V. Self, B. G. Pollet, A. Ingram & W. Bujalski (2013) High temperature (HT) polymer electrolyte membrane fuel cells (PEMFC) – A review. *Journal of Power Sources,* 231**,** 264-278.

CONTENTS

FIGURES

TABLES

GLOSSARY OF TERMS AND ABBREVIATIONS APPEARING FREQUENTLY IN THE TEXT

AC	Alternating current
A	Area of cross section of membrane
DI Water	Deionised Water
DC	Direct current
DMFC	Direct methanol fuel cell
DMAc	Dimethyl acetamide
DMF	*N,N*-dimethylformamide
DMSO	Dimethyl sulfoxide
DTU	Technical University of Denmark
EIS	Electrochemical impedance spectroscopy
GDE	Gas diffusion electrolyte
GDL	Gas diffusion layer
GO	Graphene oxide
GO-N	Graphene oxide functionalised by azo-coupling of sulfanilic acid
IT	Intermediate temperature
IEC	Ion exchange coefficient/capacity
L	Distance between voltage probes

MEA	Membrane electrode assembly
MPTMS	3-mercaptopropyltrimethoxysilane
OCV	Open circuit voltage
PFSA	Perfluorinated sulfonic acid
PTMS	phenyltrimethoxysilane
PBI	Polybenzimidazole
PEO	Poly(ethylene oxide)
Pt	Platinum
PEFC	Polymer electrolyte fuel cell
PEM	Proton exchange membrane
PEMFC	Proton exchange membrane fuel cell
%RH	Relative humidity percentage
R	Resistance
rt	Room temperature
σ	Sigma
SGO	Sulfonated graphene oxide
SPESK	Sulfonated poly(arylene ether sulfone ketone)
SPEEK	Sulfonated poly(ether ether ketone)
SPI	Sulfonated polyimine
SPSU	Sulfonated poly sulfone

UOB	University of Birmingham
UOY	University of Yamanashi
WU	Water uptake

CHAPTER 1 INTRODUCTION

1.1 Background

Often described as an efficient successor to the internal combustion engine and sometimes as the miracle power source which will mitigate climate change and our dependency on fossil fuels; fuel cells promise a future of quiet, clean and renewable energy.

The absence of the Carnot inefficiency and the electrochemical reaction producing only water vapour has resulted in great enthusiasm for fuel cells. Proton exchange membrane fuel cells (PEMFCs) in particular, offer an opportunity to run automobiles, personal electronics and combined heat and power systems without the need for fossil fuel. An enormous amount of research has been carried out in an attempt to optimise the component materials of fuel cells for efficient and cost effective units suitable for commercialisation. Research has not only focussed on the chemistry and physics of the materials or the engineering of the fuel cell system, but also on the broader requirement of a hydrogen infrastructure, social acceptance of a new type of energy generator and the economic repercussions of the commercialisation of a new energy vector [1-3].

Figure 1-1 shows the number of publications on fuel cells between 1960 and 2014. The peaks and troughs coincide with the major developments in the technology.

3

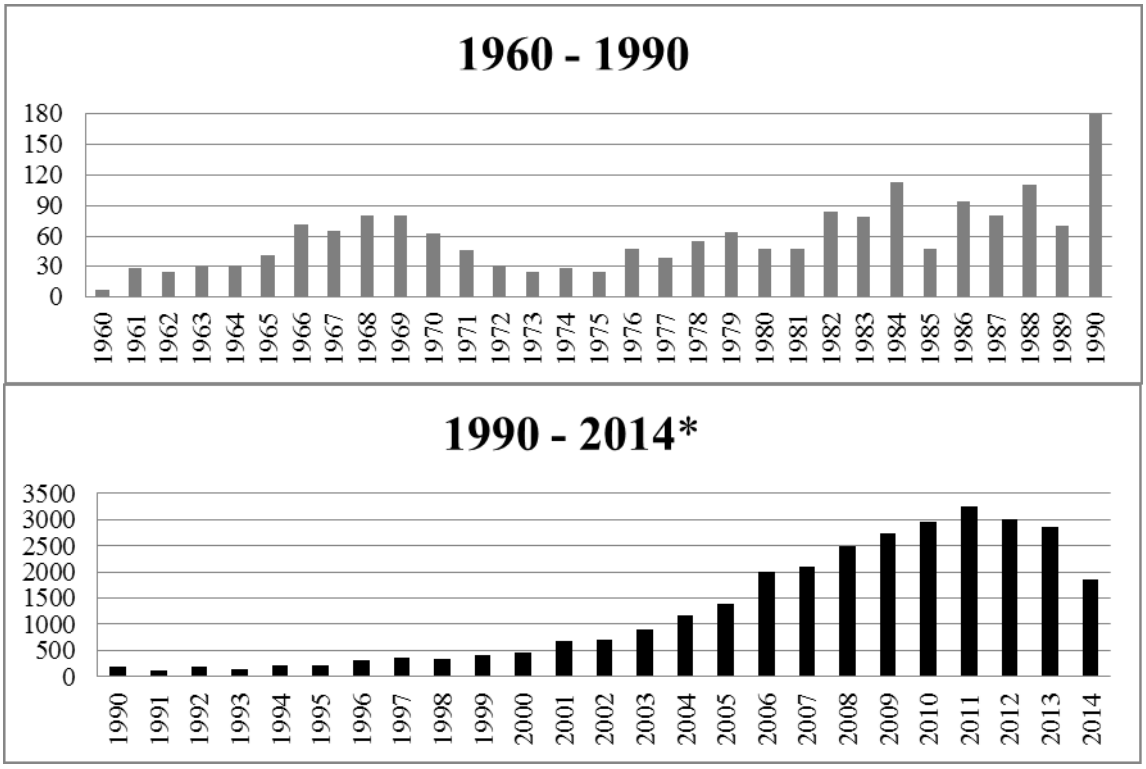

*Figure 1-1 The number of publications with the words "Fuel Cell" in the title, taken from Web of Science. (*2014 data was extracted at the end of September 2014.)*

Research began in earnest in the 1960's with the NASA space programs, but theoretically, fuel cells have been around since the 1800's when Sir William Grove demonstrated that the reaction between hydrogen and oxygen can be harnessed to generate electrical power [1]. In the 1960's, General Electric (GE) developed 1 kW proton exchange membrane fuel cell (PEMFC), containing a sulfonated polystyrene electrolyte, in the form of a thin polymer film. The film, or membrane, is sandwiched between two catalysts layers, usually comprised of a catalyst applied to a microporous gas diffusion layer (GDL), and forms the core of the fuel cell [4]. The membrane electrode assembly (MEA), illustrated in Figure 1-2, is the site of the electrochemical reactions which convert hydrogen and oxygen into water and electrical power. The diagram shows a PEMFC, which is the focus for this study. Many other types of fuel cells are in use, tuned for specific applications, and are briefly described in section 1.3.

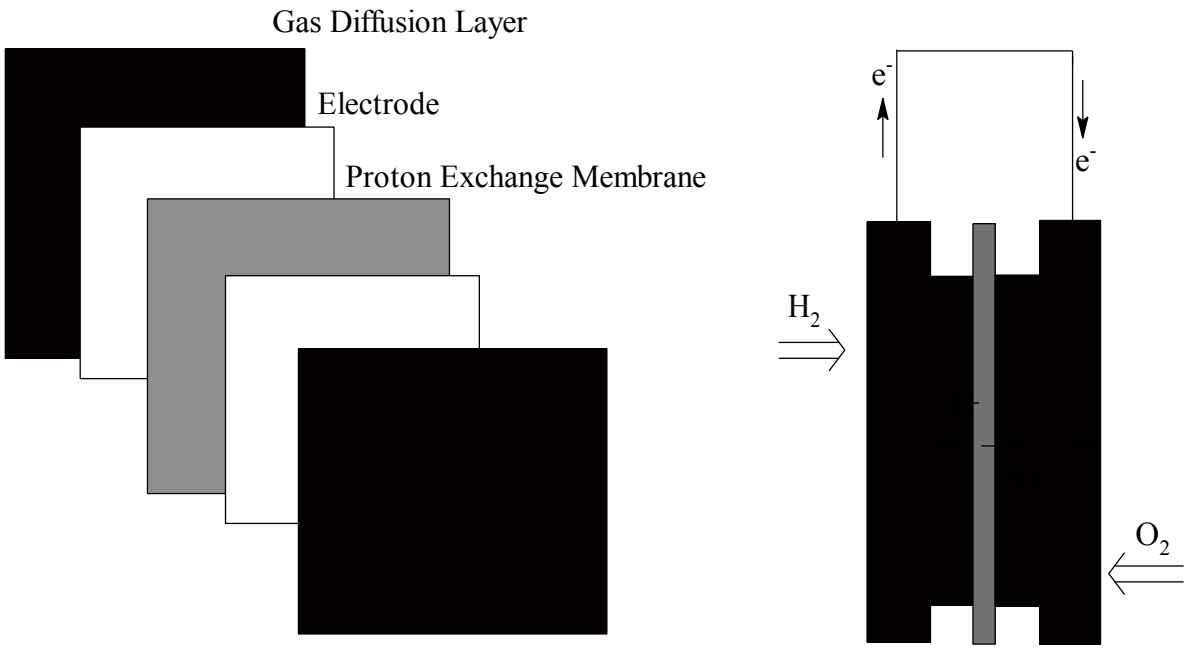

Figure 1-2 A schematic representation of a proton exchange membrane fuel cell (PEMFC) membrane electrode assembly (MEA).

The GE PEMFC, which contained a significant quantity of platinum catalyst, could generate specific energy of 0.4 kWh/kg, enough to power the fifth Gemini Earth Orbit Mission [5] for 200 hours, which at the time, was higher than that which could be obtained by battery power [5]. The PEMFC was replaced by an alkaline fuel cell (AFC) for the Apollo Missions in 1967 [6], mainly due to degradation of the proton exchange membrane (PEM) [4]. The specific energy was increased to 1.2 kWh/kg, due to increased voltage and was rated to last 400 hours [5]. GE developed and supplied the power plant on board the Biosatellite Spacecraft in 1967. A 350 W PEMFC generated the power and contained an improved membrane (compared to the sulfonated polystyrene) called Nafion. This perfluorinated sulfonic acid (PFSA) polymeric membrane developed by DuPont is still the industry standard PEM today [4].

When the first drive for automotive fuel cells started in earnest in the late 1990's, PEMFCs were identified as the system of choice due to high power density, rapid start up, high efficiency, modular design, low weight and an immobile electrolyte [7]. The deposition of the platinum catalyst as nanoparticles on a conductive support material, drastically reduced the cost compared to the NASA models and the shorter target range for automotive fuel cells (due to the possibility of refuelling and the utilisation of atmospheric air as oxidant), allowed for simplified engineering.

During the late 1990's to the early 2000's ambitious forecasts were made by companies like Honda, Ford, Toyota, General Motors, Daimler-Chrysler and Renault/Nissan, claiming that commercial production of fuel cell cars would start around 2003-2005 [8] and 189 prototypes were manufactured between them [9]. By around 2001 these projections had to be adjusted, mostly due to cost and technical performance issues [10]. It's possibly at this stage where the saying; "Fuel cells are always 10 years away from commercialisation" was first uttered [9]. At this time the crucial debate started over which needed to be developed first, fuel cell automobiles or the hydrogen infrastructure required to refuel the vehicles. Slow realisation of the projected commercialisation led to the reduction of funding and uncertainty regarding the future of fuel cells and their applications. Publications continued to increase however, showing that in certain sectors the commitment to research and development remained firm [9]. This resulted in the launch of the first fuel cell saloon car by Toyota, available for general sale in Japan at the end of 2014. Honda has projected a roll out in 2016 and other original equipment manufacturers (OEMs) are set to follow.

The commercialisation of fuel cells will be governed by more than just scientific progress. The role of politicians, economists and industry leaders will be crucial to the future of the

hydrogen and fuel cells. This lies outside of the scope of this project though and in the remainder of this report, the focus will be on the scientific principles underlying fuel cells and the properties that make PEMFCs the fuel cells of choice for automotive application. In particular, it has been identified that the operation of PEMFCs at the elevated temperature of around 120 °C could improve the performance of the state of the art models which operate at around 90 °C. The advances are predicted based on faster electrode reactions, reduced complexity and increased tolerance of impurities.

1.2 Basic Principles

A fuel cell is a type of galvanic cell, which produces electricity due to a spontaneous chemical reaction that takes place inside it. The chemical reaction can be described as two half reactions which take place at the anode and cathode respectively [11]. Hydrogen is oxidised at the anode releasing electrons which flow through the external circuit to the cathode. The protons migrate from the anode to the cathode, through the electrolyte which separates the two electrodes. The electrons and protons recombine at the cathode where oxygen is reduced resulting in the formation of water. Figure 1-3 shows a PEMFC, but the principle is the same for all fuel cells (although the anodic reaction will depend on the fuel used). The half reactions (written by convention as reductions) and overall reaction for a PEMFC is shown in equations 1-3:

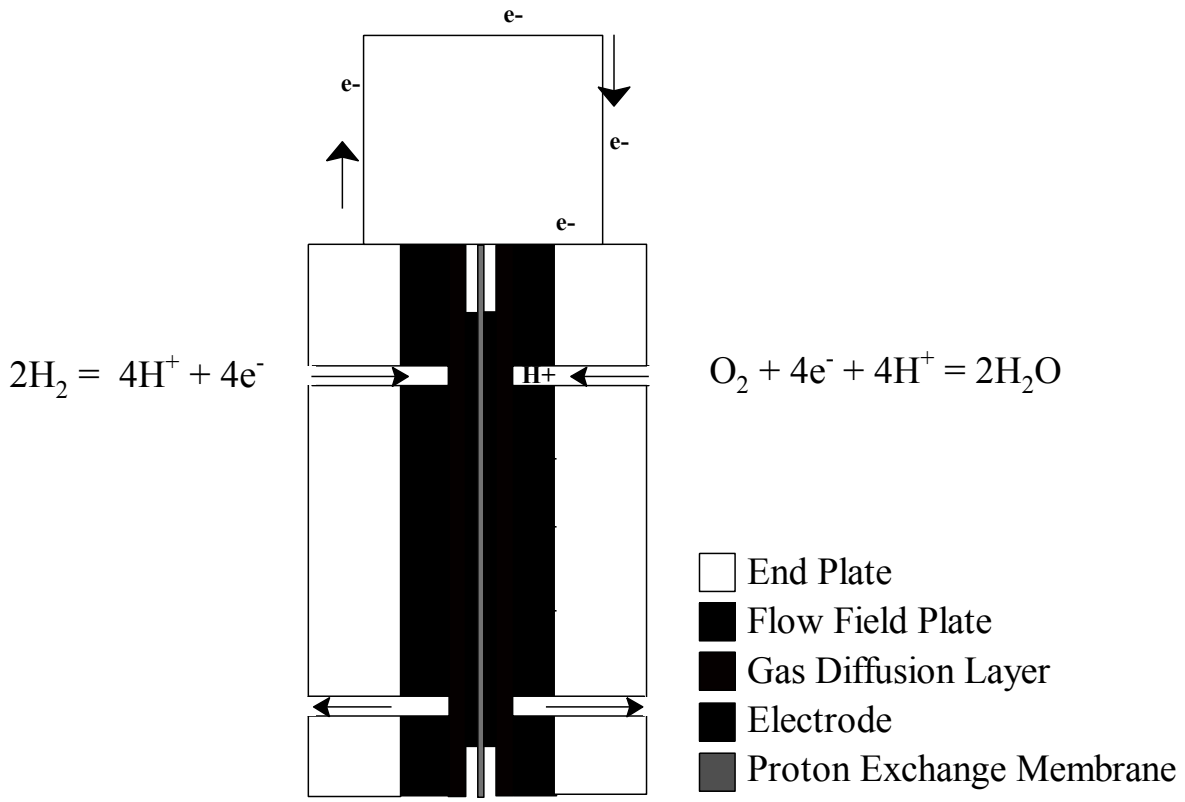

Figure 1-3 Polymer Electrolyte Fuel Cell

$2H_{2(g)} = 4H^+ + 4e^-$ 1

$O_{2(g)} + 4H^+ + 4e^- = 2H_2O$ 2

$2H_2(g) + O_2(g) = 2H_2O_{(l)}$ 3

For the cell to be reversible, and therefore not suffer any losses, the value for the Gibbs free energy of formation of water must be equal to the electrical work done in moving the electrical charge around the system.

Expressing the overall reaction as:

$H_2(g) + ½\ O_2(g) = H_2O_{(l)}$ ……..……..4

And stating that the Gibbs free energy for the formation of water (at standard temperature and pressure (STP)) as:

$\Delta G_f = -237.1$ kJ/mol

The reversible open circuit voltage (OCV) of the hydrogen fuel cell at STP (for liquid water) can then be calculated as follows:

$\Delta G_f = -2FE$ …….....……5

and

$E^0 = (-\Delta G_f)/2F$

$= 237.1$ kJ/mol/(2 x 96 485)

$= 1.23$ V

Fuel cell efficiency is usually expressed in terms of the fuel that is being used. The electrical energy produced in the electrochemical reaction which results in the formation of water, is compared to the calorific value of burning hydrogen as a fuel. This is expressed as the enthalpy of formation for either steam or liquid water. These terms are referred to as the higher and lower heating value respectively (HHV & LHV), with negative values indicating a release of energy.

$\Delta H_f = -241.83$ kJ/mol (LHV)

$\Delta H_f = -285.84$ kJ/mol (HHV)

This enables a calculation of the thermodynamic efficiency of the hydrogen fuel cell using:

Maximum efficiency (HHV) = $(\Delta G_f/\Delta H_f)$x 100 % ……6

= (-237.1 kJ/mol/-285.84 kJ/mol) x 100 %

= 83 %

This means that even though the maximum reversible OCV is 1.23 V, there is an efficiency limit of 83 % for hydrogen fuel cells. The 17% loss is due to the change in entropy when one and a half mole of gas is converted to one mole of liquid water (the term $-T\Delta S$). This pressure and volume work on the system is "non-useful" work and is released as heat.

As the fuel cell is free from Carnot inefficiencies, which describe the efficiency limits of a heat engine, it means that overall the fuel cell is more efficient than an internal combustion engine which loses about 50% of its energy due to heat loss. There are however, a host of other factors which play a role in the overall performance of a fuel cell.

Fuel utilisation is an important factor as some of the fuel passes through the cell unreacted. This is accounted for by a fuel utilisation coefficient (μ_f), often estimated at 0.95 [6]. The cell efficiency can hence be expressed in terms of the operating voltage (V_c) and fuel utilisation:

μ_f = (mass of fuel reacted in cell)/(mass of fuel input to cell) ……7

E = $(-\Delta H_f/2F)$ = 1.48 V (HHV)

Cell efficiency = μ_f * (V_c/1.48 V) * 100 %

It should be pointed out however, that un-used fuel is recirculated in the system and not necessarily lost. The efficiency overall therefore depends on the integrity of the system with respect to gas leaks.

The effect of the pressure and concentration is taken into account as fuel gases (hydrogen and oxygen) are not 100 % pure. The effect on the Gibbs free energy is expressed by the Nernst Equation:

$$E = E^0 + \left(\frac{RT}{2F}\right) \times \ln[\left(P_{H2} \times P_{\frac{1}{2}O2}\right)/(P_{H2O})] \quad \text{.....8}$$

The voltage losses are higher at lower temperatures, and the heat from higher temperature fuel cells is more useful because it can be recycled in the system and makes cooling of the system less complex.

The reason for elaborating on the underlying processes taking place in the fuel cell is to emphasise how important it is that each component performs at an optimum level and justifies the intensive materials research which has been carried out in the individual constituents used to manufacture a fuel cell. A simple diagnosis for the performance of a complete single cell (current collector, bipolar plate, electrodes and membrane) is an in-situ test which results in a polarisation curve as shown in Figure 1-4. Such a curve is obtained at specific operating conditions (temperature & relative humidity) and gives some indication to the performance of the electrodes, the membrane and the integrity of the complete cell under operating conditions. Referring to Figure 1-4, the losses occurring in all fuel cells are categorised as activation losses due to sluggish reaction kinetics (region A), losses due to

resistance in the membrane (region B) and mass transfer losses due to insufficient fuel or flooding (region C). In reality the curve usually has a much steeper slope in Region B.

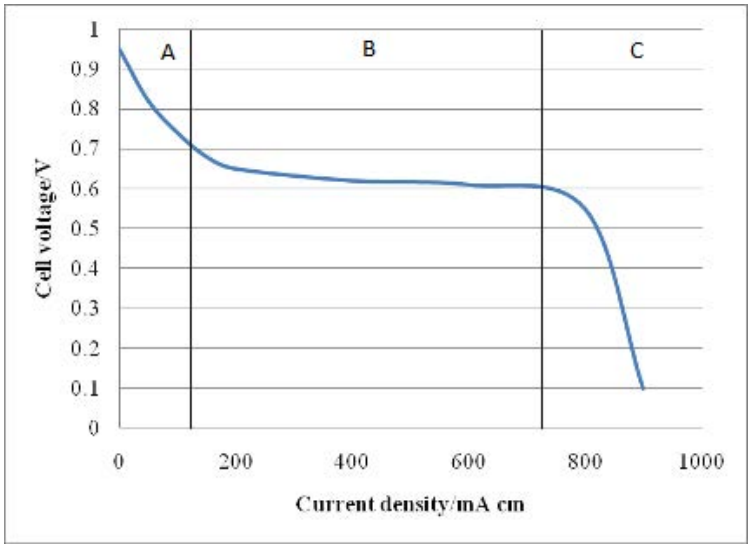

Figure 1-4 Typical Polarisation Plot of a PEM fuel cell

The performance of the cell can be analysed using electrochemical impedance spectroscopy (EIS). Impedance spectroscopy entails applying a small sinusoidal (AC) voltage or current over a wide range of frequency (from mHz-kHz or greater), and measuring the effect that this has on the AC amplitude and phase response of the electrochemical cell. Figure 1-5 is an illustration of the data that can be obtained during in-situ testing and at different current ranges. This method allows for the further analysis of the different components within the single cell. With respect to membrane performance, the intercept on the Z' axis provides the membrane resistance. It can be seen that the resistance changes at different current levels and this again can be related to the polarisation plot in Figure 1-4. The technique is described in further detail in Chapter 3.

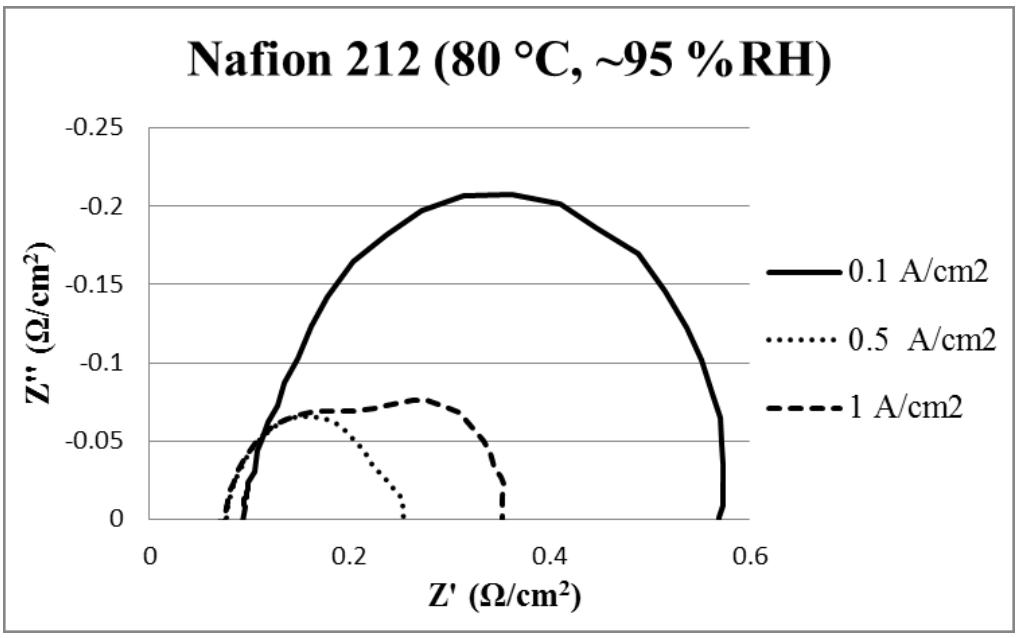

Figure 1-5 EIS plot for a composite membrane MEA at different current ranges.

Using the resistance value for the membrane obtained as described above, the proton conductivity of the membrane can be calculated using Formula 9.

$$\sigma = \frac{1}{R} \times \left(\frac{L}{A}\right) \quad \text{.....9}$$

Where σ = proton conductivity in S/cm

R = membrane resistance in Ω

L = distance between voltage probes in cm

A = area of cross section of membranes in cm^2

To test the performance of the membrane independent of the other components of the single cell, a membrane sample can be tested ex-situ. EIS can be performed in the same way as for the single cell. Alternatively the resistance of the membrane can be measured directly from Ohm's Law if the voltage and current can be measured in such a way that other types of resistance can be eliminated in the system. This provides a method to relate the ex-situ and

in-situ performance of the material. This is very useful, since ex-situ testing requires smaller amounts of membrane material, and does not require the use of the costly electrode materials, allowing for the screening of membrane materials prior to MEA preparation and testing.

The experimental details for both the in-situ and ex-situ performance testing are described in detail in Chapter 3.

1.3 Types of Fuel Cells

The choice of electrolyte dictates at which temperature a particular type of fuel cell can operate. In Table 1-1 it can be seen that PEMFCs operate at relatively low temperature when compared to solid oxide fuel cells (SOFCs). The main implication of this low operating temperature is the requirement of platinum as the catalyst to drive the reaction. The other apparent difference is the charge carrier, which will result in different half reactions taking place at the anode and cathode in the fuel cell.

For fuel cell operation, the efficiency, balanced with the operating cost and the ability of the system to withstand the effects of contamination are further factors that will determine which system is chosen for a particular application.

PEMFCs are most suitable for automotive application. This project, with objectives suggested by TMETC (Tata Motors Engineering Technical Centre), was focussed on materials for automotive application, and hence focussed on this type of fuel cell. PEMFCs, along with direct methanol fuel cells (DMFCs), are furthermore well suited to personal electronics applications and advances in materials could hence find many useful applications.

Table 1-1 Different types of fuel cells [6, 8, 12]

Type	**Electrolyte**	**Operating Temperature (°C)**	**Catalyst**	**Charge Carrier**	**Fuel Cell Efficiency (%)**	**Applications**
Direct Methanol Fuel Cell	Polymeric ion exchange membrane	20-120	Platinum	H^+	40	Automotive, portable
Proton Exchange Membrane Fuel Cell	Polymeric ion exchange membrane	60-160	Platinum	H^+	40-60	Automotive, stationary, portable
Alkaline Fuel Cell	Potassium hydroxide	50-200	Nickel	OH^-	60-70	Automotive, space
Phosphoric Acid Fuel Cell	Phosphoric acid	160-220	Platinum	H^+	36-42	Stationary
Molten Carbonate Fuel Cell	Alkali carbonate	600-700	Nickel	CO_3^{2-}	50-60	Stationary
Solid Oxide Fuel Cell	Solid oxide	500-1000	Nickel	O_2^-	50-60	Automotive, stationary

1.4 Proton Exchange Membrane Fuel Cells

The proton exchange membrane fuel cell (PEMFC) is also referred to as a polymer electrolyte fuel cell (PEFC) in some cases, to indicate that different types of membranes are in use. PEMFCs employ an acidic polymer as the electrolyte and the positively charged hydrogen ion is the charge carrier which passes through the membrane. Alkaline membrane fuel cells are also being developed for fuel cell application [13] and in this case the negative hydroxide ion is the charge carrier. In this case the second term PEFC is more appropriate. In this study the focus was on acidic proton exchange membranes and the acronym PEMFC will be used throughout. The following sections give a brief description of the components in the fuel cell.

1.4.1 Electrodes

The electrodes for a PEMFC are usually prepared from a platinum precursor which is deposited on a (traditionally) carbon support. In order to maximise the catalyst surface area, the platinum particles are in the nanometre scale and the carbon support is maximised to enhance the three-phase interface between the fuel gas, the catalyst and the contact with the electrolyte. In an attempt to reduce the cost, other metals have been investigated for catalyst application and usually focus on a platinum-metal alloy or core shell structure [7]. Carbon supports are typically small spherical particles, but reduced graphene oxide and carbon nanotubes have also been widely researched in optimisation studies. Other materials have also been considered and a recent review of catalyst support materials summarises results on carbon materials and also on metal oxides and conductive polymers which have been considered for this purpose [14].

1.4.2 Gas Diffusion Layer (GDL)

In order to promote the transport between the catalyst layer and the electrolyte, a porous hydrophobic gas diffusion layer is used in one of two configurations. One method is to deposit a liquid catalyst ink onto the GDL and, after solvent evaporation, to hot press the two resulting gas diffusion electrodes (GDEs) with the active area facing inwards, onto the membrane. A binder prepared from a suitable polymer (usually the same as the electrolyte) is used to laminate the three components together. Alternatively, the catalyst layer can be prepared as a separate component by either preparing a decal on a Teflon blank or by applying the ink directly onto the membrane. The MEA is then formed in the same way as the first method, by hot pressing all the components together. The GDL is commonly made from carbon paper or woven carbon fibres.

1.4.3 Electrolytes

The electrolyte is a solid polymeric membrane which is sandwiched between the two GDLs or GDEs. As the central part of the MEA, the membrane must show a degree of mechanical integrity. The industry standard polymeric membrane is prepared from Nafion, a robust Teflon-type polymer. Nafion and other types of electrolytes are discussed in more detail in the following section.

1.4.4 Bipolar Plates/Flow Field Plates

On either side of the MEA, a bipolar plate provides structural integrity to the cell and the gas channels distribute the fuel gasses evenly over the active area of the MEA. Bipolar plates are prepared from graphite but some resin and metal plates have been developed in order to

increase the durability and reduce the weight of the cell. The configuration of the flow channels are either serpentine or parallel, but other configurations have also been investigated in an attempt to optimise the fuel distribution and availability for reaction over the whole of the active area of the cell.

1.4.5 Current Collectors

Current collectors are required to complete the circuit between the two electrodes and carry the electrical charge to the system. For this reason a highly conductive material like gold (or a gold plated metal) is usually employed.

1.4.6 Balance of Plant (BOP)

As mentioned in the introduction, the BOP includes the auxiliary components which are required for the fuel cell to operate at the conditions for which it has been developed. This includes heating, back pressure units, fuel supply (and connections to the cell) and the electrical control units.

1.5 Higher temperature proton exchange membranes (PEMs)

The trend in papers published for proton exchange membranes mirrors that of the publications for fuel cells, with a maximum of 400 per year in 2011 and with the figure for 2014 at around 325, in the last quarter of the year.

There have been many comprehensive reviews on proton exchange membranes [15-39]. The proton exchange membrane can be considered in two parts. Firstly, the polymer used to prepare the electrolyte, including the rigid backbone, and side chains and any fillers or support materials that have been added to enhance the physical stability of the material [40]. This structural component can contain conductive species, such as the sulfonic acid groups on the Nafion backbone, or can be completely non-conductive to ions, which is the case for polybenzimidazole (PBI). Secondly, the proton carrier, which is either water and/or an ionic medium such as phosphoric acid (H_3PO_4), sulfonic acid groups (HSO_3^-) or ionic liquids such as 1-butyl-3-methylimidazolium tetrafluoroborate ($BuMeImBF_4$) [41].

For all types of proton carriers there are similar considerations. Firstly, the membrane material must absorb an optimal amount of this medium; too much weakens the membrane, too little results in inadequate proton conductivity. Secondly, the membrane material must retain the maximum amount of the medium under operating conditions over a long period of time (5,000 hrs for automotive use, 40,000 hrs for stationary use). The loss of the conducting medium results in the reduction of conductivity, degradation of the membrane, damage or flooding of the electrodes and blockage of flow field plate (FFP) channels.

Conductivity takes place via diffusion (due to a concentration gradient), proton hopping or a combination of both. The mechanism that takes place depends upon which proton conducting medium is present. Figure 1-6 illustrates the different mechanisms for water, phosphoric acid and an ionic liquid (1-butyl-3-methyl imidazolium bis (trifluoromethyl sulfonyl) imide).

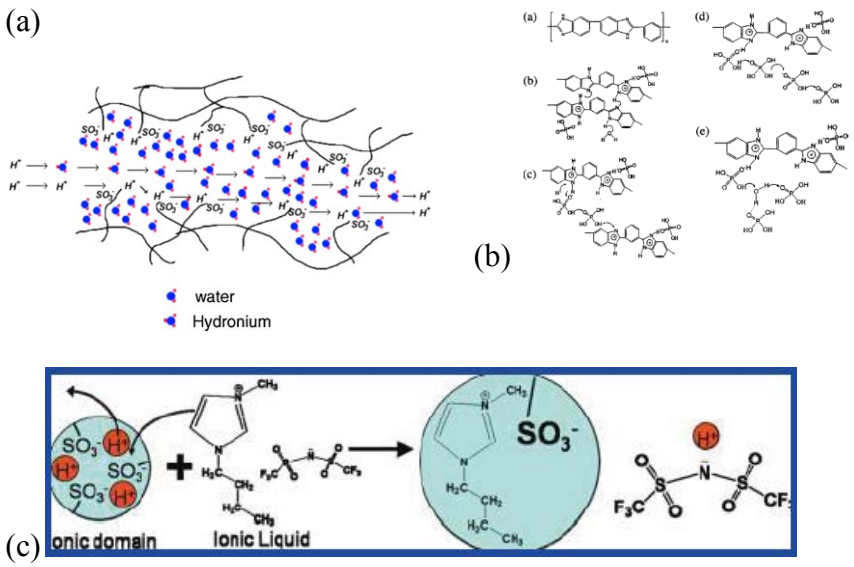

Figure 1-6 Proton conduction in (a) water, (b) phosphoric acid and (c) ionic liquids (1-butyl-3-methyl imidazolium bis(trifluoromethyl sulfonyl) imide) [42-44]. Figures reprinted from the referenced journals (Journal of Power Sources (Copyright 2005), Journal of the Electrochemical Society (Copyright 2004) and Langmuir (Copyright 2009)) with permission from the publishers (Elsevier, The Electrochemical Society and ACS).

Water containing membranes include Nafion, other fluorinated membranes and a large class of sulfonated aromatic hydrocarbons. The non-water membranes include acid-base systems such as (PBI) doped with phosphoric acid (or other acids) and materials rendered conductive by ionic liquids. To increase the uptake of the proton carrier, the concentration of the polar group (acid or base) on the polymer backbone must be maximised. In Table 1-2 the structure for some of the most common base polymers used for PEM materials are shown.

Table 1-2 Structures of common PEM materials

Name	Structure	Ref
Nafion/ PFSA	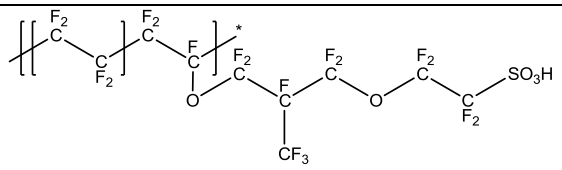	[45]
PBI	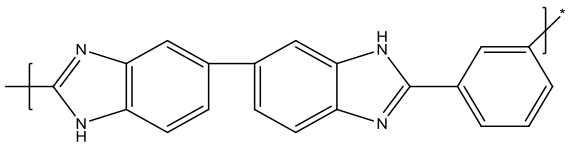	[46]
SPEEK	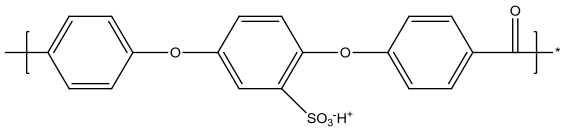	[47]
SPI	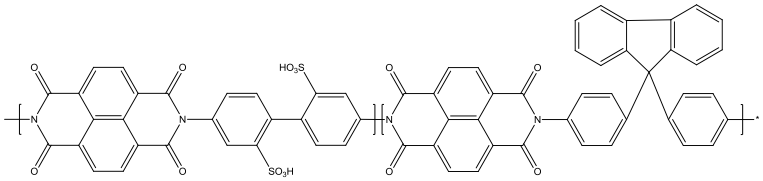	[48]
PSU	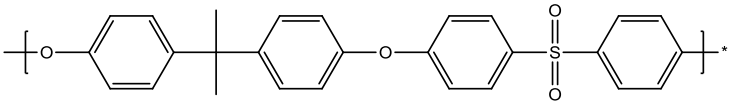	[49]

PFSA = perfluorinated sulfonic acid, PBI = polybenzimidazole (phosphoric acid present for conductivity), SPEEK = Sulfonated poly ether ether ketone, SPI = Sulfonated polyimide, PSU = Sulfonated polysulfone.

Table 1-3 summarises data on promising high temperature membrane materials and the entries that are highlighted have met DOE targets for 2015. It should be pointed out at this stage that it is very difficult to compare published conductivity values for membranes from different studies. The reason for this is the different preparation methods of the materials and non-standard test conditions and techniques. Often data is quoted without reference conductivity of commercial materials tested under exactly the same conditions. This was one of the main objectives of this study, to systematically test a series of membranes using exactly the same conditions in each series of tests.

Table 1-3 Summary of potential high temperature membrane materials

Membrane Material	Conductivity/Temp/%RH	Ref
Nafion/(5 wt%) SPPSQ*	0.157 S cm^{-1} at 120 °C and 100 %RH	[50]
PBI/H_3PO_4/(40%)SiWA	0.177 S cm^{-1} at 150 °C and 0 %RH	[51]
Recast Nafion **	0.002 S cm^{-1} at 130 °C and 100 %RH	[52]
Nafion*	0.035 S cm^{-1} at 120 °C and 30 %RH	[53]
Nafion 117/(20 wt%)ZrSPP Recast Nafion/(20 wt%)ZrSPP*	0.1 S cm^{-1} at 100 °C and 90 %RH 0.05 Scm^{-1} at 110 °C and 98 %RH	[54] [55]
Recast Nafion*/SGO	0.047 S cm^{-1} at 130 °C and 30 %RH	[53]
SPEEK/ZrP-NS	0.079 S cm^{-1} at 150 °C and 100 %RH	[56]
SPI with fluorene groups	1.67 S cm^{-1} at 120 °C and 100 %RH	[48]
SPI with sulfophenoxypropoxy pendants	1 S cm^{-1} at 120 °C at 100 %RH	[57]
SPU with fluorene	0.5 S cm^{-1} at 110 °C and 50 %RH	[58]
CF_6-PBI SO_2-PBI	0.12 S cm^{-1} at 175 °C and 10 %RH 0.12 S cm^{-1} at 180 °C and 5% RH	[59] [60]
PBI/SPAES	0.045 S cm^{-1} at 200 °C no external humidification	[61]
SPU with pyridine and hydroquinone groups	0.02 S cm^{-1} at 120 °C 0 %RH	[62]

* Membrane cast from 5 wt% Nafion 1100 solution, DuPont. ** Membrane cast from Nafion resin, Shandong Dongyue Polymer Material Co. Ltd.

SPPSQ = sulfonated poly(phenylsilsesquioxane), SiWA = silicotungstic acid, ZrSPP = Zirconium sulphophenylphosphonate, SGO = sulfonated graphene oxide, ZrP-NS = Zirconium phosphate nanosheets, SPI = sulfonated polyimide, SPU = sulfonated polysulfone, SPAES = sulfonated poly arylene ether sulfone.

The following sections briefly describe some of the most promising materials for higher temperature application.

1.5.1 Composite PEMs

Composite membranes are attracting a great deal of attention as a means for increasing the temperature tolerance of conventional PEM materials. They are manufactured by doping a polymer with a filler material and was recently classified by Dupuis [15]. The main objective of adding a filler is to improve water uptake and retention [63, 64] and by implication the conductivity at high temperature and low humidification. Most types of polymer electrolytes have successfully been doped with inorganic fillers such as hygroscopic oxides (SiO_2, TiO_2, ZrO_2, Al_2O_3), clays (montmorillonite), zeolites, mineral acids (HCl, H_3PO_4), heteropoly acids and zirconium phosphates (ZrP). Recent success has also been reported with polymeric micro or nano capsules and pure and functionalised graphene oxide (GO) which formed the focus of this study. It can be seen from Table 1-3 that it is particularly at higher humidification that the composite materials appear to perform well, suggesting an interesting area for developement.

1.5.2 PBI

Extensive reviews of these materials have recently been published by Assensio *et al.* [46] and Li *et al.* [65]. Recently Lin *et al.* reported increased mechanical strength and single cell performance for an epoxy (diglycidyl ether bisphenol-A) crosslinked PBI achieving a maximum power density of 172 $mWcm^{-2}$ at 160 °C and 0 %RH (at around 0.25 V) [66]. Increased mechanical strength by using an epoxy cross-linker has been confirmed by Wang *et al.* [67] using 1,3-bis(2,3-epoxypropoxy)-2,2-dimethylpropane and by Han *et al.* using 4,40-

diglycidyl(3,30,5,50-tetramethylbiphenyl) epoxy resin [68] and in both cases proton conductivity levels were retained. Kim *et al.* measured proton conductivity of 0.12 Scm^{-1} at 150 °C at 0 %RH for a benzoxazine cross-linked PBI membrane [69] and Aili *et al.* obtained in-plane proton conductivity of 0.14 Scm^{-1} at 150 °C and 20 %RH for a PBI crosslinked with divinylsulfone [70]. A new type of sulfonated PBI prepared by random copolymerisation of disodium 4,6-bis(4-carboxyphenoxy)benzene-1,3-disulfonate, 4,4_-dicarboxydiphenyl ether and 3,3_-diaminobenzidine was recently reported with relatively high conductivity of 0.037 S cm^{-1} at 170 °C and 0 %RH (and promising single cell performance of around 300 $mWcm^{-2}$) [71] and impressive conductivity of 0.376 S cm^{-1} 180 °C and 0%RH was reported by Mader and Benicewicz [72, 73] for a block copolymer consisting of sulfonated and non-sulfonated PBI segments.

1.5.3 Inorganic or Solid Acid Membranes

Inorganic or solid acid membranes are another promising class of membranes for higher temperature fuel cells. This class of materials undergo a superprotonic phase transition; when passing through a specific temperature, their proton conductivity increases by several orders of magnitude. An extensive review of the materials is provided by Dupuis [15] categorising the materials in three classes; $MHXO_4$, MH_2XO_4, $M_3H(XO_4)_2$ (with M = K, Rb, Cs, Tl, Li, or NH_4 and X = P, S, As or Se). The most promising material appears to be $CsHSO_4$ with a superprotonic temperature of 140 °C. As early as 2001 this class of membranes was reported in Nature [74] when it was first tested in a fuel cell at 150-160 °C, more recent studies showed conductivity of 0.04 S cm^{-1} at 200 °C [75], and blending with microporous zeolite improved conductivity [76]. However, the published single cell performance for these materials is poor. Other groups have investigated the use of ferroxane [77] obtaining proton conductivity in the region of 10^{-2} Scm^{-1} at room temperature. These

materials offer a promising alternative to polymer membranes but challenges of water solubility, mechanical instability and compatibility with other cell components need to be addressed.

It is clear that various materials exist which satisfy high temperature requirements. It appears that relative humidity remains one of the key factors which affect performance, with materials such as PBI performing best at the lowest levels, and hydrocarbons performing better under wetter conditions. The performance of PBI is furthermore optimal at the upper ranges of PEMFC operation (~180 °C) with materials such as Nafion being better suited for operation temperature in the intermediate range (up to ~120 °C).

1.6 Scope of Research

Based on the initial review of the literature summarised in Sections 1.5, and initial scoping experiments described in Chapter 3 of this thesis, the scope of this project was limited to the use of commercial Nafion polymer. This was in order to systematically investigate the effect of the filler material properties and loading in the composite membrane performances. The filler material identified as most promising was Graphene Oxide based on the small but promising amount of literature data available at the time and expertise available at UOB.

In order to carry out a systematic study of the materials identified, it was necessary to standardise the manufacture of the test samples and optimise the test protocol. In this way the differences in samples and irregularities caused by the experimental set up could be eliminated and meaningful performance data could be extracted. Most studies reviewed in the literature reported different sample preparation methods and a wide range of test

conditions; this is detailed in Chapter 2, the literature review on graphene oxide composite materials. With this strategy in mind, the following objectives were identified for this project:

1. The optimisation of the solution cast method of preparing the composite membranes.
2. Evaluation and development of the optimal filler material for use in the study, and to prepare this filler material in-house.
3. Sourcing, installation and calibration of High Temperature PEM/PEMFC Test Equipment.
4. Ex-Situ analysis of composite membrane in a temperature range of 80 – 120 °C and 25 – 95 % relative humidity.
5. In-Situ testing of composite membranes to evaluate the performance in a single cell in the same temperature and humidity range.

The objectives identified allowed, in the final stages of the project, for the preparation of membranes to the same standard each time. It was decided to prepare the filler materials in-house for the same reason. In this way a situation could also be avoided where a particular material became unavailable for any reason and it was cost efficient. In-house testing allowed for a high volume of tests and control was maintained over the integrity of each test. By carrying out the ex-situ and in-situ tests, both in-house and on the same equipment, this allowed for the correlation of the two sets of data.

Chapter 2 is a summary of the published data available for intermediate temperature proton exchange membranes prepared with graphene oxide with the main focus on Nafion-GO

composites. Some data for other composite membranes doped with GO is included to allow for comparison. Chapter 3 details the research methodology and experimental work.

Following this, the research is presented and discussed in the order of the 5 objectives. Chapter 4 and 5 describe the optimisation of the membrane preparation procedure and the preparation and characterisation of graphene oxide, the filler material selected for this study. Chapter 6 focuses on the commissioning, installation, optimisation and calibration of the test equipment and is followed in Chapter 7 and 8 with the ex-situ and in-situ results obtained for the composite Nafion-GO membranes. Chapter 9 summarises the findings of this study and gives suggestions for continuation studies relating to this work.

CHAPTER 2 LITERATURE REVIEW

2.1 Introduction

Elevated operational temperature for proton exchange membrane fuel cells (PEMFCs) is desirable due to enhanced reaction kinetics at the electrodes, increased carbon monoxide tolerance, and simplified heating and humidification management at these temperatures. As described in Chapter 1, the choice of electrolyte largely dictates the operating temperature of the cell. As conventional electrolyte materials for PEMFCs require operating temperatures of around 80 °C and full humidification, it follows that the electrolyte must be modified if the fuel cell is to be operated above this temperature.

Research in elevated temperature systems has recently focussed on an intermediate temperature (IT) range of 90 – 120 °C. Operation of the PEMFC in this temperature range is attractive because it makes it possible to focus development on conventional polymers, such as Nafion, and to tune the performance of these fairly well understood materials by the addition of filler materials which can mitigate the deterioration in performance due to dehydration. In the higher temperature range, up to around 160 °C, doping of polybenzimidazole (PBI) polymers with various fillers have the advantage of allowing a reduction in the acid loading and reducing the negative effects of acid leaching [78].

Many composite systems have been investigated based on the main types of polymers mentioned in Chapter 1. In this respect, polymers like Nafion [79], sulfonated poly(ether ether ketone) (SPEEK) [80], sulfonated poly sulfone (SPSU) [81], and polybenzimidazole

(PBI) [78, 82] have been doped with inorganic materials such as metal oxides, heteropoly acids, and graphene oxide with promising high temperature or low humidification results.

Of particular interest are Nafion-graphene oxide (GO) composite materials due to the wealth of published data on Nafion membranes and the commercial availability of polymer dispersions and films. The superior qualities of GO have furthermore been reported with respect to thermal stability up to at least 200 °C [83] and very low electrical conductivity [82].

For the purpose of this Chapter, the literature was reviewed up to the last quarter of 2014, with the aim of providing a broad overview of the GO composite materials that had been reported up to this time. The focus throughout was on materials developed for intermediate temperature (90-120 °C), but, where relevant, some studies at low temperature (20-80 °C) and high temperature (up to 160 °C) are briefly mentioned. Further detailed analysis of available data accompanies the relevant chapters in the rest of the thesis, where they were related to the measured data. The first section is a summary of the main filler materials that have been reported for composite membrane preparation. This is followed by a brief description of GO synthesis and the functionalisation of the material. The main sections follow with detailed descriptions of GO functionalisation, membrane preparation methods, characterisation and performance results. The final section summarises the implications of the literature review for this project.

2.2 Composite Materials

The main challenge for proton exchange membranes operating at elevated temperature is the evaporation of water and resultant loss in performance. One mitigation strategy is to replace water with an acid or ionic liquid as the charge carrier. A polymer can be doped with a medium such as phosphoric acid or 1-butyl-3-methyl imidazolium bis(trifluoromethyl sulfonyl) imide as illustrated in Chapter 1, Figure 1-6. PBI-phosphoric acid membranes in particular show high proton conductivity at temperatures up to above 160 °C. A serious drawback for these materials however is leaching of the ion conductor under operating conditions due to the formation of water at the electrode. This leads to reduced proton conductivity and corrosion of the other components in the fuel cell system [84]. This is clearly undesirable for automotive application.

Another strategy is to prepare composite membranes by doping a conventional low temperature membrane with a suitable filler material. Hydrocarbon polymers are very sensitive to humidification conditions, showing a remarkable drop in proton conductivity at reduced humidification. In order to increase their tolerance to higher temperature and reduced humidification, many studies have been published reporting promising results for these types of membranes. As mentioned in Chapter 1, various hygroscopic oxides, clays and zeolites among others have been investigated as filler particles to increase the water uptake and retention in proton exchange membranes (PEMs). It is also possible to improve the performance of PBI membranes, mentioned above, by adding fillers, as this reduces the quantity of acid or ionic liquid required in the polymer matrix. Table 2-1 summarises some of the filler materials that have been reported for Nafion composites and particularly for higher temperature application. In the table, the type of filler is given in the first column,

with the filler loading indicated in brackets. The water uptake and proton conductivity performance is given in the next two columns with the operating conditions indicated in brackets.

Table 2-1 Nafion-composite membranes reported in recent literature. The inorganic filler is shown in the first column (the filler loading is given in brackets) and the performance, relating to water uptake and proton conductivity, with reference to pure Nafion, is given in the second and third column (the operating conditions are given in brackets).

Class	% Water uptake vs. reference membrane	Proton conductivity vs. reference membrane	Ref
TiO_2 nanoparticles (5 wt%)	2.75 % vs. 1.6 % (100 °C) *	0.007 S/cm vs. 0.0005 S/cm (110 °C 0 %RH)	[85]
TiO_2 nanowires (5 wt%)	Decreased water uptake with increasing filler loading.	0.12 vs. 0.09 S/cm (90 °C, 50 %RH)	[86]
Acid activated Laponite clay (3 wt%)	71.1 % vs. 52.6 % (90 °C)	0.270 vs. 0.135 S/cm (110 °C, 100 %RH)	[87]
Analcime zeolite (15 wt%)	40 % vs. 6 % (25 °C)	0.4373 S/cm vs. 0.0642 S/cm (80 °C, 100 %RH) Rapid deterioration of proton conductivity above this T.	[88]
Cesium/molybdenum heteropoly acid (10 wt%)	76 % vs. 33 % (rt)	0.06 S/cm vs. 0.002 S/cm (120 °C, 0 %RH)	[89]
Phosphoric acid (34 %)	N/A	0.03-0.04 S/cm (130 °C, 16-18 %RH)	[90]
Graphene oxide (4 wt%)	37.0 % vs. 21.2 % (rt)	0.05 S/cm vs. 0.01 S/cm (120 °C, 100 %RH)	[91]
Sulfonated graphene oxide (10 wt%)	23 % vs. 29 % (rt)	0.028 S/cm vs. 0.0034 S/cm (120 °C, 20 %RH)	[92]
Hollow silica particles (10 wt%)	82 % vs. 50 % (100 °C)	0.044 S/cm vs. 0.0022 S/cm (130 °C, 100 %RH)	[52]

* Water content, as opposed to water uptake % was reported in this study.

Overall it can be seen that the incorporation of suitable filler materials have a positive effect on the water uptake and proton conductivity properties of the membrane material. The ideal filler material would have both high water uptake and increasing proton conductivity with increasing temperature. In the cases of the titanium nanowires and the zeolite detailed in Table 2-1, this is not the case. Acid activated clay, heteropoly acids, graphene oxide and hollow silica particles possess both the required attributes.

When preparing composite membranes, the following factors must be considered.

The first consideration is the degree of filler doping. The filler loading should be low enough to prevent deterioration in mechanical integrity of the membrane and blocking of the proton conduction mechanism through the plane of the membrane. On the other hand, it should be high enough to increase the water uptake ability of the pristine polymer and enhance the water retention at elevated temperatures [93].

A second factor is the filler distribution in the base polymer. Non-uniform distribution or agglomeration of particles can lead to mechanical failure in the material, either due to a disruption in the homogeneity of the polymer film, or by the formation of hot spots during operation [94]. The distribution of filler particles is affected by the chemical interaction between the polymer and the particle, the particle dimensions, and the dispersion of the filler in the casting solvent.

Finally, the chemical, mechanical and thermal stability of the filler material should match that of the base polymer.

2.3 Graphene Oxide

2.3.1 Background

The exceptional properties of GO have been widely reported and the material has been considered for applications ranging from medical delivery to highly specialised mechanical composites. The material is constructed of a disrupted sp^2 network, and the absence of an extended π-conjugated orbital system renders the material effectively electrically insulating, [95-97] a prime requirement for a composite membrane filler. The two dimensional carbon-monolayer sheets, with high surface area, are decorated with oxygen functional groups allowing for hydrogen bonding of water molecules and facile hopping sites for protons [98]. The material is highly thermally, mechanically and chemically stable at high operating temperatures, stable in de-ionised (DI) water solution, and relatively easy and cheap to synthesise using commonly available chemicals [83].

In the literature reviewed, two methods are reported to prepare GO for application in composite membrane preparation. Staudenmaier [99] developed a method following on from the initial work carried out by B. C. Brodie [98], but this method does not seem to be widely used in membrane preparation. Hummers and Offeman [100] developed the synthetic route that is chosen by the majority of researchers [91, 92, 101-103]. This method is usually referred to as the Hummers Method. The Staudenmaier method was first reported early in the 20^{th} century and comprises the addition of potassium chlorate in multiple aliquots over time to a slurry of graphite in fuming nitric acid and concentrated sulphuric acid. The Hummers Method was developed almost sixty years later and, in this case, graphite is reacted with

potassium permanganate and concentrated sulphuric acid. In both cases, a similar C:O ratio of around 2:1 is achieved [98].

The most notable modification to the original Hummers synthesis employed in different studies is the ratio of graphene oxide to potassium permanganate added in the initial stages of the reaction. The ratios vary from 1:25 [91] to 1:3 [92, 100-102]. Only one study was found to report the Staudenmaier method and, in this instance, the ratio of oxidizing agent to graphite was 1:20 [104].

Historically, the characterisation of graphene oxide has been complicated due to the variation in shape, size and composition between different samples, and a poor understanding of ideal characterisation techniques. Various structures have been suggested, and were summarised by Dreyer *et al.* [98] in an extensive review of the synthesis and functionalisation of graphene oxide. Whereas there is general agreement on the presence of alcohol and ether groups on the carbon structure, the presence of carboxylic acid is not universally agreed upon and the overall structure and location of the functional groups is in slight dispute [105].

One of the widest accepted and referenced structures, by Lerf and Klinowski, is a nonstoichiometric amorphous structure [106]. As illustrated in Figure 2-1, it was concluded that the carbon atoms were all quarternary and that tertiary alcohol groups, 1,2-ether groups and a mixture of alkenes form the bulk material. Later refinement led to the conclusion that the double bonds were either aromatic or conjugated and that small quantities of carboxylic acid was present on the edges of the sheets. The characterisation techniques employed included solid state nuclear magnetic resonance, magic angle spinning experiments and Fourier transform infrared spectroscopy (FT-IR).

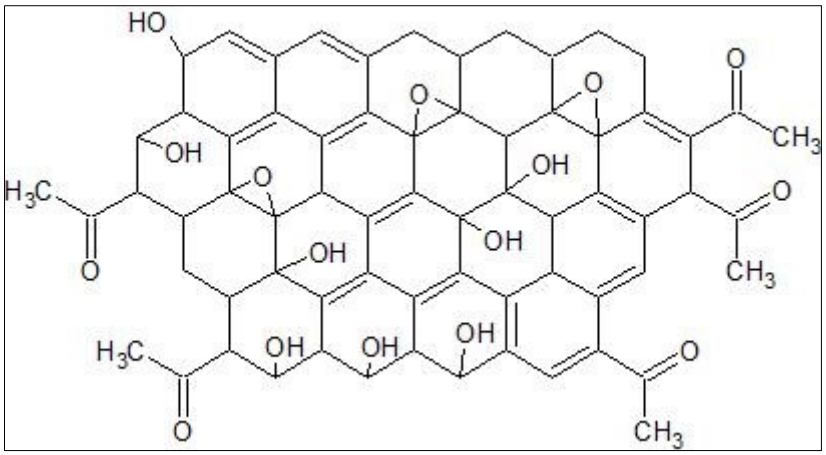

Figure 2-1 The nonstoichiometric amorphous structure of GO, suggested by Lerf and Klinowski (adapted from ref. [98]).

A further conclusion from early structural investigations conducted by proton nuclear magnetic resonance (^{1}H NMR) studies was the very strong interaction between water and graphene oxide over a wide temperature range, up to around 200 °C. This is illustrated in Figure 2-2, showing the interaction between two graphene oxide sheets via hydrogen bonding [107].

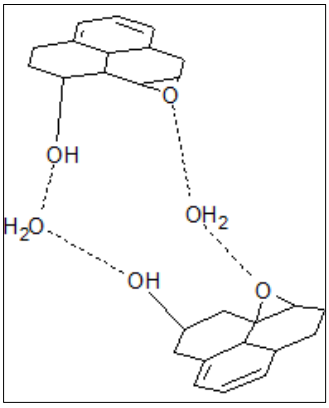

Figure 2-2 Hydrogen bonding between two graphene oxide sheets (adapted from ref. [98]).

An alternative structure was modelled sequentially by Ruess, Scholz-Boehm and Dekany [98]. The structure is comprised of trans-linked cyclohexyl species interspersed with tertiary

alcohols and 1,3-ethers and a corrugated keto/quinoidal network. If the material is further oxidised all aromaticity is lost by the formation of 1,2-ethers. This model does not predict the presence of carboxylic acid.

It is difficult to conclude which model is correct, but most studies using GO in the process of composite membrane preparation rely on chemical analysis techniques which allow the identification and quantification of chemical groups present in the bulk material and assume the Lerf-Klinowski model of planar sheets.

2.3.2 Functionalisation

For composite membrane application, GO is often functionalised to increase the ion exchange coefficient and to enhance the water uptake and retention ability. This is achieved by functionalisation of the epoxy and hydroxyl groups at the basal planes or the carboxylic acid groups on the edges of the GO sheets [98].

Epoxy groups are functionalised by ring-opening reactions and subsequent amidation. Primary and secondary aliphatic amines have been grafted onto the GO surface by nucleophilic substitution reactions on the epoxy groups [104].

Dehydration of the alcohol groups by 3-mercaptopropyltrimethoxysilane (MPTMS) or phenyltrimethoxysilane (PTMS) is another functional group conversion route and results in a precursor material that can be oxidised with hydrogen peroxide [92] or sulfonated by reaction with sulphuric acid [108] to result in sulfonic acid functionalised GO. Xue *et al.* [82] reacted GO with tert-butyl isocyanate to convert both the alcohol and the carboxylic acid groups to isocyanate groups.

Carboxylic acid groups can be converted to sulfonic acid groups by microwave reaction with concentrated nitric and sulphuric acid [103] and can also be activated by various groups such as 1-ethyl-3-(3-dimethylaminopropyl)-carbodiimide (EDC) followed by the coupling of a suitable nucleophilic species such as sulfanilic acid [109].

The functionalised GO resulting from the above techniques contains sulfonic acid as the site for ion exchange, and hence still requires humidification under test conditions. In this respect, some efforts have been made towards the development of self-humidifying membranes [101]. The addition of platinum nanoparticles could act as a reaction site to form water molecules in-situ, and with the presence of another filler material (such as GO) the membrane would be able to retain the humidification. Difficulties can occur however, due to the formation of radical species and electronic short circuit, and a further study explored the immobilisation of a sulfanilic functionalised Nafion-GO composite in a sulfonated zeolite structure [110]. Sulfanilic acid was bonded to the carbon backbone of GO by an azo-coupling reaction. It was theorised that the addition of the nitrogen-containing sulfanilic acid could act as a catalyst for water generation in the membrane [111].

Table 2-2 summarises some of the functionalisation reactions that will be described in detail in Section 4.

Table 2-2 GO functionalisation.

Functional group added	Reaction site on GO	Method	Samples tested for proton conductivity	Ref
Aliphatic amines	Epoxy	Stirring in water.	None	[104]
Sulfonated propyl	Alcohol	Reaction in toluene and oxidation.	SGO* 5, 10 %	[92]
Sulfonic acid	Carboxylic Acid	Microwave reaction with nitric/sulphuric acid.	SGO* 0.5 %, GO 0.5 %	[103]
Platinum	Oxygen groups on GO basal plane.	Microwave reaction with chloroplatinic acid and sodium hydroxide.	0.5, 3, 4.5 % both functionalised and pristine GO.	[101]

* SGO refers to sulfonated graphene oxide.

It should be pointed out that many reactions are possible at more than one functional group at the same time and that the composition of the starting material is not always fully known [98].

2.4 Graphene Oxide Composite proton exchange membranes

This section will firstly describe the functionalisation of GO and the preparation of composite membranes as reported in literature. The discussion in this chapter focuses on publications reporting on GO composites for higher temperature application. The membrane preparation process and GO synthesis is described in broader detail in Chapter 4 and 6. This is followed by a brief description of the characterisation techniques employed for the materials. The final

section compares and discusses the proton conductivity and in-situ data which have been reported for the composite materials described.

2.4.1 Preparation methods and test conditions

It has already been mentioned that Nafion polymer was the material of choice for this study, in order to focus on the properties of the filler in the overall performance of the membrane. For completeness, in this Chapter, detail is given of graphene oxide composite membranes, which were prepared from a range of polymers, in order to illustrate the different experimental techniques and results reported for composite membranes in the literature. A comparison further allows for conclusions to be made on the performance of Nafion, compared to other polymers. The focus is on high temperature studies, but as the literature is sparse, and not all studies show both in- and ex-situ data, some low temperature studies are included in order to fully investigate the techniques and trends.

2.4.2 Nafion

Nafion is usually obtained commercially as a film or as a 5-20 wt% solution in water and alcohol. Nafion is synthesised by reacting tetrafluoroethylene (TFE) with sulfonic acid to form a sultone. The sultone is converted into an acid fluoride with a sulfonyl fluoride end group which is then reacted with hexafluoropropylene oxide and pyrolysed to form sulfonyl fluoride perfluorovinyl ether. Copolymerisation of this product with TFE in a perfluorinated solvent leads to a fluorinated precursor (SO_3F) which can be neutralised to the salt form (SO_3Na) or hydrolysed to the acid form (SO_3H) [112].

Enotiades at al. [104] prepared functionalised GO by dispersing GO in water and adding aliquots of four different amine derivatives in water. The reaction was stirred for 24 hours, washed with water, centrifuged and air dried. The derivatives were chosen because of the presence of amino, alcohol and sulfonic acid functional groups and were 3-amino-1propanesulfonic acid (SULF), 2-amino-3-hydroxypropanoic acid (SER), 2-([2-hydroxy-1,1-bis(hydroxymethyl)ethyl]amino)ethane sulfonic acid (TES) and 5-aminovaleric acid (VAL). In an optimised procedure, the filler was added directly to the Nafion solution (20 %), sonicated for 1 day at room temperature and stirred for 1 day, after which the solvent was evaporated at 80 °C overnight. Resultant membranes were hot pressed at 150 °C for 15 minutes between two Teflon plates and treated with nitric acid (1M), hydrogen peroxide (3 %), DI water and sulphuric acid (0.5M). This treatment is carried out to oxidize and remove organic impurities, rinse and remove metallic impurities respectively, and is a common feature in membrane preparation methods [113]. A further treatment with ethylenediaminetetraacetic acid (EDTA) was carried out to remove paramagnetic contaminants like copper, which can be incorporated during the manufacture of Nafion [114] and which would hamper NMR analysis. Unfortunately proton conductivity and single cell performance were not reported, but extensive materials characterisation was undertaken, and promising results were obtained for further development of this type of composite for high temperature application.

One of the earliest studies on Nafion-GO composites for high temperature application was reported by Zarrin *et al.* in 2011 [92]. Sulfonated GO (SGO) was prepared by reacting GO with 3-mercapto-propyl trimethoxysilane (MPTMS) in toluene at 110 °C, under reflux conditions, for 24 hours. The mercapto groups were oxidised in 30 wt % hydrogen peroxide at 25 °C for 24 hours, washed in ethanol and water, and dried overnight prior to use.

Composite membranes were prepared by mixing Nafion (5 wt % solution), SGO and ethanol, sonicated for 30 minutes, and heated at 60 °C until half the solution evaporated. The solution was then evaporated at 100 °C for 2 hours and 140 °C for 1 hour prior to washing in hydrogen peroxide (3 %), DI water, and sulphuric acid (0.5 M) respectively. Data is reported for the functionalised composite membranes with filler content of 5 and 10 wt %. The thickness of the membranes is not stated. Proton conductivity was measured using a 4-electrode system measuring the impedance between 1MHz to 0.1 Hz and a perturbation voltage of 5 mV. Data is reported for 80, 100 and 120 °C over a humidification range of 20-100 %RH.

Membrane electrode assemblies (MEAs) were prepared for the 10 wt % membrane by painting a catalyst ink (20 wt % Pt/C, 5 wt % Nafion solution and glycerol) onto a Teflon blank and drying sequentially until a platinum loading of 0.2 mg/cm^2 (cathode) and 0.1 mg/cm^2 (anode) was achieved. The membrane was washed in a dilute sodium peroxide solution, rinsed and hot pressed to dry. The MEA was prepared by hot pressing the membrane between two decals at 210 °C for 5 minutes at 110 lbs/cm. The active area was 5 cm^2 and testing was carried out with 0.2 and 0.5 L/min hydrogen and oxygen. Data was reported for the 10 wt % membrane and recast Nafion.

In the same year a paper was published by Choi *et al.* [103]. Sulfonated GO was prepared by combining nitric acid (70 %) and sulphuric acid (97 %) with GO and treating with microwave radiation at 50 % of 900 W power under 20 psi for 3 minutes. After diluting with DI water and dialysing, the product was washed in DI water. The product was centrifuged (4000 rpm, 30 minutes, three times) and then dried under vacuum at 60 °C. The composite membranes were prepared in a similar way to that described for the previous study, by mixing Nafion

solution (5 wt %) and the filler, but in this instance *N,N*-dimethylformamide (DMF) was used instead of ethanol. The solution was stirred and sonicated for 1 hour. The solvent evaporating process differed slightly; evaporation was allowed to occur slowly between 60 to 120 °C over 12 hours. The washing procedure was similar to the Zarrin study, but 30 % hydrogen peroxide was used. The membranes were then dried under vacuum at 70 °C. Membranes were prepared to a 0.5 wt % GO loading and were around 50 μm thick. Proton conductivity was carried out via a 2-probe method and a frequency of 10^{-3} to 106 Hz with a 10mV perturbation. Tests were carried out between 25 to 100 °C. Data was reported for the functionalised composite, the unfunctionalised composite, and for Nafion 112.

MEAs were prepared, but testing is reported for a direct methanol fuel cell test at low temperature and will not be further discussed, apart from stating that the internal resistance of the composite membranes was lower than that of the reference material.

A further study published by Kumar *et al.* in 2012 [91] reported results for composites prepared from unfunctionalised GO. In contrast to the previous study, Nafion solution was first solvent cast and dried (experimental detail not given), presumably to remove the water and other solvents present in the commercial solution. A different solvent was used when the solid was dissolved in dimethyl acetamide (DMAc). A solution of GO in DMAc was then mixed into the Nafion/DMAc solution and stirred for 1 hour. The drying sequence was also different: solvent was evaporated at 70 °C and the resulting membranes were further heated at 140 °C for 2 hours after they were removed from the casting glass. The washing process was similar, but 5 % hydrogen peroxide was used, in contrast to 3 and 30 % reported in the previous two studies. The filler content was controlled at 2, 4 and 6 wt %, and the average thickness reported as 50 μm (measured at 10 random points with a digital micrometer).

Proton conductivity was measured by 4-point AC impedance between 20 kHz to 1 kHz at atmospheric pressure, between 30-120 °C and 100 % RH.

A different MEA preparation technique was used. A binder (IPA and Nafion 20 wt % solution) was sprayed onto commercial GDE (0.38 mg_{Pt}/cm^2) before sandwiching the membrane and hot pressing at 125 °C for 3 minutes at 60 kg/cm^2. The active area was 1 cm^2 and was tested using 0.1 and 0.07 L/min hydrogen and oxygen respectively. In-situ results for the 4 wt % membrane, recast Nafion and Nafion 212 is reported.

Lee *et al.* published a study in 2014 [101] reporting the deposition of platinum particles on graphene oxide. Graphene oxide, ethylene glycol, and chloroplatinic acid were combined and stirred for 3 hours, followed by sonication for 2 hours. The pH was adjusted to pH12 with sodium hydroxide, and the solution was heated in a microwave oven at 700 W for 5 minutes. The resulting product was filtered and washed with DI water and dried under vacuum at 60 °C for 12 hours. Composite membranes were prepared by evaporating the alcohol from a commercial Nafion solution (20 wt %) at room temperature for 24 hours. The filler was added, the mixture sonicated for 30 minutes, and cast using a doctor blade in an oven at 20 °C. The membrane was heated to 70 °C and kept at this temperature for 1 hour, after which time the vacuum was applied for a further 2 hours. Experimental detail for ex-situ testing was not provided. Membranes were prepared with loading of 0.5, 3 and 4.5 wt % filler material. Thickness was not given. Proton conductivity data was given for 80 °C and 100 % RH.

MEAs were prepared by combining the catalyst (Pt/C, 40 wt %), IPA, and Nafion solution (5 wt %) and sonicating for 1 hour. The composite membranes were placed on a hot plate

and the catalyst ink was painted directly onto the membrane to obtain a platinum loading of 0.2 and 0.3 mg/cm^2 on the anode and cathode side respectively. Information on the gas diffusion layer (GDL) is not given. The active area was 3 cm^2 and testing was carried out using hydrogen and oxygen at 0.1 L/min. Conditions were regulated at 80 °C and 0, 40, 60 and 100 % RH.

In a similar vein, a patent application was made in 2013 by Yeung *et al.* from the Hong Kong University of Science and Technology [111]. The strategy in this instance was to prepare composite membranes based on a zeolite-confined sulfonated graphene-Nafion composite membranes [110] to bring about in-situ water catalysation during operation under dry conditions. The principle was based on the introduction of a sulfanilic acid moiety on the carbon backbone of the graphene oxide. Graphene oxide was first partially reduced with sodium borohydride and sodium carbonate and dispersed in DI water. Sodium hydroxide was then added along with an aryl diazonium salt which was prepared from sulfanilic acid. The purified and dried product was further reacted with hydrazine and sodium carbonate to obtain sulfonated graphene. Impressive in-situ data was obtained. Under dry operating conditions at 70 °C the composite membrane showed 16.5 times higher power density than Nafion 117 [110]. As the graphene oxide was reduced in the final stages of functionalisation and since proton conductivity data is not given, this study will not be discussed in further detail.

For the studies described above, and where in- and ex-situ data is available, the experimental detail is summarised in Table 2-3 and Table 2-4.

Table 2-3 Membrane preparation variables for Nafion-GO composite membranes from literature [91, 92, 101, 103].

Variable/ Study	Solvent	Nafion solution (wt %)	Filler range (%)	Functionalisation	Membrane Thickness (μm)
Zarrin	Ethanol	5	5-10	MPTMS	Not stated
Choi	DMF	5	0.5	Sulfonation	50
Kumar	DMAc	5	2-6	N/A	50
Lee	None stated	20	0.5-4.5	Platinum	Not stated

Table 2-4 MEA preparation and test conditions for Nafion-GO composite membranes from literature [91, 92, 101, 103].

Variable/ Study	Temperature/ Humidity range	MEA preparation	Pt Loading $mg_{Pt}/cm2$	Flow Rate (L/min), (Hydrogen/Oxygen)
Zarrin	80-120 °C, 20-100 % RH	Decal catalyst layer.	0.2, 0.1	0.2, 0.5
Choi	25-100 °C, 100 % RH	N/A	N/A	N/A
Kumar	30-120 °C, 100 % RH	Commercial GDE.	0.38, 0.38	0.1, 0.07
Lee	80 °C, 100 % RH (ex-situ), 80 °C, 0-100 % RH (in-situ)	Catalyst Coated Membrane.	0.2, 0.3	0.1, 0.1

Of the four main studies reviewed, each study used a different casting solvent, filler range and type of functionalisation. In general a 5 wt% Nafion solution was used, but one study used a 20 wt% solution. Not all studies mentioned the thickness of the membranes. Proton conductivity and in-situ analysis was carried out over a range of 25 to 120 °C and from dry to fully humidified conditions. Where it was possible, the published data was related to the findings for this study in Chapters 7 and 8.

2.4.3 Polybenzimidazole (PBI)

As mentioned in Chapter 1, PBI is a high temperature polymer widely researched for application at temperatures up to 180 °C. It is synthesised by polymerisation of an appropriate diamine and carboxylic acid in polyphosphoric acid at 180-200 °C or the alternative form, ABPBI, is obtained by polymerisation of the diamine 3,4-diamonobenzoic acid under similar conditions. Conductivity for ABPBI has been reported as 0.08 S cm^{-1} at 140 °C with no hydration and 0.2 S cm^{-1} at 20 %RH [115]. The polymer can conduct ions under dry conditions due to the immobilisation of phosphoric acid which is chemically bonded to the polymer backbone. One of the main drawbacks of this material is the high acid loading that is required (at least above 3.0 molecules acid per repeat unit of polymer) and the detrimental effect that this can have on the mechanical properties and performance of the membrane and to the rest of the cell if the acid is eluted during the operation of the fuel cell. In an attempt to reduce the acid loading, the addition of functionalised GO was investigated [78].

Xu *et al.* [78] prepared PBI (poly(2,2'-m-(phenylene)-5,5'-bibenzimidazole), the structure is shown in Chapter 1, Table 2) membranes doped with GO and with sulfonated GO.

Sulfonated GO was prepared by dissolving GO in DMAc and stirring for one hour. Chlorosulfonic acid was added drop-wise over an hour, under continuous stirring. To prepare the membranes, GO and SGO were dispersed in a solution of PBI and DMAc. The solvent was evaporated at 120 °C for 12 hours. The membranes had a filler loading of 2 wt % and were approximately 70 μm thick after doping with phosphoric acid in phosphoric acid (2M) for several days at 20 °C. Proton conductivity was measured using a 4-point probe with platinum foil electrodes, between 1-20 kHz.

MEAs were prepared by spraying a catalyst ink (50 wt % Pt/C and 60 wt % PTFE in a water/ethanol mixture) onto commercial GDEs (carbon paper, Freudenburg) at 100 °C and drying at 150 °C for 2 hours. The platinum loading was 0.9 and 0.5 mg/cm^2 for the cathode and anode respectively. The electrode surface was treated with phosphoric acid and dried at 80 °C. Finally the electrodes and membranes were hot pressed at 150 °C for 10 minutes at 40 kg/cm^2. Testing was carried out with hydrogen and oxygen 0.1 and 0.050 cm^3/min respectively.

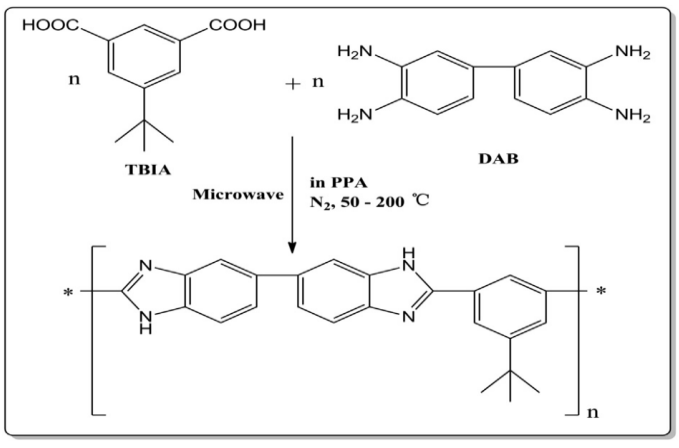

Figure 2-3 BuIPBI (3,3'-diaminobenzidine and 5-tert-butyl isophthalic acid) [82]. Reprinted from International Journal of Hydrogen Energy Copyright 2014, with permission from Elsevier.

Xue *et al.* used 3,3'-diaminobenzidine and 5-tert-butyl isophthalic acid (Figure 2-3) to prepare a BuIPBI with large alkyl groups to improve the solubility of the polymer [82]. Graphene Oxide was functionalised by dispersing in DMF, adding tert-butyl isocyanate and stirring under nitrogen for 24 hours. The resultant slurry was separated, washed in DMF, and dried under vacuum for 24 hours. The membranes were prepared by dispersing the GO in DMAc and then mixing with a PBI/DMAc solution. The solution was vigorously mixed and the solvent was evaporated at 60 °C. The membranes were between 80 to 100 μm thick (although it is not clear what the thickness was after doping with phosphoric acid), and the filler ratio of the series of membranes was between 1 to 15 wt %. The membranes were immersed in phosphoric acid at room temperature for 24 hours. Proton conductivity was carried out by 2-point probe between 0.1 to 10^5 Hz. The membranes were coated with a layer of pure polymer solution to avoid contact between the electrodes and the GO, this further increased the thickness of the material by 3-5 μm. In-situ testing was not reported.

Table 2-5 Membrane preparation variables for PBI-GO composite membranes from literature [78, 82]

Variable/ Study	Solvent	Base Polymer	Filler range (%)	Functionalisation	Membrane Thickness (μm)
Xu	DMAc	PBI	2*	Sulfonation	70
Xue	DMF	BuIPBI	1-15	Iso cyanate	80-100

*The study reported one composite membrane only.

Table 2-6 MEA preparation and test conditions for PBI-BO composite membranes from literature [78, 82]

Variable/ Study	Temperature/ Humidity range	MEA preparation	Pt Loading $mg_{Pt}/cm2$	Flow Rate (L/min), (Hydrogen/Oxygen)
Xu	175 °C, dry	Commercial GDE	0.9, 0.5	0.1, 0.05

2.4.4 Conventional Hydrocarbon Polymers

Modified and composite sulfonated hydrocarbon polymers are suitable for higher temperature PEM fuel cells. Park *et al.* recently compiled a detailed and extensive review of sulfonated hydrocarbon membranes for intermediate temperature application [37]. The starting material for SPEEK is often commercial PEEK (manufactured by Victrex or Fumatech) which is then sulfonated with concentrated sulphuric acid. Sulfonated polyimine (SPI) can be prepared by reacting a sulfonated diamine monomer, triethyalamine, naphthalenetetracarboxylic dianhydride, a hydrophobic diamine monomer, benzoic acid and m-creosol at temperatures from 150 °C to 195 °C [116]. The reports on these types of membranes doped with GO, are mostly for low temperature or direct methanol fuel cell (DMFC) application. The studies described below reported proton conductivity for composites prepared from GO and functionalised GO.

Two recent studies reported results on sulfonated poly(ether ether ketone) (SPEEK), both employing sulfonated graphene oxide as the filler material. Heo *et al.* [117] prepared

sulfonated graphene oxide by dispersing GO in tetrahydrofuran (THF) and reacting sequentially with sodium hydride, propane sultone, and hydrochloric acid to add alkyl sulfonic acid groups at the alcohol sites on GO. Membranes were prepared by dispersing GO in DMAc and combining with a SPEEK solution (also in DMAc). The solution was stirred for 12 hours and solution cast at 60 °C for 5-6 hours. Membranes were prepared with 1, 3, 5, 7 and 10 wt % filler, both for SGO and GO. Proton conductivity was measured at 25 and 80 °C with a 2 point probe between 0.1 kHz and 1 MHz. Jiang *et al.* [118] prepared sulfonated GO in the same way as Zarrin *et al.* (described above), [92] by the addition of MPTMS as sulfonic acid precursor. DMF was used as the casting solvent, and membranes were dried at 80 °C overnight and 100 °C for a further 12 hours. As a final step, the membranes were soaked in methanol, and washed in DI water to remove the residual solvent. The thickness was given as ~60 μm. A 5 wt % Nafion-GO composite, and 3-8 wt % Nafion-SGO composites were prepared. Proton conductivity was measured between 1 MHz -10 Hz with a perturbation voltage of 10 mV.

The first study did not report ex-situ testing and hence this will not be discussed further. The second focussed on DMFC application and it will simply be stated that doping with pristine GO resulted in higher maximum power density than pristine SPEEK, but lower maximum power density than commercial Nafion. Doping with sulfonated GO increased the maximum power density in the cases of 3 and 5 wt % over both pristine SPEEK and Nafion. The 8 wt % composite showed the lowest performance.

A study published by He *et al.* [94] reports results for a series of membranes prepared from sulfonated polyimide (SPI) doped with pristine GO. Membranes were prepared by dissolving SPI in dimethyl sulfoxide (DMSO), and combining with a solution of GO in DMSO, before

stirring at 60 °C. Solvent was evaporated at 70 °C for 8 hours and then heated at 120 °C for 12 hours under vacuum. Membranes were soaked in sulphuric acid and washed before drying at 120 °C for 8 hours. Proton conductivity was carried out by four-probe impedance between 1 Hz – 100 kHz. In-situ testing was again carried out under direct methanol conditions.

Poly(ethylene oxide) (PEO) was also doped with pristine GO as reported by Cao *et al.* [105]. PEO was dissolved in distilled water, and an aqueous solution of GO was added, followed by stirring for 2 hours. Water was evaporated at room temperature for 48 hours, the membrane was then removed and dried for a further 12 hours. Proton conductivity was measured between 25 to 60 °C using a four-point probe between 1- 20 kHz.

Table 2-7 Membrane preparation variables for hydrocarbon membrane-GO composite membranes from literature [94, 105, 117, 118]

Variable/ Study	Solvent	Base Polymer	Filler range (%)	Functionalisation	Membrane Thickness (μm)
Heo	DMAc	SPEEK	1-10	Alkyl sulfonic acid	
Jiang	DMF	SPEEK	5 (GO) 3-5 (SGO)	MPTMS	60
He	DMSO	SPI		N/A	
Cao	Water	PEO	0.5	N/A	80

2.5 Characterisation

Fourier transform infrared spectroscopy (FT-IR) and X-ray photoelectron spectroscopy (XPS) is frequently used as characterisation techniques for GO and functionalised GO. FT-IR is useful for confirmation of GO oxidation as graphite is IR-inactive in the region that is of interest for graphene oxide [104]. Characteristic peaks are identified for hydrogen bonded and carboxy/hydroxyl groups between 3178 and 3387 cm^{-1} in a broad band, free hydroxyl groups between 3522 and 3620 cm^{-1} [92], and aromatics at 1625 cm^{-1} [101] (also described as skeletal vibrations of unoxidised graphitic domains [119]). Carboxyl stretching vibration in carboxylic acid (C=O, 1620 cm^{-1}, weak), hydroxyl deformation (O-H, 1396 cm^{-1}, strong), carbon-oxygen bond stretching vibration (C-O, 1062 cm^{-1}, strong) and asymmetric epoxy stretching or hydroxyl deformation in carboxylic acid groups (C-O-C/O-H, 1230 cm^{-1}, weak) [104] can also be identified. The identification of sulfonic acid groups can be confirmed by peaks at around 1070 and 1354 cm^{-1} due to S=O stretching [90, 92]. FT-IR spectra for Nafion is distinctive, with the strongest peaks appearing at ~ 982 cm^{-1} for C-O-C bonds, 1057 cm^{-1} for S-O bonds, 1144 and 1203 cm^{-1} for C-F bonds, 1300 cm^{-1} for the C-C backbone, and the peaks at 1626, 1760 and 3360-3500 cm^{-1} are usually attributed to different water molecules present in the material [90, 92, 120].

XPS allows for the further confirmation of oxidation and characteristic peaks for GO are identified at the following binding energies (eV): sp^2 and sp^3 hybridized C-C/C-H (284.4 eV), C-OH (285.4 eV), C-O-C (286.6 eV), C=O (288.2 eV) and O-C=O (290.0 eV) [92, 101, 102]. XPS can be used in the same way as FT-IR to confirm functionalisation, of particular interest is C-SH at 163.1 eV (S 2p), $–SO_3^-$ at 167.1 eV (S 2p) [109] and O=S=O bonds at 532.7 eV (O s) [92].

For purposes of comparison of graphene oxide doped membranes, it would be most useful to know the carbon and oxygen content and furthermore the types of oxygen functional groups that are present on GO in order to draw conclusions about the effect of the filler on the membranes. For the studies reviewed in the previous section, this data is reported as C:O ratio (73.16 % carbon to 26.84 % oxygen) by Zarrin *et al.*, C-C:C-O ratio (0.78) by Chien *et al.* and as percentages of functional groups (C-C (62.2%), C-O-C (19.0%), C-OH (2.4%) and HO-C=O (16.4 %)) by Lee *et al.*

Characterisation of the composite membranes focuses on the properties that are required for the novel membranes to be able to perform at higher temperature and lower relative humidity. In this respect the most important characterisations are carried out to test the water uptake ability and the effect that the filler has on the membrane conductivity. The water uptake is measured gravimetrically and is usually measured in tandem with the ion exchange coefficient (IEC). The values for water uptake, IEC and proton conductivity are expected to show the same trend since the water molecules and acid sites are both involved in the diffusion transport and Grotthus hopping mechanism of the protons through the membrane. It is therefore presumed that increased water uptake and IEC will lead to increased proton conductivity.

Zarrin *et al.* [92] showed data for water uptake and IEC values increasing from recast Nafion to 10 wt % SGO filler material. This trend was echoed in proton conductivity tests at 80, 100 and 120 °C over a range of humidity. Kumar *et al.* [91] reported the trend of their materials as follows: recast Nafion < 2 wt% < 6 wt% < 4 wt% composite. It was the material with the loading of 4 wt% GO which had the highest values, and this trend was mirrored by the proton conductivity data. An exception to the agreement in these trends was reported for Nafion

membranes doped with GO functionalised with platinum [101], where the water uptake for the composite material was lower than that for recast Nafion, and decreased with increasing filler loading. This was explained by the Pt-functionalisation of GO resulting in a material which is less hydrophilic than the pristine material. The values for IEC were not reported but the proton conductivity increased with increasing filler loading, possibly confirming that the objective of in-situ water catalysis was achieved.

The thermal and mechanical properties of the composite membranes are investigated mainly by thermogravimetric analysis (TGA) and tensile testing. Unmodified Nafion has a characteristic thermal degradation trend. The degradation of the polymer takes place at three distinct temperature ranges, with the initial evaporation of residual water (25-290 °C), followed by the degradation of the sulfonic acid groups (290-400 °C) and the degradation of the PTFE back bone (470-560 °C) [121, 122]. GO functionalised with aliphatic amine sulfonic acid, and the resulting composite recast Nafion membrane showed an increased PTFE degradation temperature (395 °C) compared with recast Nafion (385 °C) [104]. Nafion functionalised with acidified laponite clay particles similarly seemed to increase the degradation temperature by 3-12 °C. As the operating temperature of any PEMFC is likely to be much lower than the 470-560 °C range, TGA is used more in respect to new polymer development. But it can be used as a diagnostic tool to ensure that a certain type of filler does not have a detrimental effect on the membrane at the temperature at which it will be expected to operate.

Tensile properties of a proton exchange membrane are crucial to its performance. The membrane is compressed during the preparation of the MEA and the assembly of the fuel cell stack and is furthermore continually subjected to swelling and contracting under operational

conditions. Increased tensile strength (14 %) and Young's Modulus (26 %) was reported for a 2 wt% composite Nafion-GO membrane [123]. A separate study reported that both the elongation at break percentage and the tensile strength increased for composite membranes up to a certain filler loading (2-4 wt% GO [91]) but that these properties deteriorated with higher filler loading (6 %). This was explained by the GO sheets aligning in the material and in this way distributing the stress through the material. With further filler incorporation the interactions between the polymer and the filler is thought to become detrimental to the overall mechanical strength of the material. A contrasting study found that the elongation at break was drastically reduced for the composite materials, compared to recast Nafion, but confirmed increased tensile strength for a GO range of 0.5 – 4.5 wt% [101]. No explanation was offered for this occurrence.

2.6 Proton Conductivity and In-situ Testing

2.6.1 Nafion

The experimental detail in Section 2.4 indicates that comparison of literature data is difficult to make. The effect of different solvents and heating regimes are discussed in more detail in Chapter 4, but it is well known that polymer membranes are sensitive to pre-treatment conditions [26, 124]. Different test conditions further contribute to disparate data ranges reported in the reviewed literature.

A summary of proton conductivity for Nafion doped with pristine GO includes the Choi *et al.* study which reported very similar proton conductivity for Nafion 112 and Nafion-GO at

0.5 wt % over a temperature range of 25 to 100 °C. It was only at the relatively high temperatures (90-100 °C) where the doped membrane showed slightly increased conductivity. Kumar *et al.* reported a proton conductivity decrease in the range of composites and commercial materials in the order 4 wt % > 6 wt % > Nafion 212 > 2 wt % > recast Nafion; over a temperature range of 30 to 120 °C with full humidification. Lee *et al.* reported data at 80 °C with full humidification with the order 4.5 wt % > recast Nafion > 3 wt % = 0.5 wt %. This data is summarised in Figure 2-4.

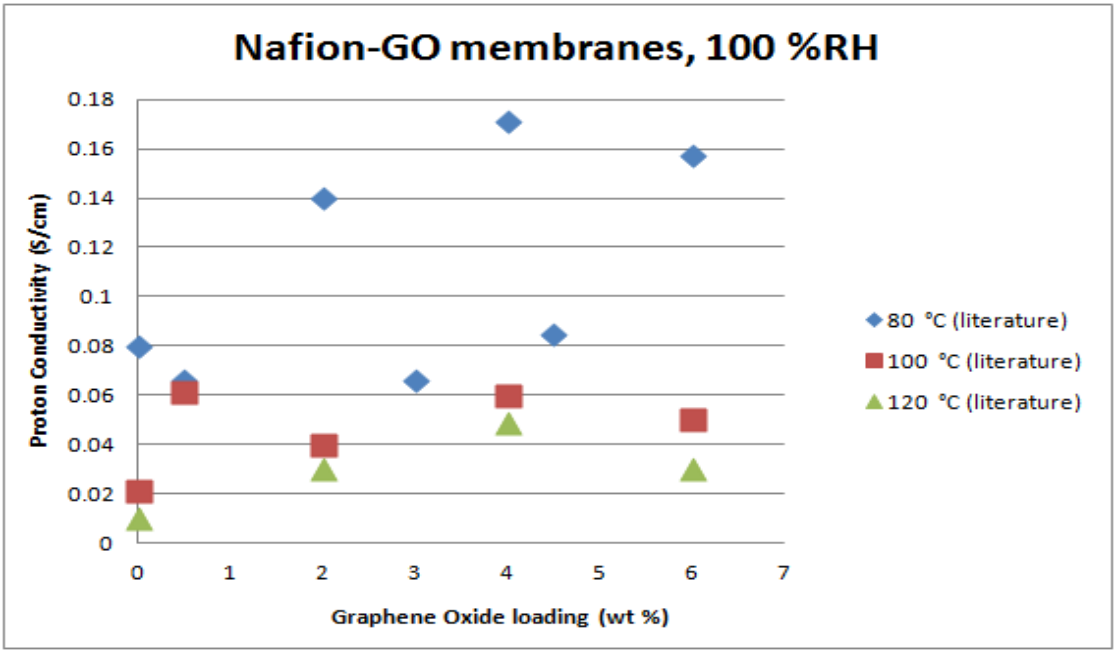

Figure 2-4 Proton conductivity for Nafion membranes doped with pristine GO as reported in recent literature [91, 92, 101, 123]. Values for recast Nafion (0 wt % GO loading) is an average as more than one value was available.

An aspect which causes considerable difficulty in the comparison of different studies is the insufficient experimental detail reported. It is very rarely stated how many samples have been tested and error bars are generally not shown. The commercial or pristine Nafion reference data is often not given, and very rarely is data for both a commercial membrane and a recast Nafion membrane included. The inclusion of both types of reference is important as

this allows an evaluation of the overall performance of the recast membranes. Furthermore, the studies which investigate functionalised GO composites do not always show data for membranes doped with pristine GO, making conclusions about the effect of functionalisation difficult. Studies choose seemingly arbitrary ranges for filler loadings, and with the differences in preparation and test conditions, this makes it unrealistic to be able to obtain a trend from different studies. Notwithstanding these difficulties, the available data was collated and summarised in order to be able to identify a trend. Where more than one membrane with the same loading was reported in different studies, an average value was calculated. Averages were also calculated for data quoted for recast Nafion in order to make sense of the trends that were reported.

While most of the Nafion-GO studies focussed on ex-situ testing with full humidification, more data was available for functionalised GO filler materials over a range of humidification conditions. A summary with the reported data is shown in Figure 2-5. It can be seen that, apart from the higher humidity ranges, the trends seems to show that proton conductivity linearly increases as the filler loading increases. This is in contrast with what is shown in Figure 2-4, where the proton conductivity seems to increase up to a maximum of around 4 – 4.5 wt % filler material, after which it drops.

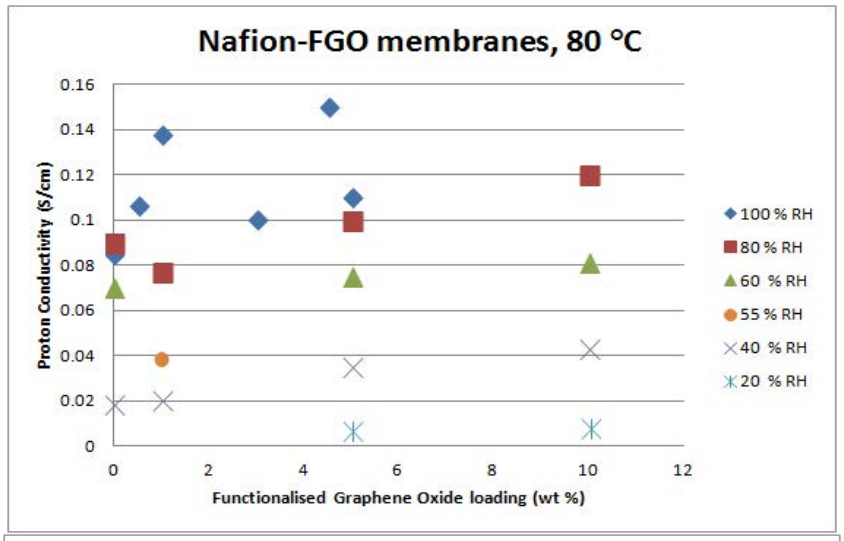

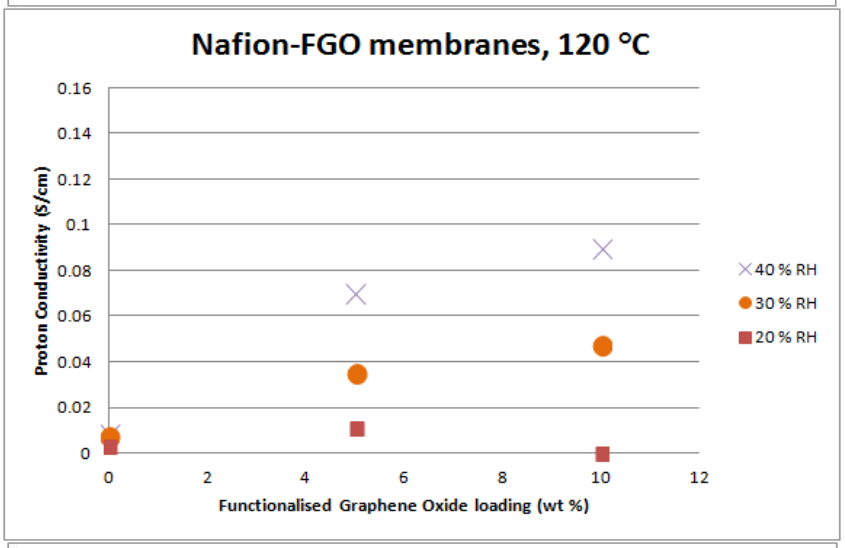

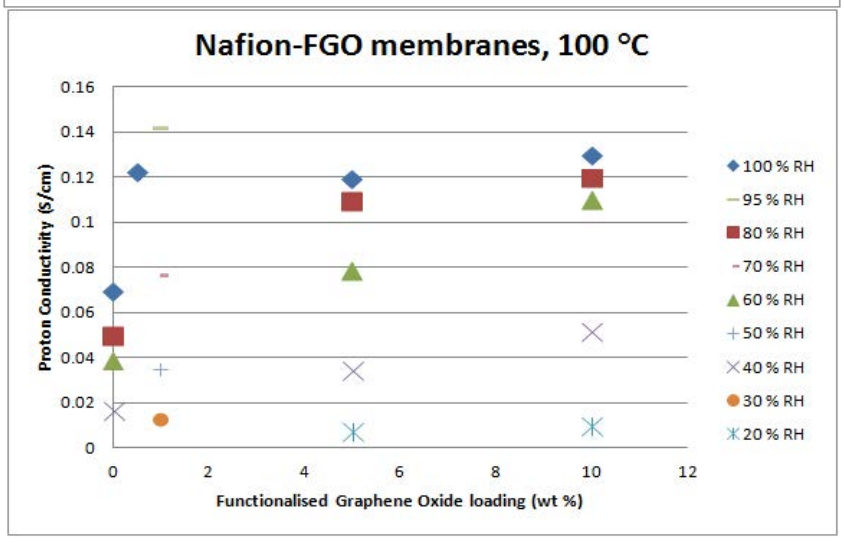

Figure 2-5 Proton conductivity for Nafion membranes doped with functionalised GO as reported in literature [92, 101, 123].

An anomaly occurs at 0.5 wt % filler loading and this is further backed up by a low temperature study by Choi *et al.* [123] on GO membranes which showed that the proton conductivity drops as the GO loading is increased from 0.5 – 2 wt %. The performance deteriorates drastically between 0.5 wt % to 2 wt %, by 55.3 % compared to recast Nafion when tested at 25 °C. In a similar study Chien *et al.* [102] reported maximum proton conductivity for composite membranes prepared with sulfonated GO between 0.5 – 1 wt % filler loading when tested at 30 °C. These studies focussed on low temperature testing because the aim of the studies was DMFC application. In this respect the reduced proton conductivity with increased filler loading could be balanced by decreased methanol crossover in the membrane.

Due to time and resource constraints ex-situ testing is often used as a means to materials selection for in-situ analysis. In this respect both Zarin *et al.* and Kumar *et al.* selected the composite material with the highest proton conductivity and used these for MEA preparation and single cell testing. The sulfonated GO composite material with 10 wt % loading was tested at 120 °C and 25 % RH. The peak power density is reported to be 0.15 W/cm^2 compared to 0.042 W/cm^2 for the recast Nafion. At 0.6 V the composite membrane and recast Nafion had a current density of 0.16 and 0.046 A/cm^2 respectively, which chimed well with the ex-situ results. For the composite with pristine GO (as reported by Kumar *et al.*), the membrane with 4 wt % filler material was selected, and outperformed both recast Nafion and Nafion 212 under two different test conditions. At 60 °C and 100 %RH, the composite material had a maximum power density of 415 mW/cm^2, compared to 300 and 272 mW/cm^2 for Nafion 212 and recast Nafion respectively. At 100 °C and 25 %RH the peak power density for the composite was 212 mW/cm^2, compared to approximately 75 mW/cm^2 and 56 mW/cm^2 for recast Nafion and Nafion 212 respectively. It should be pointed out that the

commercial Nafion 212 membrane and recast Nafion perform comparably under the first conditions, but that there is slightly better performance of the recast membrane under the hotter and dryer conditions, which is not elaborated on in the publication.

For the Lee *et al.* study on Pt-GO fillers, in-situ data is provided for 80 °C, over a range of humidity conditions, for both the unfunctionalised and the functionalised composite membranes. In all cases the 3 wt % membrane showed the best performance, which is in contrast to the proton conductivity data, where the 0.5 and 3 wt % membrane showed lower proton conductivity than the 4.5 wt % sample. At 100 %RH and 0.6 V, the current density is 0.435, 0.802, 1.27 and 0.827 A/cm^2 for recast Nafion, 0.5, 3 and 4.5 wt % Nafion-GO composite membranes respectively. This performance trend was echoed at 60 and 40 %RH. For the Kumar *et al.* study the reported current density for the 4 wt % membrane and recast Nafion at 0.6 V appears to be around 0.5 and 0.3 A/cm^2 (at 60 °C and 100 %RH) respectively. It would be inadvisable to correlate the trends due to the difference in MEA preparation techniques, but it would appear that the 4 wt % membrane resulted in lower current density compared to the reference material.

In this study, the functionalised GO membranes were prepared with platinum deposition on the GO framework in order to investigate the performance under zero humidification. In this respect, the current densities at 0.6 V were 0.27, 0.36 and 0.14 A/cm^2 for 0.5, 3 and 4.5 % Pt-GO loading respectively. This indicated that a 3 % loading was still optimal but that the performance under these conditions was very poor.

2.6.2 PBI

Proton conductivity results for the two studies detailed can be seen in Figure 2-6. Doping with both GO and with functionalised GO leads to an increase in proton conductivity, with functionalised GO showing the best performance overall. Two points to notice are that first, the pristine polymer conductivity is slightly lower for BuIPBI than for PBI, and as a result, the proton conductivity of the composite materials is also lower than that of the PBI. Secondly, the trend is slightly different for the different materials tested. PBI doped with SGO shows a marked peak at around 150 °C, PBI doped with GO increases in proton conductivity up to around 135 °C after which it plateaus. PBI conductivity continues to increase up to 175 °C. In the case of the BuIPBI, similar behaviour is seen for the pristine polymer, while the doped membranes (including the pristine GO composite) show maximum proton conductivity at 140 °C, after which performance drops. The differences are possibly due to the different types of base polymer that are used, but could also be due to the experimental techniques and the coating of the BuIPBI with an additional layer of polymer prior to testing, increasing the thickness of the membrane (70 μm vs. at least 100 μm).

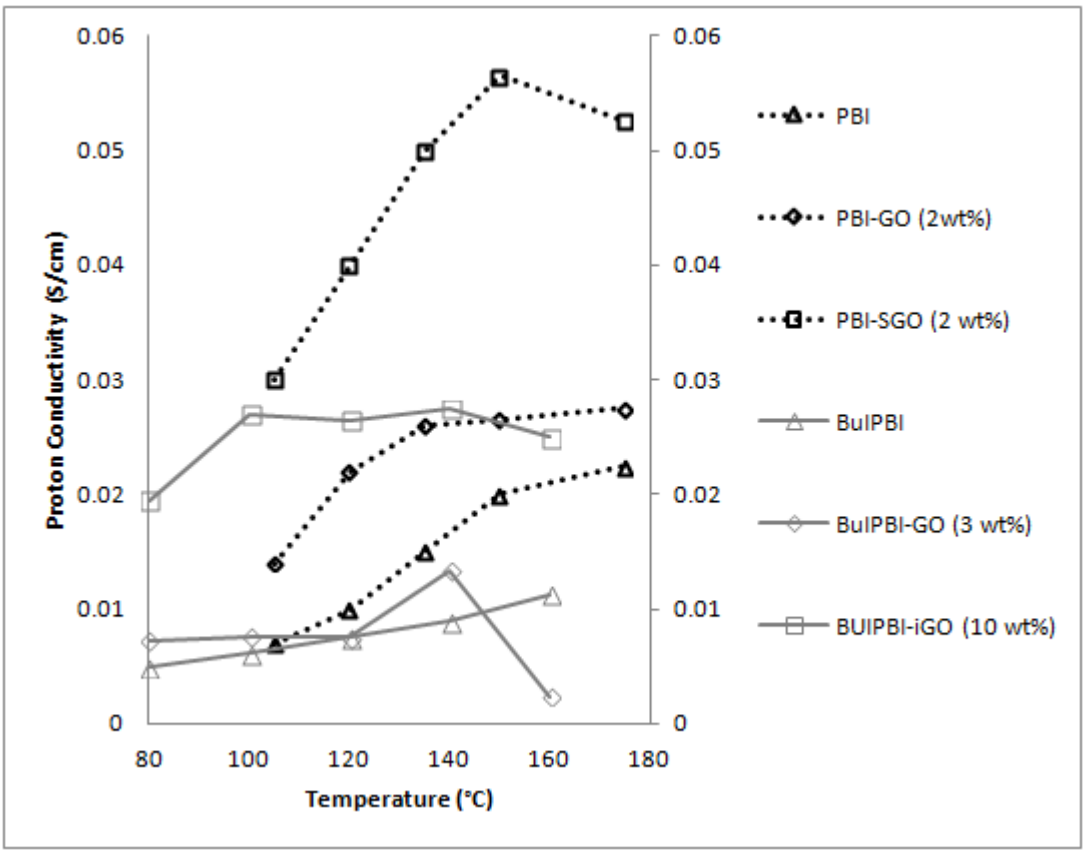

Figure 2-6 Proton conductivity for PBI membranes doped with GO, sulfonated GO (SGO) and GO functionalised with isocyanate (iGO). (Graph adapted from references [78, 82]).

In-situ testing was carried out by Xu *et al.* using both hydrogen/oxygen and hydrogen/air fuel streams, under dry conditions and at 175 °C.

The peak power density under hydrogen/air conditions were measured as 0.22, 0.38 and 0.6 W/cm^2 for PBI, PBI-GO and PBI-iGO respectively. The increased performance is ascribed to the properties of the GO. As mentioned earlier, it is thought that the acidic functional groups on GO can enhance the proton hopping mechanism. While the performance under hydrogen/air conditions was slightly lower, it was concluded that the material performed well enough to be considered for further optimisation. In particular, the

electrode catalyst layer composition and MEA preparation method were identified as the main areas for further development.

2.6.3 Conventional hydrocarbon polymers

The two studies on SPEEK-GO composites both reported increased proton conductivity on doping with pristine GO. Heo *et al.* [117] obtained a maximum proton conductivity for membranes with 5 wt %, although it should be stated that doping from 1, 3 and 5 wt % showed very similar results, 2.73, 2.80 and 2.86 mS/cm respectively. The performance dropped to 2.03 mS/cm at 10 wt %. Testing was conducted at 80 °C. Jiang *et al.* reported increased proton conductivity for the 5 wt % membrane compared to pristine SPEEK, 88.1 to 98.3 mS/cm respectively, and both materials had lower proton conductivity than Nafion 112. Testing was carried out at 65 °C, with the sample immersed in water, which could possibly explain the higher values when compared to the first study. The thickness of the membranes was not stated for the first study which could be a further reason for different values.

For the alkene sulfonic acid functionalised membranes, the highest proton conductivity was reported for the 5 wt% composite membrane. Values were 1.08, 8.41 and 5.54 mS/cm for recast Nafion, 5 wt% and 10 wt % composite respectively. The silane functionalised materials showed increased proton conductivity from 88.1 to 162.6 S/cm, with a maximum obtained for the 8 wt % membrane. The functionalised composites all showed increased proton conductivity over Nafion 112. It would have been interesting had the study included another data point to see if the performance dropped after the 8 wt % loading.

It is interesting to note that, similar to what was found by Li *et al.* for the Nafion-GO composites, the proton conductivity trend did not correctly predict the ex-situ results. Maximum proton conductivity was obtained for the 8 wt % functionalised membrane, whereas ex-situ results indicated that the membrane with 5 wt % would outperform all the other membranes in the series.

Sulfonated polyimide showed a clear increasing trend in proton conductivity as the filler loading increased [94]. At 80 °C, proton conductivity increased from 0.198 S/cm for the pristine membrane to 1.201 S/cm at 0.5 wt % loading. Increased filler loading resulted in lower conductivity from 0.664 S/cm to 0.528 S/cm for the 1 wt % and 2 wt % samples respectively. DMFC performance at 25 °C was tested and confirmed the trend from 0.5 to 1 %, but unfortunately the 2 wt % membrane was not tested.

Results for PEO were provided for one membrane only, and the filler loading was not explicitly stated. Values of 0.134 S/cm were obtained at 60 °C and 100 %RH. This is fairly high, and the report would have benefited from reference data for a pristine membrane. Degradation was also reported at temperatures above 60 °C [105]. The in-situ results are shown but at normal operating conditions (30-60 °C) no reference material data is given making it difficult to draw useful conclusions.

2.6.4 Summary of conductivity data

A summary of the conductivity data is given in Table 2-8 and Table 2-9. It can be seen that a wide range of values are obtained and that a wide range of test conditions are employed.

Table 2-8 Summary of peak performance for pristine GO membranes

Composite	**Peak proton* conductivity (S/cm)**	**Maximum power density (mW/cm^2)**	**Optimal Filler loading (wt %)**	**Ref**
Nafion (0.5%)GO	0.06 100 °C, 100 %RH	N/A	0.5	Choi[103]
Nafion (2-6%)GO	0.048 120 °C, 100 %RH	212 0.27 A/cm^2 (0.6 V) 100 C, 25 %RH	4	Kumar [91]
Nafion(0.5-4.5)GO	0.09 80 °C, 100 %RH	1.27 A/cm^2 (0.6V) 80 C, 100 %RH	4.5 (ex-situ) 3 (in-situ)	Lee [101]
PBI(2)GO	0.027 175 C, 0 %RH	380 175 C, 0 %RH	2	Xu [78]
BuIPBI(3)GO	0.0025 160 °C, 0 %RH	N/A	3	Xue [82]
SPEEK(1-10)GO	0.00286 80 °C, 100 %RH	N/A	5	Heo [117]
SPEEK(5)GO	0.0983 65 °C, immersed in DI water	N/A	5	Jiang [118]
SPI(0.5-2)GO	1.201 80 °C, 100 %RH	N/A	0.5	He [94]
PEO(0.50)GO	0.134 60 °C, 100 %RH	N/A	0.5	Cao [105]

***** At highest temperature data reported

Table 2-9 Summary of peak performance for functionalised GO membranes

Composite	**Peak proton conductivity (S/cm)***	**Maximum power density**	**Optimal Filler loading**	**Ref**
Nafion	0.009	0.15	10	Zarrin [92]
(10%)SGO	120 °C, 40 %RH	120 °C, 25 %RH		
Nafion	0.123		0.5	Choi [103]
(0.5%)SGO	100 °C, 100 %RH			
Nafion(0.5-	0.15	0.36 A/cm^2 (0.6V)	0.45 (ex-situ)	Lee [101]
4.5)PtGO	80 °C, 100 %RH	80 C, 100 %RH	3 (in-situ)	
PBI(2)GO	0.052	600	2	Xu [78]
	175 °C, 0 %RH	175 C, 0 %RH		
BUIPBI(1-	0.025	N/A	10	Xue [82]
10)iGO	160 °C, 0 %RH			
SPEEK(1-	0.008417	N/A	5	Heo [117]
10)SGO	80 °C, 100 %RH			
SPEEK(3-	0.162	N/A	5	Jiang
8)SGO	65 °C, immersed in DI water			[118]

2.7 Conclusion

The issues that become apparent from the literature are that it is very difficult to compare absolute performance values reported for similar materials due to the following factors:

- Experimental error is not given (number of test runs, error).
- The thickness of the membrane is not always stated.
- Different membrane preparation methods (drying, curing, solvents, post-treatment) are used.
- Different methods of preparing GO (resulting in varying G:O ratios and different ratios of oxygen functional groups) are used.
- GO is not always pre-processed in the same way (drying, centrifugation etc.).
- Modification in the base polymer or different types of membranes (not relevant for Nafion).
- Different ex-situ test systems and procedures (4-probe, 2-probe, shape of electrodes).
- Different methods for preparing MEAs (assembly and platinum loading).
- Different in-situ test systems, conditions and procedures (air vs. O_2, flow rates, humification).

Nafion-GO composites show promising performance in the intermediate temperature range. Nafion doped with unfunctionalised GO can increase the proton conductivity of the pristine recast membrane at elevated temperature, particularly if the filler loading is optimised. This is due to the presence of oxygen functional groups which aid water uptake and retention. Optimisation of the filler loading is required to prevent determent to the exceptional mechanical qualities of Nafion. Furthermore, optimisation prevents blockage of proton

conductivity channels. Nafion-GO membranes can further be enhanced by functionalisation of GO through sulfonation or the addition of species including isocyanates, sulfonic acid zwitterions and additional aliphatic groups. It is generally reported that the increase of sulfonic acid in the composite membrane increases proton conductivity as this increases the ion exchange coefficient. Data reported in the literature cannot be used to obtain the full trends of this type of composite material due to the varying conditions. In this respect, a systematic study on graphene oxide doped Nafion would provide a valuable addition to the literature of composite membranes.

CHAPTER 3 METHODOLOGY, MATERIALS, EXPERIMENTAL TECHNIQUES AND EQUIPMENT

This chapter describes the research methodology and experimental techniques that were used for this project. The main aim was a systematic evaluation of composite membranes for application at 120 °C and 50 %RH. The evaluation was carried out by the optimisation of preparation methods, characterisation of the materials, and testing, both ex-situ and in-situ.

3.1 Methodology

The research methodology is shown in Figure 3-1. After the selection of a suitable polymer and filler material, proton exchange membranes are usually cast from a solution. Many different materials and methods have been described in the literature, and the first step for this study was the optimisation of the casting process. Solvents were selected based on literature studies for similar types of membranes, and the casting process was optimised by using a range of heating regimes until uniform membranes were obtained. This was carried out in the framework of two scoping experiments which produced the first sets of composite membranes. For this purpose graphene oxide was obtained from a colleague.

This was followed by the evaluation and synthesis of graphene oxide. The filler was synthesised in-house and characterised. Based on the results, further experiments were carried out in an attempt to functionalise the oxygen functional groups present in the material. The preparation of the composite membranes was further optimised to ensure even particle distribution.

Initial proton conductivity testing was carried out by a third party since the facilities were not available at the University of Birmingham, but in the third year of the project, a high temperature test stand was purchased. The equipment (Scribner 850e High Temperature Test Stand) was installed, optimised, and calibrated in-house. Extensive insulation and additional heating systems were added to prevent condensation of water in the humidified gas. Calibration of the dew point settings was carried out with the use of an in-line dew point probe and humidity chamber (Vaisala DMT340).

Following the successful optimisation of the high temperature test stand, the selected composite membranes were tested for proton conductivity and single cell performance. A range of membranes with different filler loadings were tested over a range of 80-120 °C and 25-95 %RH. Membrane electrode assemblies (MEAs) were prepared using commercial gas diffusion electrodes (GDEs) in order to eliminate variations in the electrode compositions.

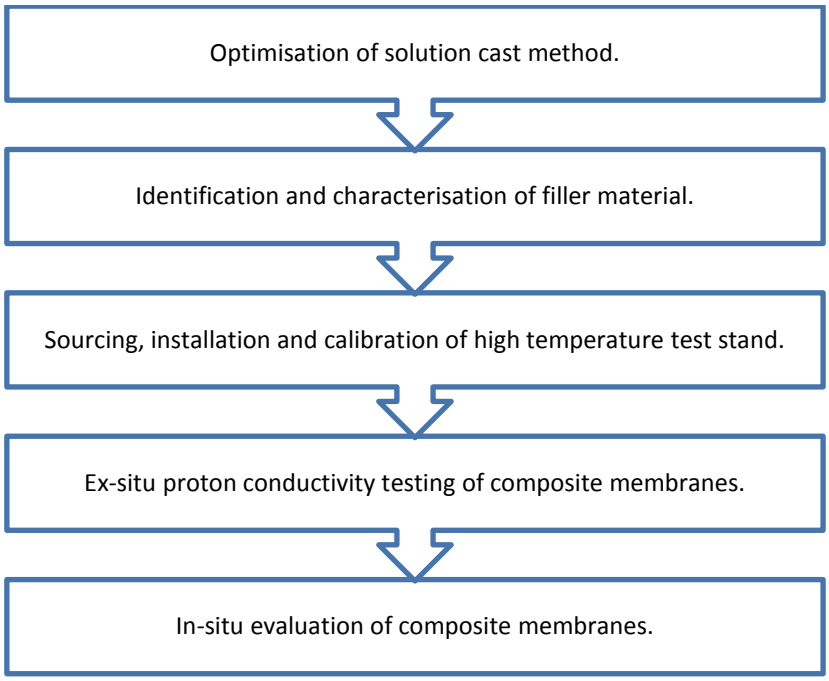

Figure 3-1 Research methodology

3.2 Materials

All materials were purchased from Sigma Aldrich and used as received, unless otherwise stated. The experimental details are given in Section 3.3.

3.2.1 Graphene Oxide and Functionalised GO

For the synthesis of GO, graphite, sodium nitrate ($NaNO_3$, >99 %), sulfuric acid (H_2SO_4, 99 %), potassium permanganate, and hydrogen peroxide (H_2O_2, 30 wt %) were used as received.

Three different functionalisation reactions were carried out. For the initial scoping experiments, GO was functionalised by the addition of sulfanilic acid. For this method, GO was obtained from a colleague and used as received. N-hydroxysuccinimide (NHS), 1-ethyl-3-(3-dimethylaminopropyl) carbodiimide (EDC) and sulfanilic acid (SA) were used in the reaction. For the sulfonation of the carboxylic acid functional groups, concentrated nitric acid (90 %) and sulfuric acid (99 %) were used. The last method comprised the addition of an azo group at the aromatic rings, and for this reaction, sodium carbonate monohydrate ($Na_2CO_3.H_2O$), sulfanilic acid, hydrochloric acid, sodium nitrate ($NaNO_3$), and sodium hydroxide (NaOH) were used.

3.2.2 Composite Membranes

Composite and recast membranes were prepared using Nafion 10 wt% commercial solution obtained from Ion Power Inc. (Newcastle, USA). For control samples, Nafion 212

commercial membrane was purchased from Fuel Cell Store and used as received. Properties of the solution and the membranes are shown in Table 3-1. Sulfuric acid (H_2SO_4, 0.5M) and hydrogen peroxide (H_2O_2, 30% solution) were used in the washing process. The ion exchange coefficient test was carried out using sodium chloride, sodium hydroxide and phenolphthalein (20% in ethanol). In initial casting experiments, a range of solvents were used and these included ethanol, IPA, *N,N*-dimethylformamide (DMF) and dimethylsulfoxide (DMSO).

Table 3-1 Properties of Nafion 10 wt % solution and Nafion 212 **[125, 126]**.

	Nafion 10 wt % solution	Nafion 212 membrane
Base	Water (VOC*, <1 %)	N/A
Equivalent Weight	1000	1100
Thickness / μm	N/A	50.8
Available acid capacity / meq/g	> 1.00	0.92 (minimum)
Total acid capacity / meq/g	1.03 to 1.12	0.95 to 1.01
Water uptake / %		50 ± 5.0
Linear expansion (50 % RH to soaked) / %		10 (23 °C)
		15 (100 °C)

* VOC = volatile organic components

3.2.3 Membrane Electrode Assembly

Gas diffusion electrode material (0.4 mg_{Pt}/g) was purchased from Johnson Matthey and isopropyl alcohol (IPA, 99.7 %) from Sigma Aldrich. Nafion 10 wt % solution, as described above, was used in the binder solution.

3.3 Experimental Procedure

This section details the experimental procedure followed for preparing the filler materials, composite membranes, and MEAs. More detail on the reactions will be given in the relevant chapters.

3.3.1 Graphene Oxide synthesis

GO was prepared by a modified Hummers process [100]. Graphite (2.5 g) was mixed with $NaNO_3$ (1.9 g) in a round bottomed flask (RBF) with a magnetic stirrer (175 rpm throughout) over an ice bath. Concentrated H_2SO_4 (84.5 mL) was added, and the mixture was stirred until homogenised. $KMnO_4$ (11.28 g dissolved in 200 mL de-ionised (DI) water) was added drop wise to the mixture, over 5 hours under constant stirring. The solution was stirred over ice for a further 2 hours, after which time the ice bath was removed, and the reaction mixture was stirred for a further 6 days. The reaction mixture was allowed to settle for 24 hours, leaving a thick slurry and a brown/red supernatant. The supernatant was removed by careful decanting and pipetting, and was then filtered. The residue was recombined with the slurry and stirred in H_2SO_4 (5 wt%, 300 mL) for two hours, followed by the addition of H_2O_2 (30 wt%, 20 mL) and a further two hour stirring period. After the first cleaning process, the reaction mixture

had a grey/green colour. The reaction mixture was allowed to settle for 24 hours, leaving a thick slurry and a grey/green supernatant. The supernatant was removed and filtered, the residue was recombined with the slurry and stirred in H_2SO_4 (3 wt%, 300 mL) for two hours, followed by the addition of H_2O_2 (0.5 wt%, 20 mL) and a further two hour stirring period. This procedure was repeated 12 times, until the solution became clear. Finally, the reaction mixture was washed in de-ionised water until the solution was neutral.

3.3.2 Graphene Oxide functionalisation

Sulfonation of the carboxylic acid groups on GO was carried out using a method reported by Chen *et al.* [109]. 0.855 g N-hydroxysuccinimide (NHS) and 1.425 g 1-ethyl-3-(3-dimethylaminopropyl) carbodiimide (EDC) were added to a 25 mL solution of GO (10mg GO per mL of deionised water) at 0 °C and stirred for 2 hours. 0.25 g sulfanilic acid (SA) was added to the mixture and stirred overnight. The sulfonated graphene oxide was filtered and washed in DI water several times.

The second sulfonation method used is a widely reported microwave process [103, 127]. GO was dried (40 °C), ground in a pestle and mortar, dispersed in DI water (~1 mg/mL), ultra-sonicated (2 hrs), and centrifuged (4000 rpm, 30 minutes x 3), each time removing the top layer for use. GO was dried at 40 °C, until no further change in weight was observed, before dispersing it in mixture of nitric acid (20 mL) and sulfuric acid (20 mL). The reaction was carried out in a microwave (CEM, MARS 5W) using 50 % of 800 W for 5 x 1 minutes. After the microwave treatment, the reaction solution was diluted with ~300 mL DI water prior to filtration and washing, using hydrophobic PTFE filters (Millipore, 2 μm), until neutral.

The azo coupling [111] was carried out by preparing a 10 mL 0.625 wt% Na_2CO_3 solution using $Na_2CO_3.H_2O$ (75mg). Sulfanilic acid (46 mg) was dissolved into this solution and stirred, after which $NaNO_2$ (18 mg) in water (9.982 g) was added whilst continually stirring. This solution was slowly added to a hydrochloric acid (HCl) (1.84 mL, 1 M) solution, over an ice bath, to obtain the aryl diazonium salt solution. GO (0.075 g) was dispersed in DI water (75 g) and sonicated. A solution of NaOH (1.53 mL, 1 M) was prepared and added to the GO solution. The aryl diazonium salt solution was added, and the mixture was stirred over the ice bath for 2 hours. The product was centrifuged, washed, and dried at 40 °C overnight.

3.3.3 Membrane Casting

The membranes, approximately 50 μm thick, were prepared using the following steps (also shown in Figure 3-2). The required amount of filler was weighed out in a glass sample vial, DI water was added (250 μl) and bath sonicated for 30 minutes. Nafion (6.7 g) solution was added to the vial and the mixture was sonicated for a further 30 minutes. Following this, a petri dish of 9 cm diameter was cleaned with soap and acetone, dried in an oven at 40 °C and wiped with lint free cloth. The mixture was spread over the petri dish to obtain a uniform covering. The heat was increased from 40 °C to 100 °C while the dish was monitored to ensure the covering remained uniform. Once all the solvent had evaporated, the membrane was cured at 100 °C for 2 hours and 140 °C for 1 hour. At the end of the heat treatment, the membrane was covered by DI water and removed from the dish. Purification was carried out at 75 °C in 300 mL each of 0.3 wt% H_2O_2 (1 hour), DI water (1 hour), 0.5 M H_2SO_4 (2 hours), and DI water (1 hour). The membrane was pressed between filter papers for 48 hours.

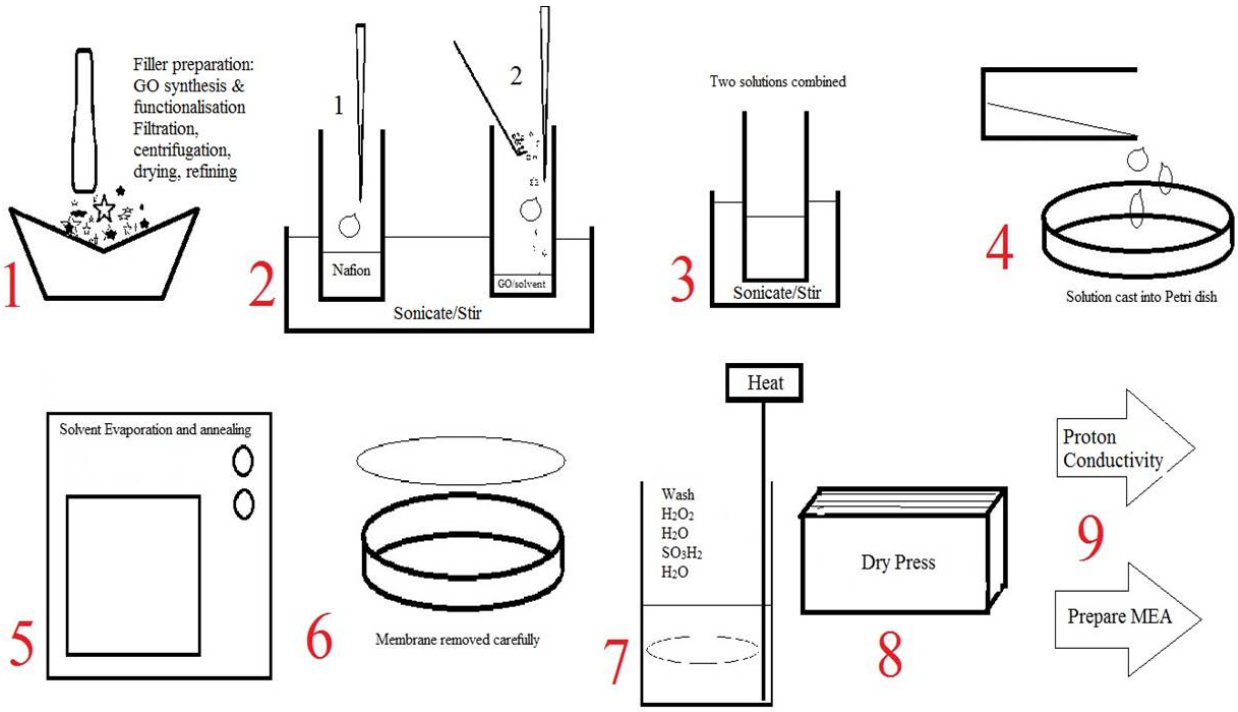

Figure 3-2 Preparation process for solution cast membranes

After several membrane samples were analysed and tested, the first step of the preparation process was amended in order to improve the dispersion of the GO in the membrane. This is discussed in more detail in Chapter 7.

3.4 Equipment

3.4.1 Fourier transform infrared (FT-IR) spectroscopy

FT-IR spectroscopy was used to identify the functional groups in the filler materials and the composite membranes. The samples were analysed by exposing them to a range of electromagnetic radiation in the infrared range ($1 > \lambda > 50$ μm) and recording the absorbance at different wavelengths as a spectrum. Chemical bonds absorb specific wavelengths of infrared radiation when the vibration of the chemical bond couples with the oscillating electric field of the infrared radiation. This results in an oscillating dipole moment also

referred to as bond deformation (stretching or bending) which has a characteristic wavenumber for each chemical bond. The frequency of the absorbed radiation can be defined by the following equation [128]:

$$v = \Delta E/h \quad (1)$$

Where v = frequency of the radiation

ΔE = energy difference between the upper and lower vibrational energy levels for the particular bond deformation

h = Planck's constant

The intensity of the transmitted or reflected light was measured as a function of its wavelength, by an interferometer. The interferogram is transformed into a single beam spectrum by a computational Fourier Transform which presents the data as a plot of wavelength against intensity. The most common absorptions are observed in the range between 4000 - 650 cm^{-1}.

A Perkin Elmer Spectrum Express was used to record the infrared spectra, and the sample was placed directly on the crystal before subjecting it to a beam of infra-red radiation. The functional groups of interest in Nafion are C-F, C-C, C-O-C, C-S, S-O and for GO are C-C, C-O, C-O-C and C=O.

3.4.2 Thermo gravimetric analysis (TGA)

TGA was used to monitor the thermal behaviour of recast and composite membranes. Using this method, a sample was heated from room temperature to a set maximum, and the loss of weight as a function of temperature was recorded. It can then be established which chemical groups in the material degrade at particular temperatures [129]. This method was also used in an attempt to confirm the filler weight % of the composite membranes. TGA was performed using a NETZSCH TG 209 system. Samples were weighed out to approximately 6 mg, and an alumina sample holder with a lid was used during the test. Nitrogen (30 mL/min) and air (50 mL/min) were applied as inert and exhaust gasses respectively. The samples were heated from 20-700 ˚C at 10 °C/min.

3.4.3 X-Ray Photo-electron Spectroscopy (XPS)

XPS was used to identify which chemical bonds were present in GO and the membranes by identifying the characteristic binding energies of carbon, oxygen and sulfur. Core level electrons are quantised and binding energies are therefore characteristic for elements. This allows for the elucidation of the chemical composition of the material [130, 131]. Analysis was carried out on the surface of the samples, which were prepared by depositing a thin film of particles onto a suitable substrate. The substrate was inserted into the equipment, and subjected to an Al Kα (1486.6eV) beam as a source of photons. This resulted in the ejection of electrons from the surface of the sample, and the intensity of the energies was recorded against the number of counts for each binding energy. At first a wide energy spectrum scan (WESS) or a survey scan was carried out to identify which elements were present followed

by high resolution energy scans for the elements of interest. The results were analysed to obtain a quantification of specific bonds present in the sample.

The analysis of GO was carried out to obtain information on the degree of oxidation of graphite and the ratio of the different bonds that were present. For this material it was particularly the carbon bonds formed with oxygen, sulfur, and nitrogen that were of interest in order to quantify the functional groups.

XPS was undertaken at the LENNF EPSRC Facility at Leeds University, Science City facilities at Warwick University, and the National EPSRC XPS Users' Service (NEXUS) in Newcastle, all operating with a monochromated Al Kα source. XPS samples were prepared by drop drying a GO/DI water solution (1mg/1mL) on an arsenic doped conducting silicon substrate until a uniform film was formed.

3.4.4 Transmission Electron Microscopy

Electron microscopes operate by passing an electron beam through an electromagnetic lens which can be charged to different degrees in order to accelerate the speed of the electrons [132]. In a transmission electron microscope, a high voltage electron beam is emitted by a cathode, and is partially transmitted through a very thin sample. The transmitted beam contains structural information about the sample, which is magnified by a series of electromagnetic lenses, and is recorded by a sensor. The images produced are black and white. The density of different types of elements generates the contrast, which allows for the analysis of particles on the nanometre scale (due to magnification by the lenses).

GO was dispersed in DI water (1mg/1mL) and dried on a copper grid. GO samples were analysed at the University of Leeds on a Philips CM200 FEGTEM field emission, under the EPSRC-funded LENNF (Leeds EPSRC Nanoscience and Nanotechnology Research Equipment Facility) program.

3.4.5 Scanning electron microscopy (SEM)

SEM was used to record surface morphology information of the sample by recording secondary electrons emitted from the material due to inelastic scattering [132]. Using this method, the primary electron beam is scanned across the sample, exciting the electrons on the surface, which are then detected to produce 3D images. Whilst TEM provides valuable information on the nanometre scale of particles, SEM can successfully be used to investigate particle distribution throughout the thickness of the membranes at both nanometre and micrometre scale. In order to investigate the particle distribution through the membrane, composite membranes were freeze dried in nitrogen and then snapped in order to expose the cross section for analysis. SEM analysis of samples prepared during this study was carried out at LENNF, as described above, using a Hitachi SU8230 SEM.

3.4.6 Water Uptake and IEC

Water uptake and ion exchange coefficient data are valuable for membrane development, as it gives an indication of how much water the material can absorb, and thus allows for the prediction of a proton conductivity trend. Water uptake was calculated using a gravimetric method and Formula 2 [79].

$$WU = \left[\frac{W_{wet} - W_{dry}}{W_{dry}}\right] \times 100 \quad \text{.....(2)}$$

Where W_{wet} = the wet weight of the membrane after soaking in DI water

W_{dry} = the dry weight of the membrane after drying under vacuum

The ion exchange coefficient is a calculation of the available acid exchange sites in the polymer and was calculated using Formula 3 [91].

$$IEC = \frac{V_{NaOH}(ml) \times M_{NaOH}(mol.L^{-1})}{W_d(g)} \quad \text{.....(3)}$$

Where V_{NaOH} = volume of sodium hydroxide added

M_{NaOH} = molarity of the NaOH solution

W_d = dry weight of the membrane as determined in the WU test

The WU was measured by weighing out around 100 mg of membrane, and immersing in around 50 mL of DI water for 24 hours. The membrane was removed from the water, surface water was absorbed using dry filter paper, and the sample was weighed. The membrane was replaced in the water for half an hour and this process was repeated three times. An average value for weight was obtained and the error was calculated. The membrane was then placed in the vacuum oven at 80 °C and 0.07 MPa for three hours. It was weighed three times at half hour intervals at the end of the experimental time.

The IEC was calculated by placing the membrane sample from the WU test in a 30 mL NaCl solution (1M) for at least two days. The membrane was removed, and 2-3 drops of phenolphthalein (20% in ethanol) indicator were added. The solution was stirred and titrated with 0.01 M NaOH until the end point was reached.

3.4.7 Conductivity Testing and Single Cell testing.

3.4.7.1 Scriber 850e Test station, BekkTech BT 112 Conductivity Clamp and Vaisala Dew Point Probe.

Membranes and MEAs were evaluated using an 850e High Temperature Scribner Associates Incorporated Test Stand (Figure 3-3). The test stand had an integrated potentiostat (885 Fuel Cell Potentiostat) and was equipped with anode and cathode stainless steel humidifiers, mass flow controllers and a pressurised continuous water supply. It had a maximum load current of 100 A, and maximum load power of 100 W. The potentiostat allowed for 2, 3, or 4 terminal connections to the test cell and had a current range of 2A, 200 mA, and 20 mA. The reference electrode had an input Voltage range between -3 to +3 V.

The cell hardware was comprised of two graphite flow field plates with single serpentine flow channels and gold plated copper current collectors. Two 100 W cartridge heaters heated the cell through channels in the anodised aluminium end plates, which also contained the reactant input/output ports and the thermocouple port.

Figure 3-3 Scribner test stand unit [133].

All components were controlled, and data was recorded, with FuelCell™ software. The temperature and dew point were regulated over a range of 80-120 °C and 25-95 %RH respectively. The system pressure was regulated by a high temperature back pressure unit connected to the outlet of the cell.

The dew point was measured and equilibrated by a Vaisala DMT340 dew point probe. The system recorded dew point data at 3 second intervals, allowing for accurate calculation of the relative humidity in the system at a particular temperature. The DRYCAP® sensor fitted to the system is not affected by water condensation or particle contamination, and allows for accurate dew point data over a range of humidity and temperature conditions. The dew point probe was supplied by Scribner with a custom built heated humidity chamber. A temperature controller was built in-house to control the temperature, details of which are provided in Chapter 7.

Proton conductivity was measured by assembling a BT-112 conductivity clamp (Figure 3-4 (left)) into the test hardware and using the potentiostat described above. The clamp allows for true 4-electrode analysis, and hence the in-plane resistance of the membrane due to charge transport can be measured accurately. Interfacial and charge transfer resistances do not influence the measurement because it is made at the membrane-electrode interface [133]. During resistance testing, the thermocouple was inserted directly into the conductivity clamp in order to accurately measure temperature at the site where the membrane was fitted. Membrane samples were cut to 1.1 cm x 3 cm strips and soaked in DI water overnight prior to testing.

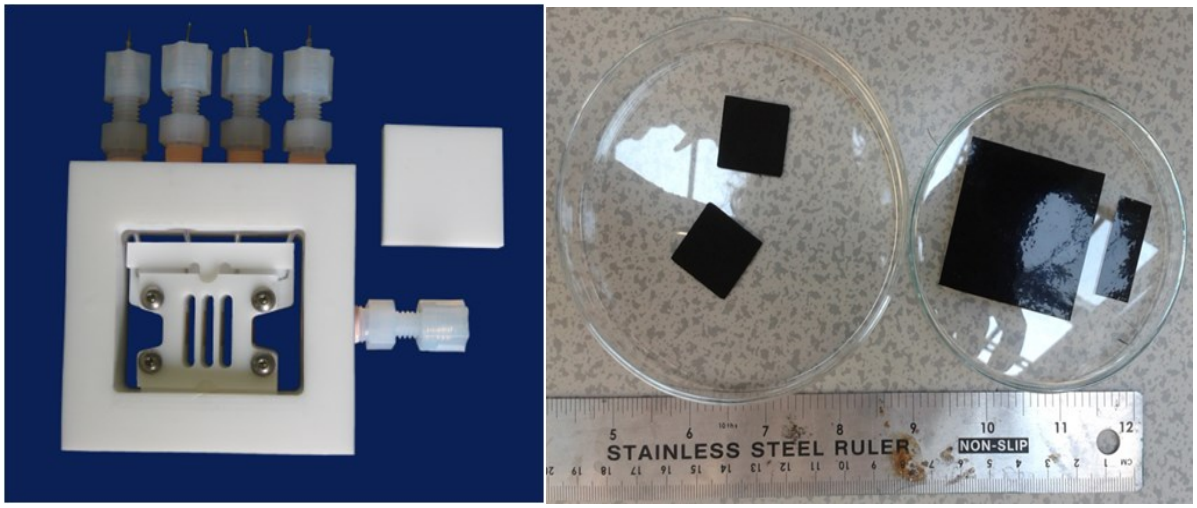

Figure 3-4 BekkTech BT 112 conductivity clamp [133] (left) and materials for membrane conductivity test and MEA preparation (right).

MEAs, with an active area of 5 cm^2, were prepared for all cell tests. A binder solution was prepared by mixing Nafion solution with isopropyl alcohol (IPA) in a ratio of 1:2, which was hand painted onto the active side of the GDE, after which the GDE was allowed to dry at 40 °C in an oven. The membranes were cut to 4.5 cm^2 and the GDEs were applied to either side. The single cell was formed by hot pressing for 3 minutes at 120 °C. Figure 3-4 (right)

shows the components for MEA preparation and membrane samples for proton conductivity testing.

3.4.7.2 Membrane resistance and Relative Humidity

Proton conductivity was calculated from the measurement of the effect of the change in voltage on the current. As the voltage was swept between 0.1V to – 0.1 V, the current change in the milliampere range was recorded on a graph of voltage vs. current. The slope of this graph gave the value for the resistance of the sample at a particular temperature and relative humidity. The measured values for the distance between the electrodes and the physical dimensions of the membrane were substituted into Equation 4 in order to calculate the in-plane proton conductivity of the membrane.

$$\sigma = \frac{1}{R} \times \frac{L}{A} \quad \text{.....(4)}$$

Where σ = proton conductivity in S/cm

R = resistance obtained from V vs I plot in Ω

L = distance between voltage probes (0.375 cm)

A = area of cross section of membranes (~ 1 cm x 0.005 cm)

In order to accurately state the test conditions (temperature and relative humidity), it was necessary to measure the dew point in the system at a specific temperature. The dew point is related to the relative humidity in the following way [134]:

$$RH = 100\% \times \left[\frac{P_{ws}(T_d)}{P_{ws}(T_{ambient})}\right] \quad \text{.....(5)}$$

Where RH = relative humidity (%)

P_{ws} = Saturation vapour pressure (hPa)

T_d = Dew point temperature (°C)

$T_{ambient}$ = System temperature (°C)

The values for T_d were obtained from data logged by the dew point probe, and $T_{ambient}$ from the Scribner test stand. By inputting these values, and that of the pressure applied to the system, into a relative humidity calculator, values for the relative humidity could be obtained for each test condition.

3.4.7.3 Cell polarisation and Impedance Spectroscopy

Performance of the single cell was evaluated by measuring the cell polarisation, and by using impedance spectroscopy at different current ranges.

The cell polarisation was determined by applying a load to the cell and obtaining a plot of voltage vs. current density, as shown in Chapter 1, Figure 1-4. In order to obtain information about the membrane resistance in-situ, impedance spectroscopy was used at low, medium, and high current ranges.

Impedance spectroscopy entails applying a small sinusoidal (AC) voltage or current over a wide range of frequency (from mHz-kHz or greater), and measuring the effect that this has on the AC amplitude and phase response of the electrochemical cell [135]. Figure 3-5 (left) illustrates how the applied perturbation affects the resultant AC waveform; they are out of

phase [136]. When a pure resistor is present in the system, the two waveforms would be the same. Since the amplitude and frequency of the perturbing voltage or current is known, the ratio and phase-relation of the response allows for the calculation of the complex impedance. The complex impedance is represented as the sum of the real and imaginary components.

In the measurement of ex-situ membrane resistance, the membrane (or resistor) is the only impeding factor to the flow of charged particles. Clearly, in in-situ testing this is not the case, and the influence of the overall cell reactions and kinetics must be factored in. Whereas the membrane conductivity cell set-up allows for the calculation of membrane resistance based purely on Ohm's law E = IR, in the single cell MEA set-up the contribution to resistance is more complex and the equation E = IZ is more appropriate [136], this can be rewritten as [137]:

$$Z(j\omega) = \frac{V(j\omega)}{I(j\omega)} \quad \text{.....(6)}$$

or

$$Z(j\omega) = Z'(\omega) + jZ''(\omega)$$

Where Z' = real or in-phase resistance

Z'' = imaginary or out-of-phase resistance

$j = \sqrt{-1}$

$\omega = 2\pi f$

f = frequency (Hz/s)

Z is the AC equivalent of resistance and includes the contribution of resistors, capacitors, and inductors present in the cell. Z' is the real resistance due to the resistor in the system, and Z''

is the imaginary or out-of-phase resistance due to other factors. Impedance data recorded by the test stand was plotted on a Nyquist Plot (Figure 3-5 (right)) using Zview™ software. The data is plotted as real vs. imaginary impedance, and the arc of the semicircle shows the values recorded at high frequency to low frequency, from left to right.

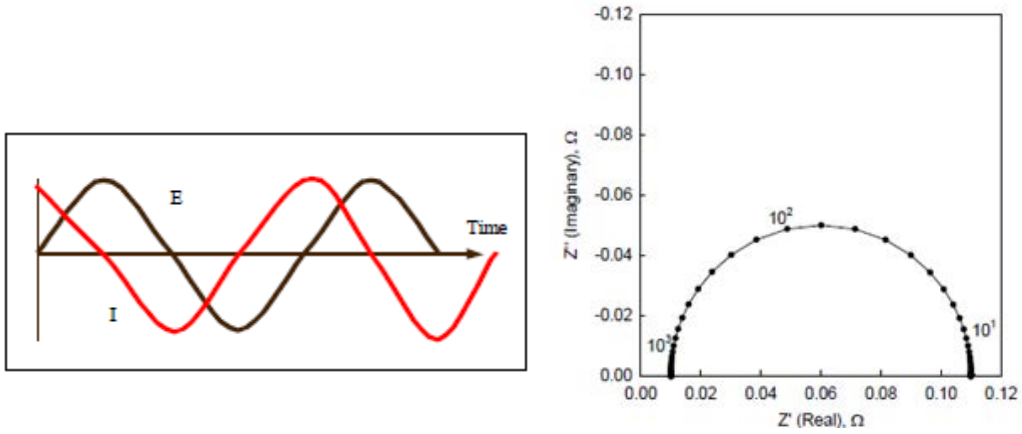

Figure 3-5 An applied voltage perturbation and the effect on the current (left) [136] and an example Nyquist Plot (right) [135].

The in-situ proton conductivity of the membrane was calculated using Equation 4. The intercept on the real axis, in the high frequency range, was taken to be the membrane resistance [138]. As this measurement is a through-plane measurement, the value for the area (A) was converted to reflect the surface of the active area of the electrodes (5 cm^2) and the thickness of the membrane (around 0.005 cm). In this study the ex-situ and in-situ membrane resistance was calculated under the same experimental conditions.

The next two chapters respectively describe the initial scoping experiments on composite membrane preparation, and the characterisation and evaluation of the filler material considered for this study.

CHAPTER 4 OPTIMISATION OF SOLUTION CAST PROTON EXCHANGE MEMBRANES

4.1 Introduction

Membranes for material development in the research process are usually prepared by solution casting. This is an efficient method for material development because small batches are prepared at one time and it is a fast way to prepare many different iterations of a similar type of material. This is particularly useful for composite membrane studies because the filler loading is varied in order to identify the optimal loading in the membrane, and often only small quantities of filler material are available at the initial stages of research.

Solution casting is preferential for a second reason: it has been shown that proton conductivity is similar in both the in-plane and through-plane direction in the membrane. In contrast, the in-plane conductivity for extruded membranes (such as Nafion 112) is anisotropic and can be much higher parallel to the extrusion process [139] compared to the through-plane direction. Solution cast membranes are therefore ideal for studies where ex-situ and in-situ properties are investigated in tandem.

Many factors are important in the casting process. In particular, the choice of solvent and the thermal treatment of the membrane can affect the mechanical strength and its performance. To this end, the starting point of the experimental work was the optimisation of the membrane preparation method and covers the first objective for this research project. This was carried out in two short projects.

The first was a collaborative project with the University of Yamanashi (UOY) using a sulfonated hydrocarbon polymer developed by the partner University, and supplied to the University of Birmingham (UOB) in order to prepare composite membranes. The sulfonated hydrocarbon polymer was supplied as a cast film and composite membranes were prepared at UOB. The cast membranes were pre-treated and tested for proton conductivity at UOY during a two-week residential period in Japan. It was only possible to test at 80 °C, but over a range of humidity and it was judged as adequate for the first scoping experiment.

The second was a more intensive project carried out at UOB. Various Nafion recast membranes and Nafion-GO membranes were prepared using different solvents (DI water, ethanol and DMSO). The casting process was optimised and MEAs were prepared from two sets.

4.2 Scoping project: SPESK-GO membranes

The scoping project was initiated following promising results published by Zarrin *et al.* [92] for recast Nafion membranes doped with sulfonated GO (SGO). As described in Chapter 2, doping of Nafion with 5 wt % and 10 wt % SGO resulted in increased proton conductivity over a temperature range of 80-120 °C and a range of humidity conditions. Promising results had also been published by Bae *et al.* [58], from the University of Yamanshi, for a series of novel sulfonated poly(arylene ether sulfone ketone) (SPESK) multi-block polymers (Figure 4-1) which were tested in similar test conditions. Both studies showed increased proton conductivity for the novel membranes when compared to Nafion (Figure 4-2). The performance at elevated temperature and low humidity was particularly encouraging.

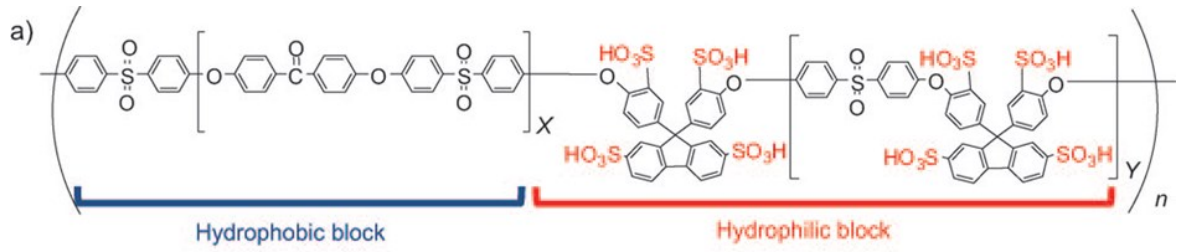

Figure 4-1 Sulfonated poly(arylene ether sulfone ketone) multi-block polymer [58]. Reprinted from Angewante Chemie-International Edition, Copyright 2014, with permission from John Wiley and Sons.

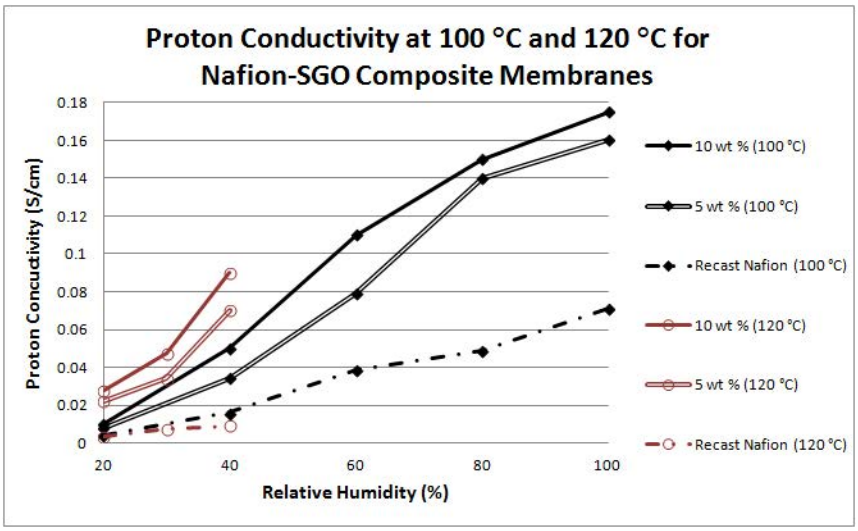

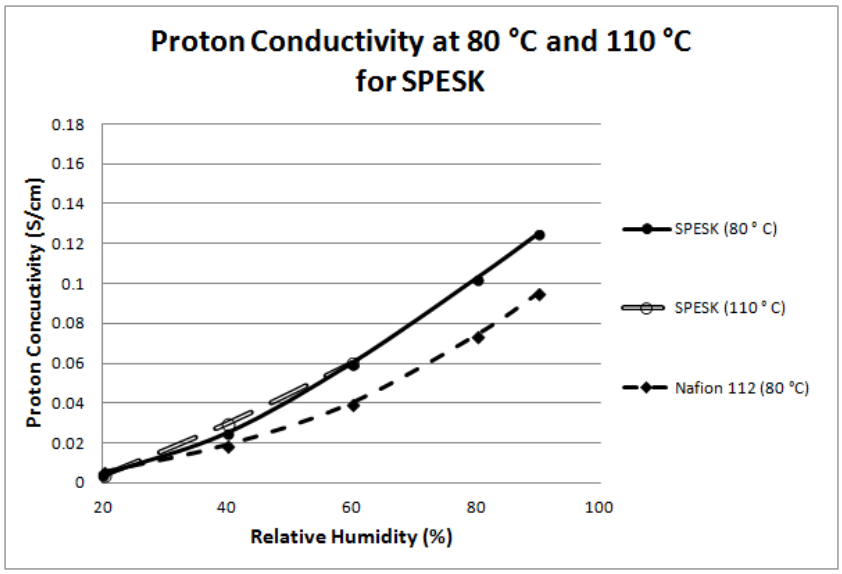

Figure 4-2 Proton conductivity reported for Nafion-SGO membranes (top) [92] and for SPESK (bottom) [58]. Graphs are adapted from literature.

Therefore, under a materials transfer agreement (MTA) between UOB and UOY a set of Nafion and SPESK composite materials was prepared to evaluate the effect of doping with GO on the proton conductivity. Following discussions with UOY, it was agreed to prepare membranes with a filler loading of 0.5 wt %, as all involved believed that higher filler loadings in the membrane could form a barrier against proton conductivity. This section will describe the preparation of sulfonated GO, casting of the composite membranes and the proton conductivity measured at UOY.

4.2.1 Sulfonated GO

GO was sulfonated with sulfanilic acid as described in Chapter 3 (Section 3.3.2) and illustrated in Figure 4-3 below. Following the reported procedure by Chen *et al.* [109], an aryl sulfonic acid group was added to GO by amide formation with the carboxylic acid groups on GO. This route was selected because, in the results reported by Chen *et al.*, it was the sulfonated material with the highest ion exchange coefficient. The range of materials that was reported on included a further aryl sulfonic acid functionalisation via a diazonium reaction, and the addition of two alkyl sulfonic acid groups using the same two methods employed for the aryl addition. Figure 4-4 shows the polymer-filler dispersions.

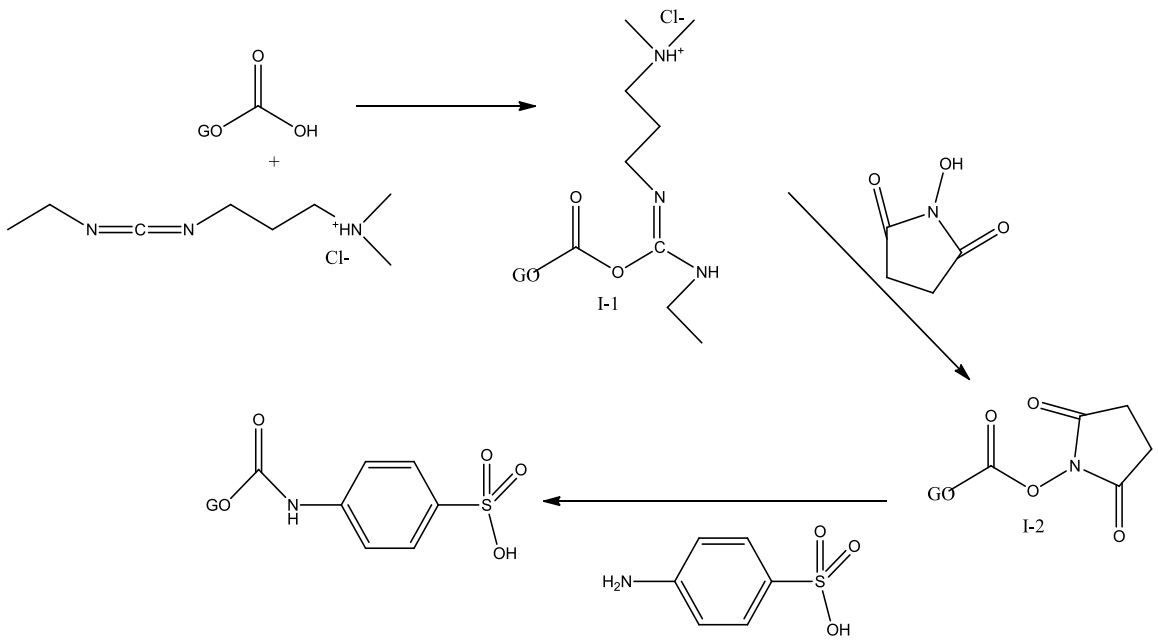

Figure 4-3 Sulfanilic acid coupling reaction via 1-ethyl-3-(3-dimethylamiopropyl) carbodiimide (EDC) and N-hydroxysuccinimide (NHS).

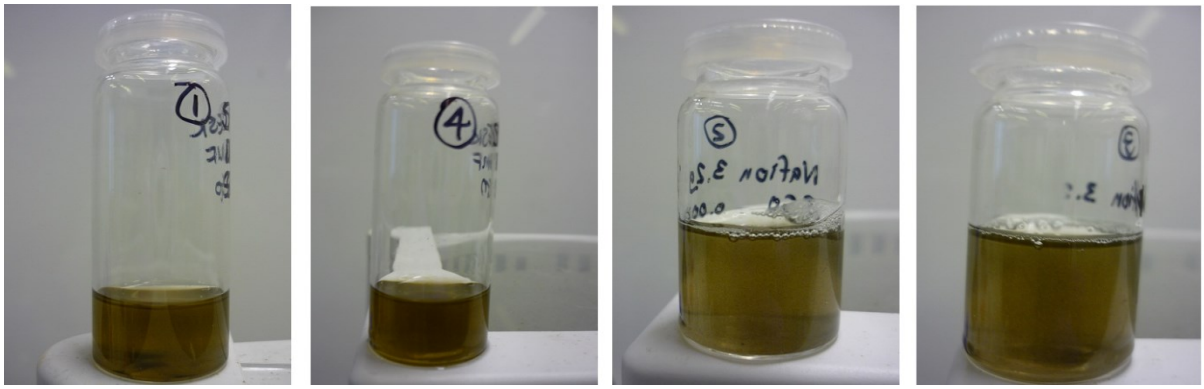

Figure 4-4 SPESK-GO and SPESK-SGO (left), Nafion-GO and Nafion-SGO (right), polymer-filler dispersions in DMF.

4.2.2 Membrane Casting

The starting point for the membrane casting was the preparation of reference Nafion membranes. The standard method for solution cast membranes was employed, by casting the solution onto glass petri dishes, after which the solvent is evaporated to form a solid membrane. The aim was to prepare membranes of around 25 μm in thickness (this was later

changed to 50 μm to enable the use of Nafion 212 membranes as a commercial reference). To calculate the volume of polymer solution required, Equation 1 was used.

$$v = \pi(r)^2 t \quad \text{.....(1)}$$

Where v = volume of the polymer solution in the petri dish

r = radius of the petri dish (4.5 cm)

t = the desired thickness of the membrane (0.0025cm)

The density of Nafion is 2.1 g/cm^3 [140] and hence 3.3 grams of the 10 wt % solution was required.

The first attempt at solvent evaporation was carried out at room temperature, but resulted in a water soluble membrane. The same process, followed by heating at 65 °C for one hour, had the same result. The process was repeated, but this time the petri dish was placed in an oven under vacuum at 80 °C and 120 °C for one hour each, following solvent evaporation. It was possible to remove the film from the petri dish with DI water, but the membrane was brittle and started to crumple as it dried out as can be seen in Figure 4-5 (left).

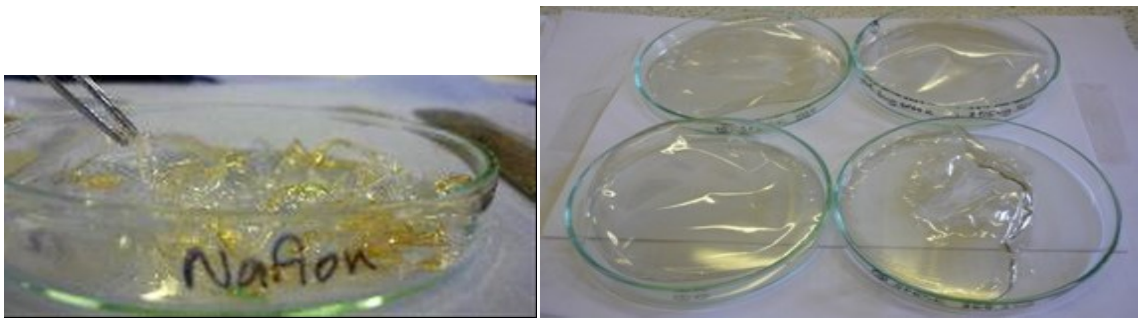

Figure 4-5 Initial attempts to prepare solution cast membranes resulted in poorly formed samples (left). The image on the right shows the two sets composite membranes prepared from SPESK-GO and SPESK-SGO.

It was decided to adhere to the process reported in the literature by Bae *et al.* [58] but to use *N,N*-dimethylformamide (DMF) as solvent in place of dimethylacetamide (DMAc). The initial casting was carried out directly from the commercial dispersion, without the addition of solvents. DMF was used for the scoping project because the successful preparation of Nafion-GO membranes had been reported previously [103, 141], and GO and SPESK formed a uniform dispersion and dissolved in this solvent respectively. The casting solution was prepared by combining the polymer (Nafion 10 wt% solution or SPESK solid) and SGO/GO (0.5 wt% to the polymer) in 5 ml DMF. The solution was sonicated for one hour, cast on a petri dish and the bulk of the solution was evaporated in the fume hood. The polymers were placed in an oven at 60°C overnight and then in a vacuum oven at 80°C for 6 hours. In total six samples were prepared: Nafion-GO, Nafion-SGO, SPESK-GO (x2) and SPESK-SGO (x2). The membranes were not all of high quality but it was possible to test the Nafion-SGO and the SPESK-SGO composites for proton conductivity. (An unsuccessful attempt was made to test the SPESK-GO membrane and is discussed with the results). The membranes were treated in 1M H_2SO_4 (2 x 2 hours, 1 x 1 hour) and washed in DI water (1 x 30 minutes, 1 x 3 hours).

4.2.3 Results and discussion

Characterisation of the SGO relied on Fourier transform infrared spectroscopy (FT-IR) as this was the only method that could be identified at the time. X-ray photoelectron spectroscopy (XPS) analysis was desirable but not available at UOB, within the time frame for the project it was not possible to access the equipment externally. Later GO studies relied heavily on XPS for characterisation as described in Chapter 5.

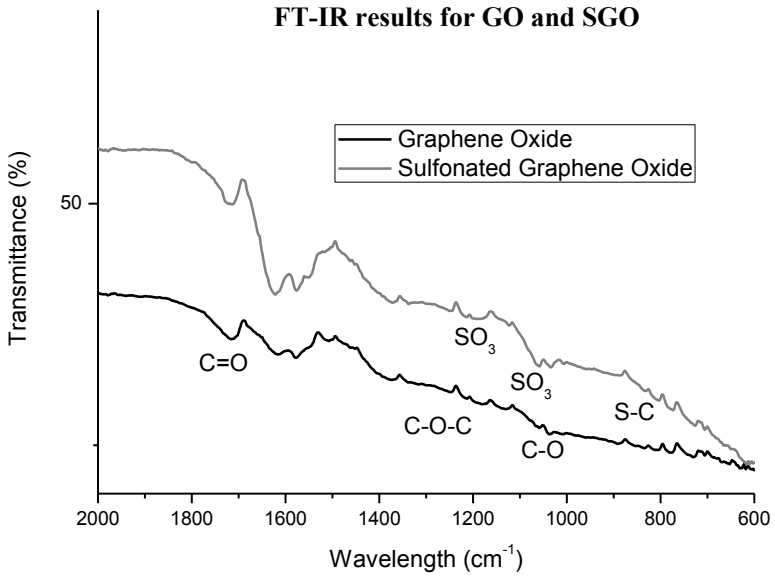

Figure 4-6 FT-IR results for GO and SGO.

Figure 4-6 shows the FT-IR results for GO and SGO taken at UOB. Peaks were observed at 1039, 1244 and 1714 cm^{-1} due to the C-O, C-O-C and C=O bonds present in GO [109]. The main peaks of interest in SGO were at 835, 1060 and 1200 cm^{-1} and were attributed to the S-phenyl stretch, SO_3 asymmetric stretch and SO_3 symmetric stretch respectively [109].

Testing was carried out at 80 °C, over a range of relative humidities between 20-100 %RH on a solid electrolyte analyser system (MSBAD-V-FC) made by Japan Bel Co. It was possible to measure the water uptake and the proton conductivity simultaneously as two samples were fitted in a magnetic suspension balance and a four-probe conductivity cell respectively in the same pressurised and humidified unit. The test sequence is shown in Figure 4-7 [142].

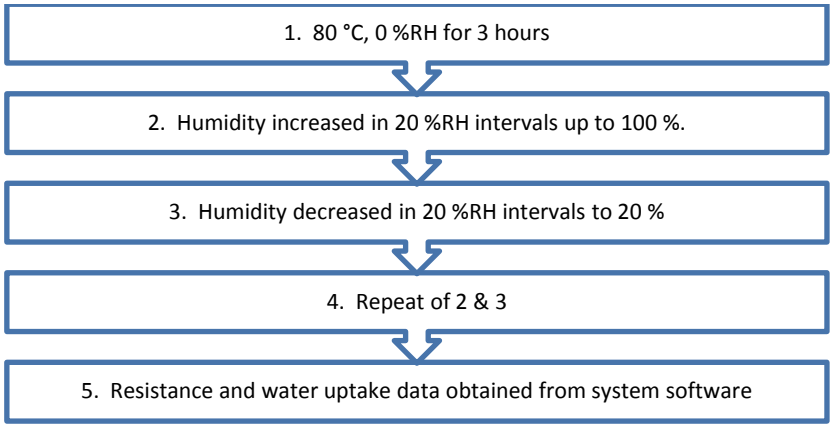

Figure 4-7 Test sequence for water uptake and proton conductivity carried out at UOY [142].

The test was carried out at 80 °C. In the first step the conditions were maintained at 0 %RH for three hours to obtain the dry weight of the polymer. The humidity was then increased and decreased by 20 %RH intervals, from 20 %RH to 100 %RH, over three cycles. At each test condition the humidity was allowed to equilibrate for 2 hours before taking a measurement. The membrane resistance was obtained from the impedance plot compiled from integrated impedance spectroscopy (Solartron 1244B and 1287), and the weight increase of the membrane was obtained from the system software. Following the analysis protocol of the UOY, data from the last increasing humidity sequence was used. The values for water uptake and ion conductivity were calculated as described in Chapter 3.

The conductivity and water uptake of the membranes are shown in Figure 4-8, conductivity for the reference SPESK sample and Nafion 212 was obtained from literature [58] and are indicated in grey. It can be seen that the proton conductivity measured for SPESK-SGO was lower than that for the pristine membrane, and also that the trend is slightly different, increasing more rapidly at the higher levels of relative humidity. The water uptake was almost the same over the whole range of humidity. It was also attempted to measure the conductivity of SPESK-GO but the test failed each time vacuum was applied. At the time, it

was hypothesised that failure could be due to degassing taking place from the graphene oxide, and that a possible solution would be to stabilise the sample for a period of time prior to assembly of the test system. Poor results were however also obtained for the next sample in the sequence, Nafion-SGO. Proton conductivity was almost negligible, and the water uptake showed an unexpected large peak around 40 %RH. It was likely due to continued issues with the vacuum sealing of the system and subsequent condensation of water. If it could be assumed that this was an anomaly, the water uptake around 80-90 %RH (as shown in Figure 4-8) suggested that doping with GO did not significantly affect the water uptake at 80 °C. Unfortunately, since each test ran for around three days, not enough time remained during the 2 week period to test the other samples.

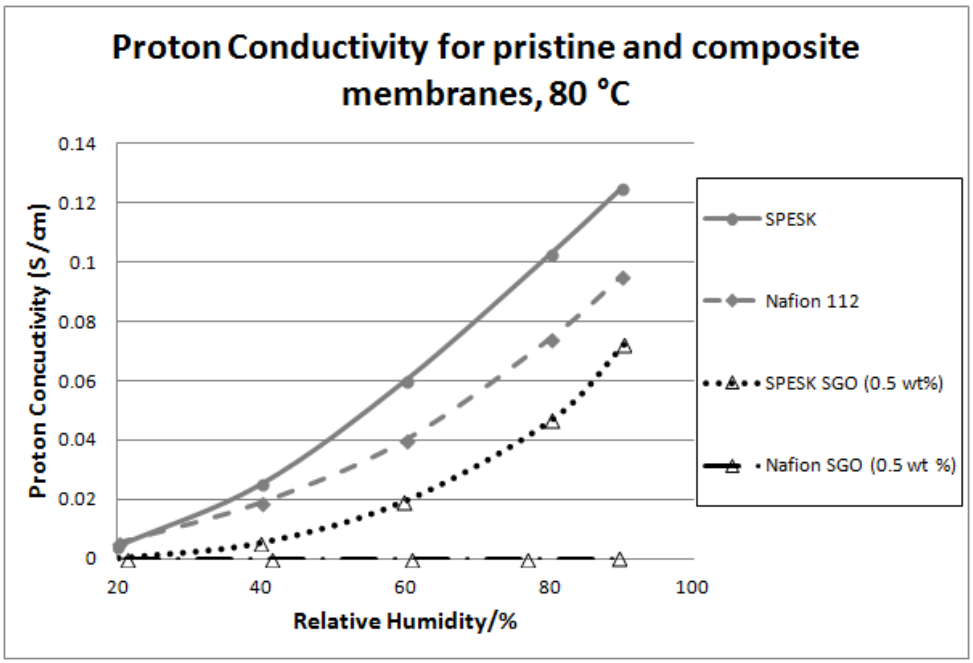

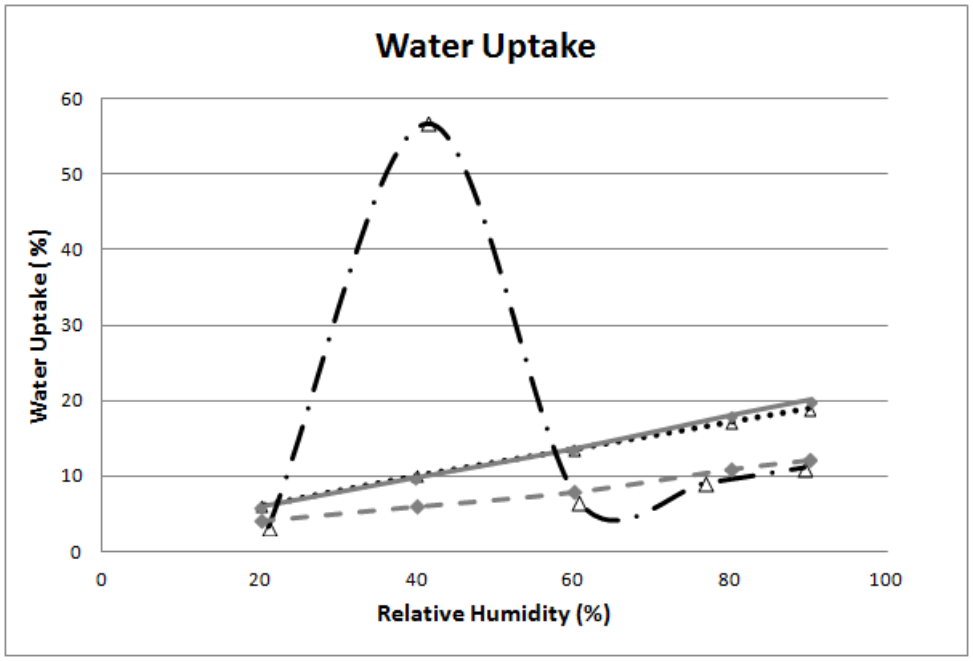

Figure 4-8 Proton conductivity (top) and water uptake (bottom) for SPESK and Nafion doped with SGO. Data for SPESK and Nafion 212 was adapted from Ref. [58] and are shown in grey.

From the proton conductivity and water uptake measurements for SPESK-SGO, it could be concluded that incorporating the filler material resulted in increasing the resistance in the membrane but that the water uptake ability was unaffected. As water uptake is a prime factor

when selecting filler materials for high temperature application, it was concluded that further study of GO as a filler would be justified.

Overall, this scoping experiment led to the following conclusions. First, the optimisation of the membrane casting procedure was necessary. In particular, the Nafion composite membranes were of poor quality. Experimental and/or equipment error could not be ruled out, but the proton conductivity data was poor. Second, the characterisation of GO and SGO would have to be a priority, in order to be able to explain the resistance trend of the membrane. Other sulfonated graphene oxide composite materials reported in literature consistently yielded membranes with increased proton conductivity (as discussed in Chapter 3) compared to the pristine membranes. Finally, being able to test membranes in-house would be the only way to test enough material in order to optimise the composite membranes. Of course, meaningful development of higher temperature materials could not be based on results from low temperature testing.

4.3 Nafion-GO membranes

Following on from the first scoping experiment, the second project was carried out with the primary aim of optimising the membrane casting method. The preparation methods for proton exchange membranes can affect the performance of the materials and some factors that are important include the choice of solvent [143, 144], thermal pre-treatment of the membranes [26, 124] and the morphology and functionalisation of the filler materials [56]. Studies also identified that extrusion led to orientated polymer chains and anisotropic water swelling as opposed to isotropic swelling observed for solution cast membranes [145].

The two main differences in the preparation technique of GO composite membranes, identified in Chapter 3, were the range of solvents that were used and the differences in the heating regimes for the curing of the polymer. Hence, studies on solution-cast Nafion membranes were reviewed in order to identify the most suitable solvents for the casting procedure, and are discussed in more detail in this section.

Silva *et al.* [141] investigated the effect of using DMSO, DMF and ethylene glycol (EG) and found that the best performance was obtained with DMF. It was theorised that this was due to the high boiling points of EG (197 °C) and DMSO (189 °C) necessitating a higher drying temperature for solvent evaporation. In the first part of this scoping study, poor performance was observed for the Nafion recast membranes from DMF solution, although the early stage of the casting procedure optimisation possibly contributed to this finding. It was however argued by Lin *et al.* [146] that Nafion membranes cast from commercial solution, using DMF, resulted in a membrane with a lower degree of hydrophobic/hydrophilic phase separation, the main reason why it is thought that Nafion is such an efficient proton conductor [147]. It was suggested that the solubility of the polymer in the solvent resulted in a more homogeneous solution, whereas the aqueous/alcohol solutions used in commercial dispersion result in the formation of hydrophilic clusters, which are preserved when the solvent is evaporated. The channels formed in the material allow for water uptake and provide the aqueous acid sites necessary for proton conductivity, as illustrated in Figure 4-9.

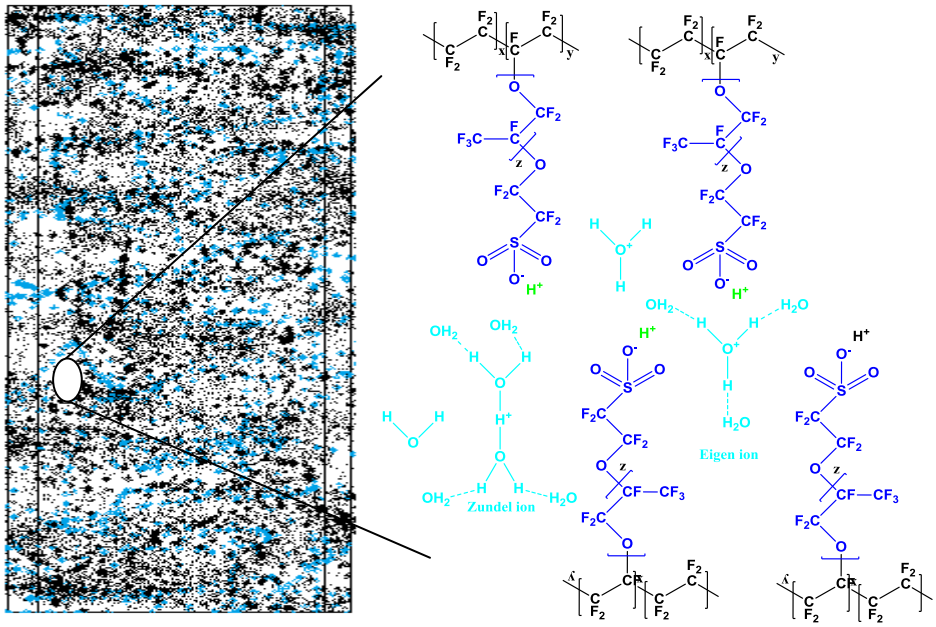

Figure 4-9 Schematic illustration of the hydrophilic channels which are formed in recast Nafion membranes.

Similar findings were reported in a separate study for re-dissolved Nafion 117 membranes, with the membranes cast from water having proton conductivity an order of magnitude higher than the membranes cast using DMF [148].

As detailed in Chapter 2, it is problematic comparing different studies empirically due to the variation in preparation techniques and test protocols. The three studies on DMF casting used a range of curing temperatures between 165 – 200 °C, and used different types of commercial reference Nafion membranes.

Commercial Nafion membranes are usually used as the reference material for experimental analysis of novel membrane materials. They are available with a range of proprieties: the series 112, 115 and 117 are prepared by an extrusion process, and the range 211 and 212 are prepared by dispersion casting [113]. The second digit indicates the equivalent weight (EW)

of the material where 1 = 1100 g = the grams of dry Nafion per sulfonic acid group, and the last number indicates the thickness in mil, where 1 mil = 25.4 μm [149]. The preparation method and the thickness of the membrane are related to its performance, hence the appropriate reference material should be chosen for each study.

Nevertheless, the conclusion was drawn that, since solvent selection would dictate the heating and curing regime, a good starting point would be to evaluate two solvents at opposite ends of the scale with regard to their boiling point. Properties of a range of solvents commonly used in solvent casting were compared (Table 4-1), and ethanol and DMSO were selected. Ethanol, with a boiling point of 78 °C, was a reasonable choice as it has been reported on in the preparation process for Nafion-GO composites [92]. DMSO was selected as the second solvent with a boiling point of 189 °C. The set of reference membranes was prepared directly from the commercial Nafion dispersion, which consists of >99% water. The three solvents (ethanol, water and DMSO) therefore covered a range of boiling points and polarities.

Table 4-1 Properties of solvents commonly used in membrane preparation [150].

	Boiling Point/°C	Dielectric constant/ε	Dipole Moment/μ
Ethanol	78	24.5	1.69
IPA	82	17.9	1.66
Water	100	80.1	1.82
DMF	152	36.7	3.86
DMAc	166	37.8	3.72
DMSO	189	46.7	3.9

Three types of membranes were cast, each consisting of a pure and a composite membrane containing 5 wt% GO, as shown in Table 4-2. The higher filler loading (compared to

0.5 wt% used in the scoping project) was chosen to enable comparison with literature values described in Chapter 2 [91, 92].

Table 4-2 Six membranes prepared using different solvents and by adding 5 wt % GO filler with reference to the 10 wt% Nafion solution.

Solvent	Pure Membranes	Composite Membranes (5 wt% GO)
None	Nafion-(W)	Nafion-GO-(W)
Ethanol	Nafion-(E)	Nafion-GO-(E)
DMSO	Nafion-(D)	Nafion-GO-(D)

4.3.1 Membrane casting

The membrane casting process was carried out in three steps. First, the preparation of recast Nafion was optimised. This was followed by adding DI water, ethanol and DMSO to the solution prior to casting and finally the method was repeated to prepare three composite membranes.

Following a slightly modified procedure reported by Zarrin *et al.* [92] a method for the casting and curing of membranes was established. Petri dishes were thoroughly cleaned, dried and wiped with a lint-free cloth prior to casting the solution. The petri dish containing the solution was placed directly into the oven and monitored as the temperature increased from 40 °C to 100 °C. After the solvent was evaporated, the temperature was maintained at 100 °C for two hours, and then increased to 140 °C for a further hour. The resulting membranes were mechanically strong, without cracks, and were easy to remove under DI water.

To prepare the membranes with additional solvent, 3 ml of DI water, ethanol or DMSO respectively were added to Nafion dispersion, after which the solution was sonicated for 30 minutes. The membranes were cast as described above. The sample with ethanol resulted in large cracks on two attempts and, as a remedy; the solvent solution was changed to a mixture of ethanol and isopropyl alcohol (IPA) in a 1:2 ratio. This produced better results but some cracking was still observed. The membranes prepared with DMSO were heated at 180 °C in the final step to allow for evaporation of the solvent [141].

Finally the composite membranes were prepared using the same method used for the pure membranes. GO was dissolved in DI water (15 mg in ~5 drops of water) and sonicated for 30 minutes, prior to adding to the solutions. The resulting solutions were sonicated for 30 minutes and cast.

4.3.2 Results and Discussion

The optimised membrane casting protocol resulted in Nafion reference membranes with no cracks, which could be easily removed from the petri dish, and which retained their shape after drying. The drying behaviour of the membranes can be explained by considering the glass transition temperature of the sulfonated perfluorinated polymer. The glass transition temperature of Nafion is around 110 °C [121, 151] and curing below this temperature will have no effect on the structure of the soluble polymer. Furthermore, evaporating the solvent over a period of time, with increasing temperature, whilst monitoring the film formation, allowed for even solvent evaporation, avoiding any gas bubble formation and subsequent cracking of the film.

The casting of the test membranes, as detailed above, resulted in three sets of membranes. Figure 4-10 shows an image of the three composite membranes, and it is clear that the membrane cast directly from the commercial Nafion dispersion and DI water resulted in the most uniform filler distribution. All membranes had a thickness of around 20 μm. The difference in the cast membranes could possibly be ascribed to the properties of the solvents, as described above. Furthermore, similar results were reported by Enotiadis *et al.* [104], who experimented with a range of solvents for solution casting of Nafion-GO membranes, including DMF and DMSO as well as direct casting from the commercial dispersion. Membranes cast directly had uniform GO dispersion, and it was concluded that, while the water interacts with the hydrophilic groups on the GO, the alcohol in the solution finds affinity with the carbon layers of GO. The organic solvents resulted in poor distribution, similar to what is shown in Figure 4-10. Overall the Nafion-(E) membranes were the poorest and still had some cracks. This was possibly due to the low boiling point of ethanol, resulting in trapped solvent escaping from underneath the partially formed membrane as the heat was increased.

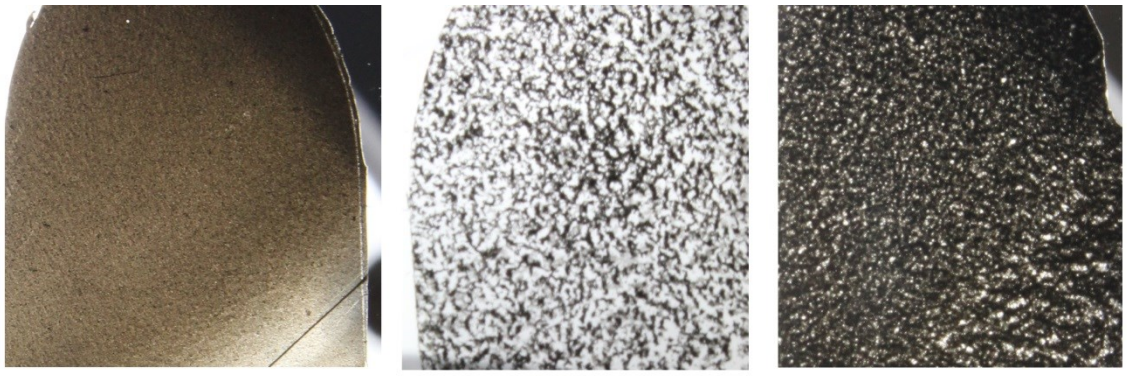

Figure 4-10 Membranes cast from the commercial dispersion (left), with the addition of ethanol/IPA (middle) and DMSO (right).

FT-IR was carried out to establish if the solvents and the doping with GO had an effect on the functional bonds in Nafion. Figure 4-11 shows that no new groups could be identified in the three sets of test samples. The expected peaks for Nafion were identified at ~968 and 982 cm^{-1} for the C-O-C bonds, 1057 cm^{-1} for the S-O bonds, 1144 and 1203 cm^{-1} for the C-F bonds, the shoulder at 1300 cm^{-1} was attributed to the C-C backbone, and the peaks at 1626, 1760 and 3360-3500 cm^{-1} were attributed to the different water molecules present in the material [90, 92, 120]. It can be seen that the same peaks are present in all the samples and it is probably due to the fact that the main functional groups that are identified for GO are the oxygen functional groups also found in Nafion. The graph for GO is included for reference.

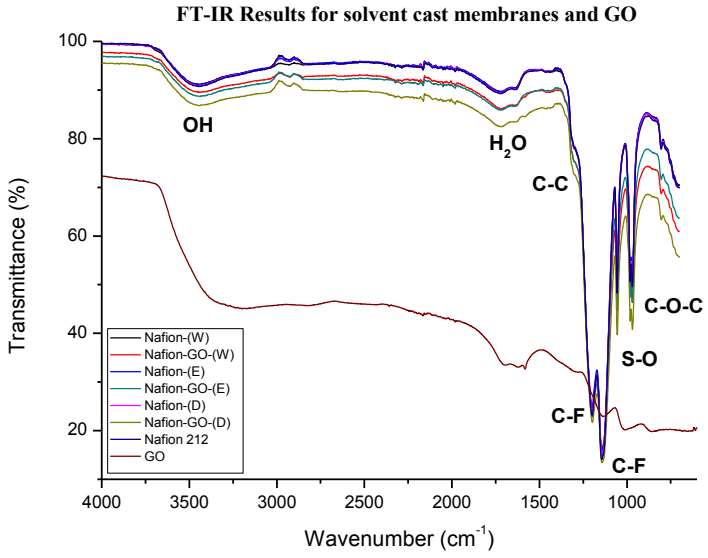

Figure 4-11 FT-IR results for the series of membranes and their composites.

Water uptake (WU) and IEC results (Figure 4-12) revealed that it was only for the Nafion-(W) membrane where the WU values increased slightly after GO doping. In each case, the IEC value decreased for the doped membranes, apart from the Nafion-(D) membranes, where a very small increase was measured. It should be noted however, that the values are very close, between 0.730 – 0.746 meq/g, and that overall, the values are lower than expected for Nafion. The expected IEC for recast Nafion is in the range of 0.95 – 1.01 meq/g, and for the

Nafion 212 membrane is 1.03-1.12 meq/g [125, 126]. This anomaly was investigated, and it was concluded that the sample size was the most important factor in the IEC measurements. In order to measure accurately the exchange of the H^+, Cl^- and the Na^+ ions between the membrane and the solution, at least 100 mg membrane was required for this measurement. Using samples of these dimensions, values for the reference materials were obtained in the expected value range, as will be seen in data reported in Chapter 7.

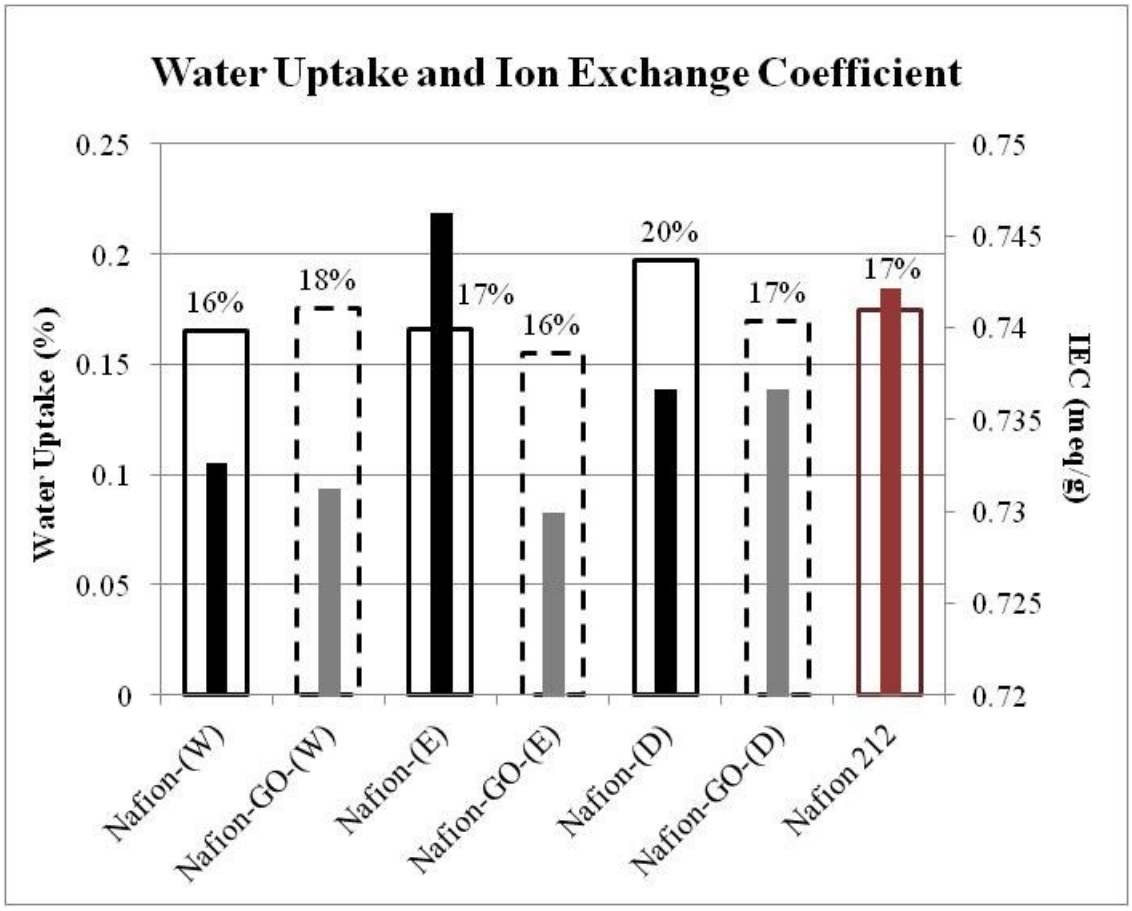

Figure 4-12 Water uptake % (outlined bars, left y-axis) and IEC (solid lines, right y-axis) values for the series of pure and composite membranes.

Due to the poor distribution of GO in the composite membranes, the size of the sample which could be used for characterisation and testing was greatly reduced. Furthermore, the WU and IEC test require fairly large sample sizes and, as this was a destructive test, the samples could not be used for further testing. Also, due also to the thinness of the membranes and the poor

formation of the Nafion-(E) samples, only limited performance data could be obtained. As a result, the Nafion-GO-(W) and Nafion-GO-(D) membranes were used to prepare MEAs, which were tested at UOB on a low temperature test stand (Paxitech). Following on from the exchange project at UOY, an opportunity existed to send a Nafion-GO sample for proton conductivity and water uptake measurement for analysis. To this end, a Nafion-GO-(W) and commercial Nafion 212 membrane sample was sent to Japan for testing.

Figure 4-13 shows that the proton conductivity for the composite membrane is lower than for the commercial Nafion 212, and that at lower relative humidity (20-60 %) the water uptake is slightly lower. The proton conductivity values are very close however, and it could be reasoned that at 5 wt% the effect of doping with GO could have a slightly detrimental effect to the movement of protons through the polymer matrix, as was theorised at the start of the scoping project with UOY.

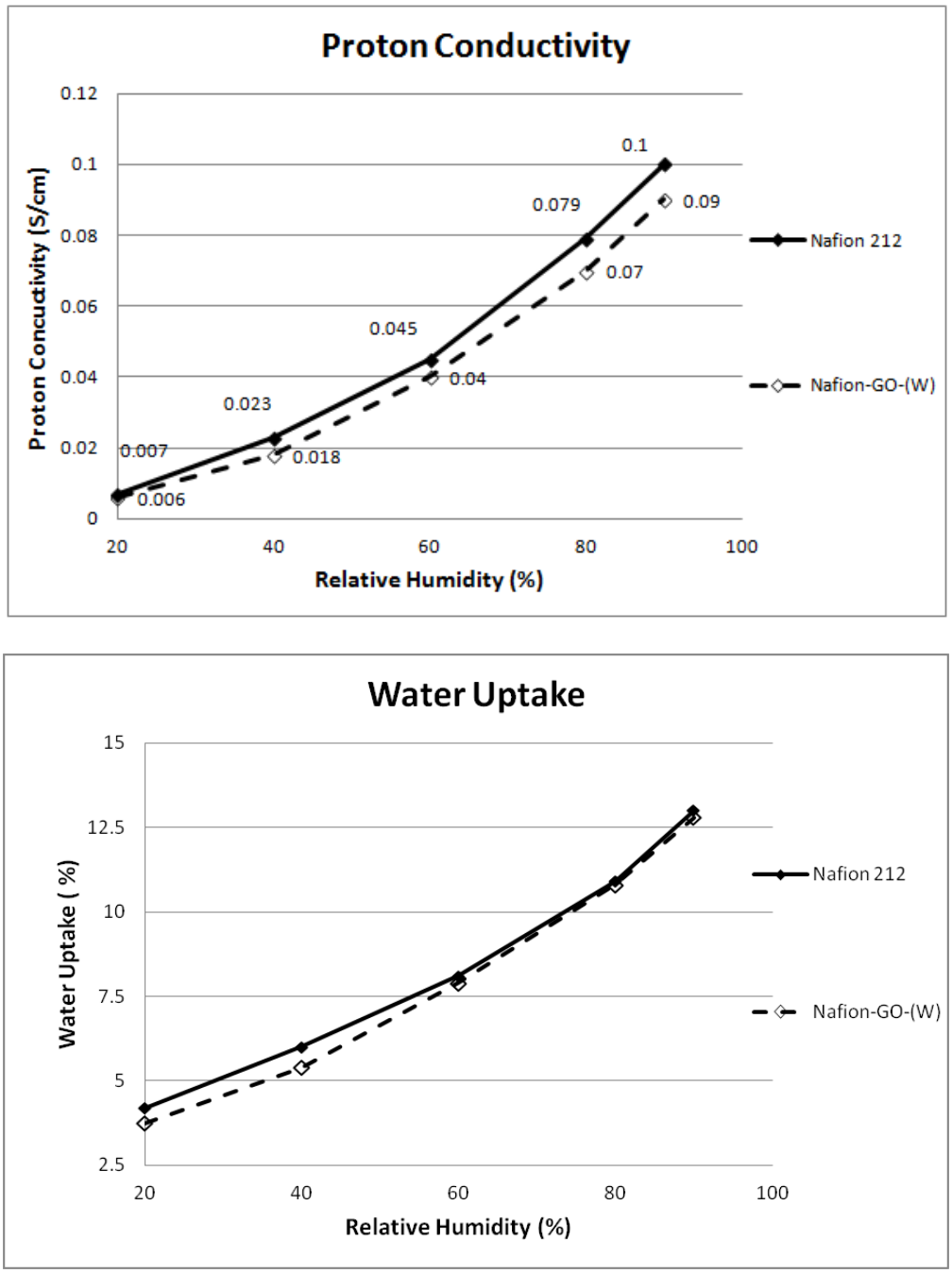

Figure 4-13 Proton conductivity (top) and water uptake (bottom) at 80 °C, measured by UOY for Nafion 212 and Nafion-GO-(W).

In-situ performance for Nafion-GO-(W) and Nafion-GO-(D) is shown in Figure 4-14. The maximum power density of the Nafion-GO-(W) membrane is slightly higher than that of the commercial Nafion 212 membrane, and the mass transport limitation is reached at a higher current density. It should be pointed out that, as the composite membrane was at least half

the thickness of the commercial membrane, slightly better performance should be expected. These results indicated that the performance of the composite membrane was at least in the same range as that of the commercial Nafion 212 membrane and warranted further investigation.

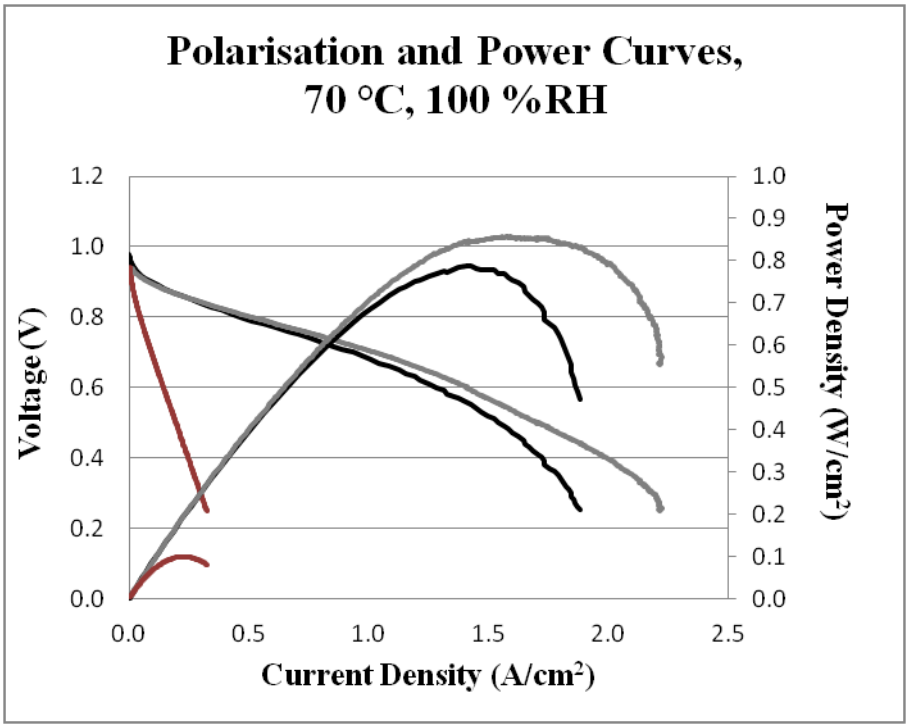

Figure 4-14 In-situ performance of Nafion 212 commercial film (black), Nafion-GO composite membrane cast from DI water solution (grey) and cast from DMSO (red).

The most apparent result from the in-situ test was that for the performance of the Nafion-GO-(D) membrane, which showed performance far inferior to both the commercial and the composite membrane prepared without addition of solvent. One reason for this could be the poor distribution of the GO filler in the polymer matrix. Another factor could be attributed to the effect that DMSO would have on the membrane formation. A study showed that, membranes cast from a range of solvents including DMF, DMSO and EG, and tested ex-situ, membranes cast with DMSO resulted in the lowest proton conductivity [141]. It was

theorised that the boiling point (and hence the increased curing temperature), and the polarity of the solvent resulted in poor hydrophobic/hydrophilic structure in the cured membranes.

4.4 Conclusion

The conclusions drawn from the two scoping projects described above shaped the experimental design of the rest of the project.

The initial tests on the composite materials did not produce results which showed increased proton conductivity over pristine membranes. However, the performance, both in-situ and ex-situ, was not in an unacceptable range, and the maintained water uptake ability of the membranes led to the conclusion that, with optimisation, the performance of the materials could be maximised for high temperature application. Due to the lack of high temperature test equipment, the results were taken at low temperature (70-80 °C), and it was possible that these conditions were not optimal to the composite membranes. Testing at high volume and at high temperature was necessary. A third party testing facility had been identified that could carry out ex-situ testing up to 90 °C, and an application was in place for the analysis of a further set of composite membranes. It was still most desirable to obtain high temperature test equipment for UOB, where ex-situ and in-situ testing could be carried out and correlated.

The characterisation of the filler material was necessary, and XPS was required in order to determine the functional groups that were present. Functionalisation of GO was carried out by oxygen functional group conversion and, if the species could not be identified in the material, it would be tenuous to conclude the success or failure of a particular reaction. The

non-uniform nature of GO is a well-known complication in the characterisation of the material. Various facilities were identified and applications were in place for XPS analysis.

Finally, the optimised preparation method for membranes was crucial to obtaining repeatable results. The use of additional solvents resulted in inferior membranes, both mechanically and based on performance. Membranes prepared from the commercial dispersion by heating to 100 °C for 2 hours and 140 °C for an additional hour resulted in strong membranes which could be handled easily. Furthermore, the addition of solvents did not have a marked effect on the water uptake and IEC, and would not be considered for further work. To prepare the composite membranes, DI water was used to disperse the filler material and resulted in similarly strong membranes. Even though the dispersion of GO was uniform using this method, further optimisation was possible and could be investigated by centrifugation, filtration, and mechanical grinding. The amount of sample material prepared in each batch also had to be increased significantly to allow for the range of characterisation and testing required to be carried out. Further refinement of the test conditions for WU and IEC was required in order to obtain published values.

The next chapter reports the findings on the synthesis and functionalisation of GO fillers.

CHAPTER 5 EVALUATION AND DEVELOPMENT OF OPTIMAL FILLER MATERIAL FOR COMPOSITE PEM – GRAPHENE OXIDE

5.1 Introduction

This chapter describes the completion of the second objective of this project; the evaluation and development of the optimal filler material for composite PEMs. As described in Chapter 2, the use of graphene oxide (GO) in composite PEMs has been shown to increase the performance at intermediate and high temperature operation, and was hence selected as the material of choice for this study. In the early stages of the project the use of hollow polymeric capsules was also considered [52], but initial attempts at synthesis and characterisation of silica shells led to poor results and this direction of study was abandoned. A brief description is provided in Appendix A1.

The enhanced performance seen in Nafion-GO composite membranes is related to the chemical properties of the material. The oxygen functional groups which are introduced during oxidation (hydroxyl (OH), epoxide (C-O-C) and carboxylic acid (COOH)) disrupt the graphene π-conjugated orbital system, making the material insulating to electrical conductivity, and enhances the tendency for the formation of hydrogen bonds. This in turn leads to high proton conductivity; GO sheets of 50 μm thickness have been shown to have in-plane proton conductivity of 0.1 S/cm and through-plane conductivity of 0.001 S/cm at room temperature and under full humidification [152]. (The anisotropic proton conductivity is due to the different routes available to the protons in the two plains.) As a comparison, published through-plane proton conductivity for Nafion 212 (50 μm) at 30 °C and full

humidification is 0.07 S/cm [91]. GO is also imperious to gas crossover and has been shown to increase the mechanical strength of composite membranes [91, 123].

Graphene oxide was synthesised via the modified Hummers Method described in Chapters 2 and 3. This chapter will focus on the chemical characterisation of GO, and the microscopic features and thermal properties as determined mainly by XPS, TEM and SEM. All XPS quantification quoted is based on at least three points of analysis on the sample. The final sections will briefly discuss the functionalised GO that was prepared in an attempt to improve the ionic conductive properties of pristine GO.

5.2 Results and Discussion

5.2.1 GO prepared in-house

5.2.1.1 Chemical Characterisation

GO was characterised by FT-IR and XPS to confirm that unreacted starting materials had been removed and to determine the degree of oxidation. The infrared spectra for graphite and graphene oxide are shown in Figure 5-1. The broad peak around 3400 cm^{-1} is due to symmetric and asymmetric stretch vibrations of residual water in the sample, and the peaks around 1720, 1600, 1050 and 1250 cm^{-1} are respectively due to the carbonyl functional groups, the graphitic vibrations of unoxidised regions, C-O bonds and ether functional groups [13]. The peak around 1645 cm^{-1} can also be attributed to the bending vibrations of absorbed water [22].

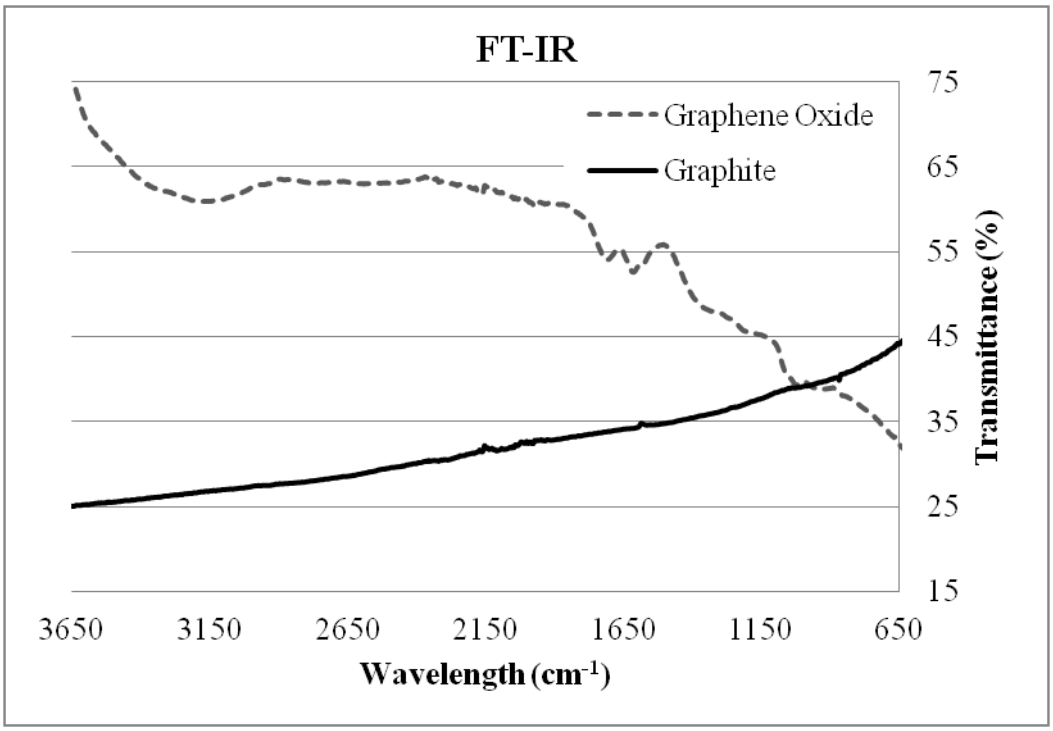

Figure 5-1 FT-IR spectra for graphite and graphene oxide

From XPS data the degree of oxidation was calculated to be 28 % with an error of ±1 %. Figure 5-2 shows the oxygen and carbon content in the GO which was successively analysed for different batches.

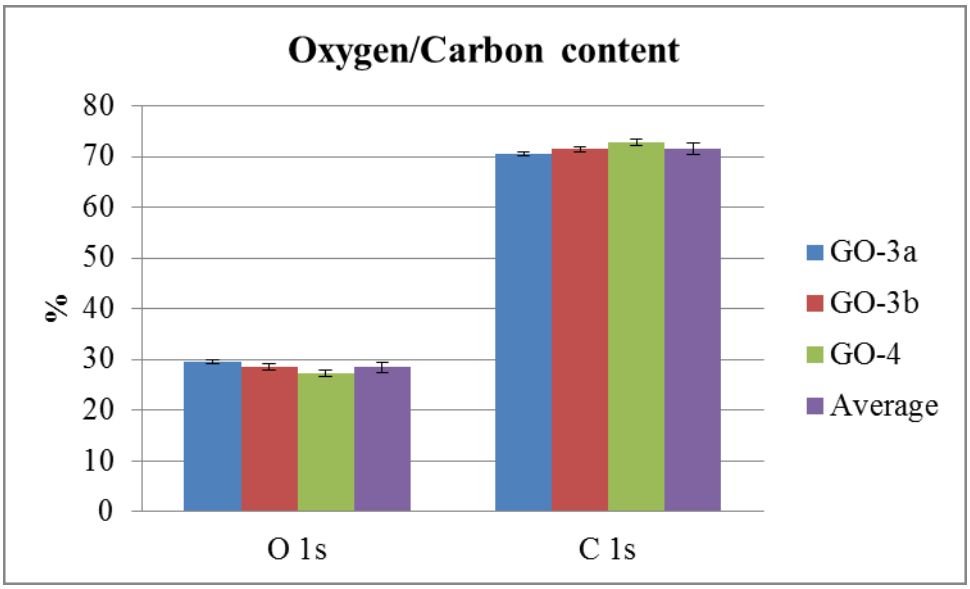

Figure 5-2 Oxygen and carbon content in GO for two successive batches.

Figure 5-3 shows the resolution of the different carbon-oxygen bonds. The peaks were assigned as C-C (284.4 eV), C-O-C (286.5 eV), C=O (287.10 eV) and HO-C=O (288.5 eV). The results agreed well with published data [92, 101].

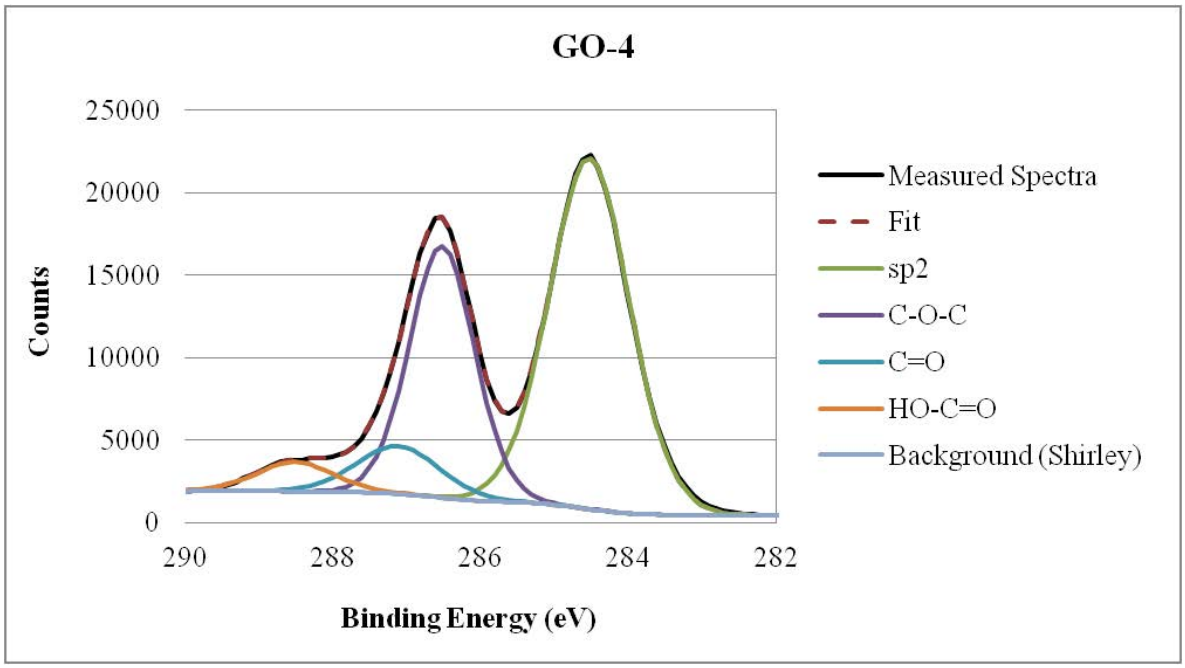

Figure 5-3 XPS spectrum for GO-4, C1s

5.2.1.2 Microscopy

TEM imaging was undertaken to evaluate the degree of exfoliation of the graphene oxide sheets and in order to establish the size range of the particles. Figure 5-4 shows representative images for dilute solutions of GO dried on copper microgrids. The particles were found to be irregular in shape and in some cases showed some stacking of sheets. The sheets were all in the micrometre range.

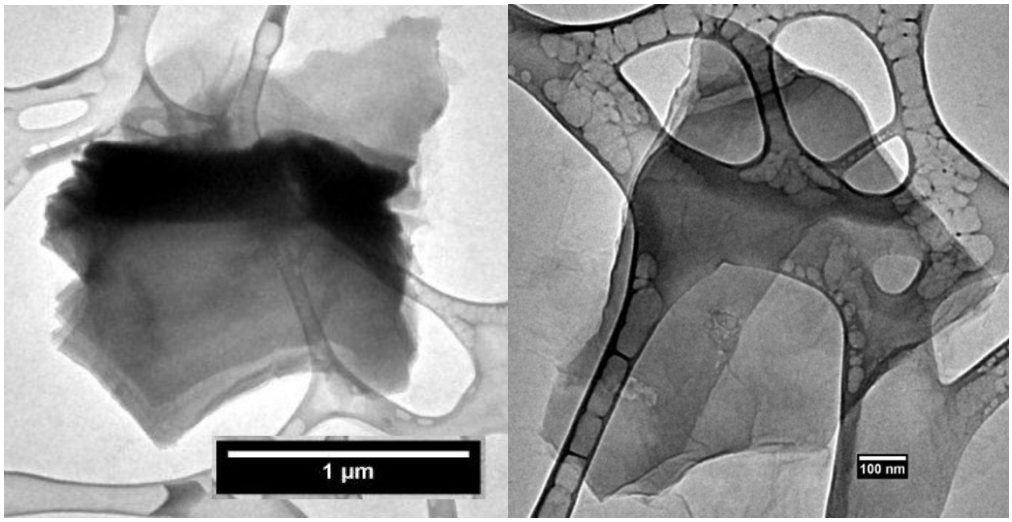

Figure 5-4 TEM images of graphene oxide particles

The TEM image of a GO sheet in Figure 5-5 shows a degree of crumpling of the particle sheet, which has been reported as a frequent occurrence in microscopic images. An explanation has been offered related to the Dekany Model mentioned in Chapter 2 [98]. The presence of the quinone groups possibly contribute to rigidity in sections of the material, where these domains end, crumpling occurs as the rigidity is lost in the aromatic or otherwise functionalised regions [98].

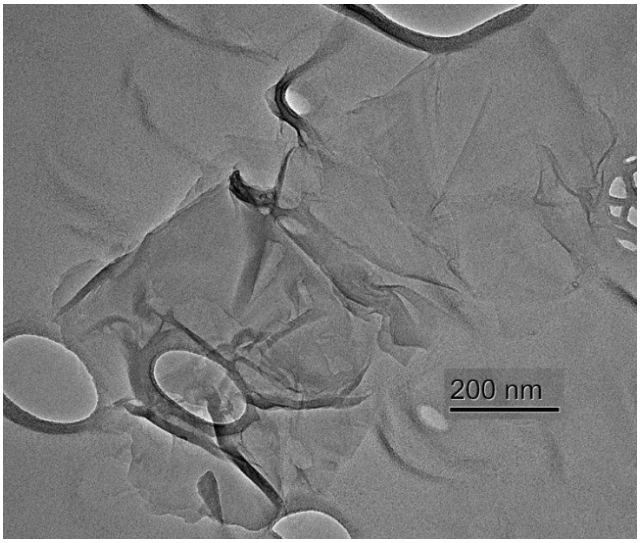

Figure 5-5 TEM image of GO showing crumpling effect

The TEM data was confirmed by Dynamic Light Scattering (DLS) (Figure 5-6), where the particle size range was found to be in the region of 300 – 700 nm in size. As the GO particles are not spherical, this was not an ideal way of characterising the size and in further optimisation procedures of the membrane preparation, efforts were focused on using a suitable centrifugation regime to separate the smallest particles from the larger sheets and layers. Removal of the largest particles and remaining stacks was confirmed when the aqueous GO dispersion remained uniform (with no sedimentation) over at least 24 hours.

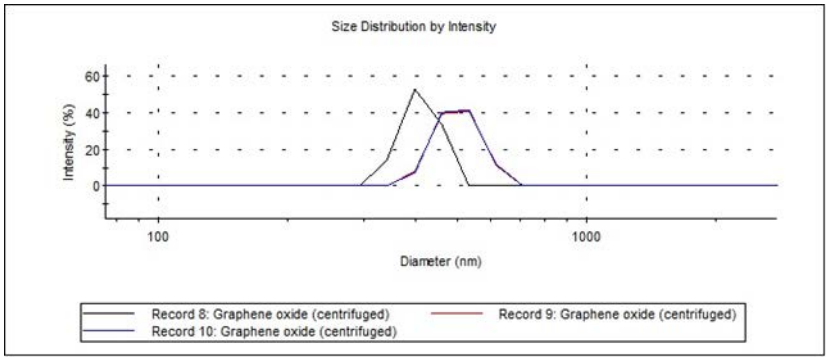

Figure 5-6 Dynamic light scattering particle size analysis for GO

The importance of the isolation of the smallest GO particles was documented by He *et al.* [94]. In the study, composite sulfonated polyimide membranes were prepared from GO synthesised from three different sizes of graphite particles. The particles with the smallest sizes, ~500 nm, showed the highest proton conductivity (at 80 °C and 100 %RH) and in-situ performance (under direct methanol fuel cell operation) when compared with particle sizes of 1 μm to 2 μm. The explanation offered for the improved performance was mainly hinged on the chemical composition, with the smaller particles containing more carboxyl functional groups than the larger particles (almost twice and three times as much respectively). As a result, smaller ionic clusters formed in the membranes, in a regular pattern, providing an unhindered path for proton migration. In the literature for intermediate temperature applications, the particle sizes were stated by Kumar *et al.* [91] in the range of ~100 nm, and

from the TEM images some particles were around 500 nm in size. Other studies did not specifically state the size of the GO sheets.

By analysing the cross sections of the composite membranes by SEM, the distribution of the filler particles could be evaluated. An initial hypothesis of particle agglomeration at the bottom of the cast membrane was disproved by the images shown in Figure 5-7. It is clear from these images that the filler particles were evenly distributed through the thickness of the membrane, but that a large degree of agglomeration had occurred. The particles were consistently orientated horizontally to the through-plane dimension and were in the tens of micrometres in width.

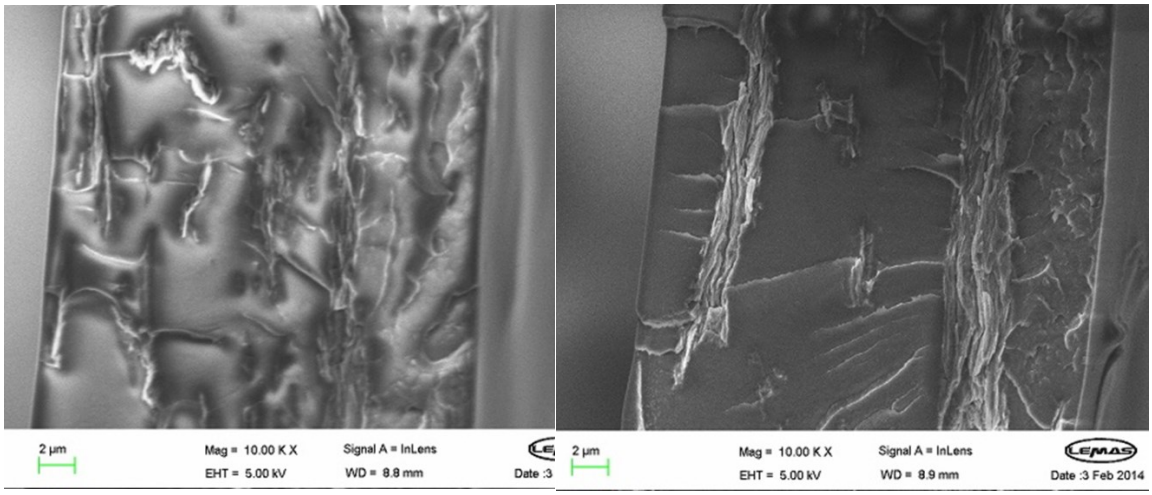

Figure 5-7 SEM images of the cross section of Nafion-GO composite membranes

After processing of the filler material by centrifugation (described in more detail in Chapter 7), SEM was repeated, and showed even distribution of sheets throughout the membrane as shown in Figure 5-8.

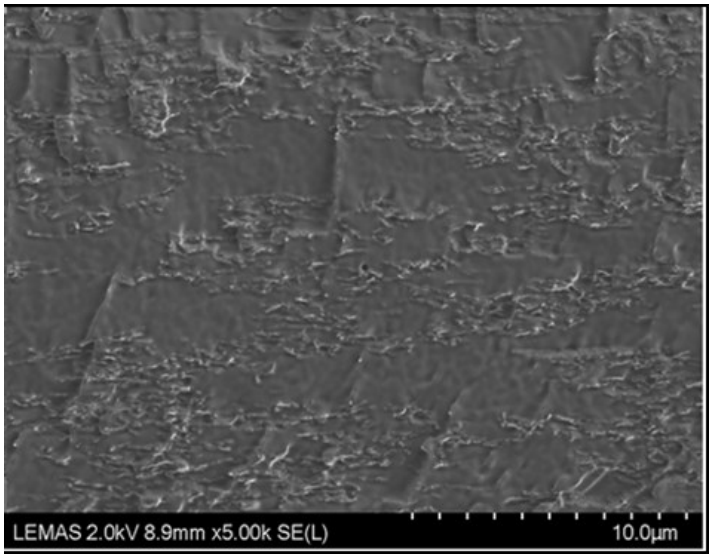

Figure 5-8 SEM image of the cross section of the composite membrane after optimised casting conditions.

The sheets were again horizontally aligned to the through plane-dimension.

5.2.1.3 Thermal Analysis

The thermal behaviour of GO is well documented and thermogravimetric analysis shows that the main mass losses are observed in distinct ranges [83]. Between 0-200 °C it is mainly water that is removed from the material. As the temperature increases from 200 – 1000 °C the carbon to oxygen ratio increases with oxygen functional groups lost in successive heating steps.

In order to evaluate the stability of GO up to 140 °C, and at different steps in the preparation process, XPS analysis was carried out on samples which were pre-treated to emulate the various steps in the process. GO powder was heated up to 140 °C to investigate the stability of the oxygen groups in the material. Figure 5-9 shows the carbon and oxygen content remains stable. Analysis of the C-O peaks revealed that a small reduction in OH-C=O bonds vs. a small increase in C-O-C bonds were the reason for the stability in the chemical content

of the material. The frequency of the bonds were 56 vs. 56 (C-C), 28 vs. 29 (C-O-C), 10 vs. 10 (C=O) and 7 to 6% (OH-C=O) in the original and heated samples respectively.

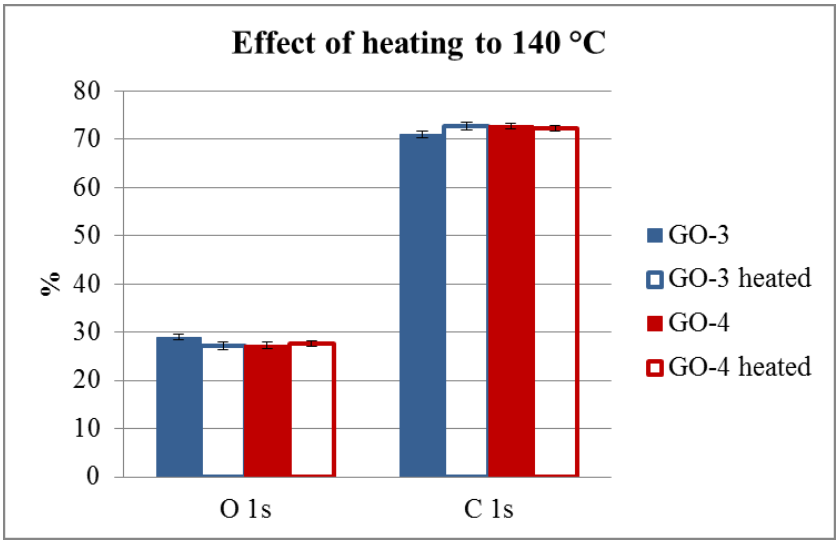

Figure 5-9 Carbon-oxygen content of two batches of GO before and after heating to 140 °C.

To evaluate the changes undergone by the composite membranes during preparation, samples were taken of pure Nafion solution, Nafion-GO mixture with solvent evaporated at room temperature and Nafion-GO composite after curing at 100 and 140 °C. In Figure 5-10 it can be seen that the elemental ratios remain very stable. Hence it can be stated that the chemical composition of GO is not altered in pure form and that the composite membrane shows no significant changes when subjected to the casting and curing process. It should be made clear that analysis reflects the surface of the material only and that the conditions were at atmospheric relative humidity or under vacuum.

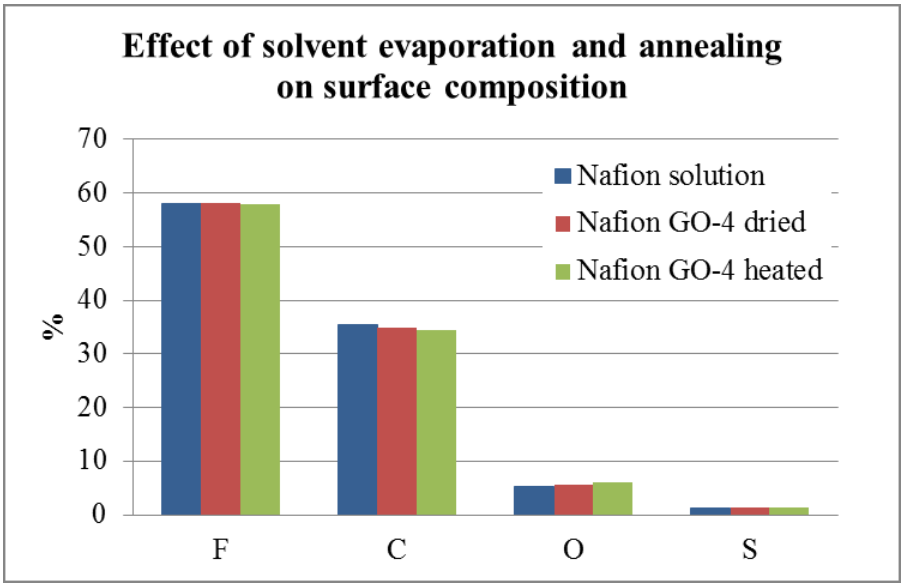

Figure 5-10 Elemental analysis of composite membranes at different stages of the casting and curing process.

5.2.2 Commercial GO

Commercial GO was obtained from Nanoinnova Technologies SL (www.nanoinnova.com). The materials characterisation received from the company included FT-IR and XPS analysis. XPS C1 analysis was reported with binding energies at 284.8 eV (35 %), 286.6 (58 %) and 288.5 (7 %), but were not assigned to particular carbon bonds. XPS on the material was repeated for verification and showed the same peaks but with slightly different content: 284.7 (49 %), 286.8 (42 %), and 288.5 (9 %) (Figure 5-11).

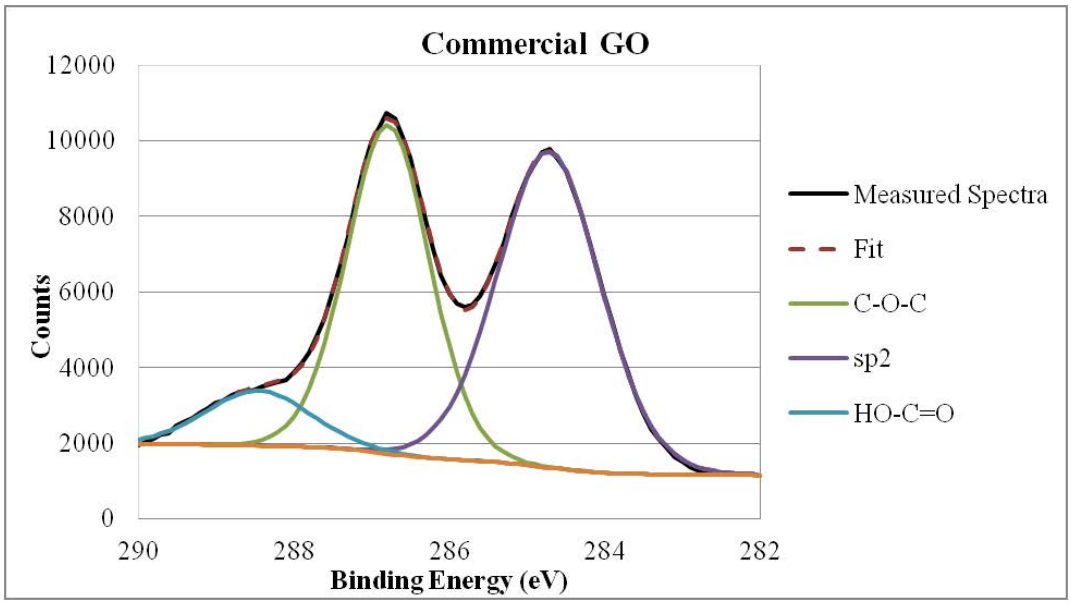

Figure 5-11 XPS for commercial GO

The effect of heating on commercial GO was investigated, as for the in-house prepared GO and it can be seen in Figure 5-12 that there is a more notable decrease in the oxygen content than for the in-house GO. The oxygen content decreases from 37 to 30 % and the carbon content increases from 63 to 70 %.

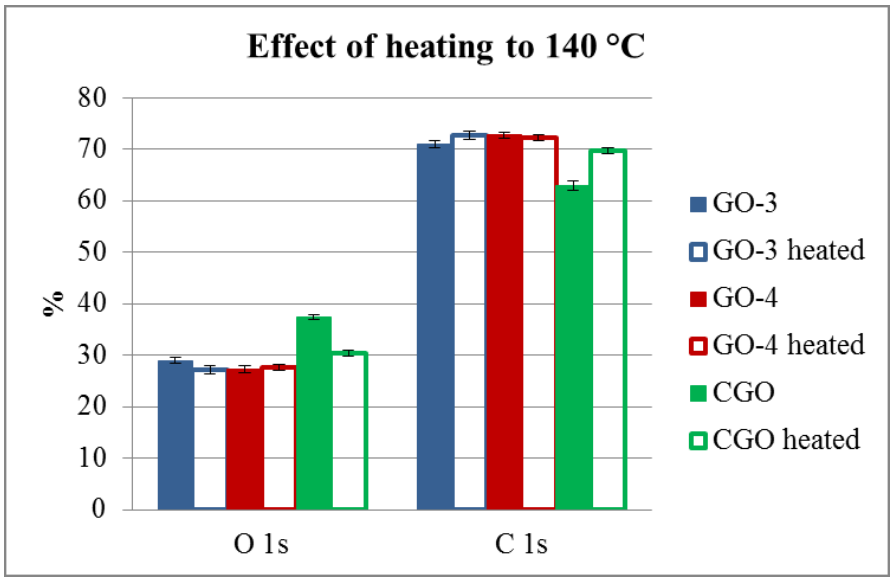

Figure 5-12 Carbon-oxygen content of in-house prepared GO and commercial GO, before and after heating to 140 °C.

5.2.3 Sulfonated GO

Both in-house prepared and commercial GO was sulfonated via concentrated sulphuric acid and nitric acid, as described in Chapters 2 and 3. Figure 5-13 shows the elemental analysis after the functionalisation and the differences in the elements appear mostly as a factor of error for the sulfonated materials. Hence it is not clear that functionalisation occurred as per the synthetic route attempted. The higher sulfur content for the commercial GO was also apparent in the starting material.

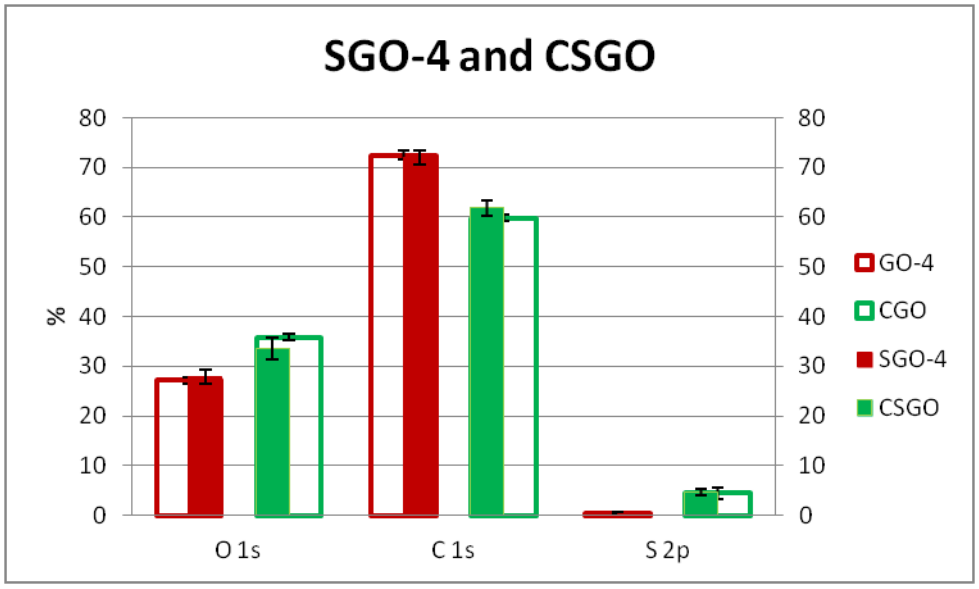

Figure 5-13 Elemental analysis of pristine and functionalised GO.

Interestingly, the appearance of the functionalised GO sheets in the cross sections of the membranes appeared to be very well separated as can be seen in Figure 5-14. It is possible that the harsh conditions employed during the functionalisation process resulted in this breaking apart of the stacks of sheets.

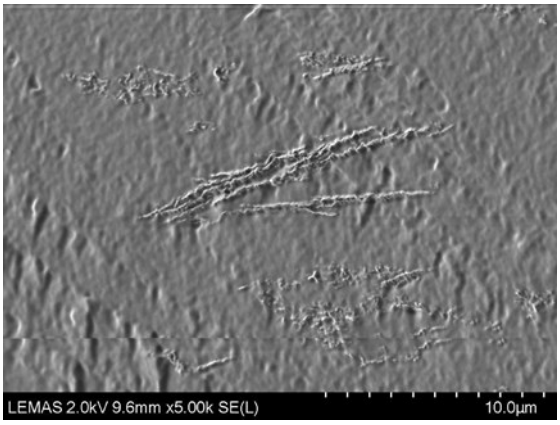

Figure 5-14 SEM image of the cross section of a Nafion composite membrane prepared with sulfonated GO.

5.2.4 Azo-coupling of sulfanilic acid

In order to evaluate the effect of different sulfonated functional groups, GO was functionalised by an azo-coupling of a sulfanilic acid compound as described in Chapter 2 and 3. Figure 5-15 shows that for this compound, when compared to the pristine and previously discussed sulfonated GO, there was a small increase in the sulfur content and a reduction in the oxygen content.

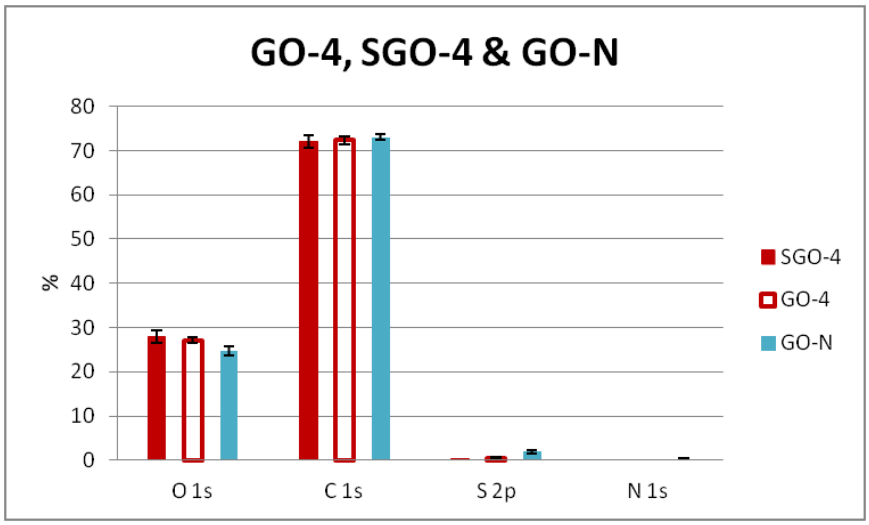

Figure 5-15 Elemental analysis of GO functionalised with azo-sulfanilic acid compound.

Analysis of the carbon C1 spectra revealed the appearance of two new peaks, the π-π* shake up satellite peaks of the sp^2 carbon network and could be an indication that some degree of delocalised π conjugation has been restored to the carbon network [83]. This could be seen as a possible explanation for the lower in-situ performance which is described in Chapter 8.

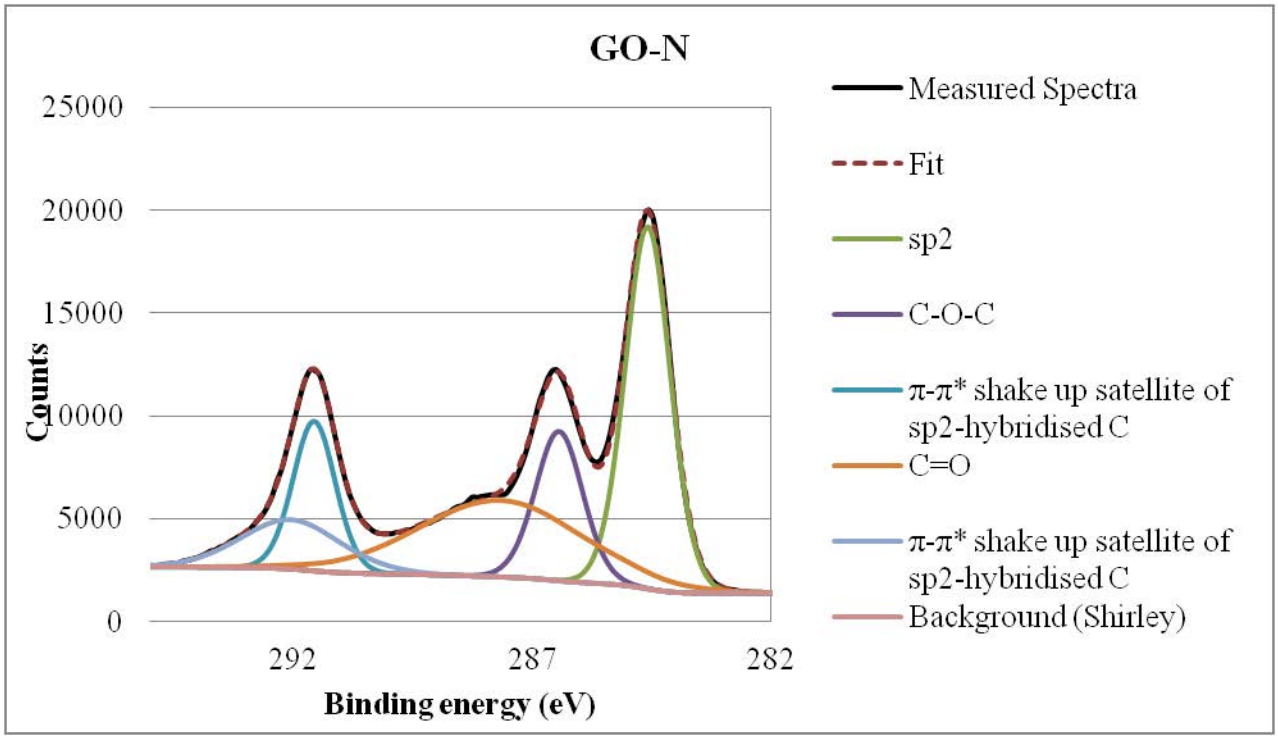

Figure 5-16 XPS spectrum for GO-N, C1s

5.3 Conclusions

Graphene oxide was synthesised in-house and characterised for chemical composition by XPS and particle size by TEM. The processing of the GO, prior to incorporation with the Nafion solution, was carried out to isolate the smaller particles of single sheets. This was achieved by centrifugation. The distribution of the particles was confirmed to be uniform, in horizontal orientation to the plane of the membrane and without stacking of sheets by SEM. It was attempted to functionalise the GO with two different sulfonic acid containing

compounds. The functionalisation resulted in change in physical appearance of the particles and in chemical composition. However, the sulfur content was not greatly increased.

CHAPTER 6 COMMISSIONING OF HIGH TEMPERATURE PEM/PEMFC TEST EQUIPMENT

6.1 Introduction

This chapter discusses the third objective; sourcing, installation and calibration of High Temperature PEM/PEMFC Test Equipment. The test stand and additional components, as described in Chapter 3, were purchased from Scribner Associates Incorporated (N. Carolina, USA) as a 'turn-key' high temperature test stand for both membrane conductivity testing and polarisation tests. The equipment was manufactured in the USA, but to UK voltage requirements and allowed for testing up to 120 °C over the full range of humidification due to the presence of a back pressure unit.

The membrane test, using a four electrode membrane clamp, allowed for the direct measurement of membrane resistance. As detailed in Chapter 3, this method is opposed to the method of measuring membrane resistance by impedance. This was desirable, as it would allow for high volume testing of materials under a range of conditions. It would further allow for testing of membrane resistance and the in-situ membrane performance on the same system with standardised operating conditions.

Extensive optimisation and calibration of the equipment was required. The first component that required optimisation was the BekkTech BT-112 membrane clamp and this is described in the first section. Following this, the insulation on the whole system was increased in order to maintain stable temperature and humidity conditions. The final stages focussed on the

calibration of the dew point with the use of an in-line dew point probe and the addition of heated and insulated sections to prevent cold spots.

6.2 BekkTech Membrane Clamp

The BekkTech BT-112 membrane clamp was supplied as part of the high temperature test stand in order to directly measure resistance in the membrane due to ion transport [153]. The membrane clamp was assembled in a test fixture (as shown in Figure 6-1). The fixture was connected to the test stand via a humidified hydrogen fuel gas line, two cartridge heaters and the potentiostat. The test sequence was programmed and controlled by the FuelCell™ program, supplied by Scribner, allowing for long term automated sequences to run without the requirement of user input.

The principle of the test is based on the measurement of resistance by Ohm's Law. The membrane clamp, with a sample inserted, is shown in Figure 6-1 (left). The membrane was inserted in-between four platinum electrodes, two platinum wires clamped the membrane down in the middle of the sample, and a voltage sweep was applied between -0.1 to 0.1 V. On either side of the platinum wires, a strip of platinum gauze measured the subsequent change in current. The data was recorded as an IV curve and from the slope the resistance was obtained.

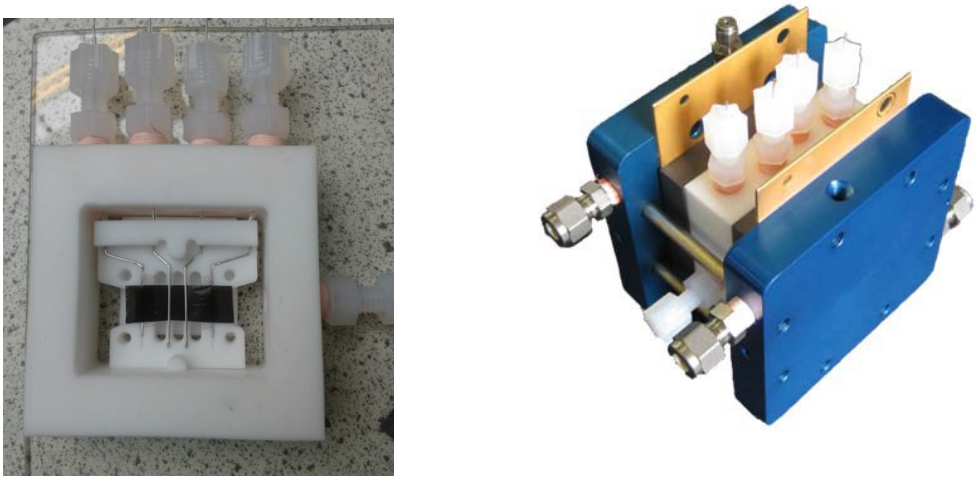

Figure 6-1 BekkTech BT112 membrane clamp (left) and Scribner test fixture (right) [153].

Figure 6-2 shows diagrammatically how the membrane clamp and test fixture is connected to the Scribner high temperature test stand.

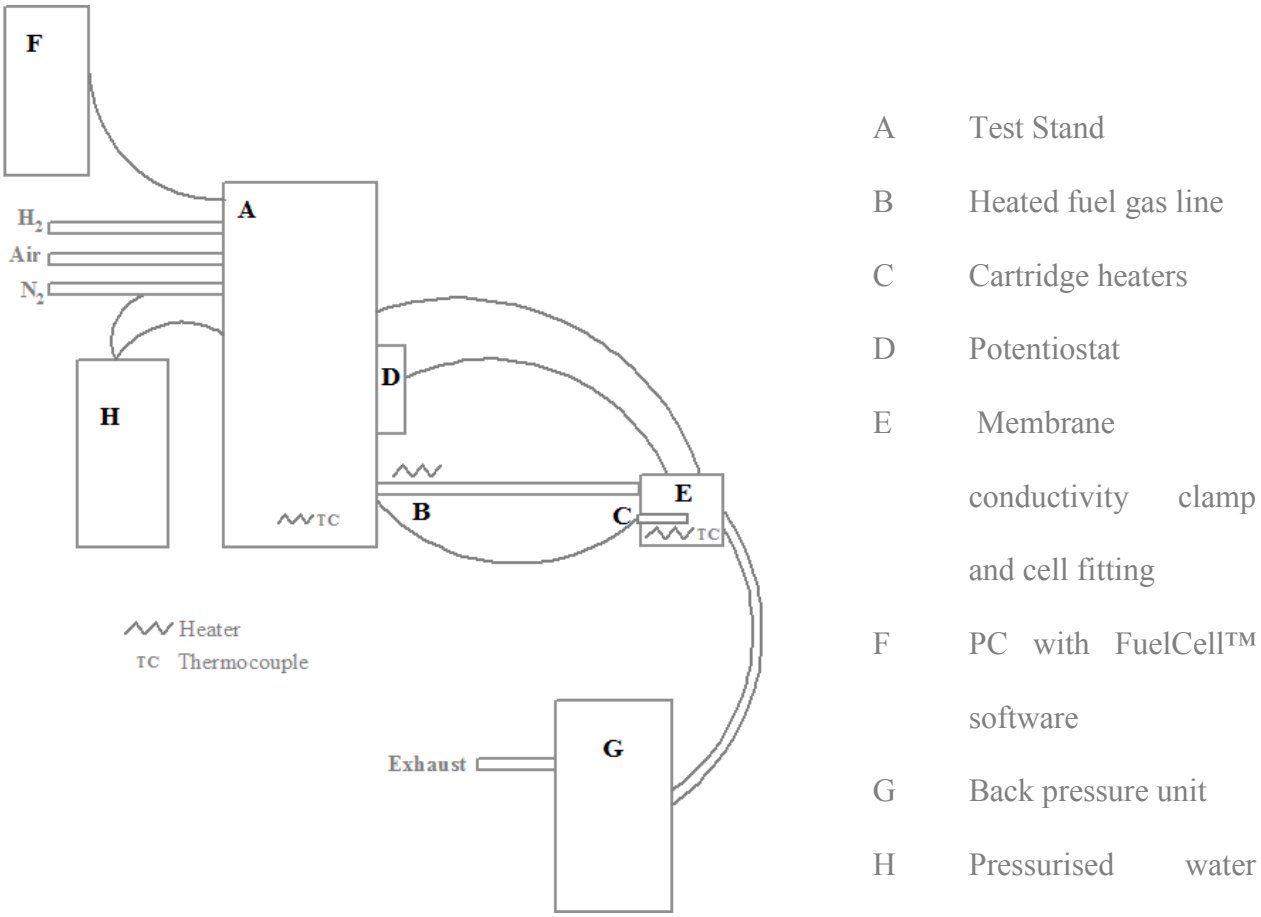

A Test Stand

B Heated fuel gas line

C Cartridge heaters

D Potentiostat

E Membrane conductivity clamp and cell fitting

F PC with FuelCell™ software

G Back pressure unit

H Pressurised water

Figure 6-2 Diagram of the test station set up for the membrane conductivity test.

Initial tests indicated a loss of contact in the cell; the voltage sweep as shown in Figure 6-3 (left) resulted in a large current anomaly and hence could not be used to calculate the resistance value.

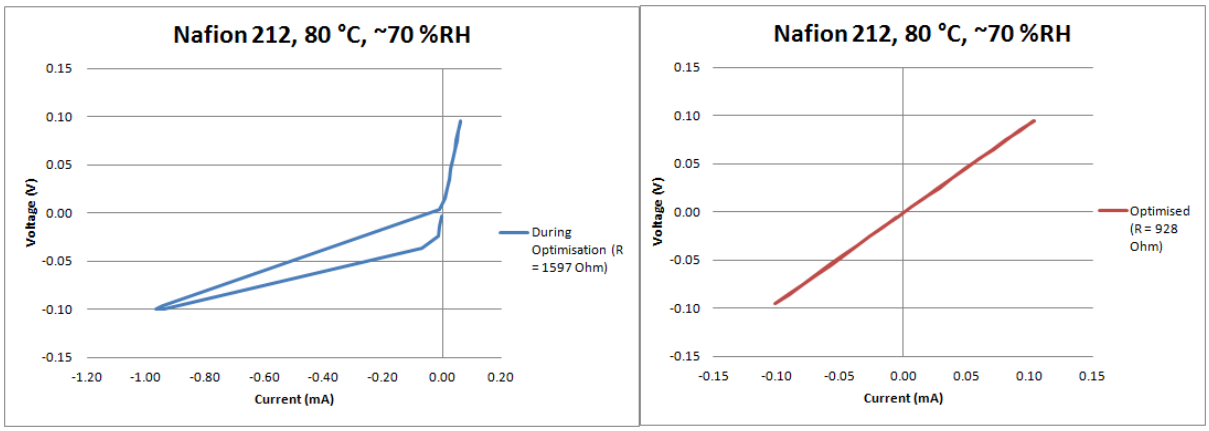

Figure 6-3 Resistance measurement during optimisation (left) and once the system had been calibrated (right).

Various strategies were employed to ensure good contact between the membrane material and the platinum electrodes. The first hypothesis was that contact was lost between the membrane and the outer electrodes when the clamp screwed into place. Platinum foil was applied to the strips of platinum gauze as shown in Figure 6-4 (left) and was followed by wrapping platinum wire around in an attempt to maintain electrode/membrane contact.

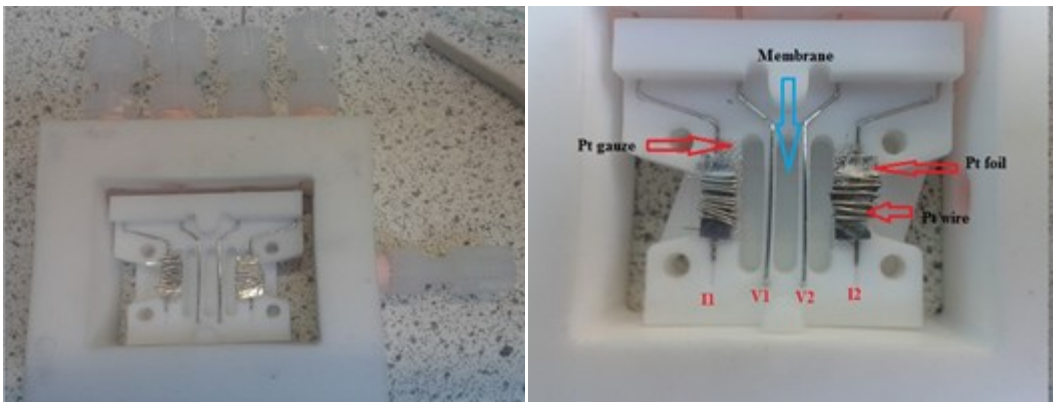

Figure 6-4 Membrane clamp adapted with platinum foil (left) and a combination of platinum foil and wire (right).

A further hypothesis was that the supplied fastening mechanism was not sufficient to maintain contact between the electrodes and the membrane throughout the test. Stainless steel screws were fastened through a top clamp and directly into the main Teflon block, and hence great care was required to avoid stripping the thread upon fastening. It was observed that the IV curve had better integrity at full humidification than at the lower relative humidity, which was possibly due to the swelling of the PEM. In order to investigate if the clamping pressure was causing the loss of contact at lower humidity, four new screws with bolts were made which could be used to securely fix the two components together. In Figure 6-5 the assembled cell is shown. This measure alone was insufficient and combinations of platinum foil and PTFE strips on the outer electrodes were added in order to maintain contact.

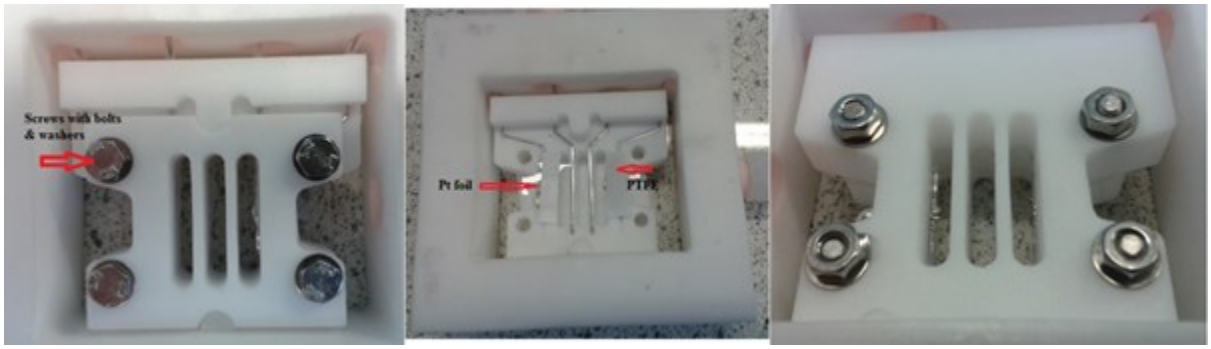

Figure 6-5 Membrane clamp adapted with custom made screws and bolts (right & left) and membrane fitted with addition PTFE strips for improved contact (middle).

The modification described resulted in improved data in some cases, but it was not consistently repeatable. Results frequently appeared as shown in Figure 6-3 (left) and on some occasions the plot did not pass through the origin, indicating serious loss in contact. To investigate the contact situation in the cell, photographic paper was inserted in the membrane clamp and it was clear from the series of samples (shown in Figure 6-6) that uniform contact was not obtained at both the current and the voltage probes at the same time.

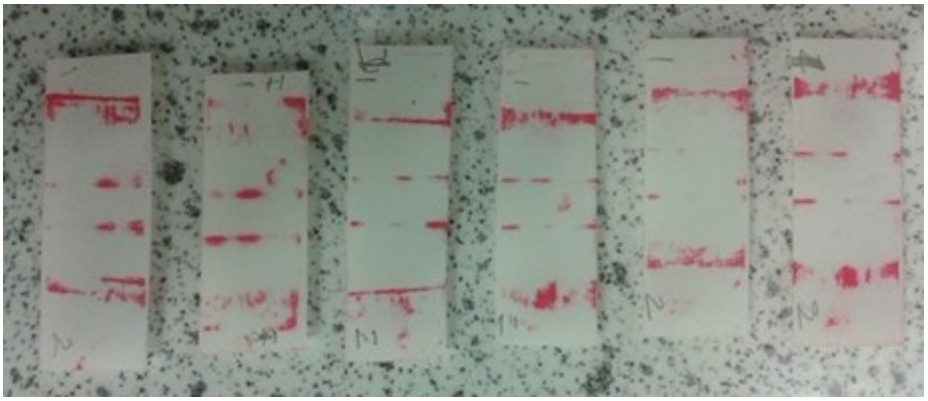

Figure 6-6 Photographic paper used to investigate the contact between membrane samples and cell electrodes. 1 and 2 marked on the samples to align the orientation.

The ultimate solution to the issues observed was the replacement of the clamp by the manufacturer. It was theorised by Scribner that a "manufacturing tolerance problem" could have led to the problematic data. All conductivity testing reported was undertaken with the replacement clamp and data throughout was taken from IV curves as shown in the right hand side of Figure 6-3. It has since also come to light that the manufacturers are developing a new type of membrane conductivity clamp specifically for high temperature application.

6.3 Insulation

The size and material of the membrane clamp resulted in the requirement for extra insulation in order to maintain the maximum measured temperature of 120 °C in the test cell during operation. An insulation fitting was made from melamine and covered with aluminium insulation tape, then fitted snugly over the cell.

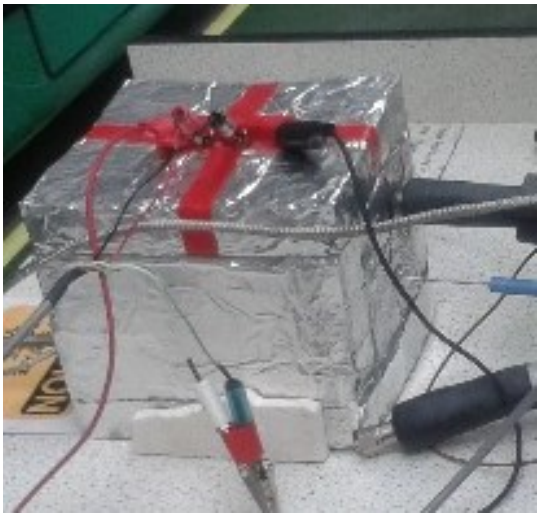

Figure 6-7 Insulation fitting prepared from melamine and aluminium tape.

Tests were carried out between 80 °C to 120 °C. The heated gas lines were connected between the test cell and the test stand, and were programmed by the manufacturer to be a few degrees above the set dew point of the system. The temperature data of the lines were not logged by the FuelCell™ software. The test cell was heated by the test station controlled cartridge heaters, and the cell temperature was logged by the system via a thermocouple immersed in the membrane clamp (so that the temperature is measured in very close proximity to the membrane) and attached to the test stand. The outlet gas was connected to the high temperature back pressure unit.

The first proton conductivity tests were carried out and revealed that further optimisation was required. Calibration of the dew point resulted in acceptable proton conductivity data but during this calibration the need for further insulation and heating was also addressed. This is described in following section.

6.4 Dew Point Calibration

The first set of data that was collected for a series of composite membranes with GO loading between 0.5 – 5 wt% is shown in Figure 6-8 (left). The slight anomalies for the 0.5 wt% membrane were possibly due to loss of contact between the membrane and the platinum electrodes as the material shrunk at lower humidity or due to water drops forming in the system due to cold spots. At this stage 25 μm membranes were still being prepared, as described in Chapter 4, and was an indication that thicker samples (i.e. 50 μm) would be a better standard to use for in the Scribner system.

The conductivity trend very clearly indicated that the resistance in the membrane increased as the GO loading increased. These results are discussed in more detail in Chapter 7, but at this stage, what was concerning was the very high proton conductivity values calculated from the resistance data. The expected proton conductivity for Nafion 212 is around 0.1 S/cm under optimal conditions which are around 80 °C and 100 %RH. Comparing the two sets of data presented in Figure 6-8, which includes the proton conductivity measured at the University of Yamanashi (as described in Chapter 4); it was clear that the conductivity measured with the Scribner test stand was too high to be accurate.

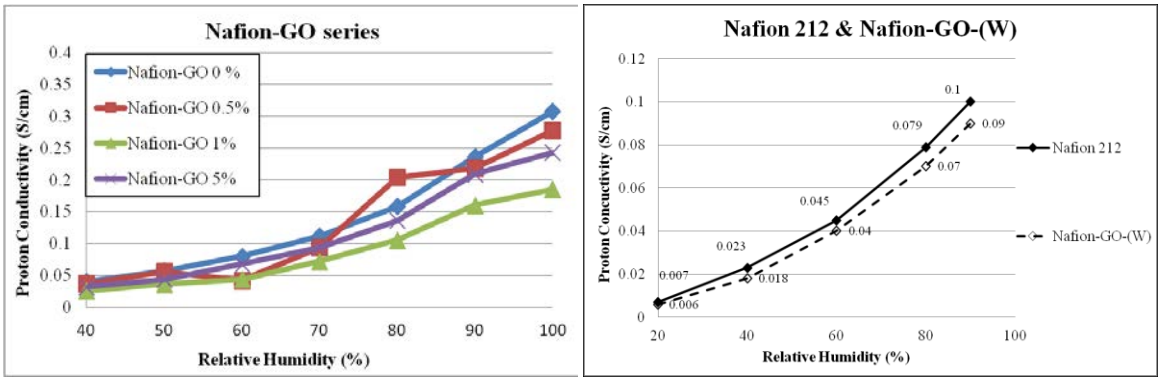

Figure 6-8 Initial proton conductivity data for Nafion-GO membranes in the range of 0 – 5 wt% filler material (left). Proton conductivity data for Nafion 212 and Nafion-GO with 5 wt% filler (Nafion-GO-(W)) and tested by UOY (reported in Chapter 4) (right).

The importance of establishing a good quality baseline and a testing protocol which is repeatable and accurate was illustrated in a recent paper by Kreuer, a renowned expert in the area of proton conductors. It was in response to a study published by Wang *et al.* [154] reporting astonishingly high proton conductivity of 5.5 S/cm for a trimesic acid and melamine whisker [155]. After repetition of the reported experiment by Prof. Kreuer's group it was concluded that experimental error had led to the measurement of this very high value. At 5.5 S/cm it was almost an order of magnitude higher than that for phosphoric acid which has been shown to be the compound with the highest intrinsic proton conductivity [155]. Hence, if proton conductivity is being reported, it should be ensured that the measurement is free of interference from other factors.

In order to validate the data obtained and reported in Figure 6-8, the Technical University of Denmark (DTU) agreed to the use of their equipment and assistance in setting up comparable test conditions in an existing membrane conductivity test rig. Over one week their system was modified (to increase and stabilise different levels of relative humidity) and thus allowed this researcher to collect membrane conductivity data under different conditions, in order to obtain a good base line for future proton conductivity data for the Nafion-GO composite

membranes. Figure 6-9 shows proton conductivity data for composite membranes with 5 % GO tested at the University of Yamanashi (described in Chapter 4) and the Technical University of Denmark (DTU). The measured value for Nafion 212 from UOY is included as a reference.

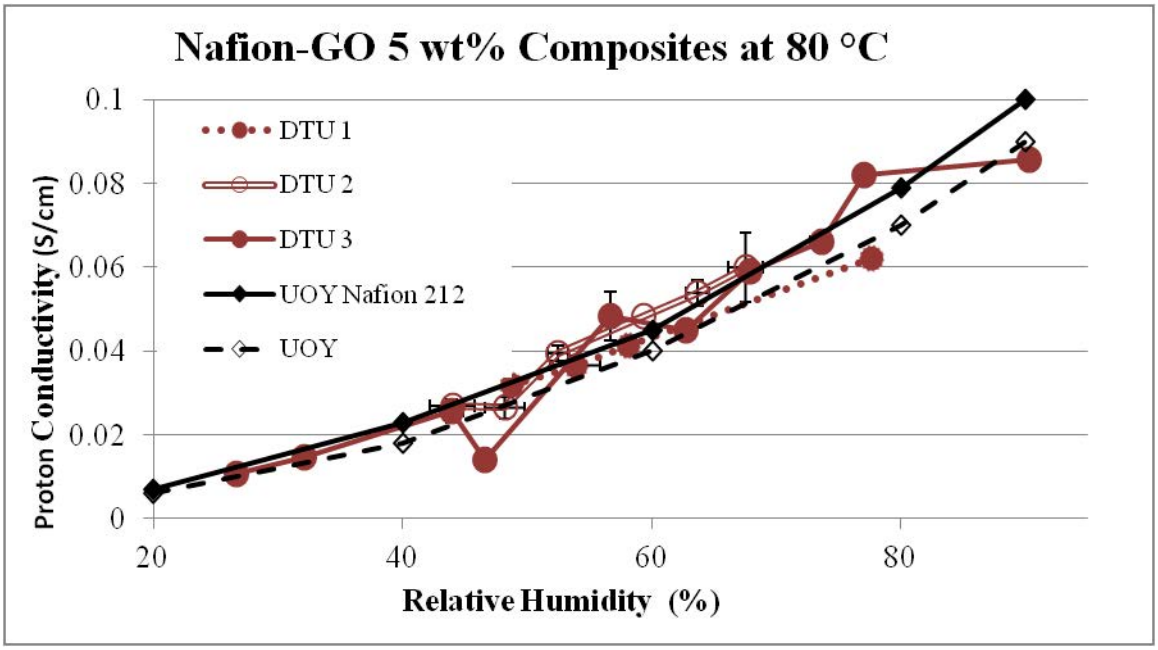

Figure 6-9 Proton conductivity measured for Nafion-GO 5 wt% at DTU and UOY. Nafion 212 data is included for reference.

The three test runs carried out on the 5 wt% composite at DTU are shown as the red lines. The noise in the data was observed because of the adapted test system. Humidification was added to a system which was optimised for operation at very low humidity and was hence difficult to control over a wide range. Measurements were taken using a four electrode measurement, in the plane of the membrane and samples were cut from the same membrane sample as tested at UOB. The humidity was measured by a dew point probe situated in the system exposed to the same heat and humidity as the test cell in a circulation oven. The data showed a smooth trend for proton conductivity from low humidity to higher humidity and more reasonable numerical values than those measured at UOB. Figure 6-10 includes the

data, (from Figure 6-8) showing the proton conductivity measured at UOB on the Scribner high temperature test stand before optimisation and dew point calibration.

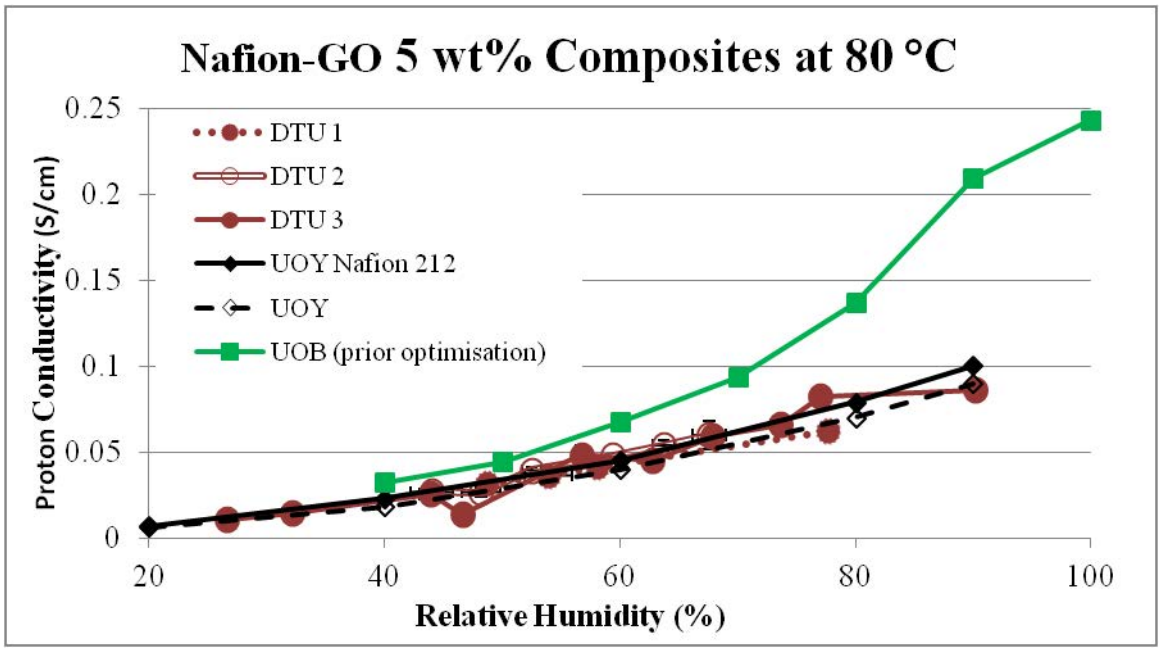

Figure 6-10 Proton conductivity measured for Nafion-GO 5 wt% at UOB (green), showing unrealistically high values for proton conductivity.

The most realistic explanation for the recorded data was that the dew point set on the Scribner test stand, and the real dew point in the system were not the same. Particularly at the higher ranges, 60 – 100 %RH, it appeared that the humidity was in fact much higher than indicated by the test stand. A dew point probe, fitted in a heated chamber was connected in-line to the system between the heated gas fuel line and the test cell. In Figure 6-11 this is indicated as I. The heated chamber was connected to the test cell (E) with a stainless steel pipe heated by a rope heater (J). The heated dew point chamber with thermocouple was supplied by Scribner.

The melamine and aluminium tape insulation described in section 6.3 was extended to include the two heated gas lines (B and J). This way the heat in the system was maintained

for the full flow journey of the humidified gas. Two control boxes (L) were built in-house to control the constant heating of both the chamber and the additional gas pipe.

With these systems in place calibration was carried out by running a test sequence, between 25 to ~95 %RH and at 80, 100 and 120 °C, with the theoretical dew point set by the test stand and measuring the actual dew point with the probe. Following the analysis of the measured dew point and temperature data, the dew points were sequentially set until the target and the measured relative humidity correlated. It should be pointed out at this stage, that the measurement of the dew point and the temperature in different locations (I and E respectively) is not ideal, but every effort was made to ensure that the pressurised and humidified gas stream was at a constant temperature throughout the system by monitoring the heating of the gas lines (at B and J).

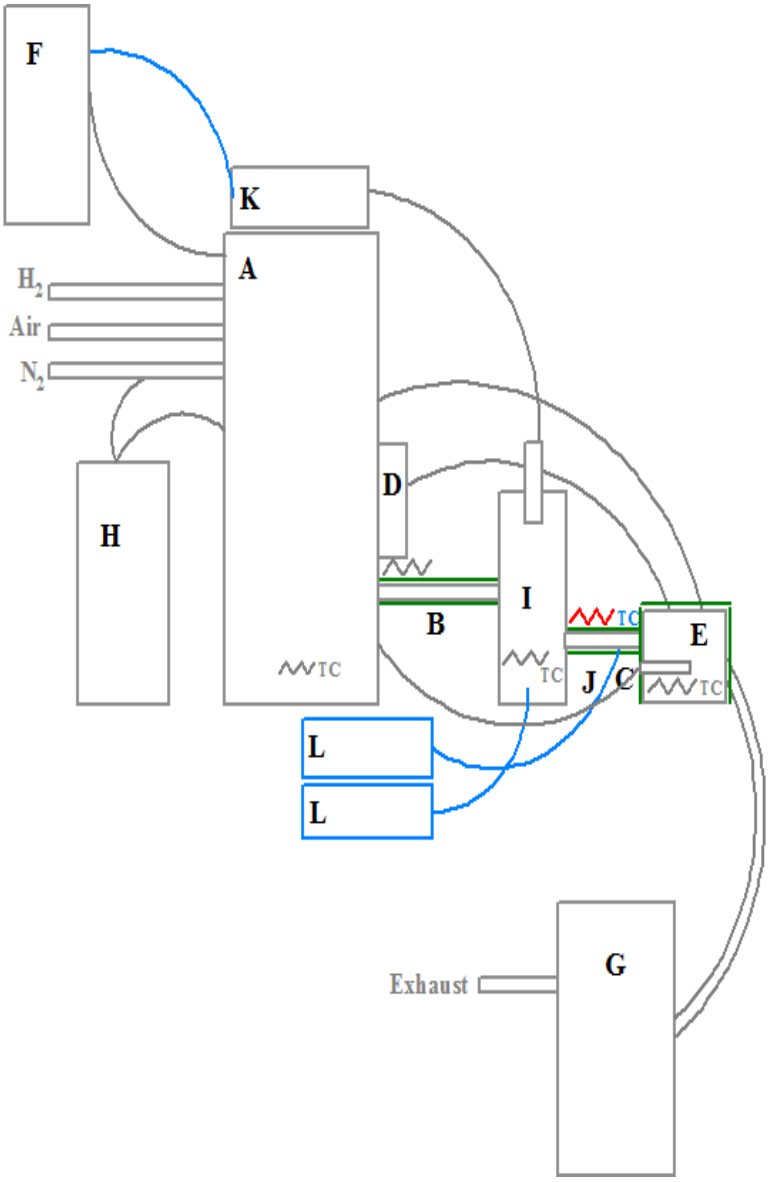

A Test Stand

B Heated fuel gas line

C Cartridge heaters

D Potentiostat

E Membrane conductivity clamp and cell fitting

F PC with FuelCell™ software

G Back pressure unit

H Pressurised water supply

I Heated dew point chamber

J Heated fuel gas line

K Vaisala dew point probe and data logging unit

L Control boxes for I and J

Figure 6-11 Diagram of the test station set up for the membrane conductivity test with additional insulation, heating and temperature control indicated in green, red and blue respectively.

Initial dew point data indicated a cold spot in the system which appeared as spikes in the dew point data. Figure 6-12 shows the measurement of the dew point at 120 °C but this data was characteristic of measurements over the full test range.

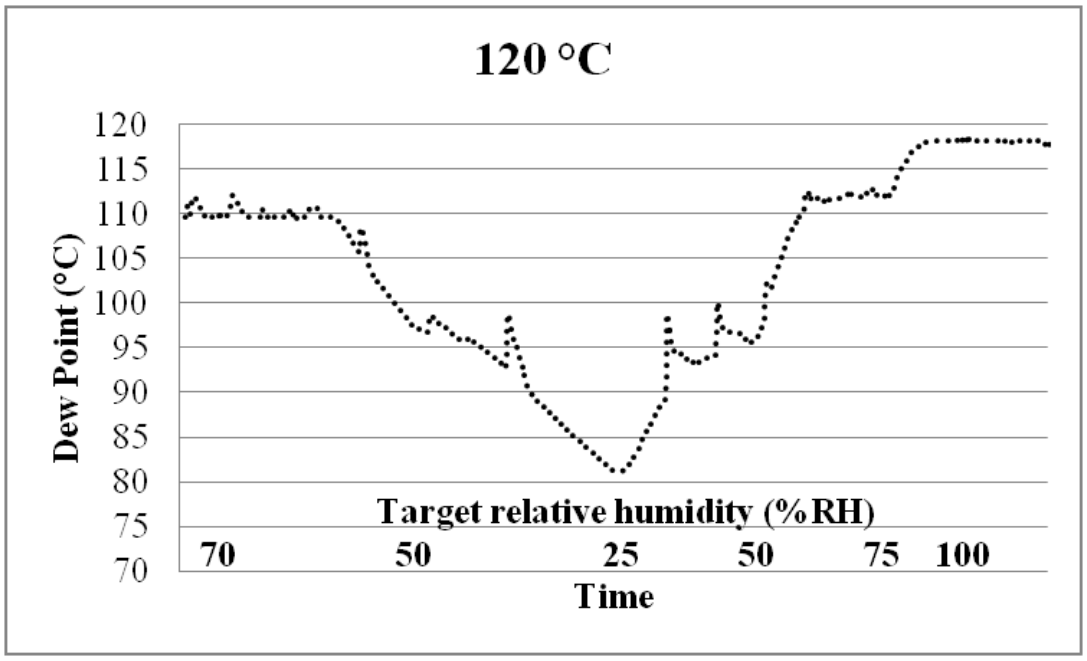

Figure 6-12 Initial dew point measurements indicating cold spots in the system.

A possible cold spot was identified at the Swagelok connection between the heated gas line from the test stand and the dew point chamber (B & I) and/or at the input port for the dew point probe (at the top of I). The line heating from the new gas line between the chamber and the cell (J) was extended to cover the Swagelok fitting, allowing combined control of the two components via the control boxes (L). As the thermocouple from the control box (L) was imbedded in the gas line insulation at J, a freestanding thermocouple (M) was inserted between B and I to monitor the temperature of the heated gas line at the point where it enters the dew point chamber. Additional insulation was added at the dew point port and to avoid gas leaks, a safety wire was applied to secure the probe to the Teflon fitting at the top of the heated chamber (I). The four input fittings for the platinum probes at the top of the membrane clamp (E) had to be adjusted frequently to avoid gas leaks, possibly adjusting slightly under heating/cooling conditions. A hydrogen monitor was used throughout testing to detect gas leaks. Figure 6-13 shows the final system which was used for all data reported in Chapters 7 and 8.

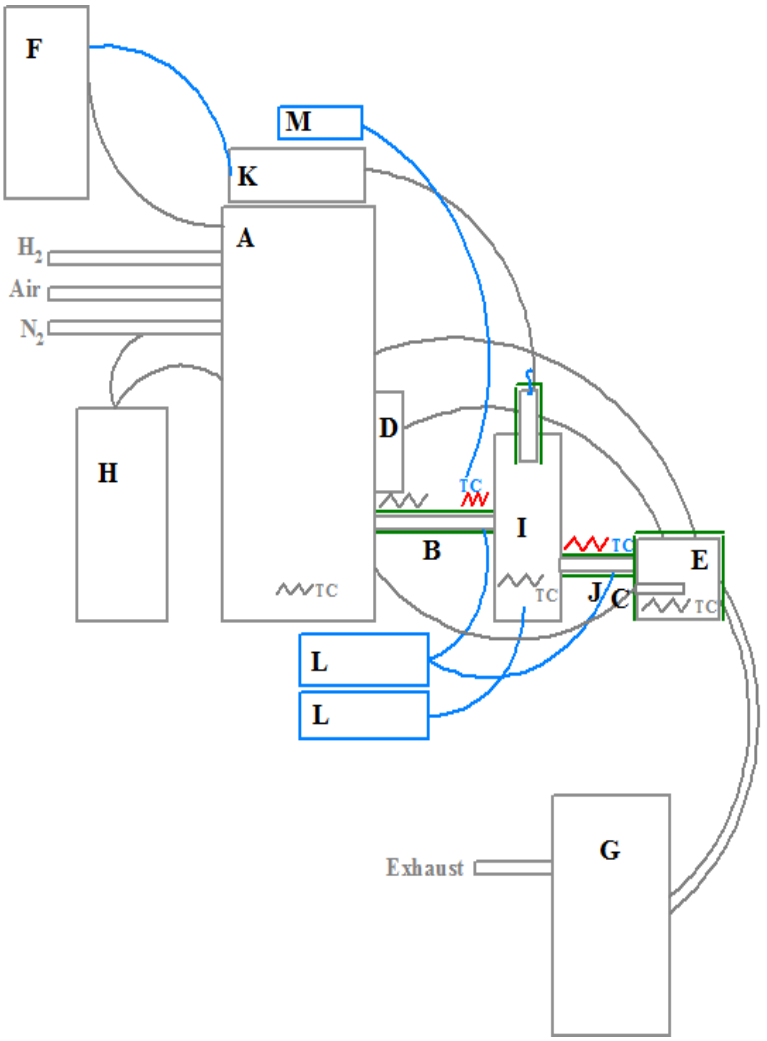

A Test Stand

B Heated fuel gas line

C Cartridge heaters

D Potentiostat

E Membrane conductivity clamp and cell fitting

F PC with FuelCell™ software

G Back pressure unit

H Pressurised water supply

I Heated dew point chamber

J Heated fuel gas line

K Vaisala dew point probe and data logging unit

L Control boxes for I and J

M Multimeter

Figure 6-13 Schematic of the optimised test

Figure 6-14 shows the results of the dew point calibration process. The dotted line shows the measured optimised dew point through the test cycle for membrane conductivity. The circles show the target dew point and the squares the temperature that was set on the test stand in order to obtain the target values. It was observed that, particularly at the higher humidity levels, and increasing with temperature, that the dew point setting had to be adjusted downwards on the test stand to obtain the desired measured values.

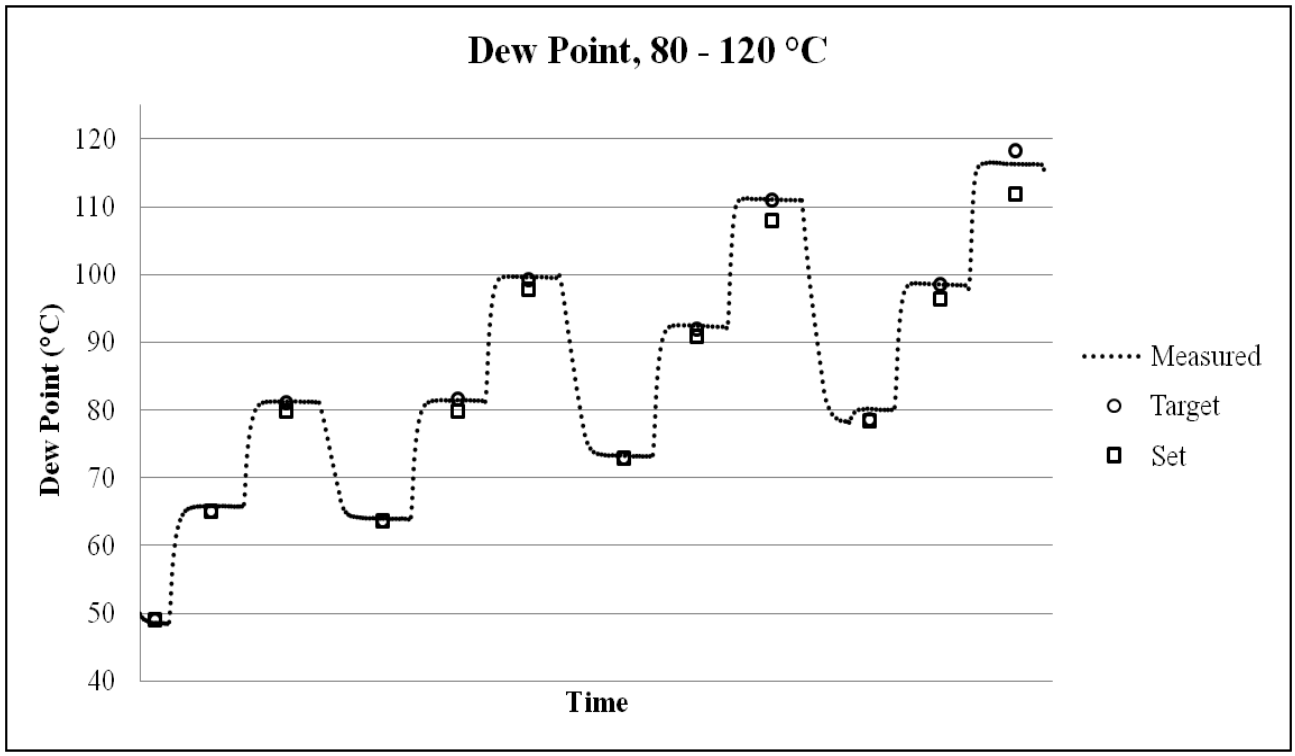

Figure 6-14 Target dew point values, measured values and the respective values set on the test stand. The test run was carried out at 25 %RH for 80 °C, 100 °C and 120 °C, then it was repeated for 50, 75 and ~95 %RH. The time scale reflects the duration of the test regime (around 36 hours).

The data for the same test sample shown in Figure 6-10, but tested under the calibrated dew point settings, is shown in Figure 6-15. It can be seen that the proton conductivity measured was now in-line with measurements taken under the same operating conditions, at three different sources, at least up to ~95 %RH.

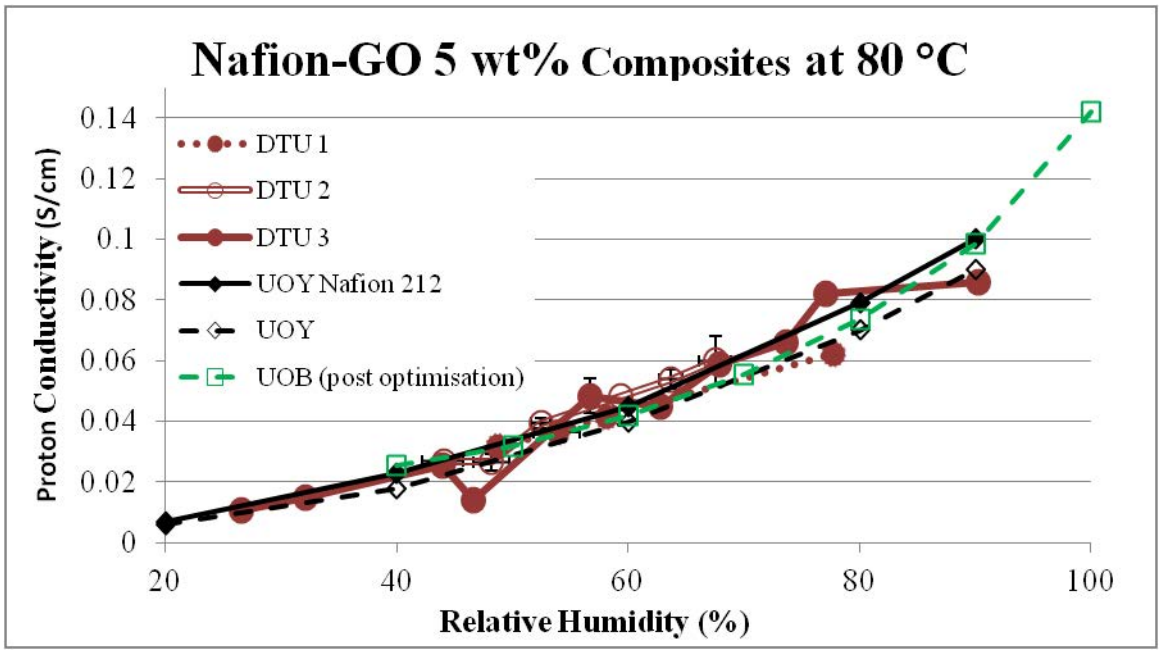

Figure 6-15 Proton conductivity measured for Nafion-GO 5 wt% at UOB (green), under calibrated dew point conditions.

6.5 Test Protocol Optimisation

The main benefit of the automated high temperature test station was the ability to run membrane conductivity or polarisation tests through the full set of test conditions without the need for user input. This allowed test time to be maximised as tests could be programmed to run overnight.

The test stand, as manufactured, and used without modification, could be programmed by the supplied software to operate in this way. Due to the optimisation of the test system, required to maintain the temperature and humidity settings, some modification of the test procedure was required in order to allow for the continuation of automated test sequences as much as possible.

First, due to the top operating temperature of 120 °C, the system required pressurisation to maintain humidification up to ~100 %. The back pressure was not controlled by the software, but manually adjusted by dials on the back pressure unit. In initial testing sequences, separate runs were programmed for the three target temperatures. Testing at 80 and 100 °C was undertaken at atmospheric pressure after which the pressure was increased for the 120 °C sequence. The ultimate goal was a continuous test sequence through the temperature and humidity ranges to ensure repeatability of test conditions and allow for the accurate comparison of data. Hence the back pressure was set at 1.3 bar (2.3 bar total) for all tests. The dew point values calibrated and shown in Figure 6-14 were representative of these operating conditions.

Second, the additional two control units for the heating of the dew point chamber and the extra section of heated fuel gas line (L in Figure 6-13) were not integrated into the commercial test stand, and hence also not controlled by the software. The temperature of both units was set at 130 °C in order to maintain the temperature above the dew point throughout the test sequences. Timer switches were installed, as a safety measure, in order to be able to switch the heating off at the end of the test run. The test sequence ran over more than 24 hours and therefore required one user interaction in the duration. The other functions of the test stand could be programmed so that at the end of the test run, the cell and humidifier temperature adjusted to 25 °C. Pressure loss (caused by a gas leak) would result in automatic shutdown of fuel gas and under these conditions nitrogen would flow freely through the system. The test could therefore be run safely overnight and 7 day per week. The only limitation to testing was if the centrally supplied nitrogen or hydrogen ran out or if a power cut was experienced. If a test sequence was interrupted (which happened frequently),

a fresh sample was prepared and the test restarted to avoid any effects on the proton conductivity caused by test conditions.

The final step in the optimisation and calibration of the test stand was to obtain a set of base line data for Nafion 212 which would be used as reference for composite membrane data. Figure 6-16 shows the result of three complete runs with error values included. The full test sequence is described in Chapter 7, but it can be seen that data is collected at three temperatures and 4 levels of relative humidity. As a reference, the conductivity measured for Nafion 212, at 80 °C, by UOY is plotted and shows good agreement. The samples were soaked in water prior to testing as this was found to produce the proton conductivity values closest to published data (this is discussed in Chapter 7).

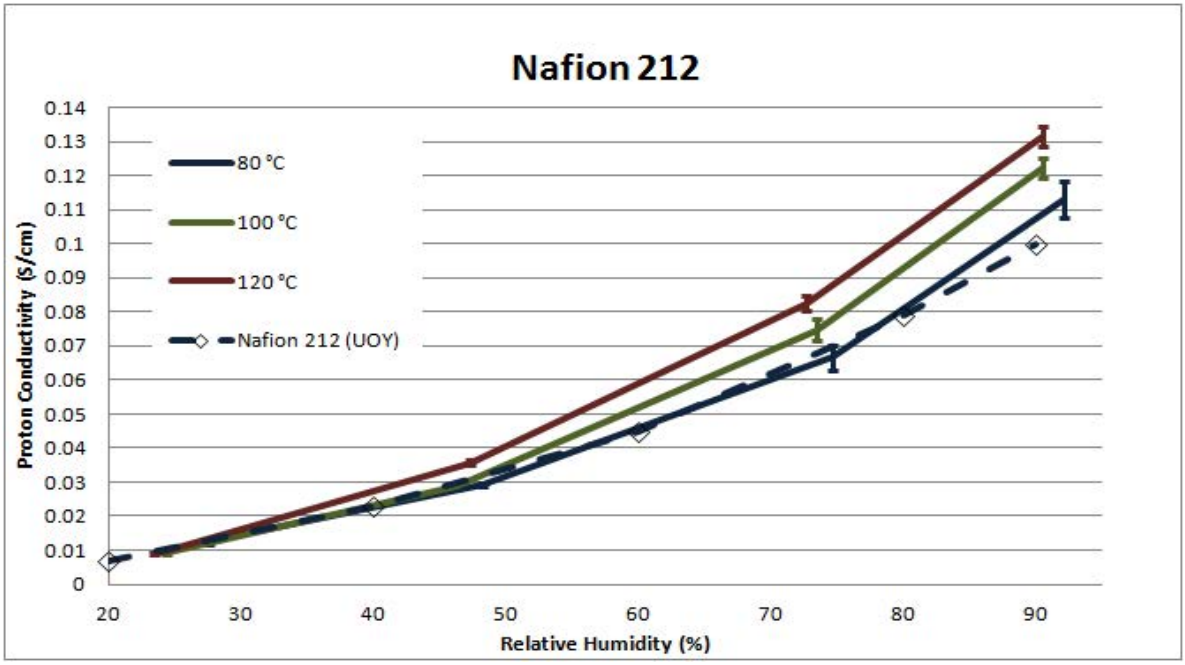

Figure 6-16 Proton Conductivity for Nafion 212 tested at 80, 100 and 120 °C over a range of relative humidity. The black dotted line is data obtained at UOY at 80 °C and is intended as a reference.

The final test sequence in the test protocol was a 6 hour test at stable conditions of 120 °C and 50 %RH. Measurements were made at half hour intervals to investigate the stability of the material under these conditions. The results are shown in Figure 6-17 for the same three runs and the mean of the three measurements is given. Proton conductivity for Nafion 212 at 120 °C and 50 %RH was measured to be 0.04 S/cm and agreed with published literature values [156].

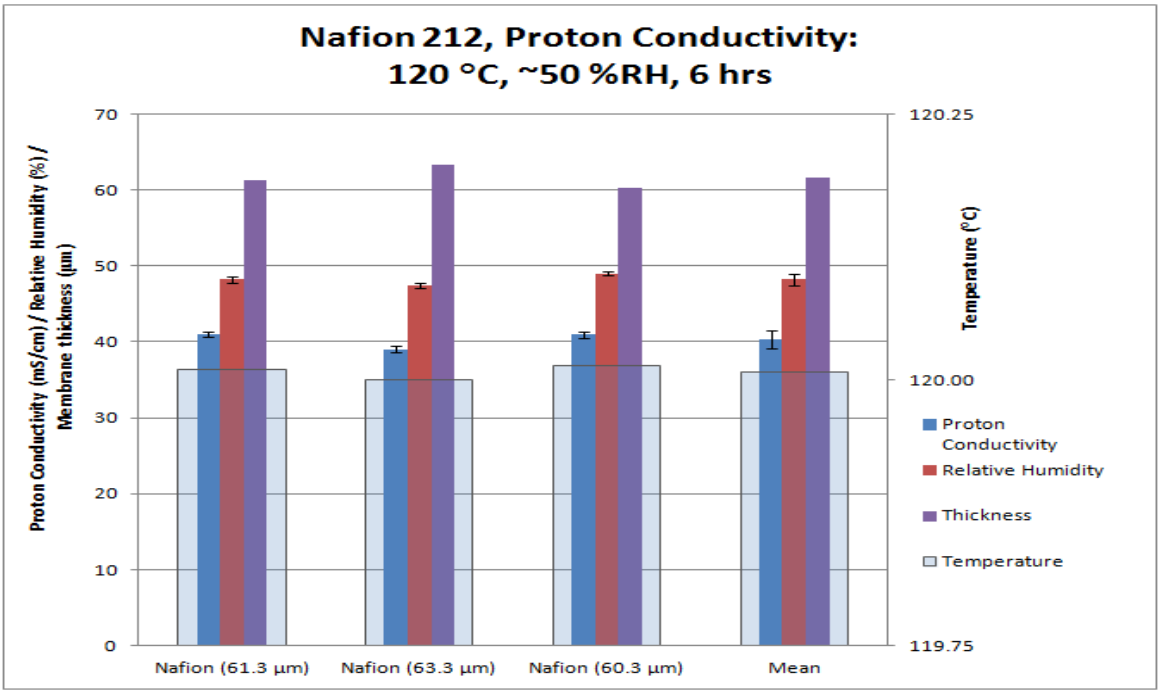

Figure 6-17 Proton conductivity for Nafion 212, measured over six hours. The data for three runs and the mean data are shown.

6.6 Conclusions

The Scribner high temperature test stand was commissioned and calibrated in the Fuel Cell lab at the University of Birmingham to enable in-house testing of membrane samples and MEAs. Extensive optimisation of the system was required for the accurate control and measurement of the dew point, temperature and resistance measurements.

Poor contact of the membrane samples with the platinum electrodes resulted in the requirement of a replacement membrane clamp due to some manufacturing irregularities. It also led to the conclusion that thicker membranes, ~50 μm, were best suited for use in the equipment. The system required extensive insulation of the test fixture and gas lines to maintain stability at 120 °C of both the temperature and the dew point. The dew point settings had to be adjusted from the theoretical values set on the test stand due to discrepancy between the set values and the values measured by the in-line dew point probe. As a result of additional gas lines and a heated dew point chamber, two extra control units were required to regulate the heating of these parts. Data collected was compared to measurements conducted at the University of Yamanashi and the Technical University of Denmark, and after calibration and optimisation, good agreement was found. Baseline data was measured for Nafion 212 and was used as the reference value in further resistance testing.

At the end of this part of the project, it was possible to conduct continuous test runs, with accurate measurement of dew point, temperature and resistance values. The system was continuously heated and insulated and operated at elevated pressure to maintain the humidity at 120 °C.

The last two chapters report the resistance data for the composite membranes and the in-situ polarisation for MEAs prepared from the same samples.

CHAPTER 7 CHARACTERISATION AND EX-SITU TESTING OF COMPOSITE-PEMS FROM LOW TEMPERATURE TO INTERMEDIATE TEMPERATURE

7.1 Introduction

This chapter addresses the fourth objective for this project; ex-situ analysis of composite membranes in a temperature range of 80 – 120 °C and 25 – 95 % relative humidity.

The first section discusses the characterisation of the membranes for water uptake ability and ion exchange capacity. Following this the proton conductivity data is presented and discussed.

The data is presented in two parts, for two reasons. At the start of the project proton conductivity was tested off-site, until the high temperature test stand (as described in Chapter 6) was purchased in the third year of the project. The results from these initial tests are presented first and formed the basis for pursuing the investigation into composite membranes prepared with GO and Nafion. The second reason for presenting the data separately is that the first sets of membranes were prepared to be 25 μm thick. For reasons that were explained in Chapter 6 and to enable comparison with the commercial standard, Nafion 212, the thickness was changed to 50 μm, and the bulk of the data reported focuses on these membranes.

The second set of data is hence from measurements taken in-house, on the Scribner high temperature system and includes a brief section on the final optimisation of the GO doping and casting. The first sections shows proton conductivity for various sets of tests carried out

to investigate the effect of the thickness of the membranes (brought about by water swelling) and the different types of GO fillers (which were described in more detail in Chapter 5). The last section is on a full set of composite membranes and the data presented a different trend to what was obtained externally. Findings throughout are related to the literature on GO-Nafion composites which were discussed in the literature review in Chapter 2. The ex-situ MEA data is described in Chapter 8.

In the discussion, the Nafion 212 membrane is referred to as the commercial membrane. The recast membranes are respectively referred to as the pristine membrane, for the 0 wt% GO loading, and the composite membranes, for the 0.25-10 wt% GO loading, where the distinction is required. The membranes sets are named GO-1, GO-2 etc. to indicate the different batches which were prepared. GO-1 and GO-2 were from a batch of GO prepared by a colleague and was used to prepare the thinner membranes. The remainder of the membranes were prepared from one batch of GO which was prepared purely for this study.

7.2 Composite Membranes – 25 µm, off-site proton conductivity measurement

7.2.1 Water Uptake and IEC

The water uptake (WU) and ion exchange coefficient (IEC) for the thinner membranes are shown in Figure 7-1 to Figure 7-3. The first set of data showed a clear trend of increasing WU from Nafion 212 to the membrane with 5 wt% GO, after which values dropped for the membrane containing 10 wt% GO. The IEC values for the recast membranes were lower than for Nafion 212 and appeared in similar range for the 0 – 5 wt% membranes (with a slight

downward trend as the GO loading increased), after which it dropped sharply at 10 wt%. As it was not clear where the maximum was, i.e. between 0 - 5 wt%, a second set of membranes were prepared with an extended range of filler loadings. Following on from the WU and IEC, as well as the proton conductivity data (which is described below), the series was extended between 0 – 1 wt%, but omitted the 10 wt% loading due to poor performance.

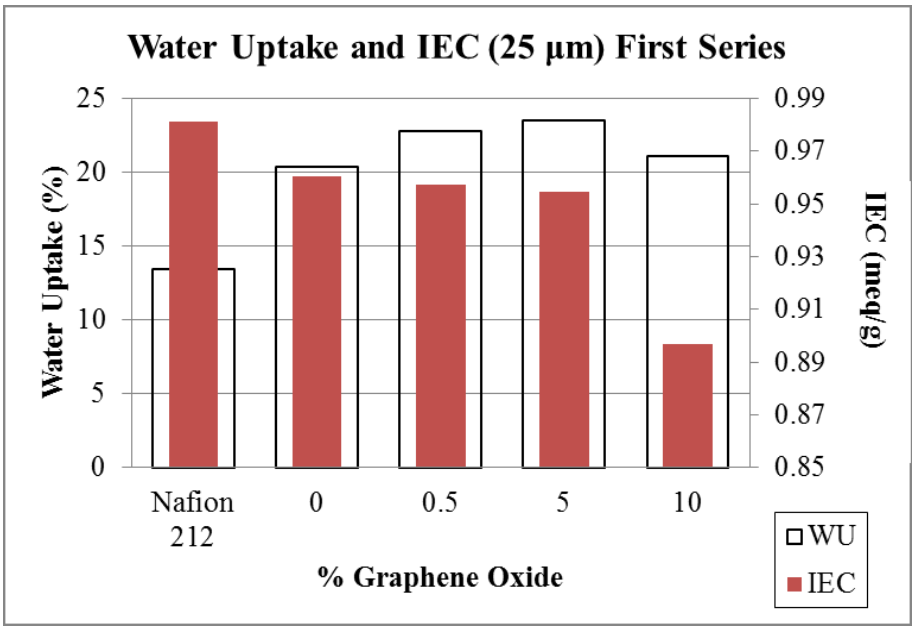

Figure 7-1 WU and IEC for the first set of Nafion-GO composite membranes

With respect to the WU (Figure 7-2), the trend was slightly unclear, but the recast membranes maintained higher values than that measured for Nafion 212. The composite membranes all showed lower values than the pristine recast membrane (0 wt% GO) and the highest values were measured for 0.5 and 1 wt%. IEC values were consistently higher than both the commercial and the pristine membrane, but the trend was interrupted between 0.5 wt% and 1 wt%, indicating that a maximum would lie anywhere between 0.5 and 5 wt%.

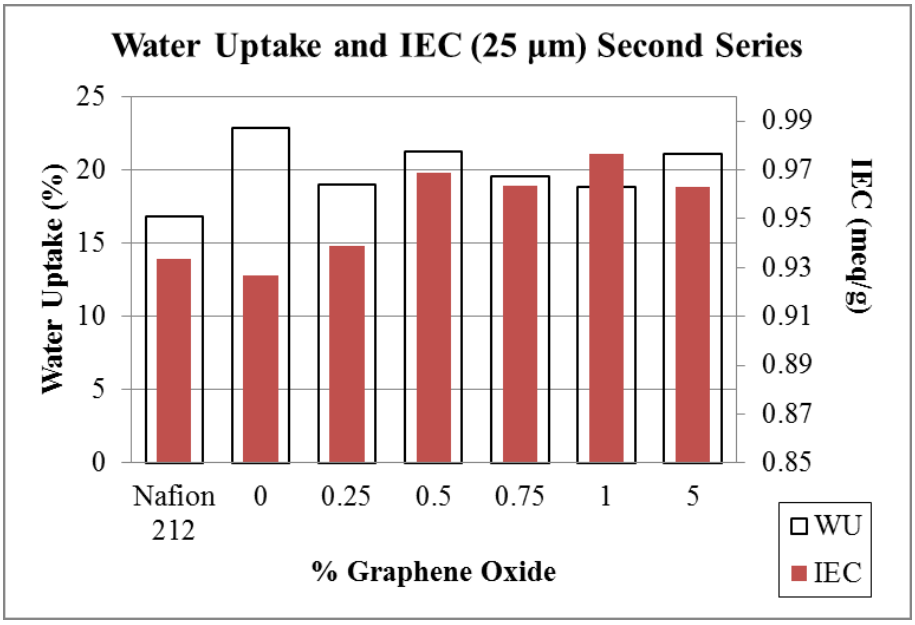

Figure 7-2 WU and IEC values for second set of Nafion-GO composite membranes, with a larger range of filler loading (10 wt% was omitted due to poor WU, IEC and conductivity data)

It was clear from a comparison of the two sets of data that the values for both the WU and IEC varied to a fairly large extent. The accurate preparation of the membranes with small amounts of GO filler was judged to be the most important factor in these anomalies. In order to establish an accurate and repeatable data set, 2 further sets of the membranes in the series were prepared and the WU and IEC were measured. Since the most data was available for the 0, 0.5, 1 and 5 wt% membranes, further studies were focussed on this range. The data for the first two sets were included in the mean values shown in the top part of Figure 7-3. The increased WU for the recast membranes was confirmed, but the values decreased as the GO loading was increased up to 1 wt%, after which it rose. The IEC values increased smoothly up to 1 wt% membrane and then dropped. When the data was evaluated including the error (at this stage data from 4 sets were collected), as is shown in the bottom part of the figure, the trends remain largely consistent, but the largest error (particularly for the IEC measurement) was present for the composite membranes.

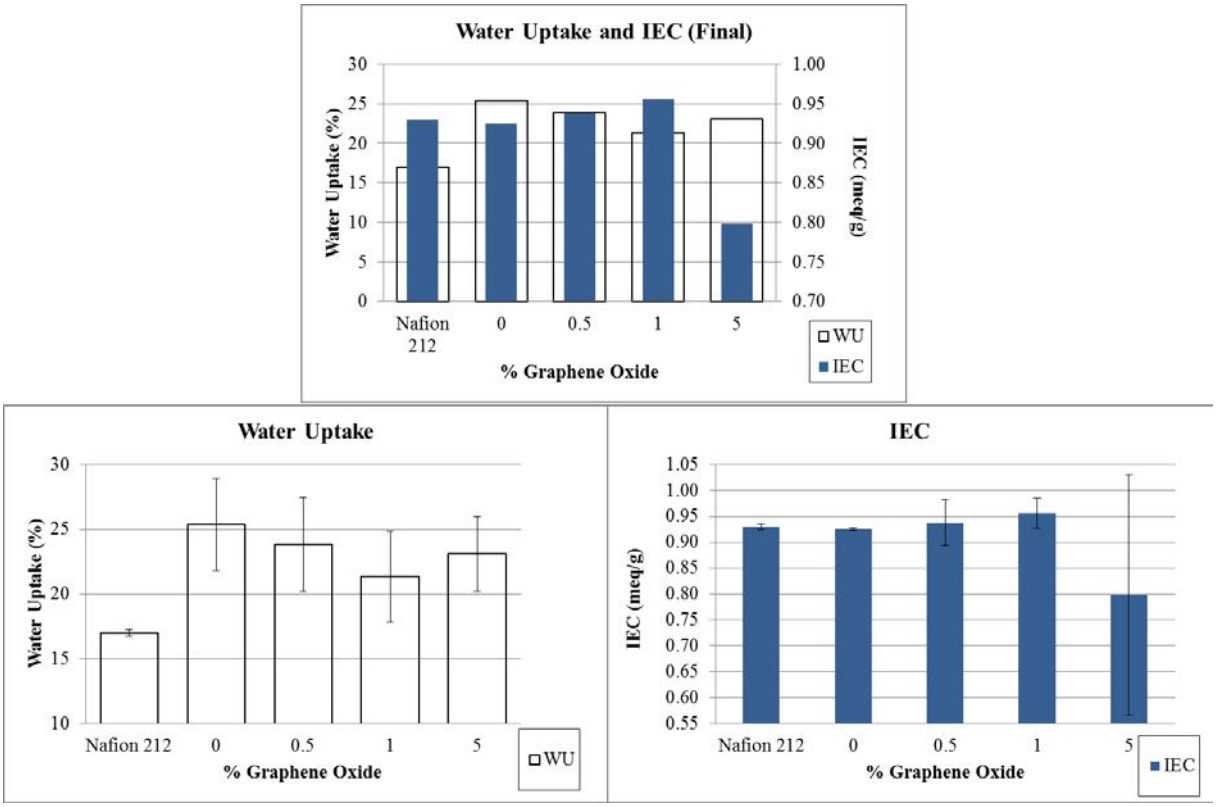

Figure 7-3 Combined data for all 25 µm Nafion-GO membranes prepared

Various reasons could be given for the large error ranges. The most apparent reason, already mentioned, was ascribed to the difficulty in controlling the filler level in the membrane. As the quantity required to prepared these membranes was so small, and due to the hygroscopic nature of the material – combined with the health and safety directive for nanomaterials, requiring the weighing of GO in a desktop fume hood – the accurate control of the filler loading between samples proved challenging. Each set of membranes throughout the study was prepared freshly for testing. This was to insure that the Nafion solution that was used was of the same quality and that the membranes had all been subjected to exactly the same temperatures and laboratory conditions.

The GO used in this part of the study was obtained from a colleague (prepared following the modified Hummers Method described in Chapters 2 and 3), in dried batches as required. It is

therefore possible that small compositional differences between the batches were present. As described in Chapter 6, one batch of GO was prepared and used solely for this study, and the thicker membranes were all prepared from this one batch of GO. Frequent XPS analysis was carried out to confirm the C-O ratio throughout to confirm the uniformity and consistency of the large batch of the prepared GO.

A further effect was possibly related to the samples used for the WU and IEC tests. For accurate WU and IEC measurements around 100 mg of sample was required, ideally in one continuous membrane section. This unavoidably incorporated some of the variations in the sample thickness and the distribution of the GO, which could not be avoided in preparing the samples. The explanations seemed reasonable when the error for the Nafion 212 samples were considered, i.e. that they were in a much smaller range than the composite membranes. This was a further indication that thicker membranes (and hence larger quantities GO and smaller dimension samples) would provide more robust data.

7.2.2 Proton conductivity

Membranes were sent to UNIDO ICHET facility in Turkey for proton conductivity Testing at this facility was carried out using the same membrane conductivity system as which had been selected for the University of Birmingham high temperature test stand. The BekkTech membrane clamp was used and measurements could be made up to 90 °C and over a range of humidity. The turn-around time was lengthy however, and control of the testing sequences was not always reliable notwithstanding the request that was placed, and will be pointed out as the data is discussed. In each case it was requested that the membranes were tested in the

full temperature range available and at each humidification step. At least three measurements for each data point were requested.

The first set of data is shown in Figure 7-4 for the membrane series with 0 – 10 wt% GO. Testing was carried out at 80 and 90 °C and between 25-100 %RH. No conductivity was measured for Nafion 212, the reason for this was not apparent, but was possibly caused by confusion with the double backing layers on the commercial membranes. Only one measurement was made at each data point. At both temperatures the 0.5 wt% membrane showed the highest conductivity and the conductivity dropped for the higher loadings. Hence the proton conductivity data matched the IEC measurements for the composite membranes only (as seen in Figure 7-1, the IEC values are 0.5 > 5 > 10 wt%), and the WU trend was only upheld between the 0 wt% and the 0.5 wt% membranes (with one exception, at 90 °C and 75 %RH). A possible explanation for this was ascribed to the fact that WU and IEC measurements were made at room temperature, as per convention.

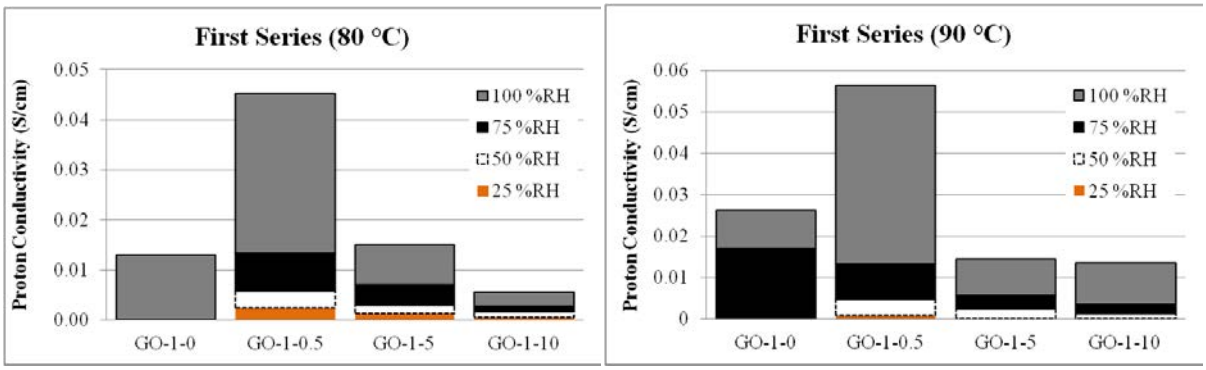

Figure 7-4 Proton conductivity for the first series of 25 µm recast membranes

Furthermore, at 80 °C and reduced humidification, the 0 wt% membrane showed no proton conductivity. At 90 °C the 0 wt% membrane had the highest proton conductivity at 75 %RH compared to the composite membranes, but under other humidity conditions the conductivity

was higher for the 0.5 wt% membrane. This could possibly indicate that at 90 °C and 75 %RH, the actual conditions in the system were closer to the ideal conditions of 80 ° and ~100 %RH showing that some optimisation of the system was perhaps necessary as was the case for the system commissioned and calibrated at UOB (as described in Chapter 6).

The proton conductivity for the second series is shown in Figure 7-5. Testing was carried out at 80 and 90 °C, both at full humidification only. Three measurements were taken for each sample, and where more than one resistance value was reported, the error is indicated. No measurement was possible for the 0 wt% sample and at 90 °C no measurements were reported for the 0.5, 0.75 and 1 wt% membranes. The composites all showed lower proton conductivity than the Nafion 212 sample (which in this case showed much lower resistance compared to the performance at 80 °C), in contrast to both the WU and IEC values in Figure 7-2. At the lower temperature range a trend appeared for the recast membranes, with a maximum at 0.75 wt%. As it can be seen from the absence of an error bar however, only the measurements for 0.5, 1 and 5 obtained more than one value. At 90 °C the proton conductivity for the composites was negligibly low.

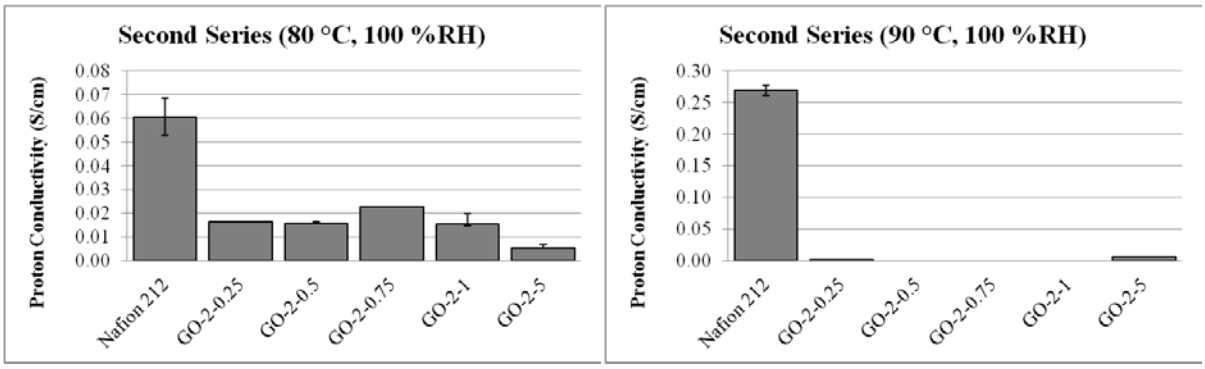

Figure 7-5 Proton conductivity for the second series of 25 µm recast membranes

At this stage in the project, the UNIDO-ICHET facility announced its closure, and Figure 7-6 shows the collated data for the two sets of membrane tests. Again, where more than one value was available, the error was calculated. Even though there was apparently a clear trend at 80 °C, which reached a maximum at 0.5 wt% GO loading, a conclusion in this line would have been tenuous. Firstly, the error indicated that for 0.5 and 1 wt% a large margin of proton conductivity values would have had to be considered and secondly, not enough data points existed for some samples.

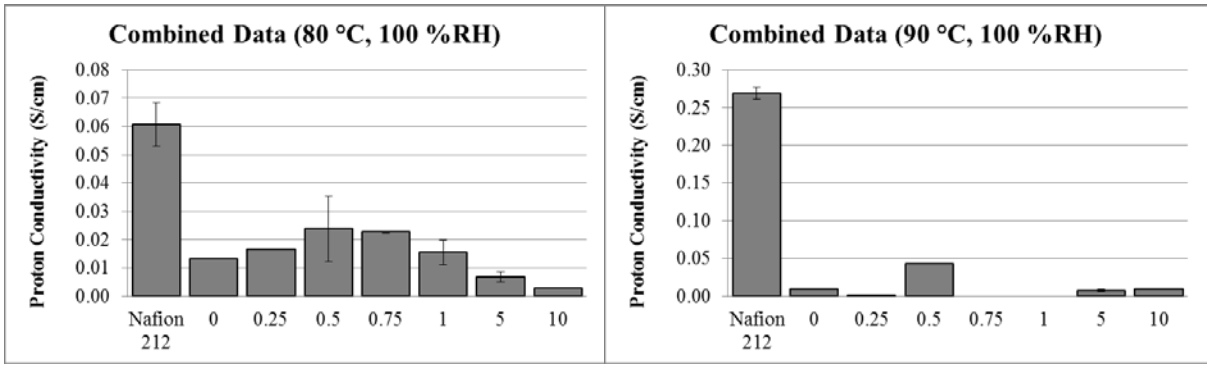

Figure 7-6 Combined proton conductivity data for the first and second 25 μm composite membrane series.

The following conclusions were drawn. The water uptake for recast membranes was consistently higher than for Nafion 212. This could not have been due to remaining solvent or water in the recast membranes, since they were dry pressed for two days prior to testing and heated in the vacuum oven until no further difference in weight was measured. The increased WU therefore must have been a result of a slightly different polymer structure after casting. Water uptake values were the least consistent with proton conductivity. Proton conductivity showed some semblance to the ion exchange coefficient. When all the data was collated and the error calculated, IEC values predicted a maximum between 0.5 – 1 wt% and this was, to some extent confirmed by the proton conductivity measurements at 80 °C. It was reasonable to conclude that the optimal filler loading would be between 0.5 and 5 wt%, as the

first series indicated low IEC and proton conductivity for the 10 wt% membrane. As the ex-situ proton conductivity was measured in-plane, it was concluded that the highest quantity of filler loading disturbed the optimal equilibrium between the quantity of polymer and filler material. Further detrimental implications for in-situ testing were predicted, as the through-plane motion of the protons would become more tenuous and increase the resistance.

The membranes for all further tests were prepared to be 50 μm in thickness, and the maximum filler loading was 5 wt%. The GO used for these membranes were all from one batch that was synthesised solely for this study.

7.3 Composite Membranes – 50 μm, in-house proton conductivity measurement

7.3.1 Water Uptake and IEC

The first step in the continuation of the membrane WU and IEC testing was to obtain a standard data range for Nafion 212. All the chemicals used for the test (sodium hydroxide, sodium chloride and hydrochloric acid) were replaced and five measurements were made. The values were obtained as shown in Table 7-1. For each set of recast membranes that were tested subsequently, a Nafion 212 sample was included, and if the values for the commercial membrane did not fall within the shown range, the data was rejected for the whole set. This was in order to eliminate any external factors that could influence the values.

Table 7-1 Standard data range for Nafion 212

	Mean	Standard Deviation
Water Uptake (%)	16.80	± 0.5
Ion Exchange Coefficient (meq/g)	1.04	± 0.02

Continuing on from the first set of experiments, the thicker membranes were prepared in the filler range of 0.5 – 5 wt% and the data is shown in Figure 7-7 and Figure 7-8. To broaden the range, a membrane with 3 wt% GO was prepared to establish an optimum filler loading. The trend resembles that which was found in the first part of the study, for the thinner membranes. Overall the recast membranes had higher water uptake than the commercial membrane, and the WU decreased from the pristine membrane down to the 1 wt% membrane, after which it increased again. In this case however, the membrane of 3 wt% which was added showed a WU value which was at least as high as the pristine membrane.

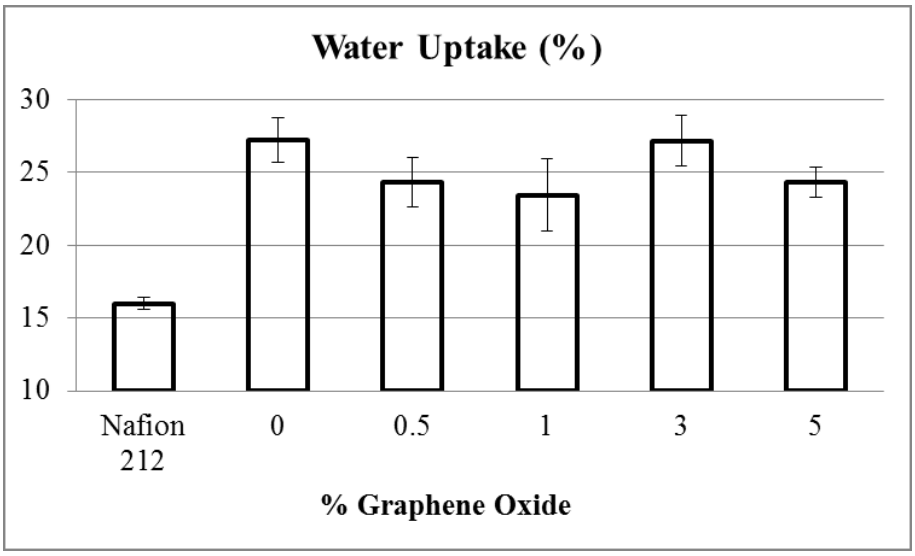

Figure 7-7 WU for the 50 µm Nafion-GO membranes prepared

The IEC values showed a similar trend to the first set, with values increasing from the pristine membrane up to 3 wt% (with the exception of the 1 wt% membrane) after which it

dropped at 5 wt%. It appeared that the highest IEC values, higher than for Nafion 212 would be found between 3 – 5 wt%, when the error was taken into account. Overall the measured IEC was higher than which was measured in the first set (by around 0.1 meq/g for Nafion 212) and possibly reflected the replacement of all the chemicals used for the test, and the refinement of the test protocol. The largest error was still in the measurement for the 5 wt% membrane, but for most of the measurements the error range fell in the same range as that for Nafion 212. A possible explanation for this was the larger quantity of GO in the membrane, and hence the increased variation of oxygen functional groups present.

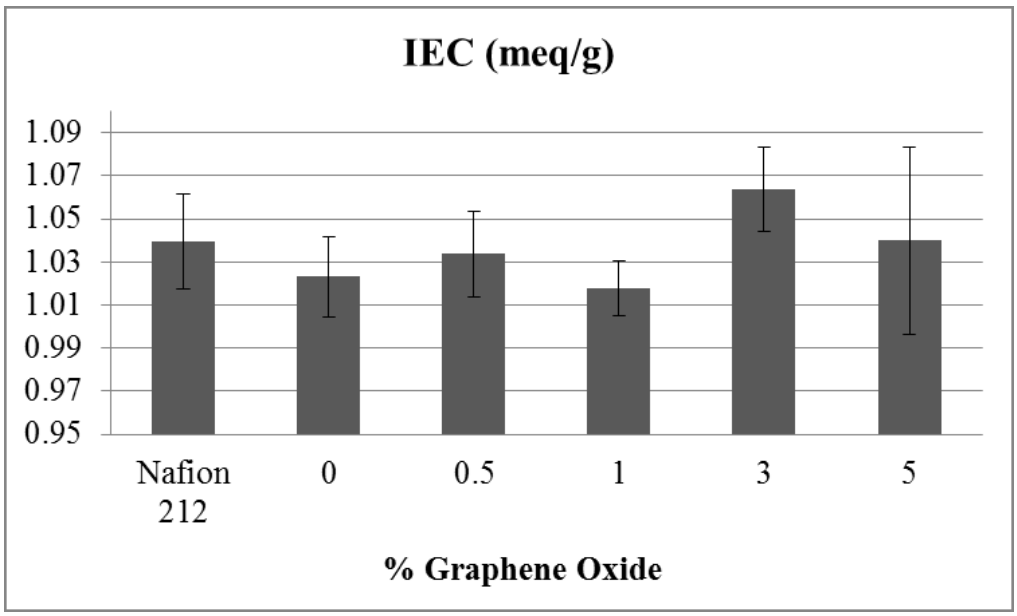

Figure 7-8 IEC for the 50 µm Nafion-GO membranes prepared

Hence both the WU and IEC values indicated that, within this range, and optimum filler loading was at 3 wt%.

When the values were compared with the literature which was reviewed in Chapter 2, it was found that each study presented different value ranges and dissimilar trends. Figure 7-9 and Figure 7-10 show the data (if it was given) for the WU and IEC for membranes prepared with GO (without functionalisation) to allow comparison. For the WU, it was clear that a wide

range of values were presented and that, particularly at the higher filler loadings, a large degree of variation occurred. At lower filler loadings this study showed the closest resemblance to the trend reported by Lee *et al.* [101], with an initial drop in WU from the pristine membrane to 0.5 wt% GO. Whereas Lee *et al.* reported an evening out of values between 0.5 – 3 wt% (data was only given for 0, 0.5, 3 and 4.5 wt%) , this study showed a further decrease to 1 wt%, after which the maximum value was obtained at 3 wt%. This presented some similarity with the Kumar *et al.* [91] results which showed an increase in values from pristine to the maximum at 4 wt%. Whilst both this study and Kumar *et al.* reported a decrease in values after the maximum, the Lee *et al.* report showed no further data after the maximum value given at 4.5 wt%. Hence the maximum between the three studies was shown between 3 – 4.5 wt%, and it was possible that this could be attributed to the weighing/measuring issues attributed to the highly hygroscopic GO or possibly due to uneven distribution of GO in the membrane.

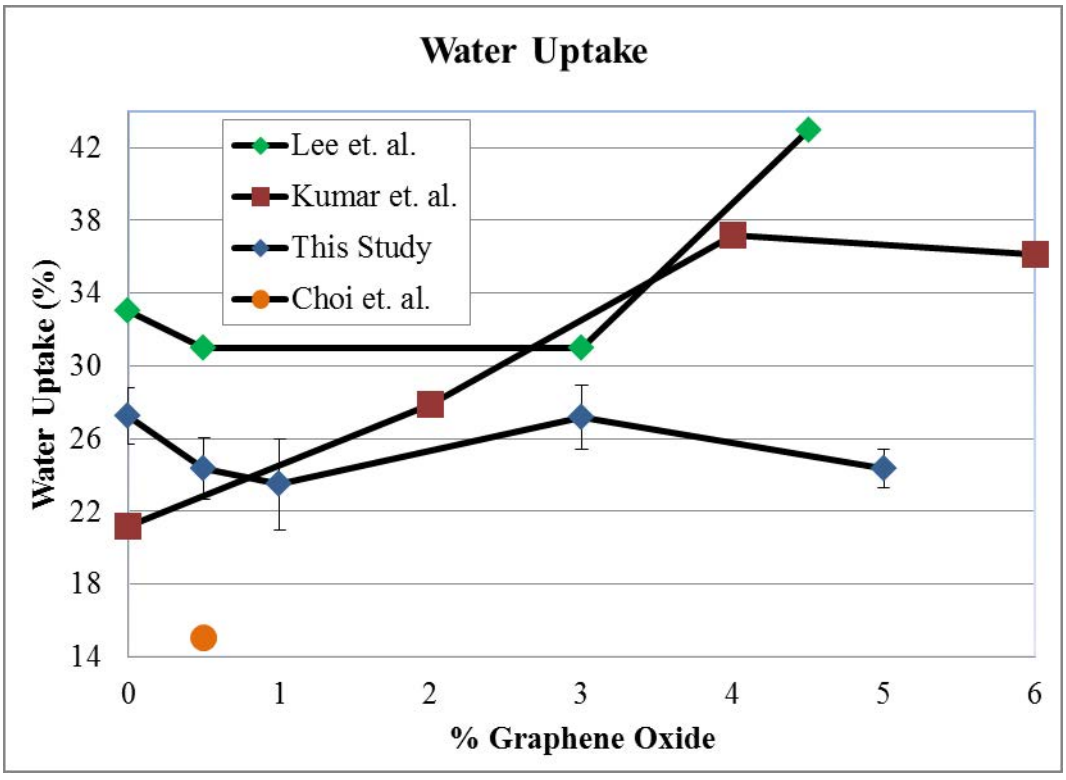

Figure 7-9 Comparative water uptake values from literature and this study [91, 101, 103]

In general, the literature that was reviewed did not report data for the confirmation of filler loading in the composite membranes. The most accurate way to measure the presence of fillers in a composite membrane would be by thermogravimetric analysis (TGA). This is however not always possible due to the corrosive nature of Nafion to the internal parts of the equipment. A source of error in TGA data would also be presented by the changing nature of GO over the temperature range required to analyse a Nafion composite, which is between 0 – around 600 °C. It has been shown that pure GO shows mass loss at under 100 °C due to water loss, at around 200 °C due to the start of the reduction process and over the range of 300-600 °C due to further loss of oxygen functional groups [83]. Analysis of the residue, after completion of the TGA run, would therefore not accurately confirm the loading. A certain range in filler loading should therefore be expected between different sets of membranes. Particularly, if it is stated that a membrane contains 3 wt% of GO, it is possible that the filler loading could fall in a range, rather than an exact percentage. It was possible to obtain some comparative TGA data for a 0 wt% and 1 wt% sample, the data is shown in Appendix A2 for information.

Little data was available for comparison of IEC data, but when compared to the WU data, it can be seen in Figure 7-10 that the IEC trend for the Kumar *et al.* study was very similar and that for this study, an exception from the trend occurred at 0.5 wt%. The WU value decreased from pristine to 1 wt%, whereas the IEC value first increased and then decreased through this range. Between 1, 3 and 5 wt% the trend remained the same.

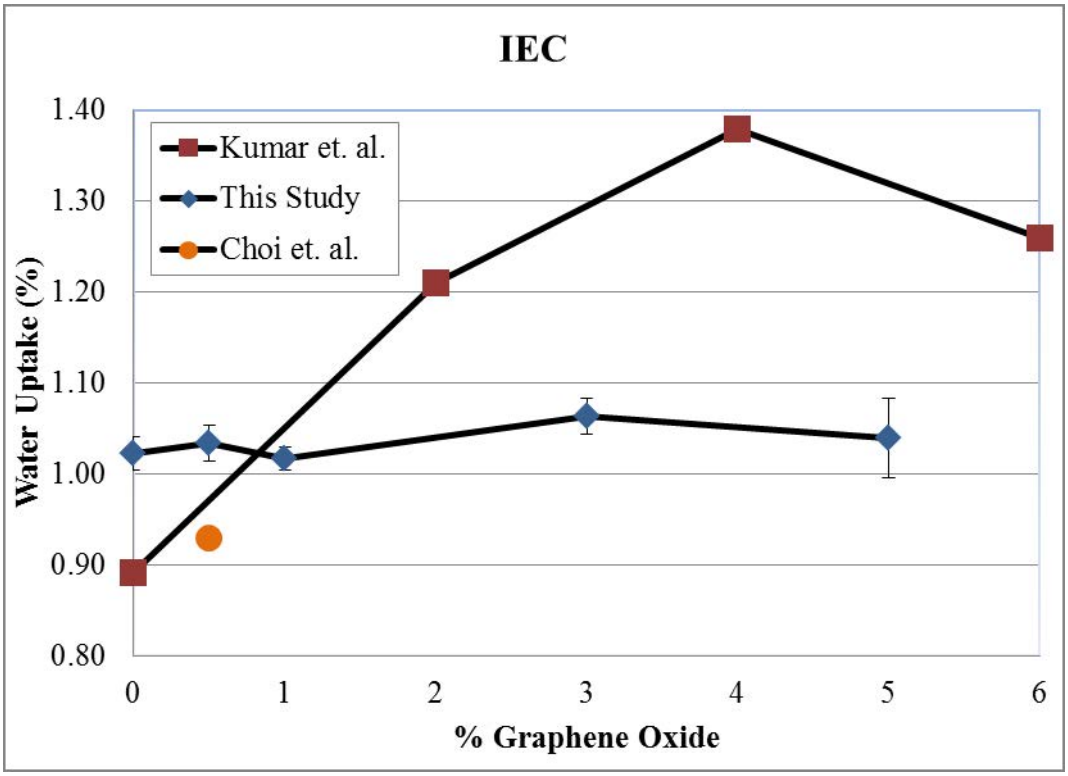

Figure 7-10 Comparative ion exchange values from literature and this study [91, 103]

7.3.2 Final Casting optimisation

Analysis of membranes prepared early in the study revealed uneven GO distribution and considerable agglomeration as is shown in Figure 5-7. The SEM analysis was initially undertaken to confirm that the GO was not accumulating at the bottom of the membrane as it was cast. Whilst this did not appear to occur, the many-sheet collections of GO was not desirable in a composite membrane, where good filler distribution is essential for optimal performance and durability of the membrane. The uneven distribution would not only lead to inconsistent proton conductivity performance in the fuel cell, but could lead to mechanical failure due to the lack of polymer binding in this region and the accumulation of absorbed

water which would lead to uneven swelling in the membrane. This could have been a further reason for the inconsistent data collected as described in the previous section.

Accordingly, the GO was pre-treated and incorporated into the membrane in a modified way from what was described in Chapter 3. Initially the weighed and dried GO was mixed with water and sonicated for 30 minutes prior to addition of the Nafion solution. It could be visually established that the GO was not well distributed using this method. Manual grinding with a pestle and mortar, prior to sonication in water produced membranes with a more uniform appearance, but the SEM images indicated that this was also not adequate. Subsequently, GO was dried (40 °C), ground in a pestle and mortar, dissolved in DI water (~3.6 mg/ml), ultra-sonicated (2 hrs) and centrifuged (4000 rpm, 30 minutes x 3), each time removing the top layer of the solution for further use. The concentration of the solution was calculated by removing a known volume and drying this in a petri dish until no further change in weight was observed. The GO (in solution) was combined with the Nafion solution to obtain the desired filler loading, stirred with a stirrer bar and dried in the oven as described in Chapter 3. The method produced the most visually uniform membranes, and was confirmed by SEM; GO sheets were evenly distributed throughout the thickness of the membrane, with no agglomeration.

7.3.3 Proton Conductivity

This section will briefly describe the test protocol used on the Scribner test stand, followed by a discussion of the proton conductivity data. The first sets of data investigated the effect of pre-treatment of the test samples, and different types of GO on the performance of the membranes. In order to obtain a balance between a reasonable filler loading that could be

accurately repeated, and optimal use of the finite GO stock, membranes were prepared with a filler loading of 1 wt% for these tests. The remaining tests represent testing of a set of membranes which were prepared in the range of 0.5 – 5 wt% GO loading.

7.3.3.1 Test protocol

Figure 7-11 shows the optimised test protocol which was used for membrane conductivity testing. Membrane samples were firstly soaked in water for at least two hours prior to fitting in the membrane clamp. After assembling the clamp in the test station, the temperature was set to 80 °C for the test cell and monitored until the temperature had stabilised before the heating was turned on for the humidifiers. This was done in order to prevent flooding in the test cell. Subsequently the temperature in the humidifiers was increased slowly, up to the desired dew point. The membrane sample was then allowed to equilibrate at 80 °C and 70 %RH for one hour.

The resistance measurements were then made for each temperature, starting at ~25 %RH, followed by 50, 75 and ~95 %RH. At each step the sample was stabilised at the relevant temperature and humidity for either 1 or 2 hours (as determined during the calibration described in Chapter 6), and then three measurements were taken, half an hour apart.

After the measurement was made for 120 °C and ~95 %RH, the humidification was decreased to 50 %RH and, over six hours, the resistance was measured every half an hour.

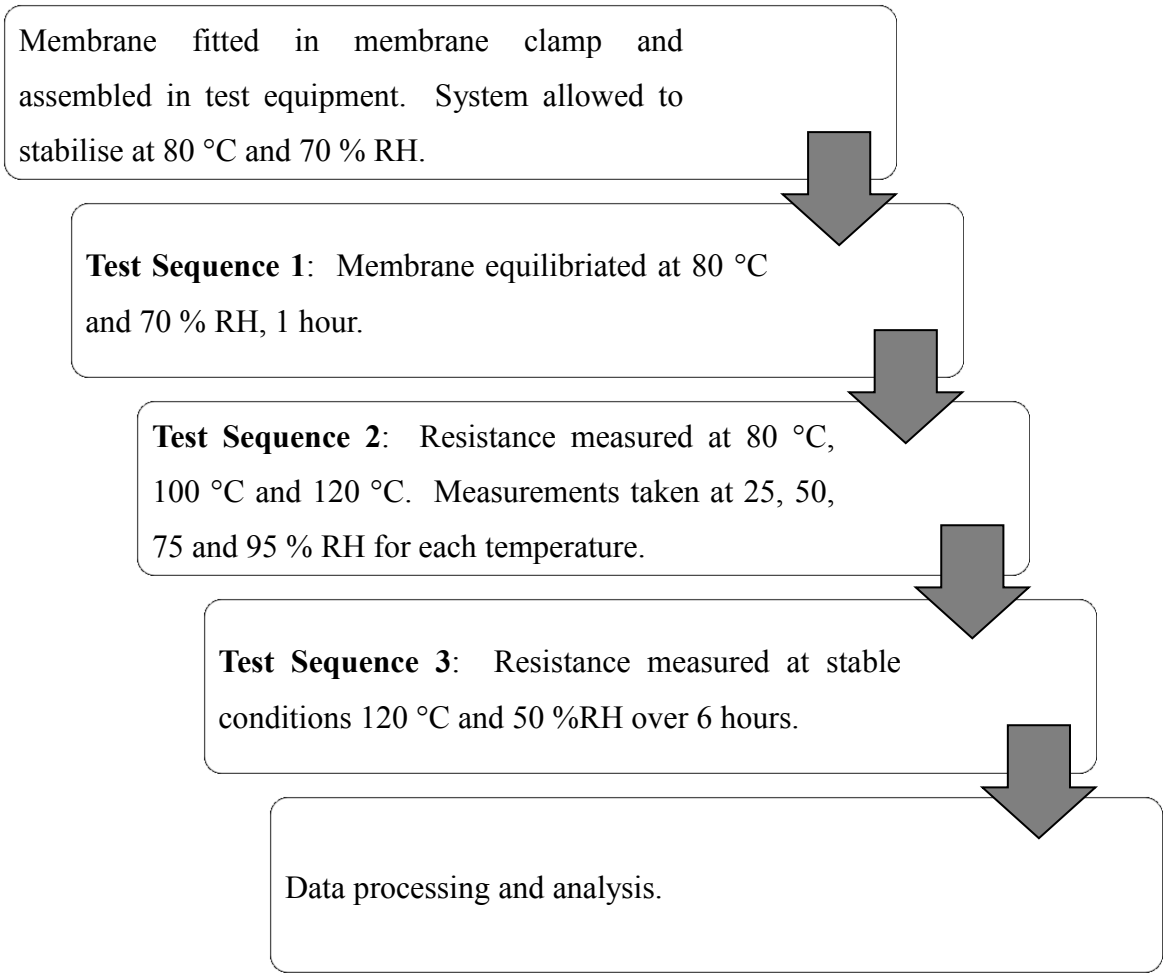

Figure 7-11 Test protocol for membrane resistance measurement

At the end of the test sequences, the proton conductivity was calculated from each resistance measurement. The membrane thickness was measured at three points and the average value was taken. The dew point measurements, as logged separately by the Vaisala dew point probe, along with the temperature measurements, from the Scribner test stand, were used to calculate the actual relative humidity.

7.3.3.2 Proton conductivity – The effect of the thickness of the membranes

The first in-situ tests were carried out to determine the repeatability of the results as well as the effect of pre-soaking and dry testing. The samples GO-3 and GO-4 were from two

batches and the two GO-4 samples were prepared from the same membrane. The results are shown in Figure 7-12, with the proton conductivity on the left and the humidity, as measured by the in-line dew point probe on the right.

At 25-50 %RH the proton conductivity was in direct line with the relative humidity – apart from at 80 °C and 25 %RH where the error in both the proton conductivity and the relative humidity was large. This was to the greatest extent related to the first measurement in each set of three measurements at this step, where the conditions had not been stabilised low enough. As 25 %RH was not the target for this project (it was 50 %RH), no further calibration was undertaken. The soaked sample showed the most stable conductivity, but with a slight decrease in value as the temperature increased. This was a clear indication that the pre-soaking resulted in more stable membrane dimensions and that the swelling of the dry samples, in the initial stages of the test, could affect the resistance. For the dry samples, the conductivity seemed to drop with temperature at 25 %RH but increased at 50 %RH. (although this was in line with the RH measurements). The conductivity for the soaked sample was the lowest under all conditions, as expected, because after water swelling it was thicker than the other two samples.

Between 75 to ~95 %RH the conductivity increased with temperature for all the samples, with one anomaly at 120 °C and ~95 %RH for the GO-4 dry sample, which was possibly due to the low measured relative humidity value. Overall the trend was the smoothest for the soaked sample, notwithstanding the variation in the relative humidity values, with the dry samples showing more irregularity.

When the conductivity was monitored in the 6 hour test the conductivity for the membranes were in the sequence GO-3-1 > GO-4-1 > GO-4-1 soaked, with values of 48, 45 and 35 mS/cm respectively. It would be expected that the two dry membranes would have approximately the same resistance under stable conditions, as they were prepared to have the same dimensions and composition.

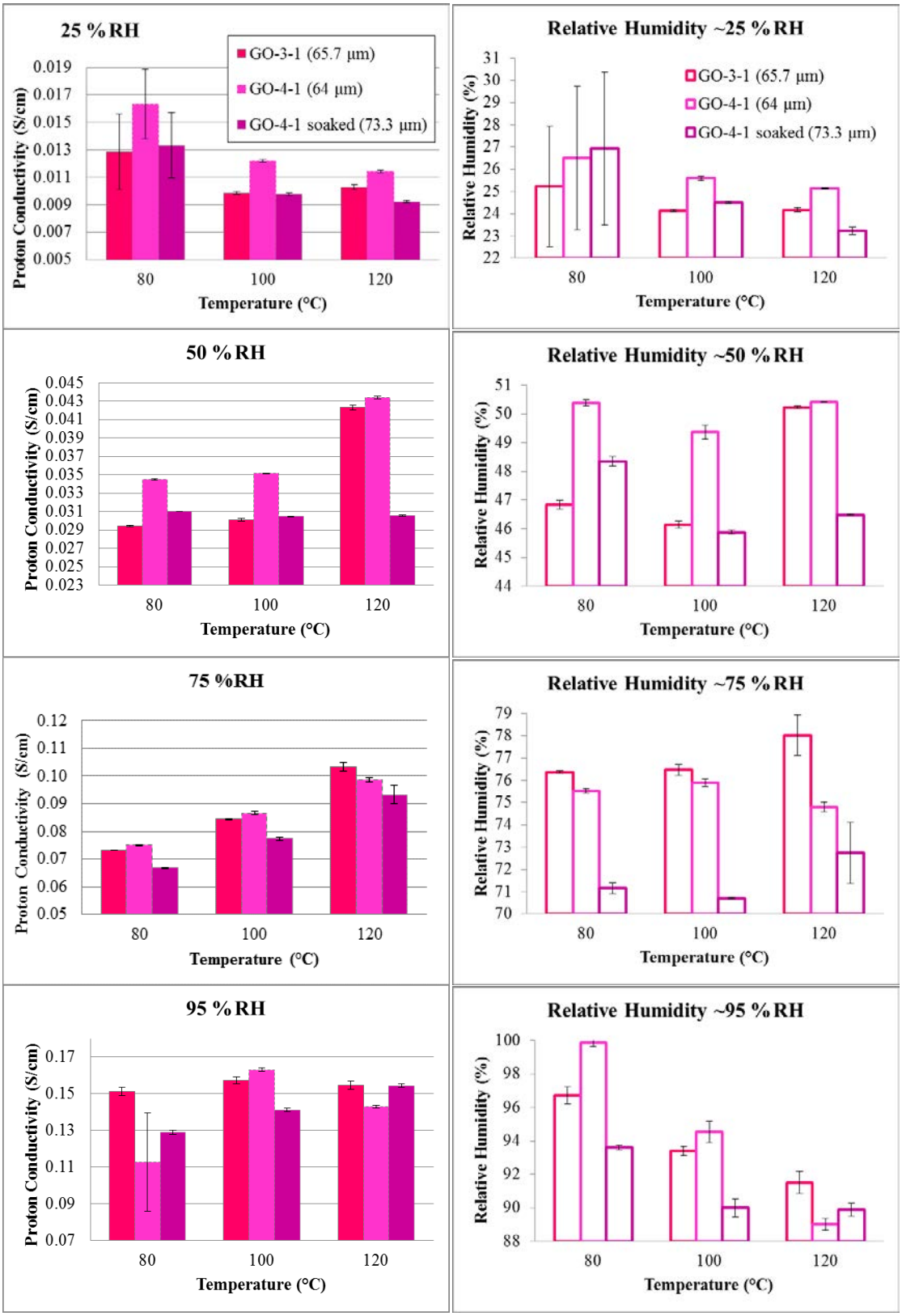

Figure 7-12 Proton conductivity measured for three 1 wt% composite membranes, two tested from the dry state and one after soaking for 2 hours prior to testing . The graphs on the left show the measured relative humidity.

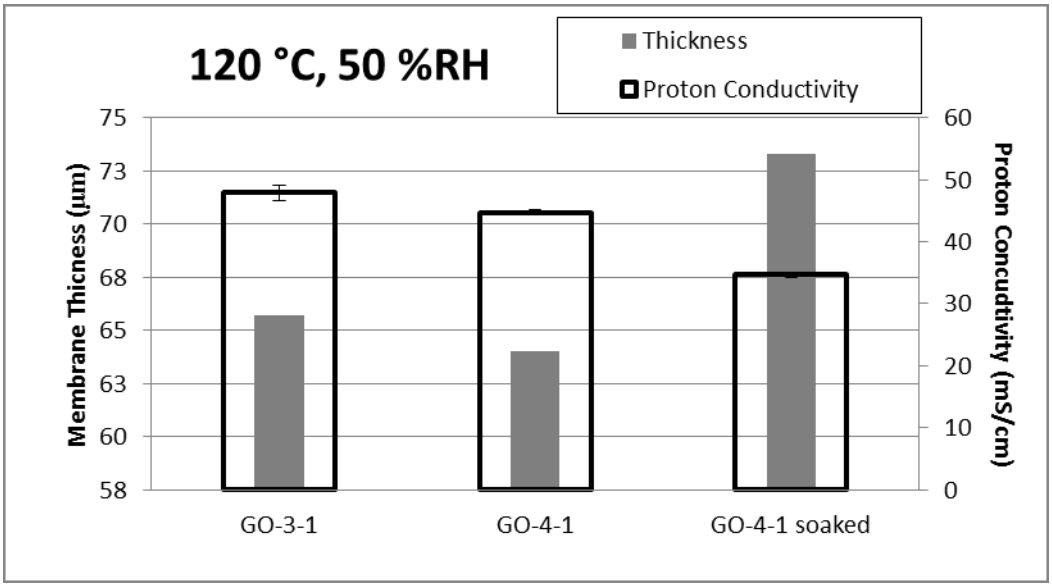

Figure 7-13 Proton conductivity measured over six hours, at stable conditions.

From this data the conclusion was taken that pre-soaking of the samples would result in the most stable data and would possibly eliminate any variations that could result from remaining solvent in the recast membranes.

7.3.3.3 Proton conductivity – The effect of different types of filler

The second set of proton conductivity was measured for membranes prepared from GO, sulfonated GO and commercial GO as described in Chapter 5. All samples were pre-soaked and were very close in thickness at 71 – 73.3 µm (the error in all cases was ~ ± 4 µm). From the data shown in Figure 7-14 it was clear that the functionalised and commercial GO resulted in lower proton conductivity overall. This was true regardless of the fact that the measured relative humidity (as shown on the right hand graphs) was always slightly higher during these tests than during the test for the pristine sample. A departure from the trend at 120 °C and 50 %RH appeared but data collected under these conditions during the 6 hour test (Figure 7-15) showed large error values for the functionalised and commercial membrane

which was possibly the result of some instability caused by the composition of the functionalised GO in the membrane under these conditions. Within these error margins it would therefore not be possible to conclude that these types of membranes showed improved performance just for this one condition step.

The conclusion therefore was that the best performance was found for the pristine GO prepared in-house.

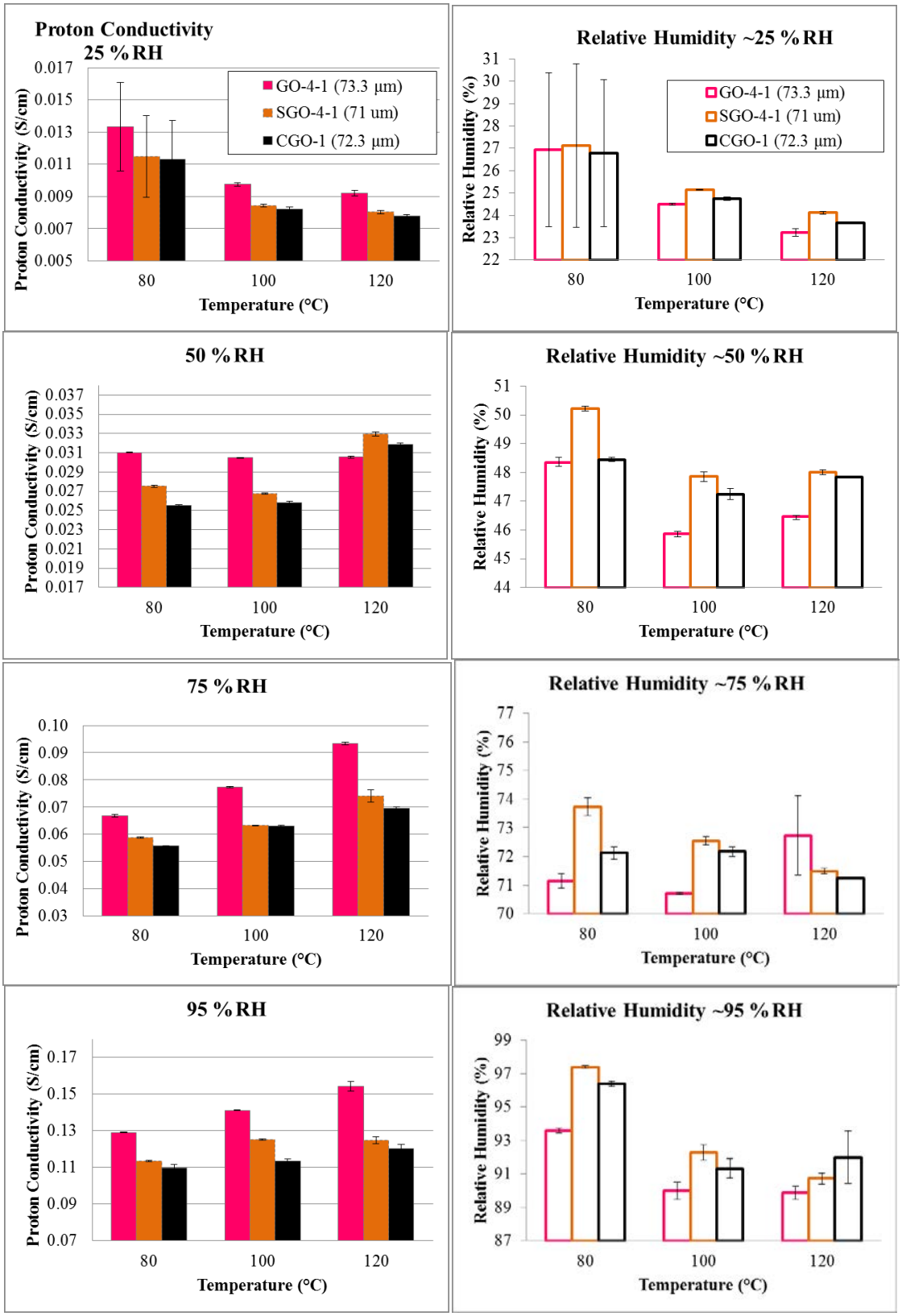

Figure 7-14 Proton conductivity measured for three 1 wt% composite membranes, prepared from GO, sulfonated GO and commercial GO. The graphs on the left show the measured relative humidity.

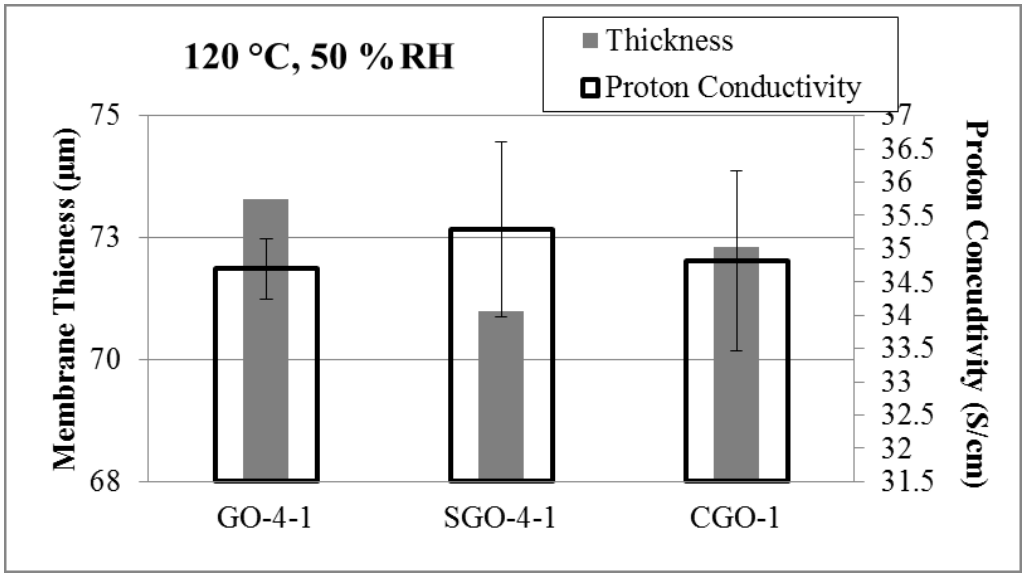

Figure 7-15 Proton conductivity measured over six hours, at stable conditions.

7.3.3.4 Proton conductivity – The effect of the filler loading

Figure 7-16 shows the results for a series of membranes prepared with 0 – 5 wt% GO, again with the relative humidity values shown on the right hand side of the figure. It should also be pointed out that the Nafion 212 values were collated data from three separate runs, as detailed at the end of Chapter 6. This explains the relatively smaller error in the values at 80 °C and 25 %RH. Also, overall, the composite membranes showed lower proton conductivity than both the commercial and the 0 wt% membrane.

At 25 and 50 %RH, the proton conductivity trend was Nafion 212 > recast > 0.5 > 3 > 5 with the possible exception of 80 °C and 25 %RH (0.5 > 0, with a large error margin) and at 100 °C and 50 %RH (5 > 3). At 75 and 95 %RH the 0 wt% membrane consistently had slightly higher proton conductivity than Nafion 212 and the trend from the lower humidity levels was repeated at 120 °C. At 80 and 100 °C the 3 wt% membrane however showed the

highest conductivity and at 80 °C and 95 %RH the 5 wt% membrane performed better than the 0.5 wt% membrane.

If the deviation from the trend was purely as a result of the fluctuations in the relative humidity, then the maximum for 3 wt% would have been expected to appear at 120 °C as well. In a similar fashion, the increased performance for the 5 wt% membrane at 100 °C and 0 %RH should have been consistent at 80 and 120 °C too.

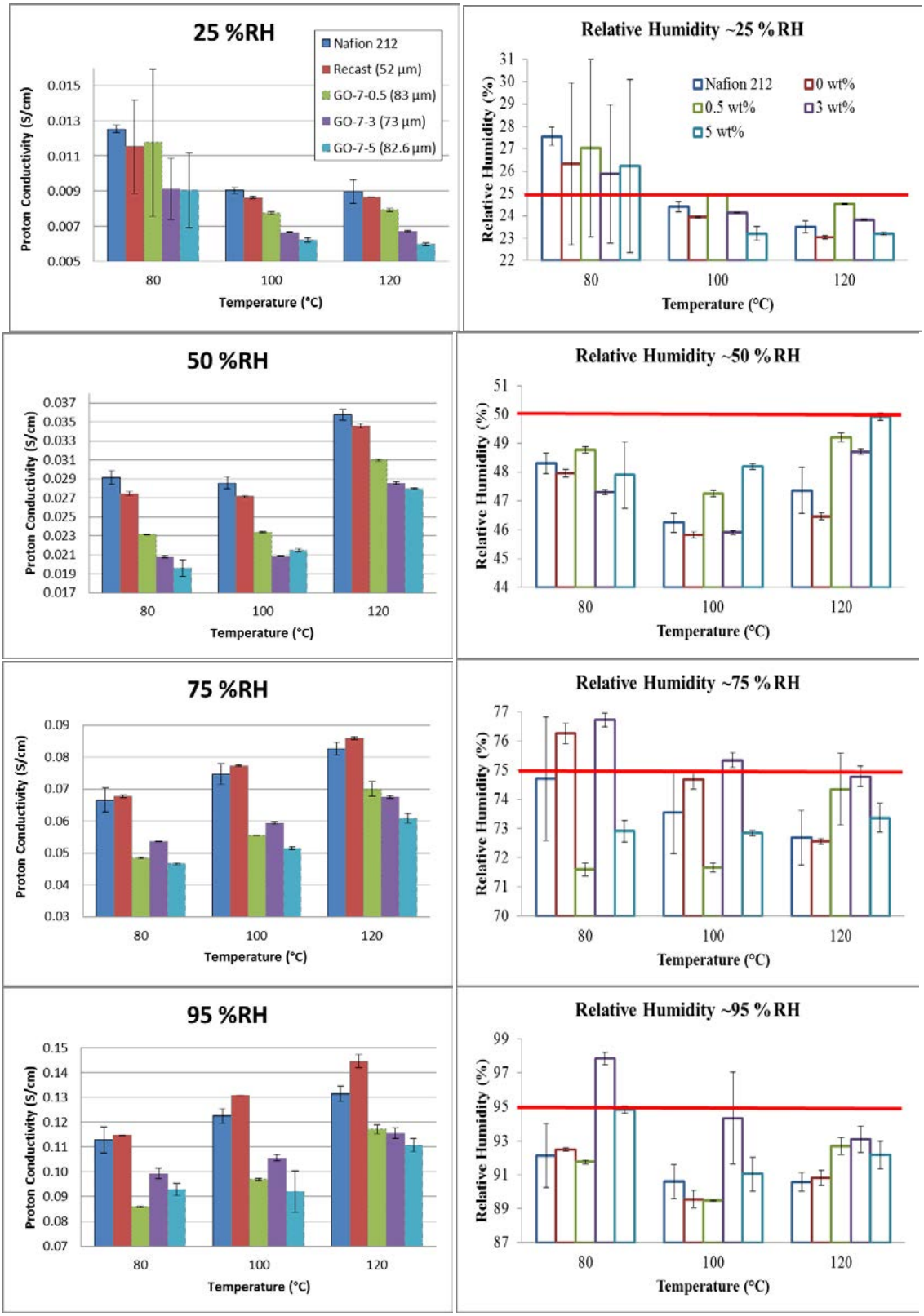

Figure 7-16 Proton conductivity measured for Nafion and a series of composites with filler loading from 0 – 5 wt% GO. The graphs on the left show the measured relative humidity.

It can be seen from the proton conductivity error values, that it was only at 80 °C and 25 %RH overall, and for the 5 wt% membrane at 80 °C and 50 %RH and 100 °C and 95 %RH, that the error was significantly larger than that for the baseline Nafion 212 data.

It appeared therefore that, at 80 – 100 °C, as the humidification increased, the performance of the 3 and 5 wt% membranes improved with respect to the 0.5 wt% membrane. It is possible that this could be a result of the swelling of the membrane allowing for better proton transport through the tortuous path along the plane of the Nafion matrix resulting from the filler particles.

For the final test sequence, where resistance was measured over 6 hours, as shown in Figure 7-17, the trend of the first sequence was confirmed, within a reasonable margin of error. The figure also indicates the thickness of the membranes. The membrane thickness increased smoothly as the filler loading increased and some degree of increased proton conductivity would have been attributable to the dimensions of the sample.

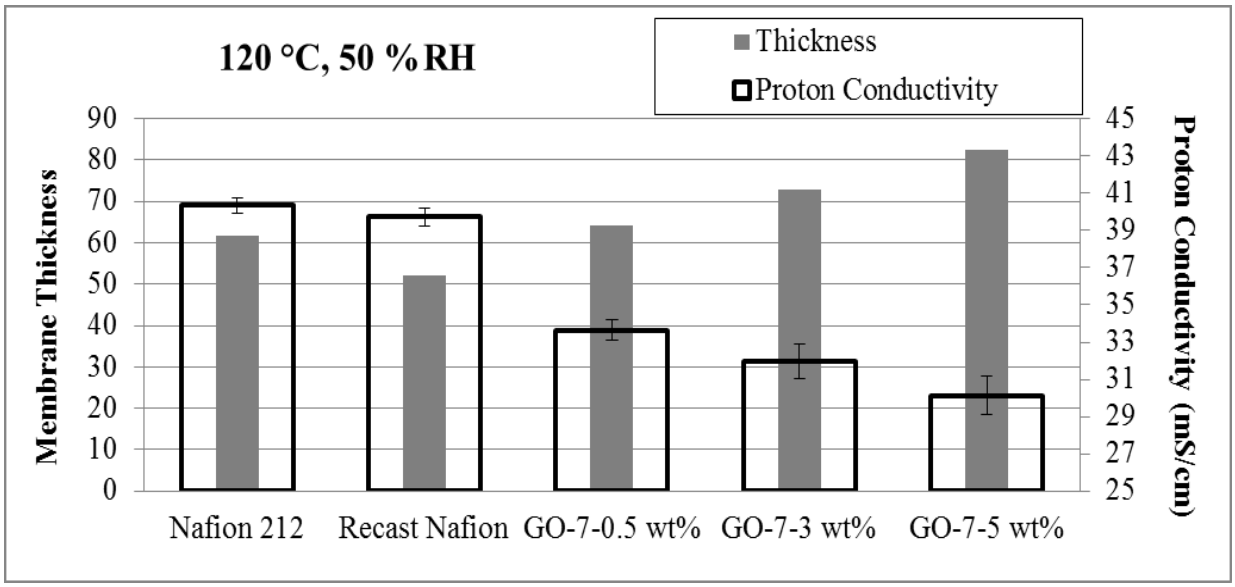

Figure 7-17 Proton conductivity measured over six hours, at stable conditions.

The data was compared with three published studies under comparable conditions, and three things were apparent. Firstly, as can be seen in Figure 7-18, the proton conductivity for this study increased as the temperature increased, whereas for the data published by Kumar *et al.*, the conductivity decreased at higher temperature. This was possibly due to the optimised test conditions in the test stand, with the applied back pressure ensuring the constant relative humidity. It was stated in the Kumar *et al.* study that the tests were carried out under atmospheric pressure, which would have led to a lower relative humidity than the target 100 %RH at 120 °C.

Secondly, the trends echoed the WU and IEC values (where it was available for comparison). At 80 °C this study measured a higher proton conductivity for recast pristine Nafion, and hence the conductivity trend first decreased down to 0.5 wt%, then increased for 3 wt% after which it declined again. This was in discord with both Kumar *et al.* which reported an increase from 0 wt% to 6 wt% after which the values dropped. The Lee *et al.* study similarly showed a fall in proton conductivity from 0-0.5 wt%, after which an evening out through 3 wt% led to an increased conductivity at 4.5 wt%. In all three cases the proton conductivity showed the same trend as the WU. The IEC was not given by Lee *et al.*, but for this study and the Kumar *et al.* study, the proton conductivity and ion exchange followed the same trend. For this study there was an exception at 0.5 wt% where the IEC value showed a small increase over the recast membrane.

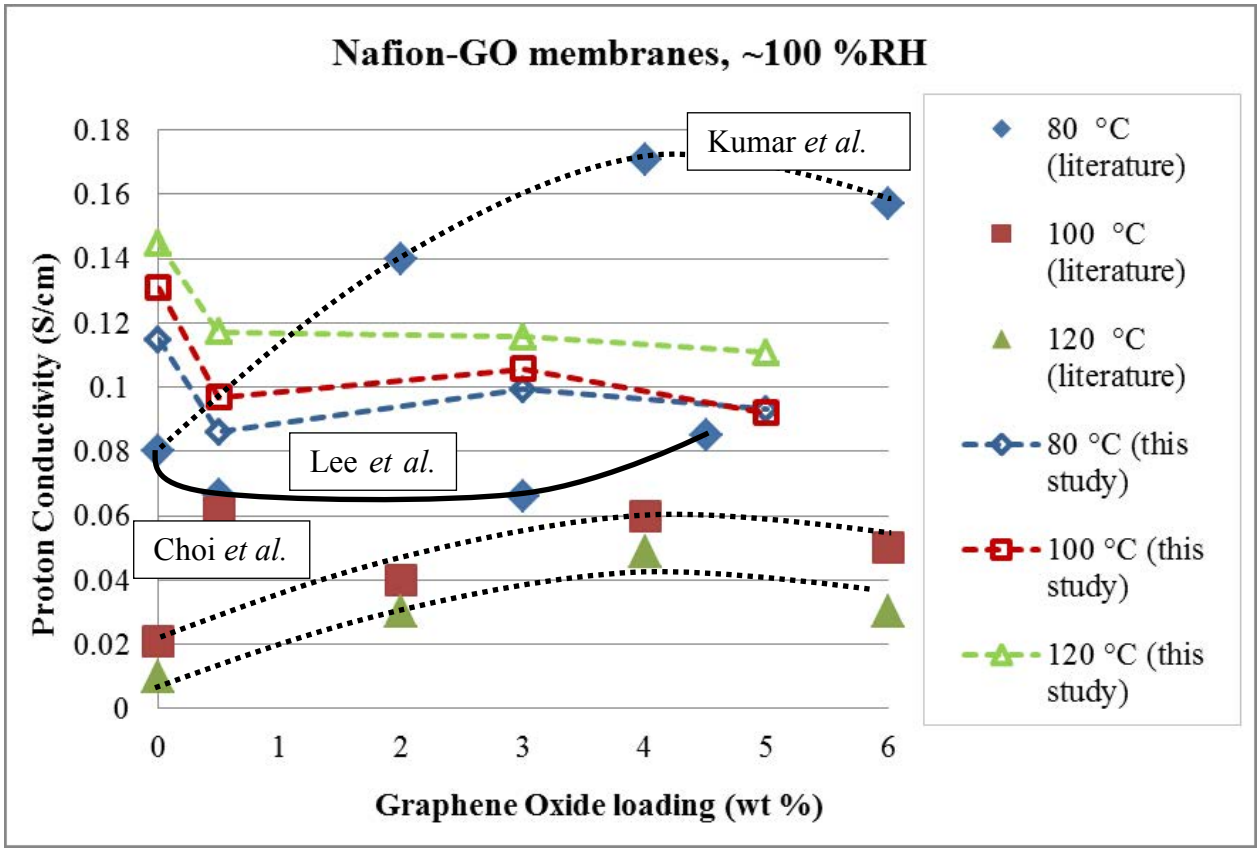

Figure 7-18 Proton conductivity data for Nafion-GO composite membranes – this study and literature.

Finally, the maximum proton conductivity values ranged from ~0.17 S/cm for a 4 wt% membrane (Kumar), to ~0.082 S/cm for a 4.5 wt% membrane (Lee), with values for this study falling somewhere in-between. It should be pointed out that the measurements for this study were made at ~95 %RH, as it was established that maintaining 100 %RH was challenging. This study also measured higher proton conductivity for the pristine membrane, and if the published value was taken, would have shown a similar trend to the Kumar study at 80 – 100 °C. In the literature for intermediate applications, the particle sizes are not always discussed, but Kumar *et al.* stated particle sizes of ~100 nm, although it would appear that some particles are up to 500 nm.

7.4 Conclusions

The ex-situ analysis of the different types of membranes allowed for the following conclusions to be made.

Firstly, in order to accurately measure membrane resistance, WU and IEC, the membranes had to be of an optimal thickness. This was in order to ensure good contact with the platinum electrodes under all test conditions, and more uniform samples for the WU and IEC tests. In order to allow for comparison with the state of the art Nafion 212 membrane, recast membranes of around 50 μm were prepared.

Secondly, the filler loading which was evaluated in the first set of tests confirmed that a GO component of 10 wt% led to deterioration in the membrane performance, possibly due to GO agglomeration and a disruption in the polymer/filler ratio. Furthermore, the in-plane performance would be exacerbated during in-situ operation and through-plane proton conductivity, as the concentration of GO particles could increase the proton tortuosity through the thickness of the membrane. The filler loading in the range of 0.5 to 5 wt% was used for further study. The incorporation of the GO in the membrane was optimised to ensure even distribution without many-sheet layers of filler in the membrane which could compromise mechanical properties of the material.

Pre-soaking of membrane samples provided stable dimensions for resistance measurements. When three membranes of the same thickness, but doped with pristine GO, sulfonated GO or commercial GO were compared, the pristine GO composite consistently had higher proton conductivity.

WU and IEC of the thicker membranes predicted optimal filler loading of around 3 wt%, but the ex-situ testing showed two different trends, at lower and higher humidity and at lower and higher temperature. At low humidity a smooth conductivity trend which dropped as the filler loading was increased was established, whereas the higher humidities resulted in improved performance for the 3 wt% membrane with respect to the 0.5 wt% membrane. This is possibly an indication that, at lower humidification, the filler particles impede the progress of the protons. As the humidification increases, the membrane swells and possibly creates less tortuous conductivity paths. Compared with literature values at full humidification, the composite membranes showed a similar trend, with a maximum at around 3 wt% and the proton conductivity values fell in between the published values, possibly due to the slightly lower optimised humidification of 95 %RH.

Following the in-situ testing, the same membranes from the GO-7 series were used to prepare MEAs and the results are discussed in the next chapter.

CHAPTER 8 IN-SITU TESTING OF COMPOSITE-PEM MEMBRANE ELECTRODE ASSEMBLIES FROM LOW TEMPERATURE TO INTERMEDIATE TEMPERATURE

8.1 Introduction

This chapter addresses the fifth and final objective for this project; in-situ analysis of composite membranes in a temperature range of 80 – 120 °C and 25 – 95 % relative humidity.

The bulk of the time for this project was spent on the commissioning and calibration of the test stand and the optimisation of the membrane resistance testing. The test stand was also shared between two full time PhD researchers and occasionally used by postgraduate students. Hence, selective in-situ testing was carried out towards the end of the project in order to verify the results obtained by resistance testing. This included in-situ testing of the GO-7 series membranes as discussed in Chapter 7. Further calibration of the relative humidity was required and three membranes were re-tested under slightly lower set dew points at the upper level. The results for both these tests showed a different trend to what was found ex-situ and, using in-situ impedance measurements, an attempt was made at correlating the ex-situ and in-situ membrane resistance. Finally, a second set of functionalised GO membranes were prepared and tested in-situ.

8.1.1 Test Sequence

The prepared MEAs were fitted into the test cell and assembled in the test stand. In a similar way as with the membrane test, the cell was allowed to reach 80 °C before the humidifiers were turned on and the dew point slowly increased to around 95 %RH. The test run was started and test sequence controlled by the programmed test steps. The MEA was conditioned at 80 °C and ~95 %RH at open circuit voltage (OCV) for 6 hours. The humidity was adjusted to 25 %RH and stabilised for 3 hours. A constant voltage of 0.6 V was applied and a further open circuit step applied for 20 minutes. This was followed by two current scans between 0-15 A at 0.1 A per 5 seconds. An open circuit step of 15 minutes was run followed by three impedance steps at 0.1, 0.5 and 1 A between 10 kHz and 0.1 Hz. These steps were repeated for the complete test run.

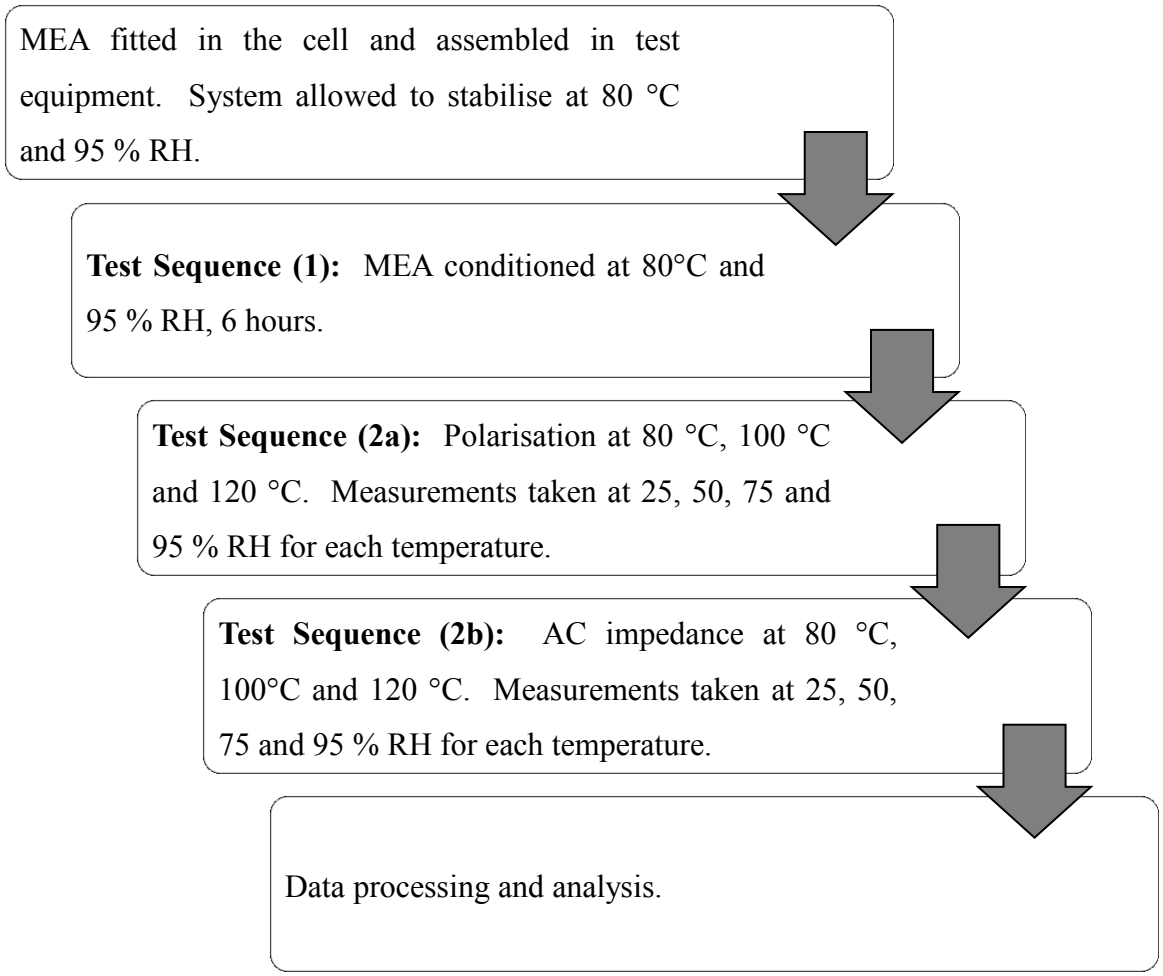

Figure 8-1 Test protocol for MEA polarisation and impedance

At the end of the test run the data was extracted and analysed using FuelCellView (for polarisation) and ZView (for impedance), both supplied by Scribner with the test stand. In all cases the second current scan was used for the polarisation analysis.

8.2 Results and Discussion

Since the optimisation of the in-situ performance of the composite membranes was an integral goal of membrane development, MEA tests were carried out right from the start of the project. For the initial thinner membranes (GO-1 and GO-2), MEAs were prepared and

tested by a colleague on a low temperature test stand which was already in place in the UOB Fuel Cell Laboratory. The test conditions were 70 °C and 100 %RH and the trends are shown in Table 8-1 (data is shown in Appendix A3). The highest proton conductivity and maximum power was found in all cases to be 0.5 wt% for GO-1. The trend was not so clear for GO-2. Ex-situ proton conductivity was measured to be the highest for 0.75 and lowest for 5 wt%, but in-situ performance resulted in the highest power output for 0.25 and the lowest for 0.75 wt%. For reasons already described, it was possible that there was not a large enough distinction between the 0.25, 0.5 and 0.75 wt% membranes, and due to possible agglomeration of the GO, a reasonable conclusion at this stage was that some of the composite membranes performed at least as good as Nafion 212 and in some cases slightly better. As the temperature varied for the tests and since the low temperature test stand had not been subjected to dew point calibration this data is not discussed further in this study.

Table 8-1 Ex-Situ and In-Situ performance trends for GO-1 and GO-2

GO-1	
Ex-Situ (80 °C, 100 %RH)	**0.5 > 5 > 0 > 10**
Ex-Situ (90 °C, 100 %RH)	**0.5 > 0 > 5 > 10**
In-Situ (70 °C, 100 %RH)	**0.5 > 0 = 10 > 5**
GO-2	
Ex-Situ (80 °C, 100 %RH)	**Nafion 212 > 0.75 > 1 > 0.25 > 0.5 >5**
Ex-Situ (90 °C, 100 %RH)	**Nafion 212 > 5 > 0.25**
In-Situ (70 °C, 100 %RH)	**0.25 > 0.5 = 1 = 5 > 0.75 > Nafion 212**

The remainder of the results presented focus on data collected for the thicker membranes which were tested on the calibrated and optimised high temperature Scribner test stand.

8.2.1 Effect of filler loading

Following on from the proton conductivity tests, which showed the two trends of Nafion 212 > 0 > 0.5 > 3 >5 wt% and 0 > Nafion 212 > 3 > 0.5 > 5 wt% under different conditions, MEAs were prepared from the same membrane samples in order to evaluate the in-situ performance. Figure 8-2 shows the results for the tests at 50 %RH and is representative of the data set (Appendix A4 shows all the data).

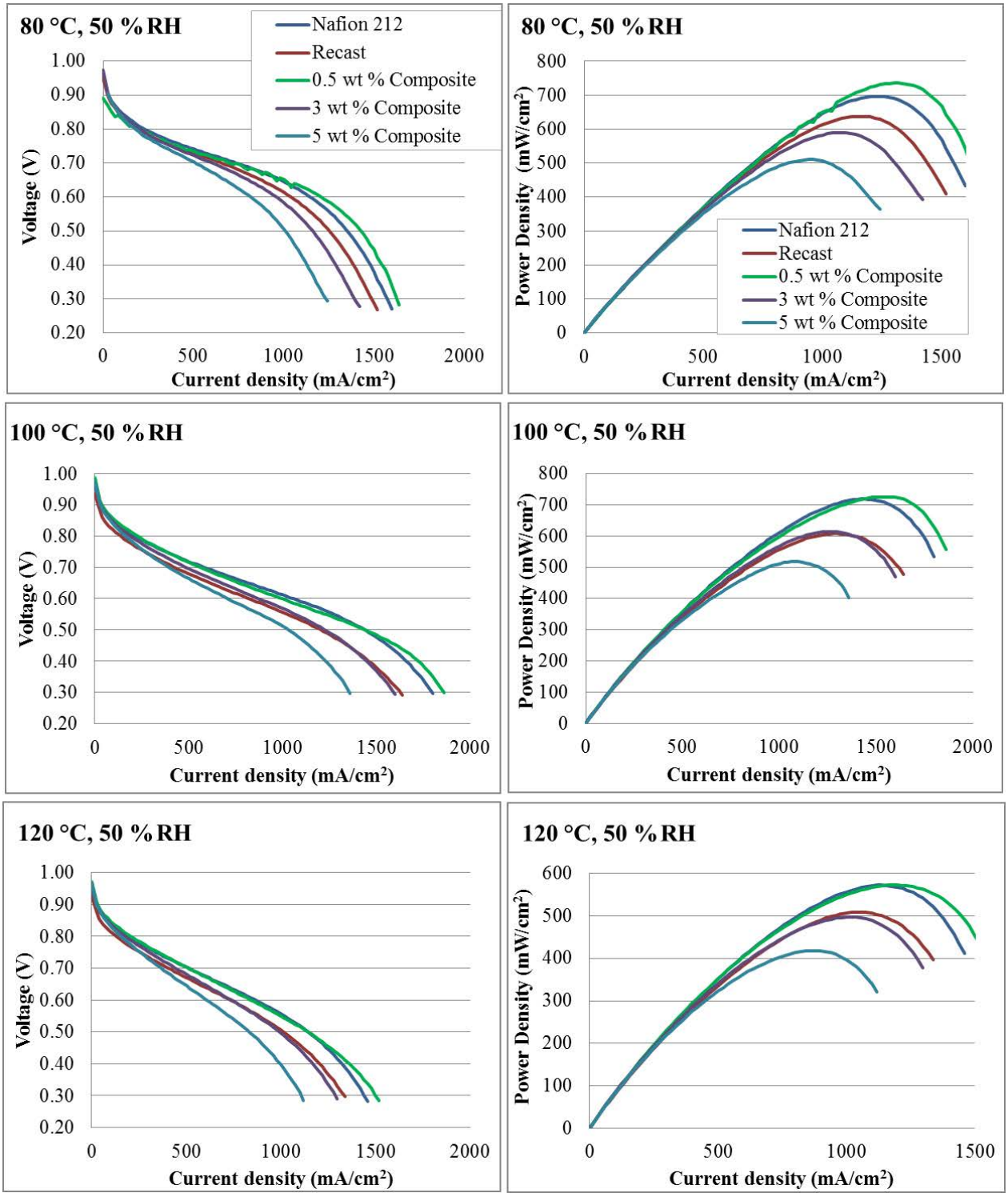

Figure 8-2 Polarisation and power curves for GO-7 series membranes, at 50 %RH.

For the composite membranes the trend was consistently in the order of 0.5 > 3 > 5 wt% in the maximum power density reached. Furthermore, the 0.5 wt% membrane performed at least as good as the commercial Nafion 212 membrane and better than the recast 0 wt%

membrane. At 100 and 120 °C the 3 wt% membrane showed maximum power very close to the recast membrane.

In order to compare the results with data from literature, the power density at 0.6 V and the maximum power density were plotted against temperature and are shown in Figure 8-3.

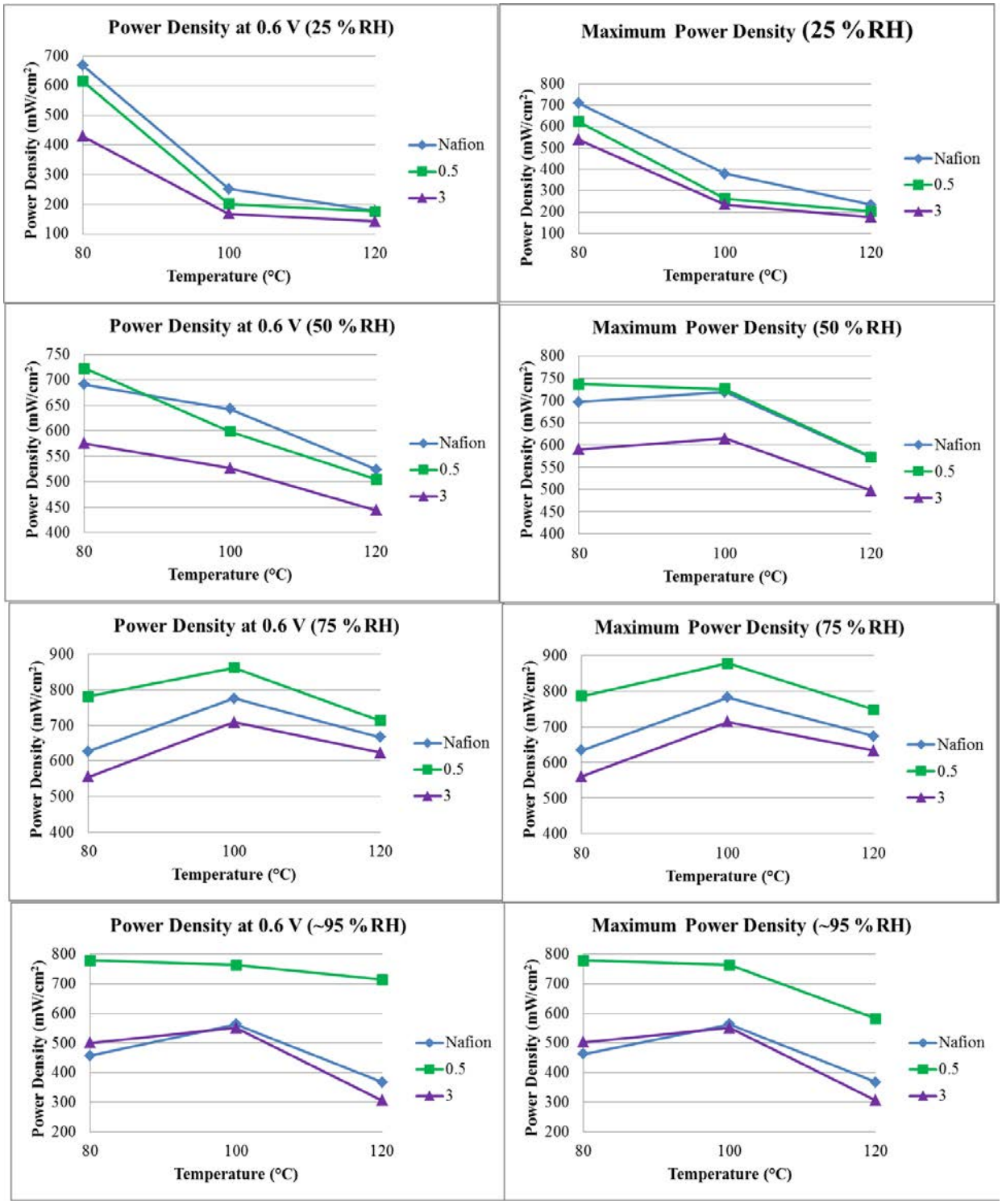

Figure 8-3 Power density at 0.6 V and maximum power density for GO-7 MEAs.

A comparison of the literature in-situ results showed a similar disparity in the reference materials that was found for ex-situ testing, in that the values measured for this study was much higher. It is difficult to speculate when little is known about the test set up, but the

Scribner test stand was calibrated and insulated thoroughly, and it can be stated with certainty that the target relative humidity was achieved. When the data for the composites are compared, the current at 0.6 V shows that for the Lee *et al.* study, where proton conductivity was in the order of 4.5 > 0 > 0.5 ≈ 3, the in-situ test showed 3 > 4.5 > 0.5 > 0 (1.27, 0.827, 0.802 and 0.435 A/cm^2 respectively). For this study the proton conductivity range was 0 > 3 > 5 > 0.5 and the in-situ maximum power was 0.5 > 0 > 3 > 5 (1.30, 0.880, 0.840 and 0.660 A/cm^2). Both studies therefore found different ex-situ vs. in-situ trends, and the membrane with the lowest ex-situ proton conductivity resulted in the highest maximum power density under comparable conditions. The current density of the reference membrane in this study was almost double that of the literature value.

Kumar *et al.* did not show data for the whole range of membranes reported in the ex-situ testing, maximum power density of 212 mW/cm^2 was reported for the 4 wt% MEA but results for the 2 and 6 wt% membrane was not given. The composite MEA power density was much higher than 56 and 75 mW/cm^2 measured for Nafion 212 and recast Nafion respectively. This study showed 263.79 and 234.61 mW/cm^2 for 0.5 and 3 wt% respectively which is in a similar range, but remarkably higher values of 380.24 and 318.52 mW/cm^2 were obtained for Nafion 212 and recast Nafion.

Whilst the focus remained on comparing trends between different studies, it is just pointed out that this study used 0.2 L/min hydrogen and 0.5 L/min air as fuel gasses, whereas both the other studies used hydrogen and oxygen as fuel at around 0.1 L/min. Furthermore the Kumar study used a similar Pt loading at around 0.4 mg_{Pt}/cm^2 and a MEA preparation technique as this study, but prepared a smaller active area of 1 cm^2. The Lee study had a lower catalyst

loading at 0.2 and 0.3 mg_{Pt}/cm^2 at the anode and cathode respectively, and used the membrane coated technique to prepare 3 cm^2 MEAs.

8.2.2 Effect of relative humidity

Initially the dew point was set on the test stand as it had been calibrated for the membrane conductivity test by using the in-line dew point probe. For the runs at the highest humidity levels, there appeared to be a large improvement in the performance of the 0.5 wt% composite membrane in the mass transport region compared to the other MEAs, as can be seen in Figure 8-4 (left).

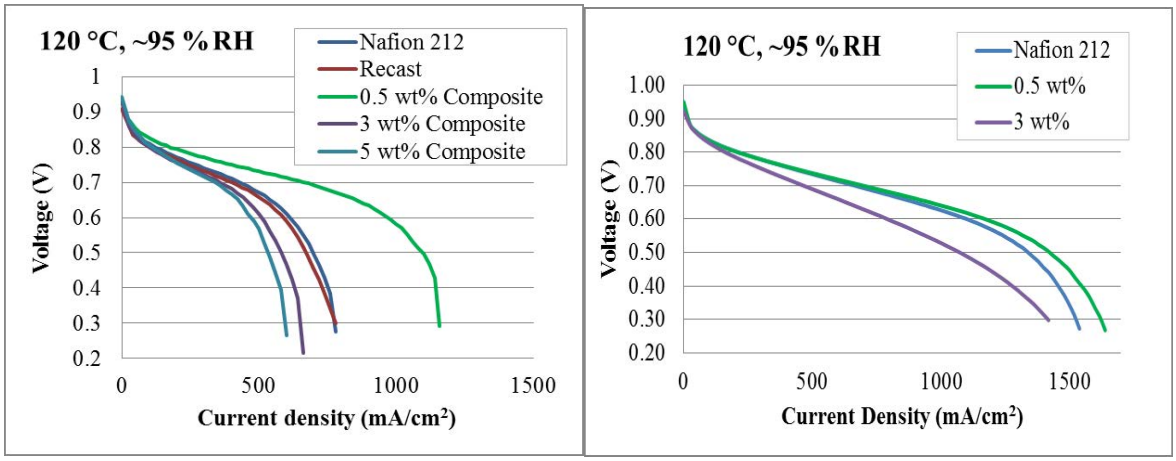

Figure 8-4 Polarisation for GO-7 series with initial dew point settings (left) and after a downwards adjustment (right).

In order to establish if this was due to the test settings or if it was a true reflection of the performance of this composite membrane, the dew point on the test stand was adjusted downwards, and three MEAs were tested again. In the right hand side of the figure it can be seen that this resulted in improved performance for all membranes, and even though the

0.5 wt% membrane still showed the best performance, that it was now very close to that of the commercial membrane.

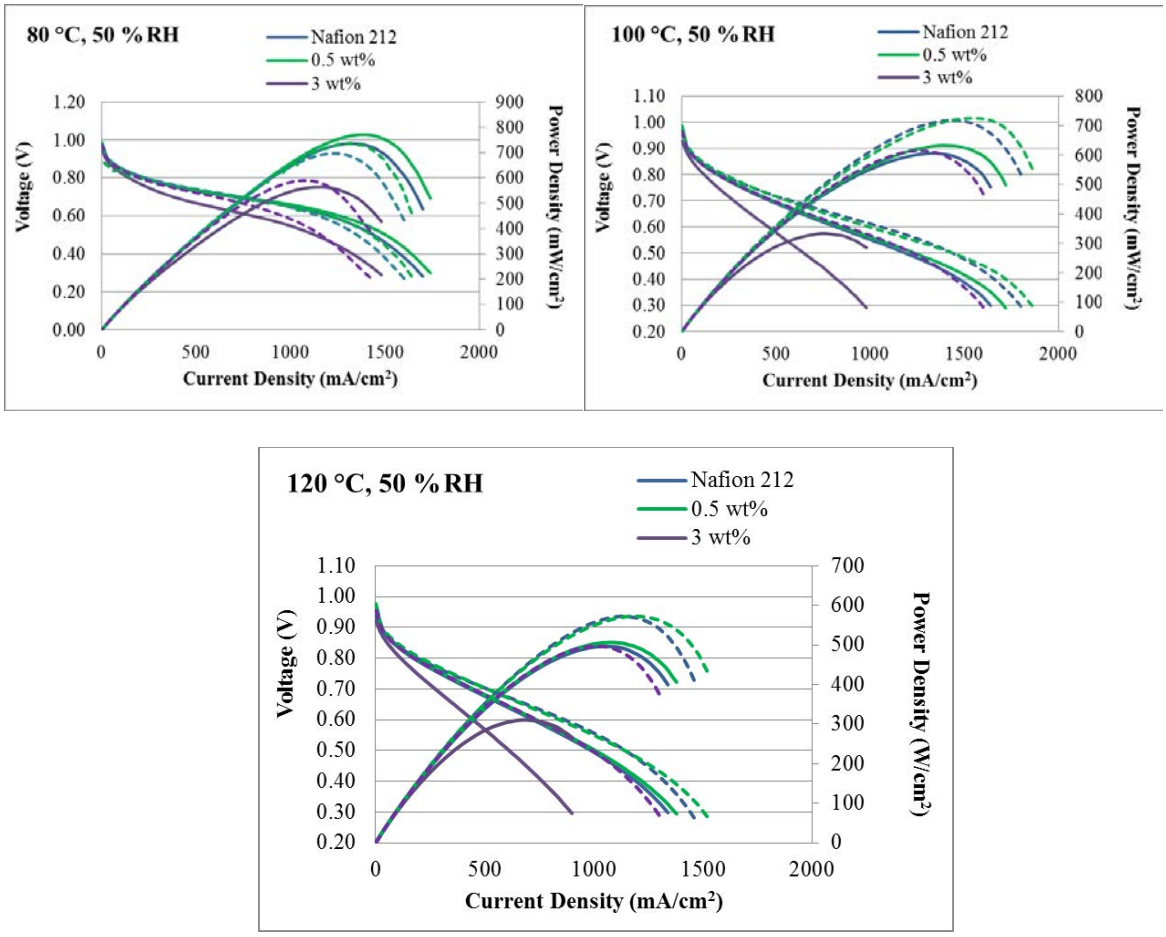

Figure 8-5 Polarisation and power curves for three MEAs retested under slightly lower dew point at the top humidity level. The dashed lines indicate the first set of tests from Figure 8-2.

Comparing the polarisation and power output with the first set of data (Figure 8-5), it was established that the trend remained the same for the three MEAs that were retested, but that the maximum power was affected by the optimised conditions. At 80 °C and 50 %RH there was a slight increase in power for Nafion 212 and 0.5 wt%, but at the higher temperatures, the power was lower. This was particularly apparent for the 3 wt% membrane, which also showed lower power at 75 %RH (Figure 8-6). Overall, the performance of the 0.5 wt% membrane remained the most stable. At the highest humidification the maximum power of

both Nafion 212 and the 3 wt% membrane showed the most improvement. This confirmed that flooding affected these membranes in the initial test run.

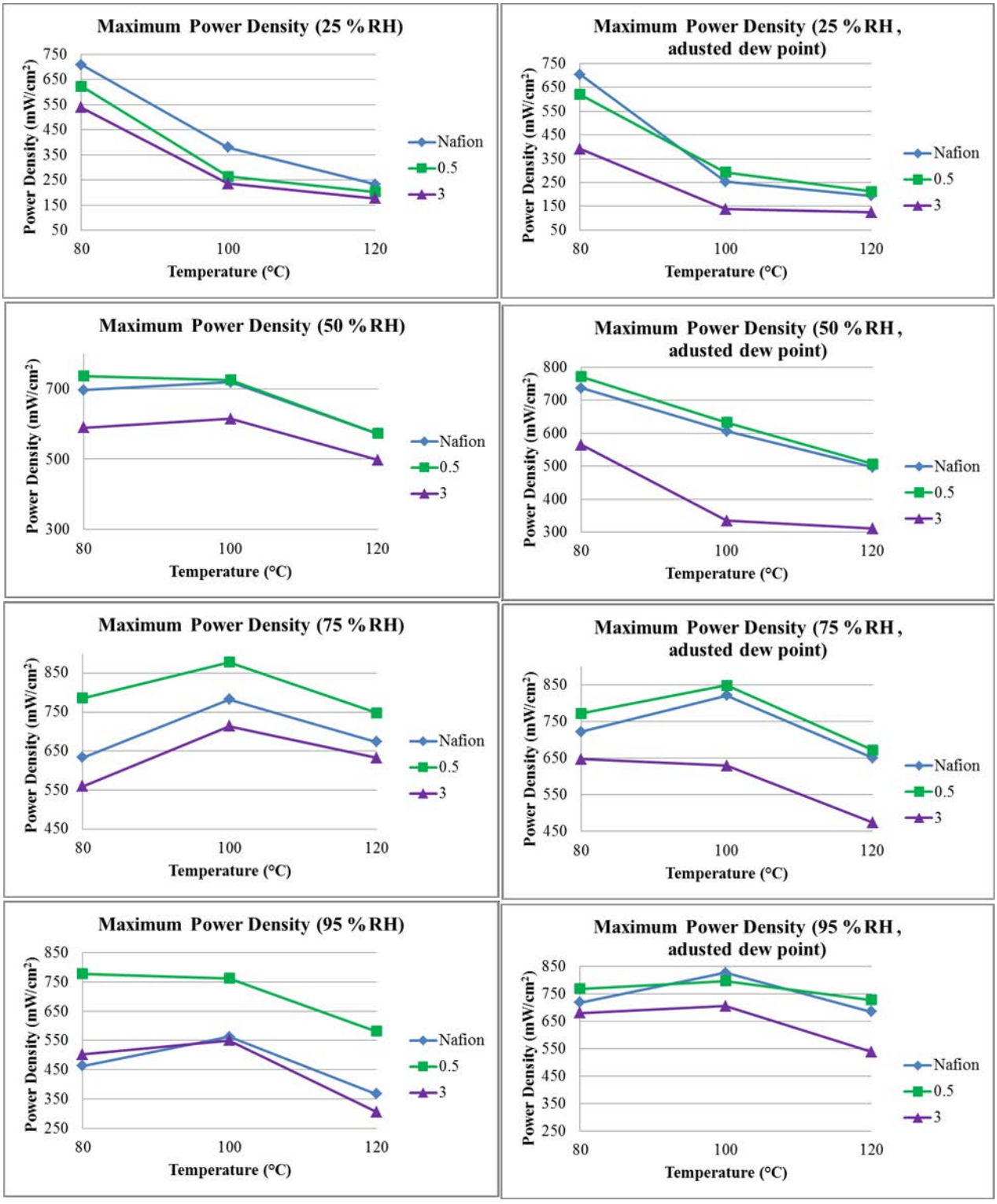

Figure 8-6 Maximum power density at initial (left) and optimised (right) relative humidity for GO-7 MEAs.

8.2.3 Ex-situ vs. in-situ membrane resistance

In order to compare the ex-situ and in-situ measurements, impedance measurements were taken at 0.1, 0.5 and 1 A during the polarisation tests under all the conditions. From this the proton conductivity was calculated and plotted, together with the ex-situ membrane conductivity and is shown in Figure 8-7 and Figure 8-8. This figures show the impedance for the first set of polarisation on the left, and the values after the dew point was adjusted on the right.

The reason why area specific resistance (ASR), was not quoted for the two sets of data was because of the inherent non-uniform nature of composite membranes, particularly under varying test conditions. The ASR is an expression of membrane resistance in terms of the dimensions of the test area.

$$ASR = R * A \quad \text{.....(1)}$$

Where R = resistance in Ω

A = area in cm^2

At 50 %RH, under both the initial and the optimised conditions, the in-situ (through-plane) membrane resistance increased with temperature in the in-situ test. This is in contrast to the ex-situ resistance, which decreased with temperature for the ex-situ test. The very low value for Nafion 212 at 80 °C and 0.1 A was an anomaly, possibly caused by a spike in temperature or drop in humidification, and it was not present when the test was repeated. The in-situ trend changed at 95 %RH, also increasing with temperature under non-optimised conditions, but was restored when the dew point was reduced.

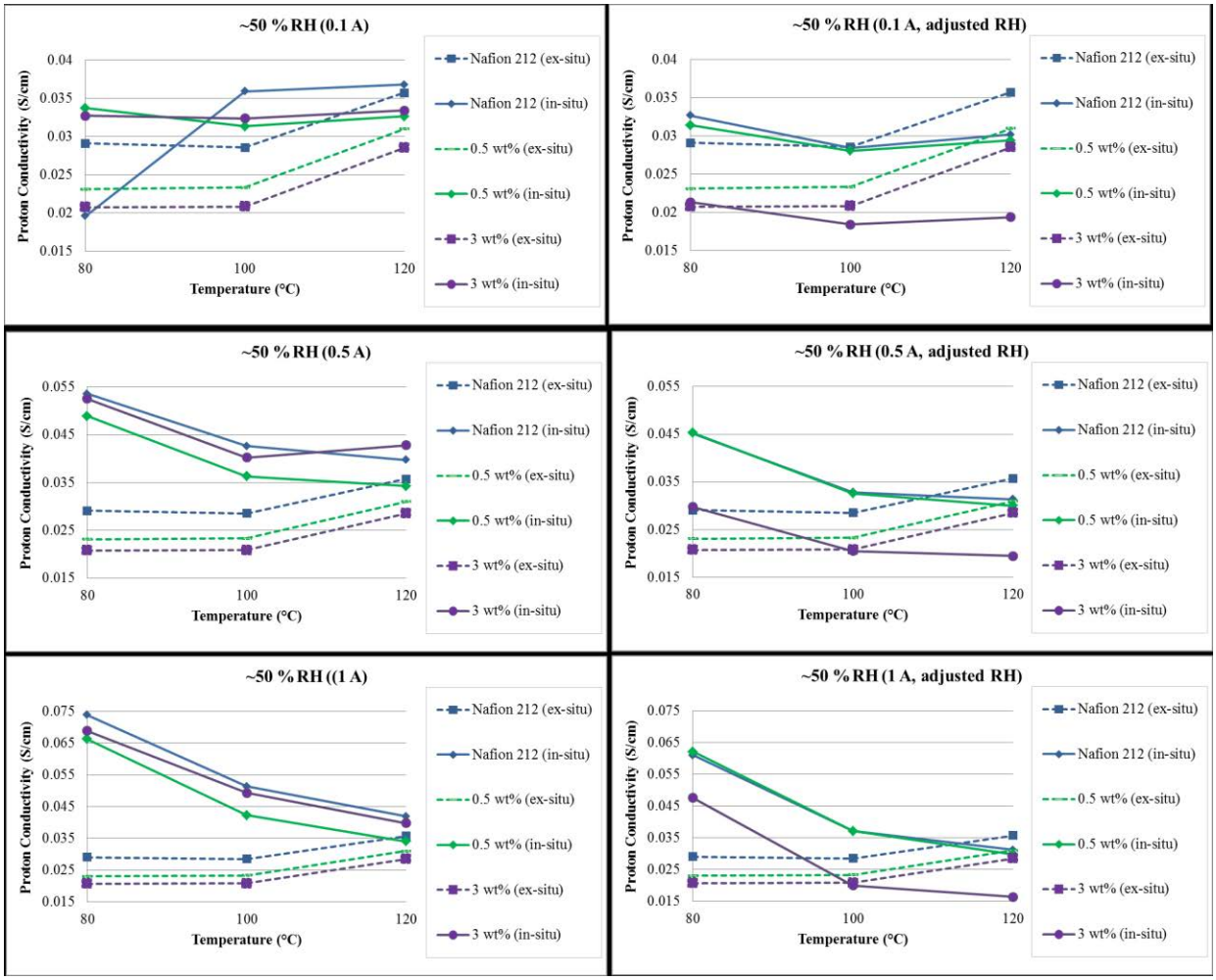

Figure 8-7 Ex-situ proton conductivity (dashed lines) vs in-situ proton conductivity (solid lines) under initial (left) and optimised (right) conditions at 50 %RH.

The ex-situ proton conductivity showed two trends. Nafion 212 > 0.5 > 3 at 50 %RH for all temperatures. At higher humidification this trend remained prominent at 120 °C, but at 80 and 100 °C, it changed to Nafion 212 > 3 > 0.5 wt%. Under non-optimised in-situ testing the trend was Nafion 212 > 3 > 0.5 wt% under most conditions with resistance values being almost the same for Nafion 212 and the 3 wt% membranes at higher current and as the humidity increased. At 120 °C and lower current, the 3 wt% had slightly lower resistance in some cases.

After the dew point was adjusted however, the trend was Nafion 212 ≈ 0.5 > 3 at 50 and 75 %RH while it was 0.5 > Nafion 212 > 3 at 95 %RH.

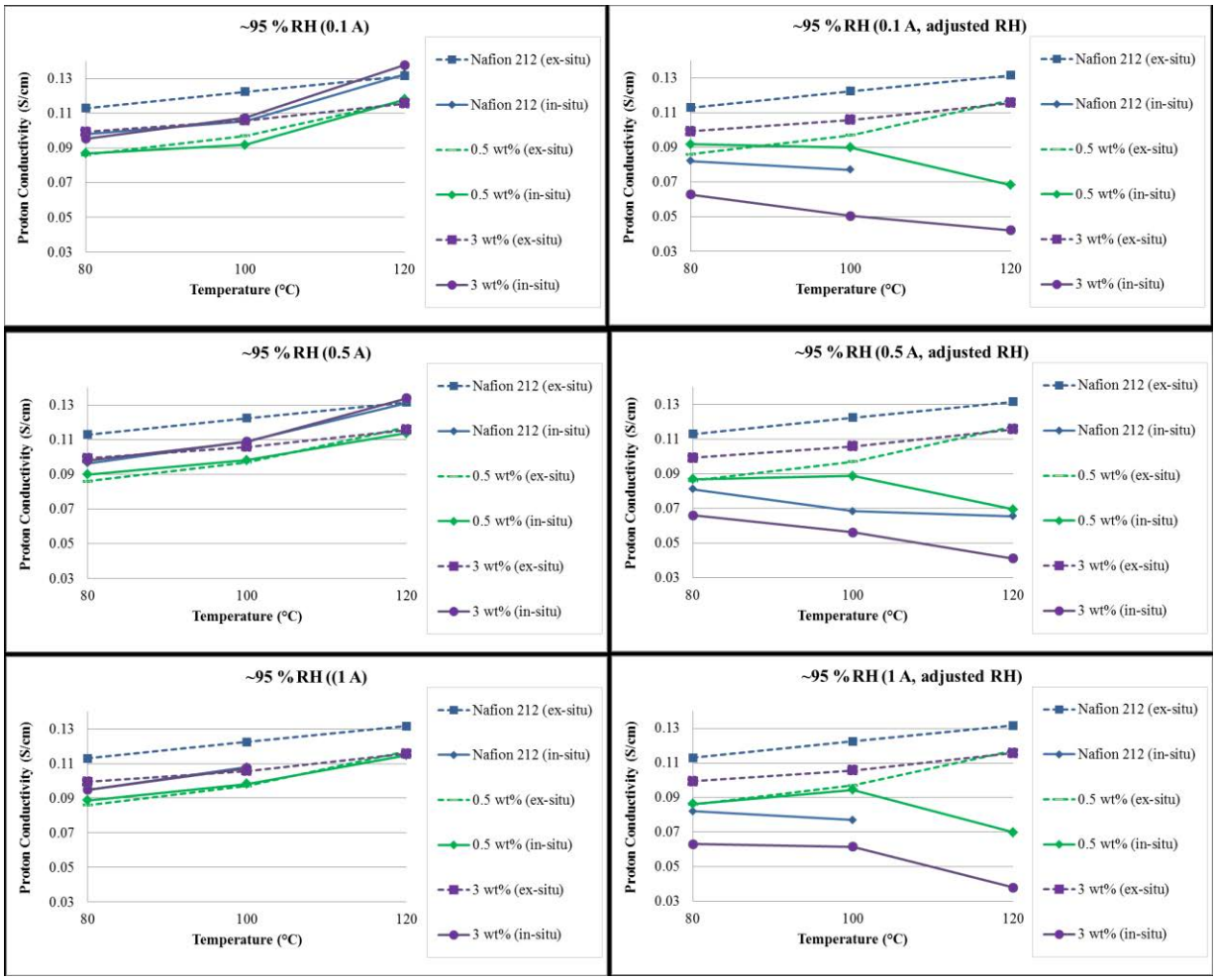

Figure 8-8 Ex-situ proton conductivity (dashed lines) vs in-situ proton conductivity (solid lines) under initial (left) and optimised (right) conditions at ~95 %RH.

The test conditions in the non-optimised in-situ test were the same as the proton conductivity test and the resistance in this case showed the same trend as was shown for the power output of the MEAs. Therefore, it was concluded that even if the membrane resistance was lower for the 3 wt% than for the 0.5 wt% membrane, under operating conditions the 0.5 wt% membrane produced better results. This result was possibly related to the flooding which was observed at the first stage of the in-situ testing.

8.2.4 Effect of filler type (GO functionalised with azo-sulfanilic acid).

The second type of functionalised GO, as described in Chapter 5, was used to prepare a set of membranes. The data is shown for 50 %RH (Figure 8-9) but is representative of all conditions (as shown in Appendix A5). The first observation was that the maximum power for the functionalised membranes was lower than for Nafion 212 and the 0.5 wt% GO-7 sample. In the case of the functionalised GO membranes, the performance appeared to improve for the 3 wt% membrane with respect to the 0.5 wt% membrane, as the temperature increased. At 100 °C the two membranes had equal performance. This agreed well with published data, as shown in Chapter 2, where proton conductivity appeared to increase as the filler loading increased for functionalised membranes and suggests an interesting area for further study.

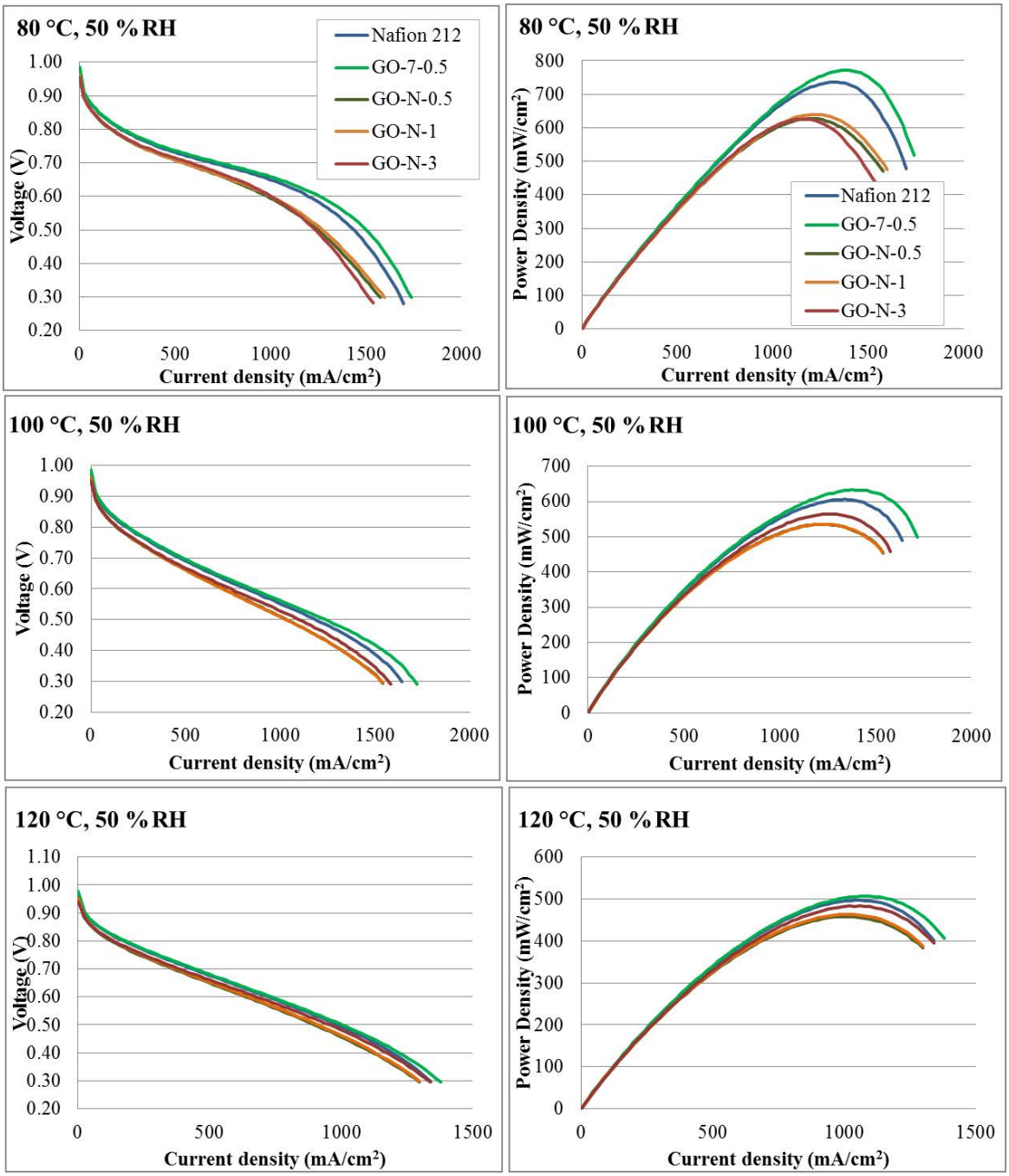

Figure 8-9 Polarisation and power curves for GO-N series of membranes prepared with functionalised GO at 50 %RH.

8.3 Conclusions

The in-situ analysis of the different types of membranes allowed for the following conclusions to be made.

For the composite membranes the trend was consistently in the order of 0.5 > 3 > 5 wt% in the maximum power density reached. The 0.5 wt% membrane furthermore performed at least as good as the commercial Nafion 212 membrane and better than the recast 0 wt% membrane. At 100 and 120 °C the 3 wt% membrane showed maximum power very close to the recast membrane. As for the ex-situ results, this study consistently measured higher performance for the reference materials (Nafion 212 and the pristine membrane) than the literature values.

In order to improve apparent flooding at the highest humidity levels, the dew point was adjusted downwards and this affected the performance of the commercial membrane and the 3 wt% membrane to the greatest extent. The performance of the 0.5 wt% membrane remained the most stable between the two dew point settings, but a marked improvement was apparent for the commercial and 3 wt% membrane. This confirmed that flooding had affected these two membranes under the initial test conditions.

In order to compare the ex-situ and in-situ proton conductivity, impedance was used to calculate the values for the in-situ through-plane proton conductivity. Whereas resistance decreased with temperature for the ex-situ tests, it increased during the in-situ test under the optimised conditions. Under non-optimised conditions, the upward trend was also found in the in-situ results. Under non-optimised in-situ testing the trend was Nafion 212 > 3 > 0.5 wt% under most conditions with resistance values being almost the same for Nafion 212 and the 3 wt% membranes at higher current and as the humidity increased. At 120 °C and lower current, the 3 wt% had slightly lower resistance in some cases.

After the dew point was adjusted however, the trend was Nafion 212 ≈ 0.5 > 3 at 50 and 75 %RH after which it was 0.5 > Nafion 212 > 3 at 95 %RH. The resistance in this case showed the same trend as was shown for the power output of the MEAs. Therefore, it was concluded that even if the membrane resistance was lower for the 3 wt% than for the 0.5 wt% membrane, under operating conditions the 0.5 wt% membrane produced better results.

WU and IEC predicted optimal filler loading of around 3 wt%, but the ex-situ testing showed two different trends, at lower and higher humidity and at lower and higher temperature. At low humidity a smooth conductivity trend which dropped as the filler loading was increased was established, whereas the higher humidities resulted in improved performance for the 3 wt% membrane with respect to the 0.5 wt% membrane. To some extent this was confirmed with the impedance results from the non-optimised test.

A second type of functionalised GO was used to prepare a set of composite membranes, which all showed lower maximum power than Nafion 212 and the 0.5 wt% GO-7 composite membrane.

CHAPTER 9 SUMMARY AND FURTHER WORK

9.1 Conclusions

This study has contributed to the knowledge of graphene oxide composite membranes by systematically evaluating the performance of a series of membranes under different humidity and temperature ranges, both ex-situ and in-situ. The study was carried out in the framework of five objectives, which were identified after a review of available literature on these materials.

The membrane preparation method was optimised by investigating the use of different types of solvents for the casting process, and different heating regimes for the curing stages. The method of incorporating the GO into the membrane was also found to significantly affect the membrane composition. It was concluded that de-ionised (DI) water was the optimal solvent for Nafion-GO composite membranes and that solvent evaporation and membrane curing at 100 and 140 °C led to the most mechanically robust membranes. Simply dispersing dry GO in DI water and combining with the polymers solution was found to result in uneven distribution and filler agglomeration. Successive centrifugation and the use of GO in solution, without drying, resulted in membranes with even distribution of sheets of filler material.

Graphene oxide from different sources and different compositions were used to prepare membranes for testing. It was found that the GO prepared in-house and in one single batch resulted in the most uniform and repeatable results. The GO was analysed by XPS each time a new batch of membranes were prepared to ensure the composition remained stable. XPS was used to confirm the C:O ratio of 2:1 was retained throughout the study.

In order to carry out in-house membrane conductivity and single cell polarisation testing, a high temperature test stand was purchased from Scribner. The test stand was fitted with a pressurised water tank for continuous humidification and a back pressure unit to maintain the humidity levels at 120 °C. The equipment required extensive optimisation and calibration in order to ensure repeatable test conditions. The most prominent source of initial error was related to insufficient insulation resulting in cold spots and condensation, and a disparity between the set and actual relative humidity. This was remedied by insulating the entire exposed area of the test set-up and addition of heated gas lines. A dew point probe was used to measure the actual dew point in-line to the test cell and the test stand was calibrated to result in the desired humidity steps of 25 to ~95 %RH. The test software was programmed to allow for continuous test sequences, again to ensure that the conditions remained the same during each test run. For data analysis the actual dew point was measured and along with the logged temperature, used to calculate the actual relative humidity at each step. This allowed for the analysis of proton conductivity with relation to the actual relative humidity in the system.

Various sets of membranes were prepared and the membrane resistance measured between 80 – 120 °C and 25 to ~95 %RH. In contrast to published data, the composite membranes consistently had higher resistance than the commercial and pristine recast membranes. When only the composite membranes were considered, the IEC and WU trends both suggested an increasing trend from 0.5 wt% to 3 wt%, after which the values dropped as the filler loading was increased to 5 wt%. The proton conductivity showed two trends. First, a smooth increase in resistance as the filler loading increased, at lower humidification (25-50 %RH) and at 120 °C overall. At higher humidification (75 to ~95 %RH) and between 80 – 100 °C, a maximum proton conductivity was measured for the 3 wt% filler loading.

Membrane electrode assemblies (MEAs) were prepared using commercial electrodes with 0.4 mgPt/cm^2 and the polarisation and impedance measured at the same optimised conditions as for the resistance measurements. The in-situ performance, based on power density, echoed the ex-situ results, at lower humidification and 120 °C, with decreasing power density as the filler loading increased from 0.5 to 3 to 5 wt%. This was maintained after dew point adjustment which was required to eliminate flooding at the highest humidification level. In contrast to the ex-situ tests, the composite membranes consistently showed higher power density for the 0.5 wt% membrane than for both the reference membranes. Analysis of impedance data showed different trends for the non-optimised and optimised dew point. The greatest effect was on the membrane with the highest GO loading changing the trend from 3 ≈ Nafion 212 > 0.5 wt% to 0.5 ≈ Nafion 212 > 3. Under non-optimised conditions, and at the highest humidity, the ex-situ and in-situ proton conductivity values were the closest and under these conditions the proton conductivity also showed an upwards trend with temperature increase.

Comparing the results from this study with literature values underlined the discrepancies which were highlighted in the literature review. A notable departure was the performance overall for the composite materials compared to the reference materials, where this study measured much lower membrane resistance and higher maximum power density than that which had been published for the commercial Nafion 212 membrane. As a result, this study could not conclude that doping of pristine membranes with graphene oxide led to increased performance. This was particularly apparent for ex-situ resistance measurements. It did however confirm that membranes with a filler loading of 0.5 wt% had in-situ power density which was at least as high, or slightly higher, at 120 °C and 50 %RH.

9.2 Further work

In terms of required further work on Nafion-GO membranes, collaborative studies between institutions is suggested in order to allow for the standardisation of membrane preparation and MEA manufacturing, and thus more meaningful comparative analysis of test results on materials with similar properties. The inclusion of standard reference materials in this respect is imperative. In a broader sense, the development of composite materials would benefit from an agreed standard set of filler loadings used in testing and the development of a characterisation technique to accurately confirm the actual percentage present. This is a particular area that would benefit from refinement with respect to graphene oxide as the hygroscopic nature makes measuring of small quantities challenging.

In terms of in-situ evaluation of composite membrane MEAs, a broad range of operating conditions should be investigated in order to optimise the performance, particularly with respect to the humidification of the fuel gasses. A small adjustment in the dew point was shown to have a significant effect on the performance of the cell for certain membranes, and an optimal setting could possibly be found with an unequal humidification at the anode and the cathode side of the cell. A proposal for further study in this respect has been accepted for a post-doctoral study at the Federal University of Rio Grande do Sul and one of the key objectives include the investigation of reduced flow rates and the effect of reduced humidification at the cathode side of the cell. A further area of interest is gas permeability testing, as composite membranes could significantly decrease fuel crossover.

Results obtained in this study showed no improvement in performance for membranes prepared from functionalised GO vs. pristine GO. As it was shown in Chapter 2 however, the

performance of composite membranes prepared with sulfonated GO appeared to show an increase in performance as the loading increased – as opposed to a peak in the performance for pristine GO – indicating that a more in-depth study could have confirmed this trend. A further comparative study on different types of functionalisation on GO could therefore show promising results.

REFERENCES

1. Moore, R. and V. Raman, *Hydrogen infrastructure for fuel cell transportation.* International Journal of Hydrogen Energy, 1998. **23**(7): p. 617-620.
2. Assefa, G. and B. Frostell, *Social sustainability and social acceptance in technology assessment: A case study of energy technologies.* Technology in Society, 2007. **29**(1): p. 63-78.
3. Granovskii, M., I. Dincer, and M.A. Rosen, *Economic and environmental comparison of conventional, hybrid, electric and hydrogen fuel cell vehicles.* Journal of Power Sources, 2006. **159**(2): p. 1186-1193.
4. Rikukawa, M. and K. Sanui, *Proton-conducting polymer electrolyte membranes based on hydrocarbon polymers.* Progress in Polymer Science, 2000. **25**(10): p. 1463-1502.
5. Scott, J.H., *Fuel Cell Development for NASA's Human Exploration Program: Benchmarking With "The Hydrogen Economy".* Journal of Fuel Cell Science and Technology, 2009. **6**(2).
6. Larminie, J. and A. Dicks, *Fuel Cell Systems Explained*. 2000: John Wiley & Sons.
7. Chandan, A., et al., *High temperature (HT) polymer electrolyte membrane fuel cells (PEMFC) – A review.* Journal of Power Sources, 2013. **231**(0): p. 264-278.
8. Bernay, C., M. Marchand, and M. Cassir, *Prospects of different fuel cell technologies for vehicle applications.* Journal of Power Sources, 2002. **108**(1–2): p. 139-152.
9. Bakker, S., *The car industry and the blow-out of the hydrogen hype.* Energy Policy, 2010. **38**(11): p. 6540-6544.
10. Konrad, K., et al., *Strategic responses to fuel cell hype and disappointment.* Technological Forecasting and Social Change, 2012. **79**(6): p. 1084-1098.
11. Atkins, P. and J. de Paula, *Elements of Physical Chemistry*. Fourth Ed. ed. 2007, Oxford: Oxford University Press & W. H. Freeman and Compary.
12. FuelCells2000. *Fuel Cells 2000 - Types of Fuel Cells*. 2015 [cited 2015; Available from: http://www.fuelcells.org/base.cgim?template=types_of_fuel_cells.
13. Hou, H.-Y., *Recent Research Progress in Alkaline Polymer Electrolyte Membranes for Alkaline Solid Fuel Cells.* Acta Physico-Chimica Sinica, 2014. **30**(8): p. 1393-1407.
14. Sharma, S. and B.G. Pollet, *Support materials for PEMFC and DMFC electrocatalysts—A review.* Journal of Power Sources, 2012. **208**(0): p. 96-119.
15. Dupuis, A.-C., *Proton exchange membranes for fuel cells operated at medium temperatures: Materials and experimental techniques.* Progress in Materials Science, 2011. **56**(3): p. 289-327.
16. Bose, S., et al., *Polymer membranes for high temperature proton exchange membrane fuel cell: Recent advances and challenges.* Progress in Polymer Science, 2011.
17. Bai, H. and W.S.W. Ho, *Recent developments in fuel-processing and proton-exchange membranes for fuel cells.* Polymer International, 2011. **60**(1): p. 26-41.
18. Peighambardoust, S.J., S. Rowshanzamir, and M. Amjadi, *Review of the proton exchange membranes for fuel cell applications.* International Journal of Hydrogen Energy, 2010. **35**(17): p. 9349-9384.
19. Gourdoupi, N., J.K. Kallitsis, and S. Neophytides, *New proton conducting polymer blends and their fuel cell performance.* Journal of Power Sources, 2010. **195**(1): p. 170-174.
20. Zaidi, S.M.J., *Research Trends in Polymer Electrolyte Membranes for PEMFC*. Polymer Membranes for Fuel Cells. 2009: Springer Science + Business Media.

21. Puffer, R.H. and S.J. Rock, *Recent Advances in High Temperature Proton Exchange Membrane Fuel Cell Manufacturing.* Journal of Fuel Cell Science and Technology, 2009. **6**(4).
22. Martin, K.E. and J.P. Kopasz, *The US DOEs High Temperature Membrane Effort.* Fuel Cells, 2009. **9**(4): p. 356-362.
23. Devanathan, R., *Recent developments in proton exchange membranes for fuel cells.* Energy & Environmental Science, 2008. **1**(1): p. 101-119.
24. Shao, Y., et al., *Proton exchange membrane fuel cell from low temperature to high temperature: Material challenges.* Journal of Power Sources, 2007. **167**(2): p. 235-242.
25. Miyatake, K. and M. Watanabe, *Emerging membrane materials for high temperature polymer electrolyte fuel cells: durable hydrocarbon ionomers.* Journal of Materials Chemistry, 2006. **16**(46): p. 4465-4467.
26. Hamrock, S.J. and M.A. Yandrasits, *Proton exchange membranes for fuel cell applications.* Polymer Reviews, 2006. **46**(3): p. 219-244.
27. Smitha, B., S. Sridhar, and A.A. Khan, *Solid polymer electrolyte membranes for fuel cell applications - a review.* Journal of Membrane Science, 2005. **259**(1-2): p. 10-26.
28. Miyatake, K. and M. Watanabe, *Recent progress in proton conducting membranes for PEFCs.* Electrochemistry, 2005. **73**(1): p. 12-19.
29. Wieser, C., *Novel Polymer Electrolyte Membranes for Automotive Applications – Requirements and Benefits.* Fuel Cells, 2004. **4**(4): p. 245-250.
30. Schuster, M.E. and W.H. Meyer, *Anhydrous proton-conducting polymers.* Annual Review of Materials Research, 2003. **33**: p. 233-261.
31. Roziere, J. and D.J. Jones, *Non-fluorinated polymer materials for proton exchange membrane fuel cells.* Annual Review of Materials Research, 2003. **33**: p. 503-555.
32. Mehta, V. and J.S. Cooper, *Review and analysis of PEM fuel cell design and manufacturing.* Journal of Power Sources, 2003. **114**(1): p. 32-53.
33. Li, Q., et al., *Approaches and Recent Development of Polymer Electrolyte Membranes for Fuel Cells Operating above 100 °C.* Chemistry of Materials, 2003. **15**(26): p. 4896-4915.
34. Glusen, A. and D. Stolten, *Membranes for polymer electrolyte fuel cells.* Chemie Ingenieur Technik, 2003. **75**(11): p. 1591-1597.
35. Kerres, J.A., *Development of ionomer membranes for fuel cells.* Journal of Membrane Science, 2001. **185**(1): p. 3-27.
36. Costamagna, P. and S. Srinivasan, *Quantum jumps in the PEMFC science and technology from the 1960s to the year 2000: Part I. Fundamental scientific aspects.* Journal of Power Sources, 2001. **102**(1-2): p. 242-252.
37. Park, C.H., et al., *Sulfonated hydrocarbon membranes for medium-temperature and low-humidity proton exchange membrane fuel cells (PEMFCs).* Progress in Polymer Science, 2011. **36**(11): p. 1443-1498.
38. El-kharouf, A., et al., *Proton Exchange Membrane Fuel Cells Degradation and Testing – A Review.* J.Energy.Inst (in press).
39. Bose, S., et al., *Polymer membranes for high temperature proton exchange membrane fuel cell: recent advances and challenges.* Progress in Polymer Science, 2011. **36**(6): p. 813-843.
40. Yu, T.L., *Overview of Electrochemical Polymer Electrolyte Membranes*, in *Electrochemical Polymer Electrolyte Membranes*. 2015, CRC Press. p. 1-60.
41. Yi, S.Z., et al., *Anhydrous elevated-temperature polymer electrolyte membranes based on ionic liquids.* Journal of Membrane Science, 2011. **366**(1-2): p. 349-355.

42. Hogarth, W.H.J., J.C. Diniz da Costa, and G.Q. Lu, *Solid acid membranes for high temperature (¿ C) proton exchange membrane fuel cells.* Journal of Power Sources, 2005. **142**(1-2): p. 223-237.
43. Ma, Y.L., et al., *Conductivity of PBI membranes for high-temperature polymer electrolyte fuel cells.* Journal of The Electrochemical Society, 2004. **151**(1): p. A8-A16.
44. Mistry, M.K., et al., *Interfacial Interactions in Aprotic Ionic Liquid Based Protonic Membrane and Its Correlation with High Temperature Conductivity and Thermal Properties.* Langmuir, 2009. **25**(16): p. 9240-9251.
45. Banerjee, S. and D.E. Curtin, *Nafion® perfluorinated membranes in fuel cells.* Journal of Fluorine Chemistry, 2004. **125**(8): p. 1211-1216.
46. Asensio, J.A., E.M. Sanchez, and P. Gomez-Romero, *Proton-conducting membranes based on benzimidazole polymers for high-temperature PEM fuel cells. A chemical quest.* Chemical Society Reviews, 2010. **39**(8): p. 3210-3239.
47. Iojoiu, C., et al., *From polymer chemistry to membrane elaboration: A global approach of fuel cell polymeric electrolytes.* Journal of Power Sources, 2006. **153**(2): p. 198-209.
48. Miyatake, K., B. Bae, and M. Watanabe, *Fluorene-containing cardo polymers as ion conductive membranes for fuel cells.* Polymer Chemistry, 2011.
49. Parvole, J. and P. Jannasch, *Polysulfones grafted with poly(vinylphosphonic acid) for highly proton conducting fuel cell membranes in the hydrated and nominally dry state.* Macromolecules, 2008. **41**(11): p. 3893-3903.
50. Nam, S.E., et al., *Preparation of Nafion/sulfonated poly(phenylsilsesquioxane) nanocomposite as high temperature proton exchange membranes.* Journal of Membrane Science, 2008. **322**(2): p. 466-474.
51. Verma, A. and K. Scott, *Development of high-temperature PEMFC based on heteropolyacids and polybenzimidazole.* Journal of Solid State Electrochemistry, 2010. **14**(2): p. 213-219.
52. Yuan, J.J., H.T. Pu, and Z.L. Yang, *Studies on Sulfonic Acid Functionalized Hollow Silica Spheres/Nafion (R) Composite Proton Exchange Membranes.* Journal of Polymer Science Part a-Polymer Chemistry, 2009. **47**(10): p. 2647-2655.
53. Zarrin, H., et al., *Functionalized graphene oxide as a new highly proton conductive composite membrane for high temperature PEMFCs*, in *Abstract #643, 219th ECS Meeting, © 2011 The Electrochemical Society*. 2011.
54. Casciola, M., et al., *Nafion-zirconium phosphate nanocomposite membranes with high filler loadings: Conductivity and mechanical properties.* Fuel Cells, 2008. **8**(3-4): p. 217-224.
55. Kim, Y.T., et al., *Nafion/ZrSPP composite membrane for high temperature operation of proton exchange membrane fuel cells.* Current Applied Physics, 2006. **6**(4): p. 612-615.
56. Kozawa, Y., et al., *Proton conducting membranes composed of sulfonated poly(etheretherketone) and zirconium phosphate nanosheets for fuel cell applications.* Solid State Ionics, 2010. **181**(5-7): p. 348-353.
57. Miyatake, K., et al., *Synthesis and properties of a polyimide containing pendant sulfophenoxypropoxy groups.* Journal of Polymer Science Part a-Polymer Chemistry, 2007. **45**(1): p. 157-163.
58. Bae, B., et al., *Proton-Conductive Aromatic Ionomers Containing Highly Sulfonated Blocks for High-Temperature-Operable Fuel Cells.* Angewandte Chemie-International Edition, 2010. **49**(2): p. 317-320.

59. Li, Q., et al., *Partially fluorinated aarylene polyethers and their ternary blends with PBI and H3PO4. Part II. Characterisation and fuel cell tests of the ternary membranes.* Fuel Cells, 2008. **8**(3-4): p. 188-199.
60. Li, Q.F., et al., *Properties, degradation and high temperature fuel cell test of different types of PBI and PBI blend membranes.* Journal of Membrane Science, 2010. **347**(1-2): p. 260-270.
61. Lee, H.S., et al., *Synthesis and characterization of poly(arylene ether sulfone)-b-polybenzimidazole copolymers for high temperature low humidity proton exchange membrane fuel cells.* Polymer, 2008. **49**(25): p. 5387-5396.
62. Kallitsis, J.K., M. Geormezi, and S.G. Neophytides, *Polymer electrolyte membranes for high-temperature fuel cells based on aromatic polyethers bearing pyridine units.* Polymer International, 2009. **58**(11): p. 1226-1233.
63. Tripathi, B.P. and V.K. Shahi, *Organic–inorganic nanocomposite polymer electrolyte membranes for fuel cell applications.* Progress in Polymer Science, 2011. **36**(7): p. 945-979.
64. Laberty-Robert, C., et al., *Design and properties of functional hybrid organic-inorganic membranes for fuel cells.* Chemical Society Reviews, 2011. **40**(2): p. 961-1005.
65. Li, Q., et al., *High temperature proton exchange membranes based on polybenzimidazoles for fuel cells.* Progress in Polymer Science, 2009. **34**(5): p. 449-477.
66. *<Colicchio 2009.pdf>*.
67. Wang, S., et al., *Novel epoxy-based cross-linked polybenzimidazole for high temperature proton exchange membrane fuel cells.* International Journal of Hydrogen Energy, 2011. **36**(14): p. 8412-8421.
68. Han, M.M., et al., *Cross-linked polybenzimidazole with enhanced stability for high temperature proton exchange membrane fuel cells.* Journal of Materials Chemistry, 2011. **21**(7): p. 2187-2193.
69. Kim, S.K., et al., *Cross-Linked Benzoxazine-Benzimidazole Copolymer Electrolyte Membranes for Fuel Cells at Elevated Temperature.* Macromolecules, 2012. **45**(3): p. 1438-1446.
70. Aili, D., et al., *Crosslinking of polybenzimidazole membranes by divinylsulfone post-treatment for high-temperature proton exchange membrane fuel cell applications.* Polymer International, 2011. **60**(8): p. 1201-1207.
71. Sheng, L., et al., *Synthesis and properties of novel sulfonated polybenzimidazoles from disodium 4,6-bis(4-carboxyphenoxy)benzene-1,3-disulfonate.* Journal of Power Sources, 2011. **196**(6): p. 3039-3047.
72. Mader, J.A. and B.C. Benicewicz, *Synthesis and Properties of Segmented Block Copolymers of Functionalised Polybenzimidazoles for High-Temperature PEM Fuel Cells.* Fuel Cells, 2011. **11**(2): p. 222-237.
73. Mader, J.A. and B.C. Benicewicz, *Sulfonated Polybenzimidazoles for High Temperature PEM Fuel Cells.* Macromolecules, 2010. **43**(16): p. 6706-6715.
74. Haile, S.M., et al., *Solid acids as fuel cell electrolytes.* Nature, 2001. **410**(6831): p. 910-913.
75. Yang, C., et al., *Approaches and technical challenges to high temperature operation of proton exchange membrane fuel cells.* Journal of Power Sources, 2001. **103**(1): p. 1-9.
76. Piao, J.H., S.J. Liao, and Z.X. Liang, *A novel cesium hydrogen sulfate-zeolite inorganic composite electrolyte membrane for polymer electrolyte membrane fuel cell application.* Journal of Power Sources, 2009. **193**(2): p. 483-487.

77. Tsui, E.M., M.M. Cortalezzi, and M.R. Wiesner, *Proton conductivity and methanol rejection by ceramic membranes derived from ferroxane and alumoxane precursors.* Journal of Membrane Science, 2007. **306**(1-2): p. 8-15.
78. Xu, C., et al., *A polybenzimidazole/sulfonated graphite oxide composite membrane for high temperature polymer electrolyte membrane fuel cells.* Journal of Materials Chemistry, 2011. **21**(30): p. 11359-11364.
79. Treekamol, Y., et al., *Nafion (R)/ODF-silica composite membranes for medium temperature proton exchange membrane fuel cells.* Journal of Power Sources, 2014. **246**: p. 950-959.
80. Xie, L., E.B. Cho, and D. Kim, *Sulfonated PEEK/cubic (Im3m) mesoporous benzene-silica composite membranes operable at low humidity.* Solid State Ionics, 2011. **203**(1): p. 1-8.
81. Furtado, A.A.M. and A.S. Games, *Sulfonated bisphenol-A-polysulfone based composite PEMs containing tungstophosphoric acid and modified by electron beam irradiation.* International Journal of Hydrogen Energy, 2012. **37**(7): p. 6228-6235.
82. Xue, C., et al., *Graphite oxide/functionalized graphene oxide and polybenzimidazole composite membranes for high temperature proton exchange membrane fuel cells.* International Journal of Hydrogen Energy, 2014. **39**(15): p. 7931-7939.
83. Ganguly, A., et al., *Probing the Thermal Deoxygenation of Graphene Oxide Using High-Resolution In Situ X-ray-Based Spectroscopies.* The Journal of Physical Chemistry C, 2011. **115**(34): p. 17009-17019.
84. Liu, Y.F., et al., *Bronsted acid-base polymer electrolyte membrane based on sulfonated poly(phenylene oxide) and imidazole.* European Polymer Journal, 2006. **42**(9): p. 2199-2203.
85. Ye, G.B., et al., *Nafion (R)-Titania Nanocomposite Proton Exchange Membranes.* Journal of Applied Polymer Science, 2011. **120**(2): p. 1186-1192.
86. Wang, Z.B., H.L. Tang, and M. Pan, *Self-assembly of durable Nafion/TiO2 nanowire electrolyte membranes for elevated-temperature PEM fuel cells.* Journal of Membrane Science, 2011. **369**(1-2): p. 250-257.
87. Mishra, A.K., et al., *Effect of peptizer on the properties of Nafion-Laponite clay nanocomposite membranes for polymer electrolyte membrane fuel cells.* Journal of Membrane Science, 2012. **389**: p. 316-323.
88. Kongkachuichay, P. and S. Pimprom, *Nafion/Analcime and Nafion/Faujasite composite membranes for polymer electrolyte membrane fuel cells.* Chemical Engineering Research & Design, 2010. **88**(4A): p. 496-500.
89. Amirinejad, M., et al., *Cesium hydrogen salt of heteropolyacids/Nafion nanocomposite membranes for proton exchange membrane fuel cells.* Journal of Membrane Science, 2011. **377**(1–2): p. 89-98.
90. Aili, D., et al., *Phosphoric acid doped membranes based on Nafion (R), PBI and their blends - Membrane preparation, characterization and steam electrolysis testing.* International Journal of Hydrogen Energy, 2011. **36**(12): p. 6985-6993.
91. Kumar, R., C.X. Xu, and K. Scott, *Graphite oxide/Nafion composite membranes for polymer electrolyte fuel cells.* Rsc Advances, 2012. **2**(23): p. 8777-8782.
92. Zarrin, H., et al., *Functionalized Graphene Oxide Nanocomposite Membrane for Low Humidity and High Temperature Proton Exchange Membrane Fuel Cells.* The Journal of Physical Chemistry C, 2011. **115**(42): p. 20774-20781.
93. Lin, C.W. and Y.S. Lu, *Highly ordered graphene oxide paper laminated with a Nafion membrane for direct methanol fuel cells.* Journal of Power Sources, 2013. **237**(0): p. 187-194.

94. He, Y., et al., *Enhanced performance of the sulfonated polyimide proton exchange membranes by graphene oxide: Size effect of graphene oxide.* Journal of Membrane Science, 2014. **458**(0): p. 36-46.
95. Stankovich, S., et al., *Graphene-based composite materials.* Nature, 2006. **442**(7100): p. 282-286.
96. Jung, I., et al., *Tunable Electrical Conductivity of Individual Graphene Oxide Sheets Reduced at "Low" Temperatures.* Nano Letters, 2008. **8**(12): p. 4283-4287.
97. Kotov, N.A., I. Dékány, and J.H. Fendler, *Ultrathin graphite oxide–polyelectrolyte composites prepared by self-assembly: Transition between conductive and non-conductive states.* Advanced Materials, 1996. **8**(8): p. 637-641.
98. Dreyer, D.R., et al., *The chemistry of graphene oxide.* Chemical Society Reviews, 2010. **39**(1).
99. Staudenmaier, L., *Verfahren zur Darstellung der Graphitsäure.* Berichte der deutschen chemischen Gesellschaft, 1898. **31**(2): p. 1481-1487.
100. Hummers, W.S. and R.E. Offeman, *Preparation of Graphitic Oxide.* Journal of the American Chemical Society, 1958. **80**(6): p. 1339-1339.
101. Lee, D.C., et al., *Nafion/graphene oxide composite membranes for low humidifying polymer electrolyte membrane fuel cell.* Journal of Membrane Science, 2014. **452**(0): p. 20-28.
102. Chien, H.C., et al., *Sulfonated graphene oxide/Nafion composite membranes for high-performance direct methanol fuel cells.* International Journal of Hydrogen Energy, 2013. **38**(31): p. 13792-13801.
103. Choi, B.G., et al., *Innovative Polymer Nanocomposite Electrolytes: Nanoscale Manipulation of Ion Channels by Functionalized Graphenes.* Acs Nano, 2011. **5**(6): p. 5167-5174.
104. Enotiadis, A., et al., *Graphene-Based Nafion Nanocomposite Membranes: Enhanced Proton Transport and Water Retention by Novel Organo-functionalized Graphene Oxide Nanosheets.* Small, 2012. **8**(21): p. 3338-3349.
105. Cao, Y.C., et al., *A poly (ethylene oxide)/graphene oxide electrolyte membrane for low temperature polymer fuel cells.* Journal of Power Sources, 2011. **196**(20): p. 8377-8382.
106. He, H., et al., *A new structural model for graphite oxide.* Chemical Physics Letters, 1998. **287**(1–2): p. 53-56.
107. Lerf, A., et al., *13C and 1H MAS NMR studies of graphite oxide and its chemically modified derivatives.* Solid State Ionics, 1997. **101–103, Part 2**(0): p. 857-862.
108. Wang, Y., et al., *Zeolite beta-filled chitosan membrane with low methanol permeability for direct methanol fuel cell.* Journal of Power Sources, 2008. **183**(2): p. 454-463.
109. Chen, G.F., et al., *Preparation of sulfonic-functionalized graphene oxide as ion-exchange material and its application into electrochemiluminescence analysis.* Biosensors & Bioelectronics, 2011. **26**(7): p. 3136-3141.
110. Han, W., et al., *Zeolite-Confined Sulfonated Graphene-Nafion Composite Membrane for Self-Humidifying PEMFC*. 2013, 13AIChE Annual Meeting.
111. Yeung, K.L., W. Han, and H.Y. Poon, *Graphene-Based Self-Humidifying Membrane and Self-Humidifying Fuel Cell*, in *United States, Patent Application Publication*, P.A.P. United States, Editor. 2013: United States.
112. Souzy, R. and B. Ameduri, *Functional fluoropolymers for fuel cell membranes.* Progress in Polymer Science, 2005. **30**(6): p. 644-687.

113. Slade, S., et al., *Ionic Conductivity of an Extruded Nafion 1100 EW Series of Membranes.* Journal of The Electrochemical Society, 2002. **149**(12): p. A1556-A1564.
114. MacMillan, B., A. Sharp, and R. Armstrong, *An n.m.r. investigation of the dynamical characteristics of water absorbed in Nafion.* Polymer, 1999. **40**(10): p. 2471-2480.
115. Wannek, C., W. Lehnert, and J. Mergel, *Membrane electrode assemblies for high-temperature polymer electrolyte fuel cells based on poly(2,5-benzimidazole) membranes with phosphoric acid impregnation via the catalyst layers.* Journal of Power Sources, 2009. **192**(2): p. 258-266.
116. Miyatake, K., T. Yasuda, and M. Watanabe, *Substituents effect on the properties of sulfonated polyimide copolymers.* Journal of Polymer Science Part a-Polymer Chemistry, 2008. **46**(13): p. 4469-4478.
117. Heo, Y., H. Im, and J. Kim, *The effect of sulfonated graphene oxide on Sulfonated Poly (Ether Ether Ketone) membrane for direct methanol fuel cells.* Journal of Membrane Science, 2013. **425–426**(0): p. 11-22.
118. Jiang, Z., X. Zhao, and A. Manthiram, *Sulfonated poly(ether ether ketone) membranes with sulfonated graphene oxide fillers for direct methanol fuel cells.* International Journal of Hydrogen Energy, 2013. **38**(14): p. 5875-5884.
119. Stankovich, S., et al., *Synthesis and exfoliation of isocyanate-treated graphene oxide nanoplatelets.* Carbon, 2006. **44**(15): p. 3342-3347.
120. Fernandes, A.C. and E.A. Ticianelli, *A performance and degradation study of Nafion 212 membrane for proton exchange membrane fuel cells.* Journal of Power Sources, 2009. **193**(2): p. 547-554.
121. de Almeida, S. and Y. Kawano, *Thermal Behavior of Nafion Membranes.* Journal of Thermal Analysis and Calorimetry, 1999. **58**(3): p. 569-577.
122. Mistry, M.K., et al., *Novel Organic-Inorganic Hybrids with Increased Water Retention for Elevated Temperature Proton Exchange Membrane Application.* Chemistry of Materials, 2008. **20**(21): p. 6857-6870.
123. Choi, B.G., et al., *Enhanced transport properties in polymer electrolyte composite membranes with graphene oxide sheets.* Carbon, 2012(0).
124. Maldonado, L., et al., *Characterization of polymer electrolyte Nafion membranes: Influence of temperature, heat treatment and drying protocol on sorption and transport properties.* Journal of Membrane Science, 2012. **389**: p. 43-56.
125. DuPont, *DuPont™ Nafion® PFSA Membranes NR-211 and NR-212* in http://fuelcellstore.com/spec-sheets/nafion-211-212-spec-sheet.pdf. 2008, E. I. du Pont de Nemours and Company
126. DuPont, *DuPont™ Nafion® PFSA Polymer Dispersions*, in http://www2.dupont.com/FuelCells/en_US/assets/downloads/dfc103.pdf. 2009, E. I. du Pont de Nemours and Company
127. Kannan, R., et al., *Domain Size Manipulation of Perflouorinated Polymer Electrolytes by Sulfonic Acid-Functionalized MWCNTs To Enhance Fuel Cell Performance.* Langmuir, 2009. **25**(14): p. 8299-8305.
128. Young, R.J. and P.A. Lovel, *Introduction to Polymers*. Second Edition ed. 1981, London: Chapman & Hall.
129. Stevens, M.P., *Polymer Chemistry, An Introduction*. Second Edition ed. 1990, Oxford: Oxford University Press.
130. Chen, C. and T.F. Fuller, *XPS Analysis of Polymer Membrane Degradation in PEMFCs.* Journal of The Electrochemical Society, 2009. **156**(10): p. B1218-B1224.

131. Parry, V., et al., *XPS investigations of the proton exchange membrane fuel cell active layers aging: Characterization of the mitigating role of an anodic CO contamination on cathode degradation.* Journal of Power Sources, 2011. **196**(5): p. 2530-2538.
132. Leng, Y., *Materials Characterization*. 2008, Singapore: John Wiley & Sons (Asia) Pte Ltd.
133. Sribner and A. Incorporated. *Fuel Cell Test Equipment and Accessories*. 2014; Available from: http://www.scribner.com/fuel-cell-and-electrochemical-hardware/fuel-cell-test-equipment.
134. Vaisala. *Humidity Converstion Formulas*. 2013; Available from: http://www.vaisala.com/Vaisala%20Documents/Application%20notes/Humidity_Conversion_Formulas_B210973EN-F.pdf.
135. Scribner. *Electrochemical Impedance Spectroscopy (EIS): A Powerful and CostEffective Tool for Fuel Cell Diagnostics* Available from: http://www.scribner.com/files/tech-papers/Scribner%20Associates%20-%20Electrochemical%20Impedance%20Spectroscopy%20for%20Fuel%20Cell%20Research.pdf.
136. Princeton and A. Research. *Basics of Electrochemical Impedance Spectroscopy*. Available from: www.princetonappliedresearch.com.
137. Katz, E. and I. Willner, *Probing Biomolecular Interactions at Conductive and Semiconductive Surfaces by Impedance Spectroscopy: Routes to Impedimetric Immunosensors, DNA-Sensors, and Enzyme Biosensors.* Electroanalysis, 2003. **15**(11): p. 913-947.
138. Yadav, R. and P.S. Fedkiw, *Analysis of EIS Technique and Nafion 117 Conductivity as a Function of Temperature and Relative Humidity.* Journal of The Electrochemical Society, 2012. **159**(3): p. B340-B346.
139. Cooper, K., *Characterizing through-plane and in-plane ionic conductivity of polymer electrolyte membranes.* Proton Exchange Membrane Fuel Cells 8, Pts 1 and 2, 2011. **41**(1): p. 1371-1380.
140. Bae, B., K. Miyatake, and M. Watanabe, *Sulfonated Poly(arylene ether sulfone ketone) Multiblock Copolymers with Highly Sulfonated Block. Synthesis and Properties.* Macromolecules, 2010. **43**(6): p. 2684-2691.
141. Silva, R.F., M. De Francesco, and A. Pozio, *Solution-cast Nafion® ionomer membranes: preparation and characterization.* Electrochimica Acta, 2004. **49**(19): p. 3211-3219.
142. Bae, B., K. Miyatake, and M. Watanabe, *Synthesis and Properties of Sulfonated Block Copolymers Having Fluorenyl Groups for Fuel-Cell Applications.* Acs Applied Materials & Interfaces, 2009. **1**(6): p. 1279-1286.
143. Kaliaguine, S., et al., *Properties of SPEEK based PEMs for fuel cell application.* Catalysis Today, 2003. **82**(1-4): p. 213-222.
144. Jun, M.-S., Y.-W. Choi, and J.-D. Kim, *Solvent casting effects of sulfonated poly(ether ether ketone) for Polymer electrolyte membrane fuel cell.* Journal of Membrane Science, (0).
145. Peron, J., et al., *Properties of Nafion (R) NR-211 membranes for PEMFCs.* Journal of Membrane Science, 2010. **356**(1-2): p. 44-51.
146. Lin, H.-L., et al., *Morphology study of Nafion membranes prepared by solutions casting.* Journal of Polymer Science Part B: Polymer Physics, 2005. **43**(21): p. 3044-3057.
147. Kreuer, K.-D., et al., *Transport in Proton Conductors for Fuel-Cell Applications: Simulations, Elementary Reactions, and Phenomenology.* Chemical Reviews, 2004. **104**(10): p. 4637-4678.

148. Laporta, M., M. Pegoraro, and L. Zanderighi, *Recast Nafion-117 thin film from water solution.* Macromolecular Materials and Engineering, 2000. **282**(1): p. 22-29.
149. Sahu, A., et al., *Nafion and modified-Nafion membranes for polymer electrolyte fuel cells: An overview.* Bulletin of Materials Science, 2009. **32**(3): p. 285-294.
150. UniversityofWashington. Available from: http://depts.washington.edu/eooptic/linkfiles/dielectric_chart[1].pdf.
151. Sone, Y., P. Ekdunge, and D. Simonsson, *Proton conductivity of Nafion 117 as measured by a four-electrode AC impedance method.* Journal of The Electrochemical Society, 1996. **143**(4): p. 1254-1259.
152. Tateishi, H., et al., *Graphene Oxide Fuel Cell.* Journal of The Electrochemical Society, 2013. **160**(11): p. F1175-F1178.
153. Scribner and A. Incorporated. *Fuel Cell Test Equipment and Accessories*. 2014; Available from: http://www.scribner.com/fuel-cell-and-electrochemical-hardware/fuel-cell-test-equipment.
154. Wang, H., et al., *High Proton Conductivity of Water Channels in a Highly Ordered Nanowire.* Angewandte Chemie International Edition, 2011. **50**(52): p. 12538-12541.
155. Kreuer, K.-D. and A. Wohlfarth, *Limits of Proton Conductivity.* Angewandte Chemie International Edition, 2012. **51**(42): p. 10454-10456.
156. Choi, J., et al., *High Conductivity Perfluorosulfonic Acid Nanofiber Composite Fuel-Cell Membranes.* Chemsuschem, 2010. **3**(11): p. 1245-1248.
157. Lensen, D., D.M. Vriezema, and J.C.M. van Hest, *Polymeric Microcapsules for Synthetic Applications.* Macromolecular Bioscience, 2008. **8**(11): p. 991-1005.
158. Bergman, S.D. and F. Wudl, *Mendable polymers.* Journal of Materials Chemistry, 2008. **18**(1): p. 41-62.
159. El-Kharouf, A., et al., *Proton exchange membrane fuel cell degradation and testing: review.* Journal of the Energy Institute, 2012. **85**(4): p. 188-200.
160. Pu, H., D. Wang, and Z. Yang, *Towards high water retention of proton exchange membranes at elevated temperature via hollow nanospheres.* Journal of Membrane Science, 2010. **360**(1–2): p. 123-129.
161. Wang, J.T., et al., *Enhanced Water Retention by Using Polymeric Microcapsules to Confer High Proton Conductivity on Membranes at Low Humidity.* Advanced Functional Materials, 2011. **21**(5): p. 971-978.
162. Liang, C., et al., *Effect of addition of organic microspheres on proton conductivity property of sulfonated poly(arylene ether sulfone) membrane.* Journal of Applied Polymer Science, 2008. **109**(6): p. 3739-3745.
163. BangsLaboratories, *Microsphere Aggregation TechNote 202*, in *http://www.bangslabs.com/sites/default/files/imce/docs/TechNote%20202%20Web.pdf* , I. Bangs Laboratories, Editor. 2013: Fishers.
164. Yun, D.S., et al., *Controlling size and distribution for nano-sized polystyrene spheres.* Bulletin of the Korean chemical society, 2010. **31**(5): p. 1345-1348.
165. Smitha, B., S. Sridhar, and A.A. Khan, *Synthesis and characterization of proton conducting polymer membranes for fuel cells.* Journal of Membrane Science, 2003. **225**(1–2): p. 63-76.
166. Graf, C., et al., *A general method to coat colloidal particles with silica.* Langmuir, 2003. **19**(17): p. 6693-6700.

APPENDIX A1 - IDENTIFICATION OF OPTIMAL FILLER MATERIAL FOR COMPOSITE PEM – SILICA CAPSULES

Introduction

This following is a short report on the investigation of in-house synthesis of hollow silica capsules.

Following a literature review three attractive applications for hollow polymeric spheres with relation to composite PEMs were identified. The first was micro/nano reactor sites where catalysts could be encapsulated in the hollow capsules. Tuning could render the shell selectively permeable to unwanted species which upon entering the shell are neutralised by the catalyst [157]. In fuel cell application this would be applicable to hydroxyl free radical species which are thought to be formed in the MEA during operation [120] or to crossover platinum catalyst particles from the electrodes [38]. A second application was the use of these particles to form self-healing polymers. Under this principle, capsules were filled with a 'healing agent' [158] which is released if a crack in the host membrane ruptures the sphere. In this way the mechanical failure is repaired. The continuous swelling and shrinking of the membrane under fuel cell operation is a common source for membrane failure in the MEA [159]. No reports were found for fuel cell membrane application, possibly due to extensive optimisation required for chemically and mechanically compatibility with known polymer electrolytes and fuel cell operational conditions.

For immediate application, the third type of polymeric fillers which were identified were hollow functionalised spheres. Promising published results showed increased water uptake and retention in composite membranes tested at increased temperature or reduced humidity.

One published strategy was the preparation of hollow polystyrene spheres and it was reported that Nafion 112 membranes doped with 20-35 wt% of the filler material [160] improved the proton conductivity over a range of temperatures from 70 to around 115 °C. The composite membrane doped with 35 wt% of particles showed the highest proton conductivity overall and maximum proton conductivity at 105-110 °C. The material with 20 wt% filler had only slightly higher proton conductivity than the commercial Nafion 112 up to 85 °C, but whereas the commercial material showed a drastic drop in conductivity after around 85 °C, the performance of the composite continued to increase up to around 115 °C. All testing was carried out under full humidification. The reported proton conductivity was in a fairly low range. This was possibly due to the fact that Nafion 112 resin in the Na^+ form was used to prepare the membranes from DMF solvent and the membranes were re-acidified after casting.

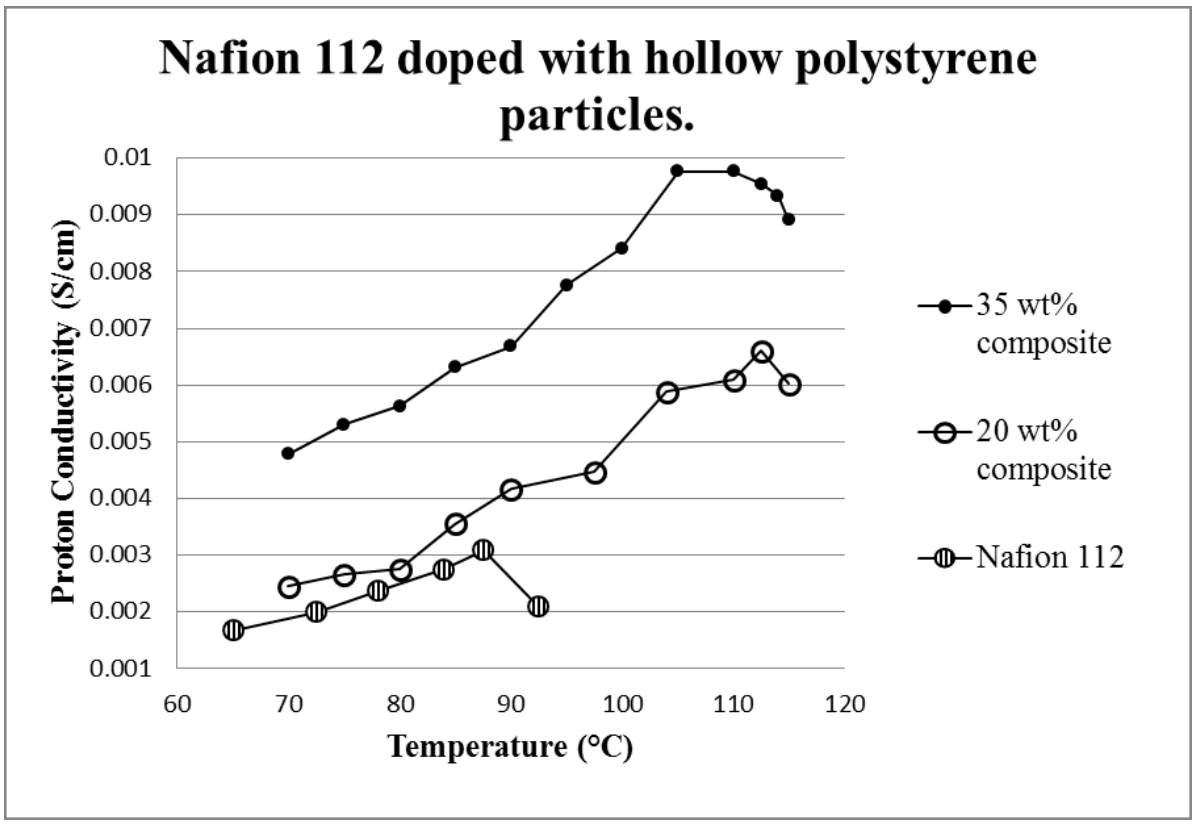

Figure A1-1 Proton conductivity for Nafion 112 membranes doped with hollow polystyrene particles. Graph was redrawn from [160].

The synthesis of the polymeric particles was carried out in two steps. First SiO_2 nanoparticles in the range of 60 nm were prepared after which a polystyrene shell was polymerised around this. The obtained core-shell particles were submerged in hydrofluoric acid to obtain the hollow polystyrene particles. Finally the particles were sulfonated with sulphuric acid to prepare the final sulfonated hollow particles which were around 100 nm in size. A similar study reported the preparation of hollow polymeric microcapsules for the doping of Chitosan membranes [161] and reported improved proton conductivity for the doped membranes over a temperature range of 20-85 °C under full humidification. The particles were prepared with different functional groups (carboxylic acid, sulfonic acid and pyridyl) and were around 500 nm in size. It was theorised that the improved performance was due to enhanced water uptake (up to 79 %) and retention in the composites when

compared to the pristine membrane. The composite membrane with 15 wt% filler material showed only 54 % loss of conductivity over 60 minutes at steady conditions (40 °C and 20 %RH), compared to 95.7 % loss for the pristine membrane.

A further study on Nafion composites was reported by Yuan *et al.* [52]. In this procedure a different strategy was followed where polystyrene particles were prepared and coated with a silica substrate (γ-mercaptopropyltriethoxysilane (MPTS)). This resulted in particles of around 170 nm in size. The doped membranes showed higher water uptake, particularly at increased temperature (up to 100 °C), and the proton conductivity for the composites were consistently higher than the recast Nafion reference membrane up to a filler loading of 10 wt%. This method was selected for particle preparation as the reported proton conductivity was in a higher range than reported for the hollow polystyrene particles. As silica particles are also more hydrophilic than the PS particles, it was possible that particle agglomeration could be avoided.

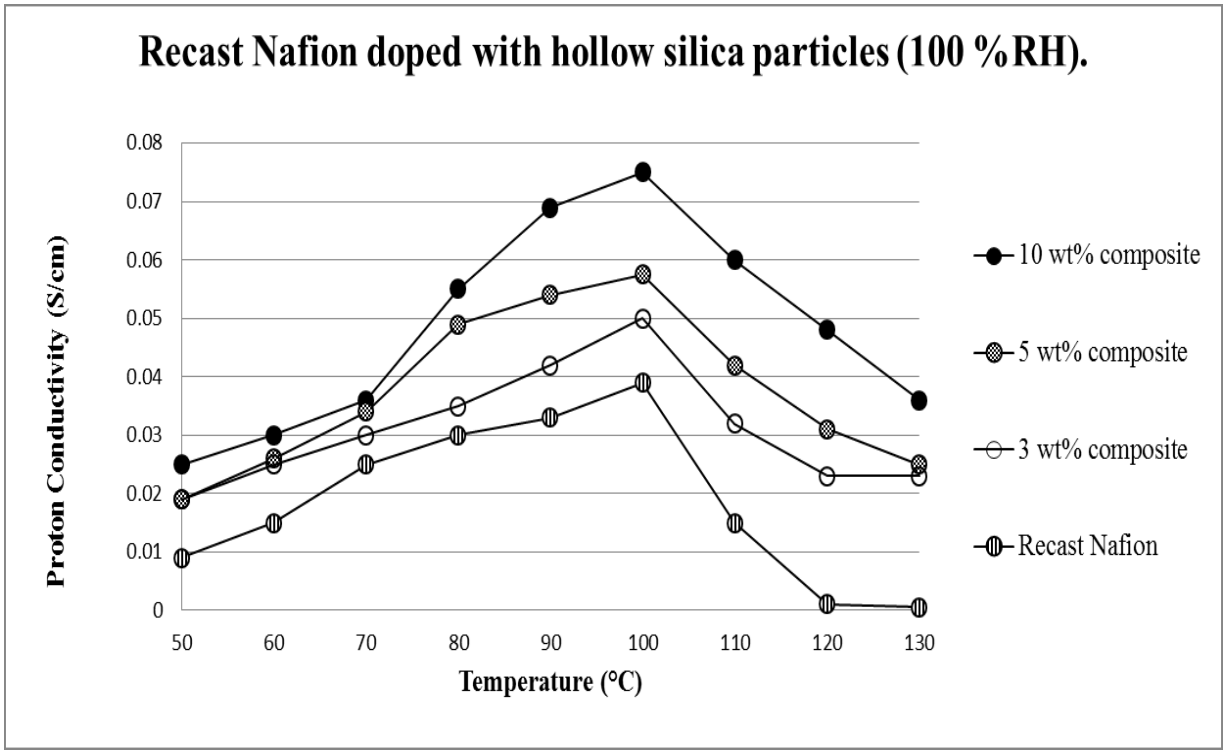

Figure A1-2 Proton conductivity for recast Nafion membranes doped with sulfonic acid functionalised hollow silica particles. Graph was redrawn from [52] (note: a different trend is shown graphically in the publication, the correct trend is shown here following correspondence with the author).

In the following sections the preparation and characterisation of the polystyrene particles and silica shells are described.

Polystyrene particles and hollow silica shell preparation.

First, two types of polystyrene particles were prepared in order to establish the optimal method. The two schemes are shown in Figure A1-3. The first type was prepared following the procedure reported by Liang *et al.* [162] using a surfactant in the solution. The emulsion polymerization was carried out to form polystyrene particles cross-linked with divinyl benzene (PS-DVB). The surfactant was included in an attempt to keep the polystyrene

particles separated after formation [163], with the size around 200 nm. The stirring speed was not reported and a rotation speed of 250 rpms. was selected.

The second procedure omitted the surfactant and polyvinylpyrrolidone (PVP) was used as dispersant in this case [52]. PVP has previously been reported as a suitable dispersant and an effective method of controlling the particle size of PS [164]. The expected particle size in this instance was around 120 nm. The method was adapted slightly by increasing the stirring speed from the reported 100 rpm to 250 rpm.

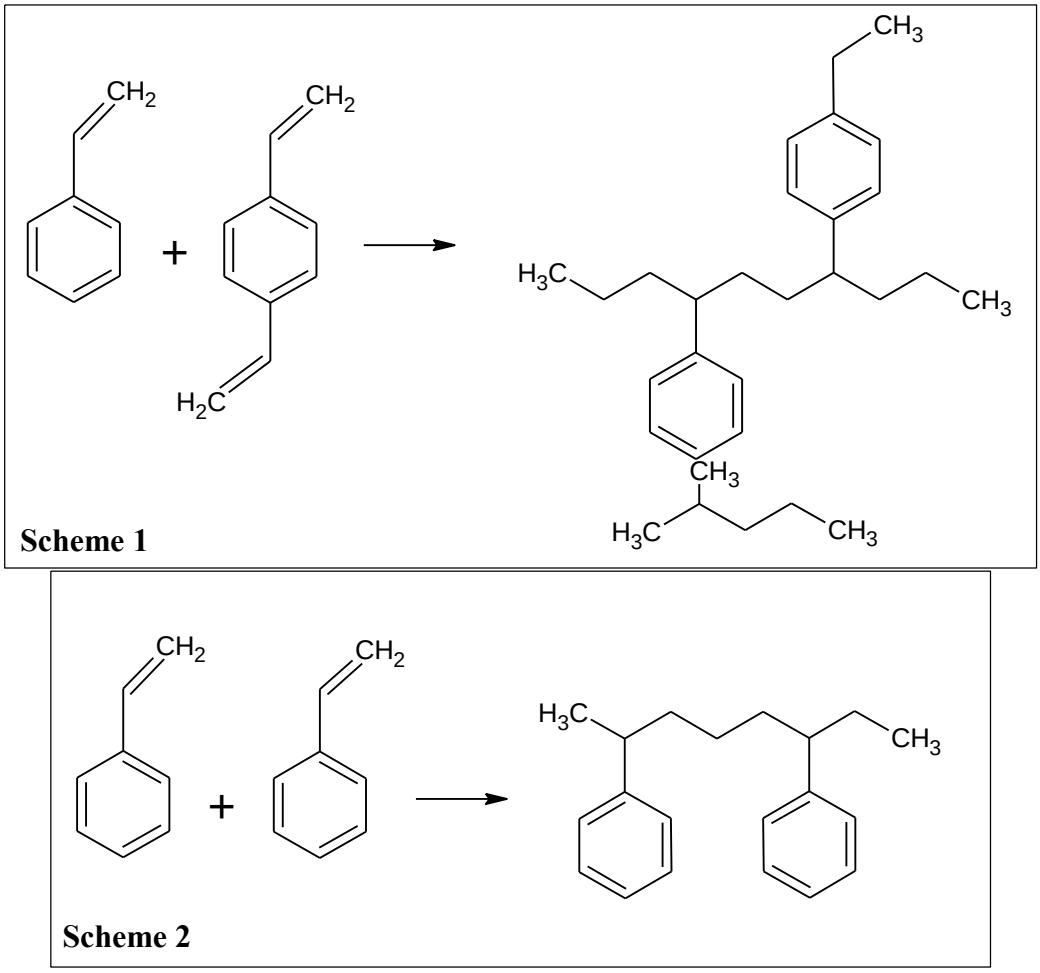

Figure A1-3 Styrene polymerisation via DVB crosslinking (Scheme 1), and with PVP as dispersant (Scheme 2).

After evaluation of the particle formation by TEM, the selected particles were used to form the silica shell. This was carried out by a modified procedure reported by Yuan *et al.* [52]. The final step in the reported procedure was the oxidation of the mercapto groups on the silica shell. For this study an additional heating step was added to remove the polystyrene core. After formation of the silica shell by 3-mercaptopropyl trimethoxysilane (MPTMS) and oxidation of the mercapto groups the product was separated, dried and heated at 550 °C for 4 hours in a furnace.

Results and discussion

The two procedures resulted in particles of two different sizes. It can be seen in Figure A1-4 that the PS-DVB particles which were prepared with sodium dodecyl sulphate as surfactant were around 30-50 nm in size. It was also found that the particles showed considerable agglomeration and that many particles were connected to each other, rather than free spheres.

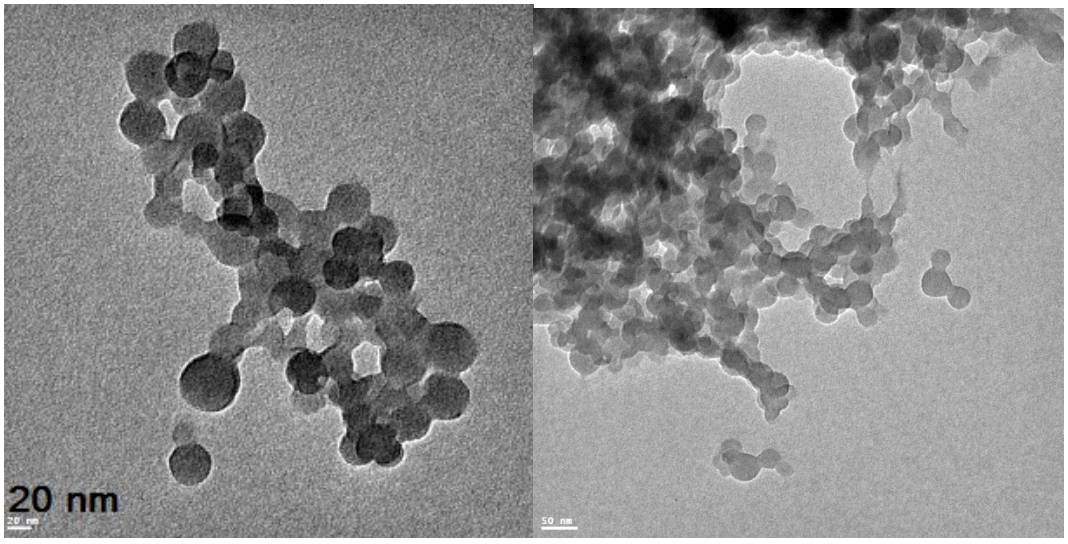

Figure A1-4 PS-DVB particles

Figure A1-5 shows the PS-PVP particles which were larger at150-200 nm but more disperse. Due to the more distinct and separate polystyrene particles, the second batch was used as the template for the formation of the silica shells.

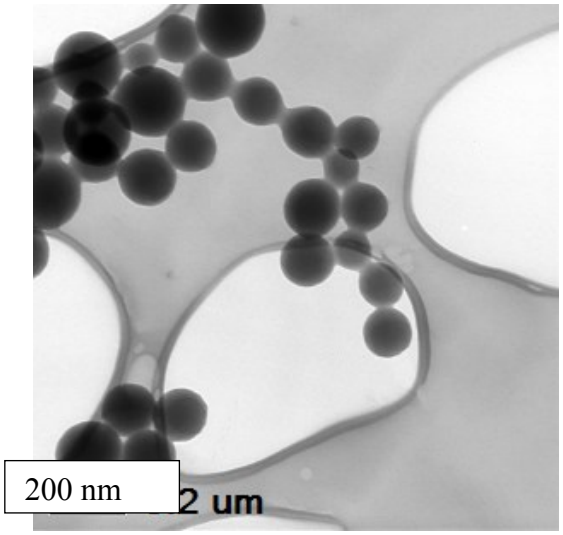

Figure A1-5 PS-PVP particles

The particles were analysed by TGA, FT-IR and XPS. Figure A1-6 shows the thermal decomposition for the polystyrene particles and this agrees well with published TGA results. The main decomposition of the material takes place at around 400 °C and the drastic weight loss between 350 °C to 450 °C has been attributed to the possible splitting of main chains or the evaporation of residual solvent [165]. The high temperature for solvent evaporation is explained when it is considered that the solvent is trapped within the rubbery state of the polymer matrix.

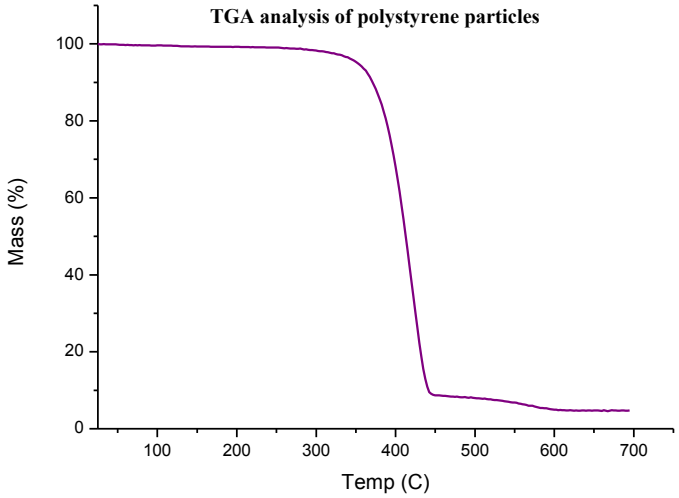

Figure A1-6 TGA for polystyrene particles

The samples were analysed by FT-IR with the characteristic peaks indicated in Figure A1-7. The peaks at 3000, 1700 and 1440 cm^{-1} are due to the C-H and C-C aromatic stretching. The peaks at 750-690 cm^{-1} are C-H out-of-plane bending.

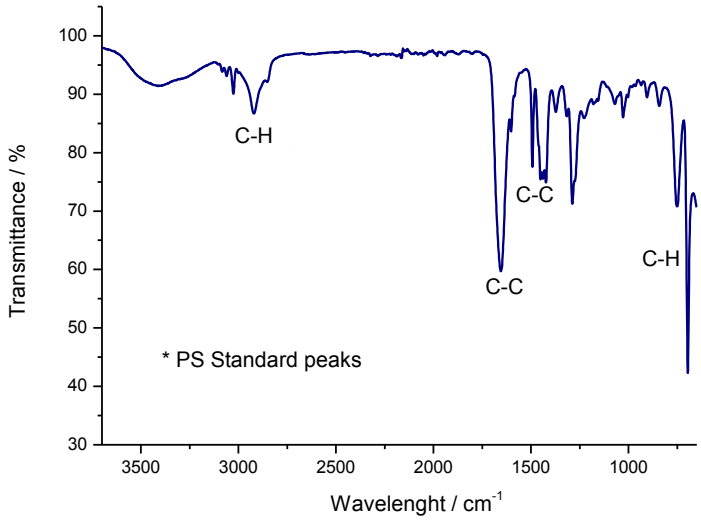

Figure A1-7 FT-IR for PS-PVP particles

The final stage of the synthesis, according to the literature, was carried out by the addition of MTPMS and oxidation with hydrogen peroxide. The images in Figure A1-8 are of the

particles after this step was carried out on the left and reference images from literature on the right. It was not apparent that the silica shell formation was successful, some smaller, less dense particles were present in the sample, but EDX was not available, making it impossible to draw firm conclusions.

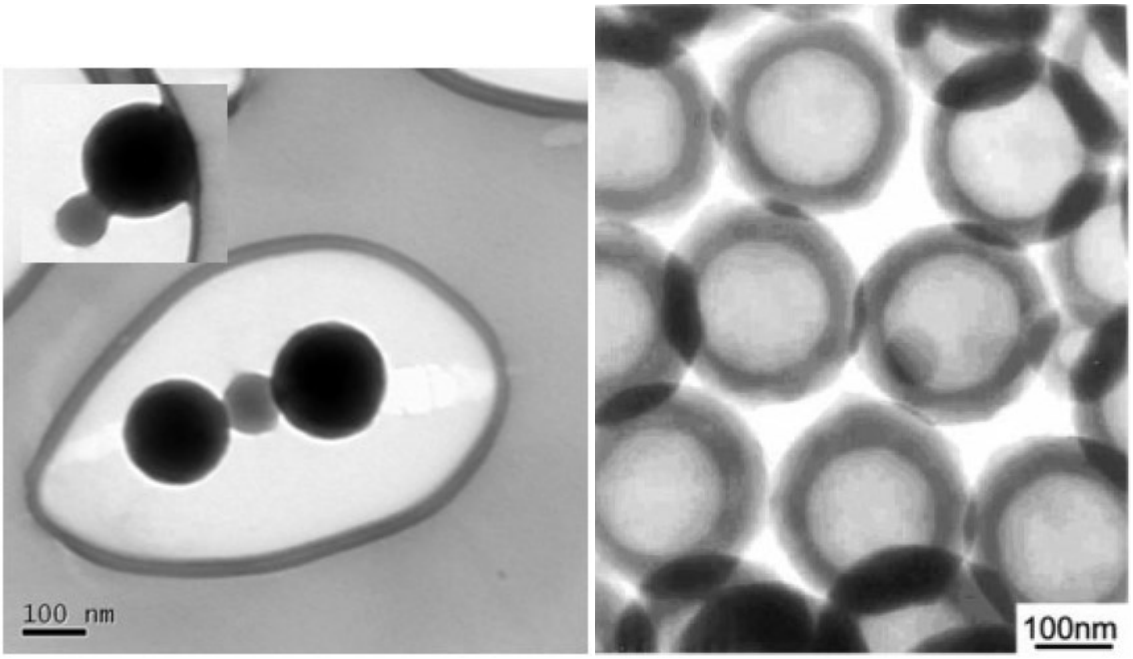

Figure A1-8 PS-PVP particles after MPTMS shell formation reaction (left) and image from literature using the same method (right) [52]. Reprinted from Journal of Polymer Science Part a,Copyright 2009, with permission from John Wiley and Sons.

Elemental analysis by XPS indicated that the material composition had changed very little between the two stages of the synthesis. Figure A1-9 shows the analysis; the carbon, oxygen and silicon composition varied by very small quantities (less than 1% in all cases). The only observable difference was that the starting particles showed no sulfur content, whereas the modified particles have 0.7 % sulfur relative to carbon, oxygen and silicon.

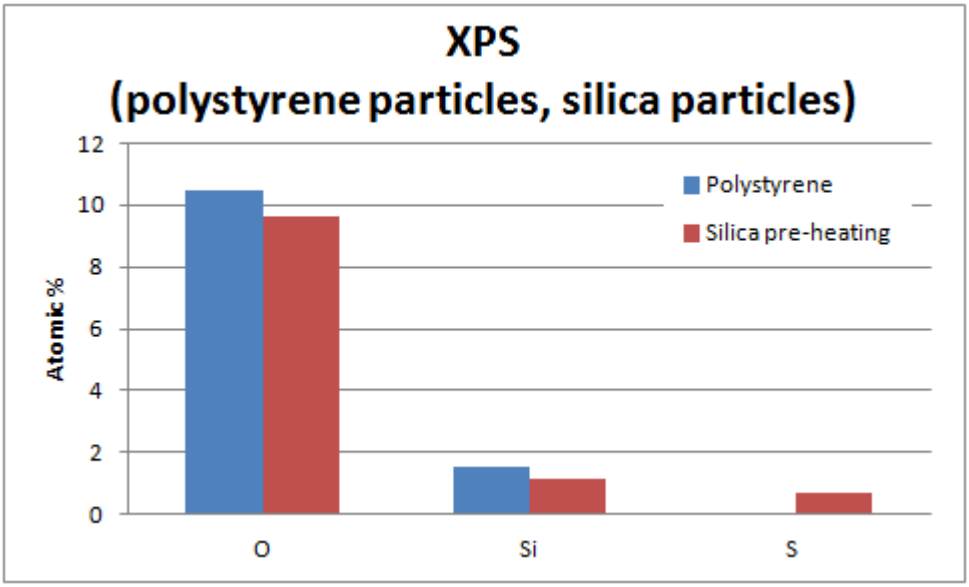

Figure A1-9 XPS analysis of the polymer particles before and after the silica shell reaction. For clarity, carbon was omitted from the graph.

The results were verified by FT-IR. In Figure A1-10 the peaks for polystyrene and for the particles used for the silica synthesis step are shown in black and red. From this data it appeared that the silica functional groups were present, due to the peak observed around 1067 cm^{-1}. It was possible that the shell had formed but that a large amount of polystyrene was still present. The final step was carried out in an attempt to remove the polystyrene through heating the sample to 550 °C over 4 hours. The results are shown in Figure A1-10 .

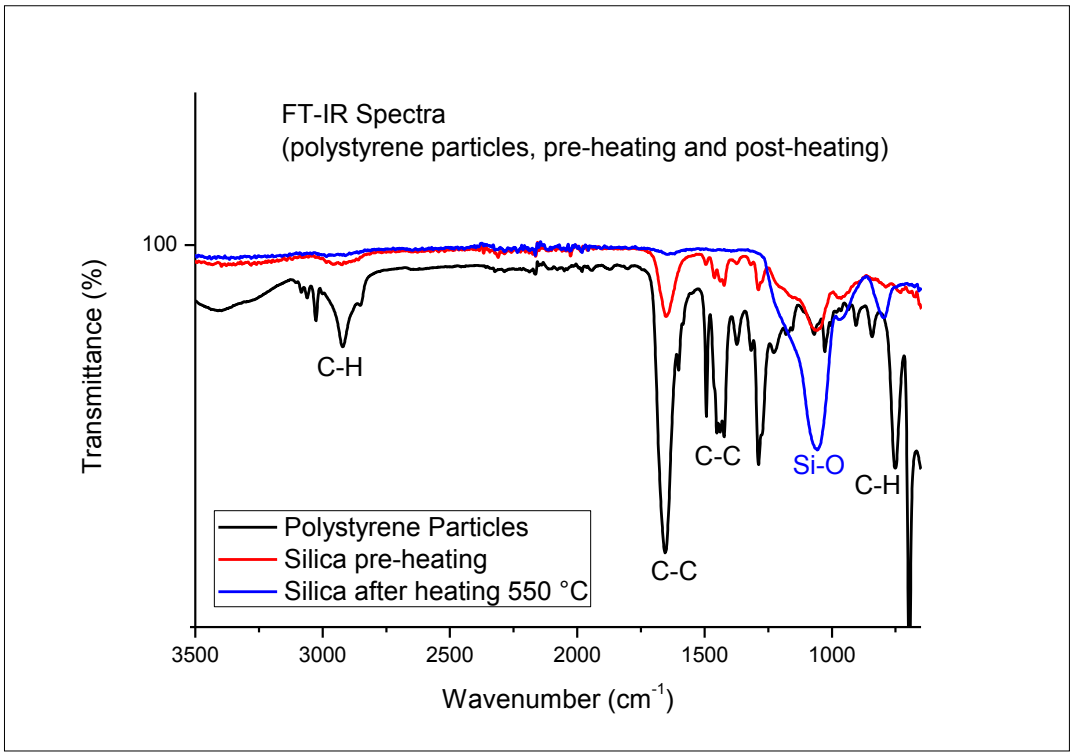

Figure A1-10 FT-IR of polystyrene and silica coated particles.

The final product appeared to have lost all the carbon functional groups and the main peaks that were present were the Si-O peaks as observed for the intermediate product. The particles were analysed by TEM, as shown in Figure A1-11. Particles in the range of 50-200 nm were observed with EDX indicating the presence of only carbon, oxygen and silicon. The rough appearance of the particles was also found in a separate study by Graf *et al.* [166] where smaller particles formed a similar rough surface.

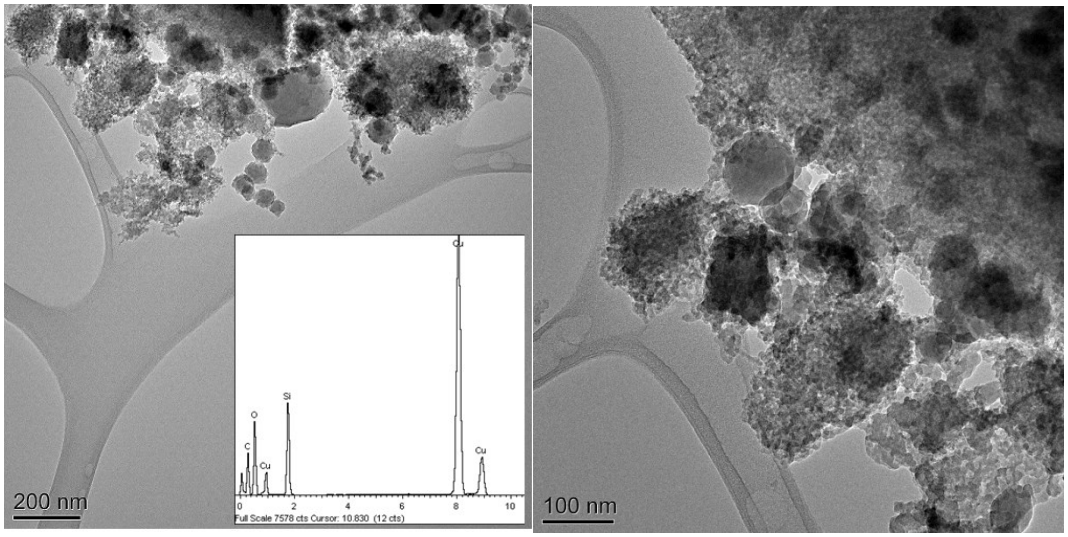

Figure A1-11 Silica shell particles showing multiple smaller contamination particles.

Even though this direction of research was clearly promising for composite membranes, it was decided that the optimisation of the silica particles would be too time intensive and that the necessary equipment for this work was not reliably available for this project. Frequent TEM and XPS would be required which could not be guaranteed. Sole use of a high temperature furnace and distilling apparatus would also be necessary to avoid contamination of the samples with conducting elements, such as nickel, which was widely used by colleagues and could not be justified for one researcher.

Conclusions

Hollow polymeric capsules were identified as a promising filler material for intermediate temperature PEMs. The preparation of silica shells were carried out on template polystyrene particles after identifying an optimal preparation method for the preparation of the core spheres.

The characterisation of the silica particles showed poor formation of spheres and large quantities of contamination, possibly due to elements present in the high temperature furnaces which were regularly used to prepare electrodes for other projects. It could not be foreseen that a furnace would be made available for the sole use of this project. As a route for further study it is however recommended as a promising direction with few publications in the literature.

Based on the findings in this part of the project, it was decided to focus on GO for the remainder of the project as the filler material for the composite membranes.

APPENDIX A2 – TGA FOR NAFION 212, RECAST NAFION AND GO-4-1

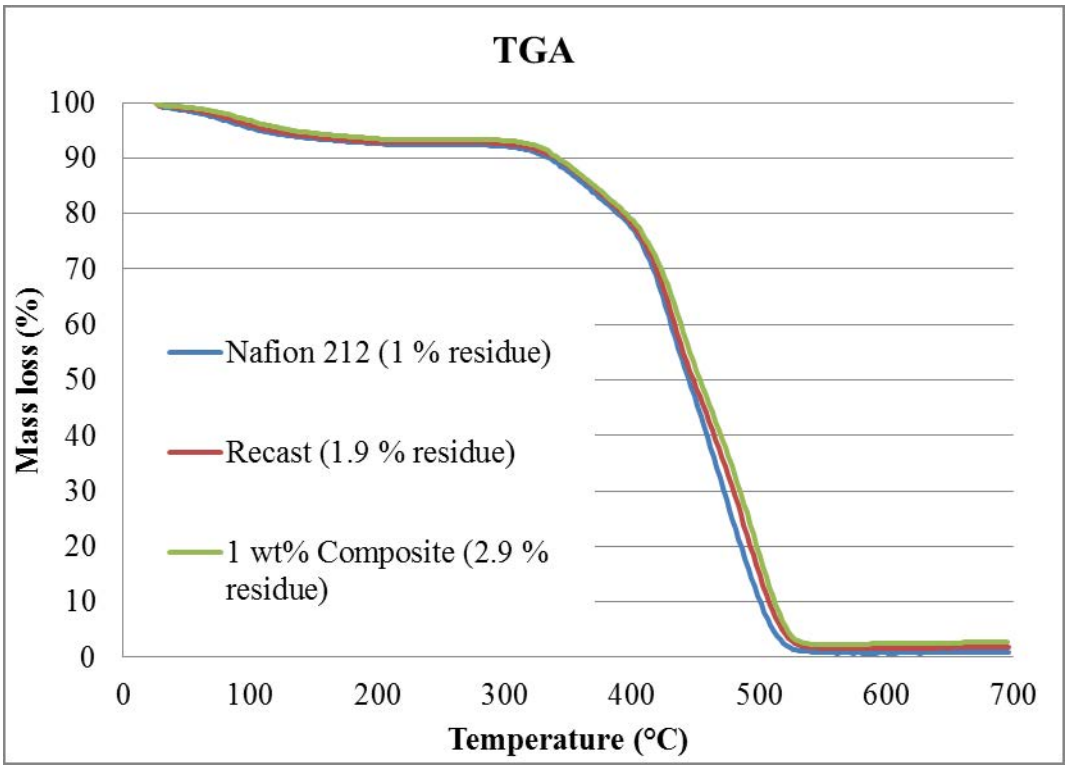

Figure A2-1 TGA for Nafion 212, recast Nafion and 1 wt% Nafion-GO composite membrane samples.

APPENDIX A3 – IN-SITU POLARISATION AND POWER PLOTS FOR GO-1 AND GO 2 SERIES TESTED AT 70 °C AND 100 %RH

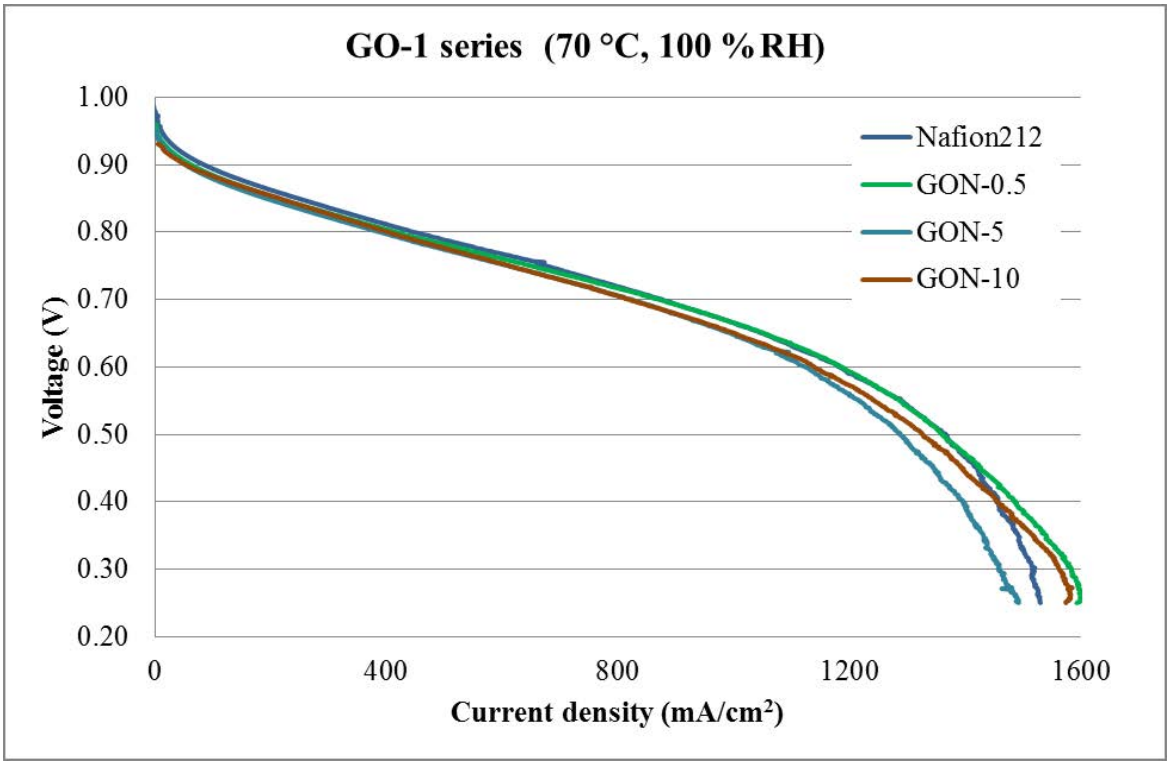

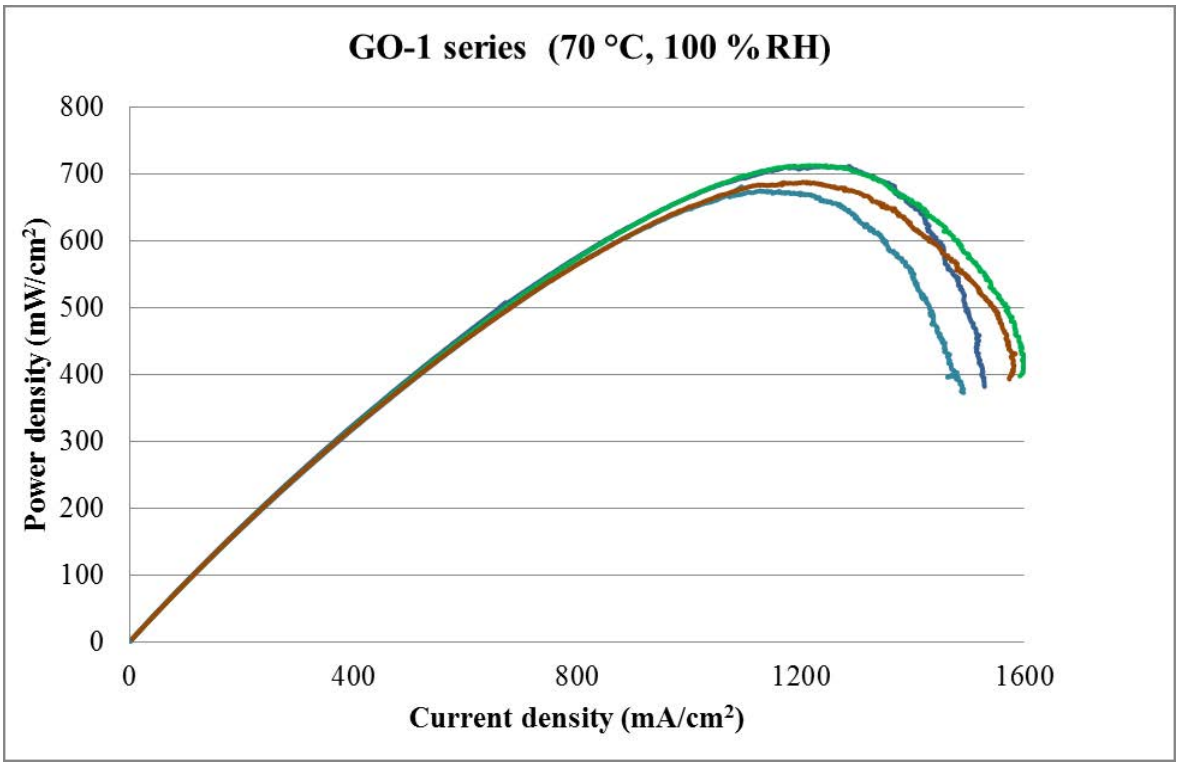

Figure A3-1 Polarisation and power curves for GO-1 series membranes.

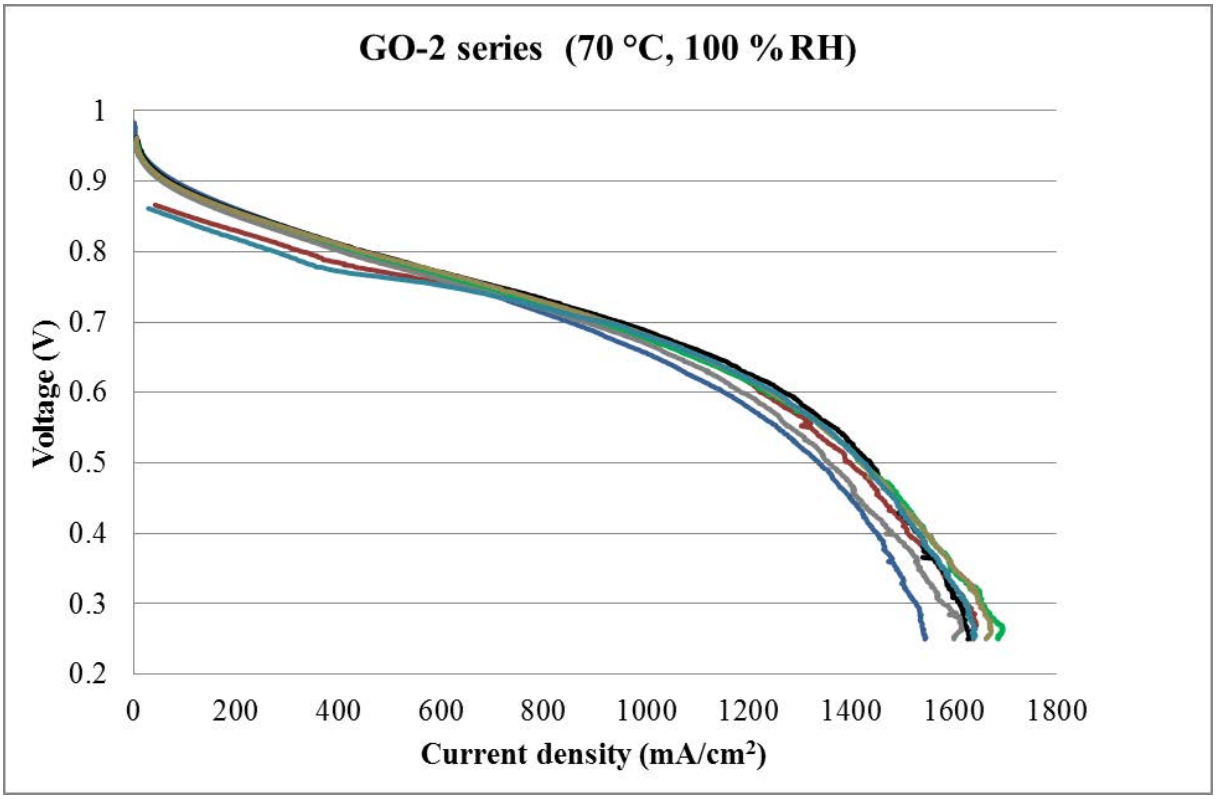

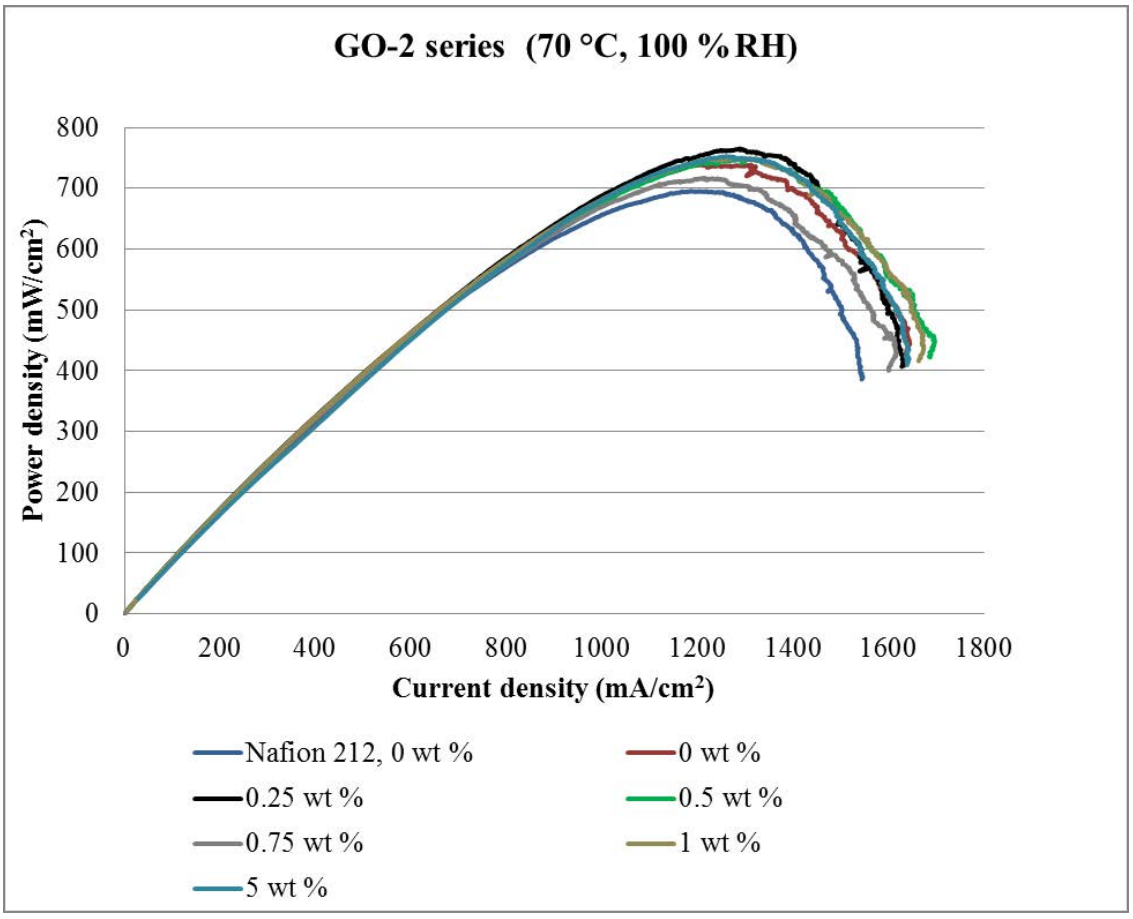

Figure A3-2 Polarisation and power curves for GO-2 series membranes.

APPENDIX A4 – POLARISATION AND POWER CURVES FOR GO-7 SERIES MEMBRANES.

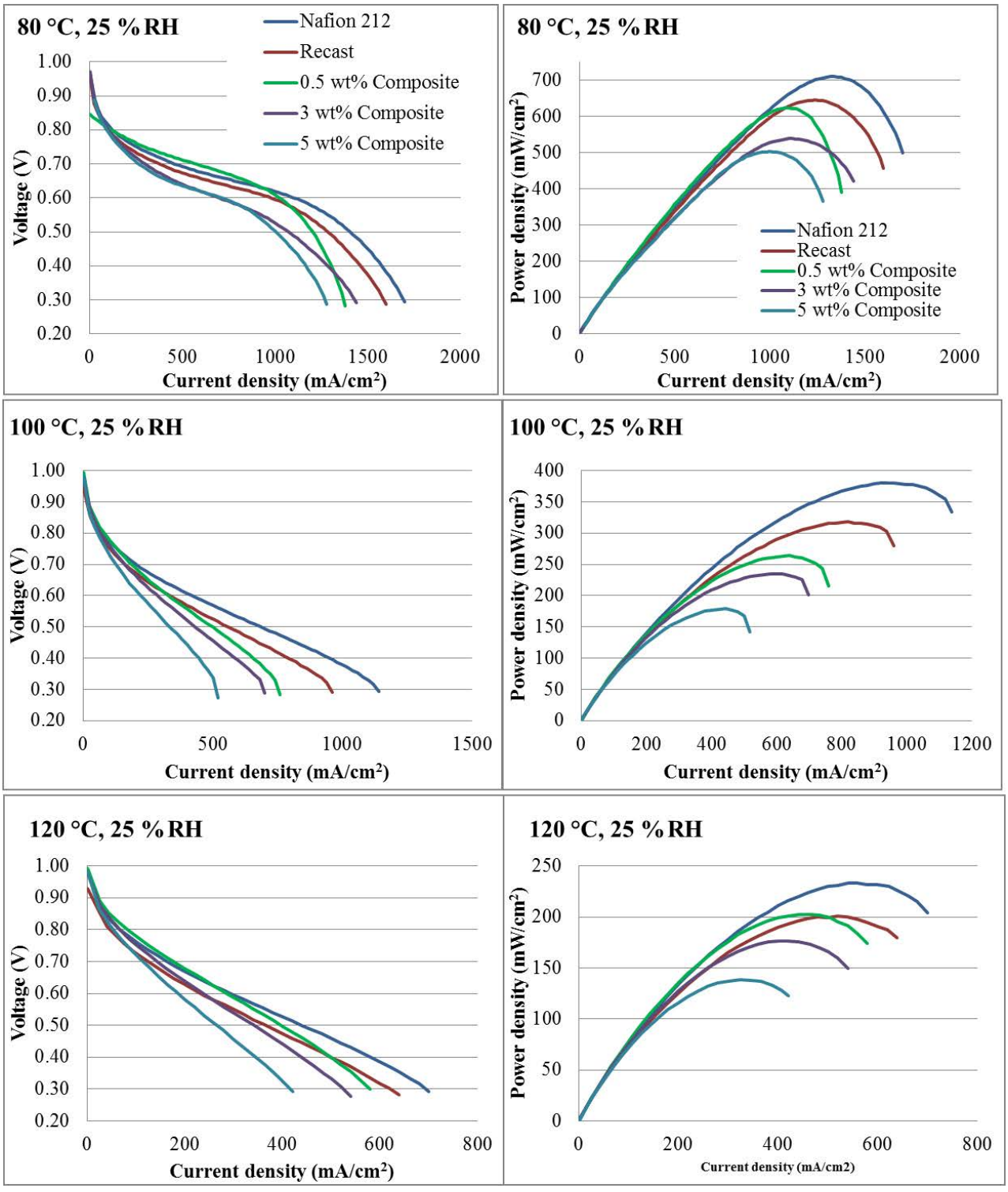

Figure A4-1 Polarisation and power curves for GO-7 series membranes, at 25 %RH.

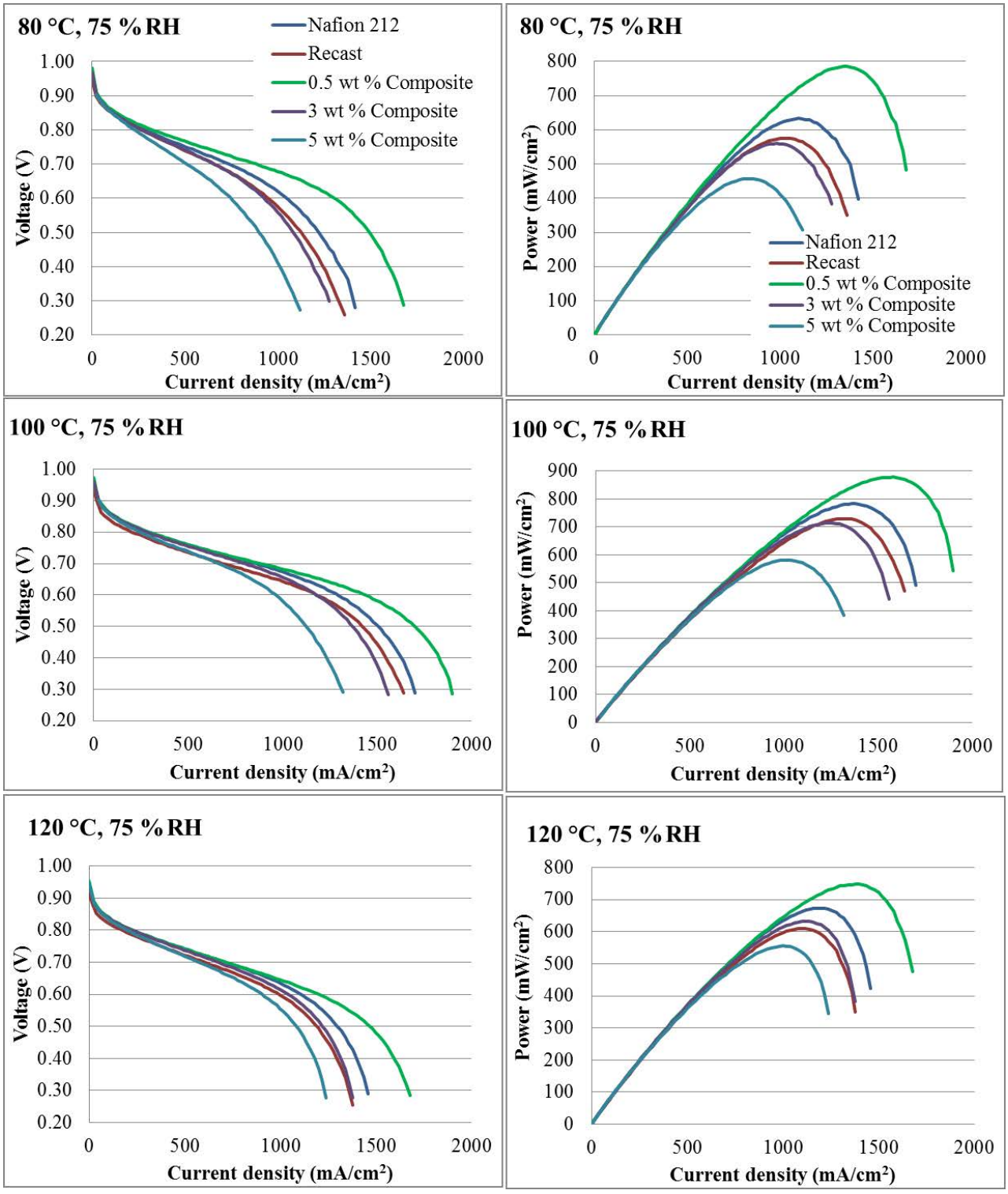

Figure A4-2 Polarisation and power curves for GO-7 series membranes, at 75 %RH.

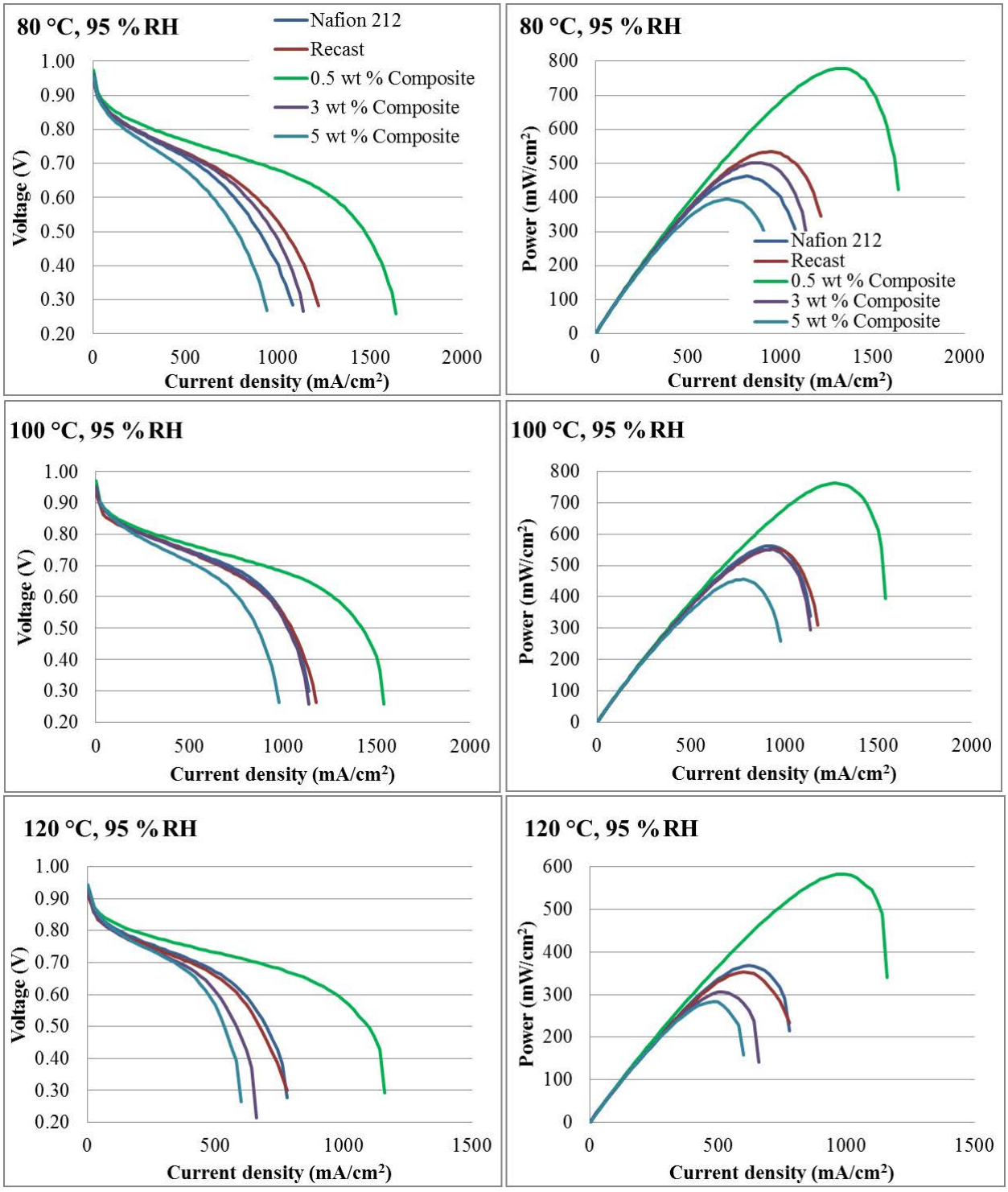

Figure A4-3 Polarisation and power curves for GO-7 series membranes, at 95 %RH.

APPENDIX A5 - POLARISATION AND POWER CURVES FOR GO-N SERIES OF MEMBRANES PREPARED WITH FUNCTIONALISED GO

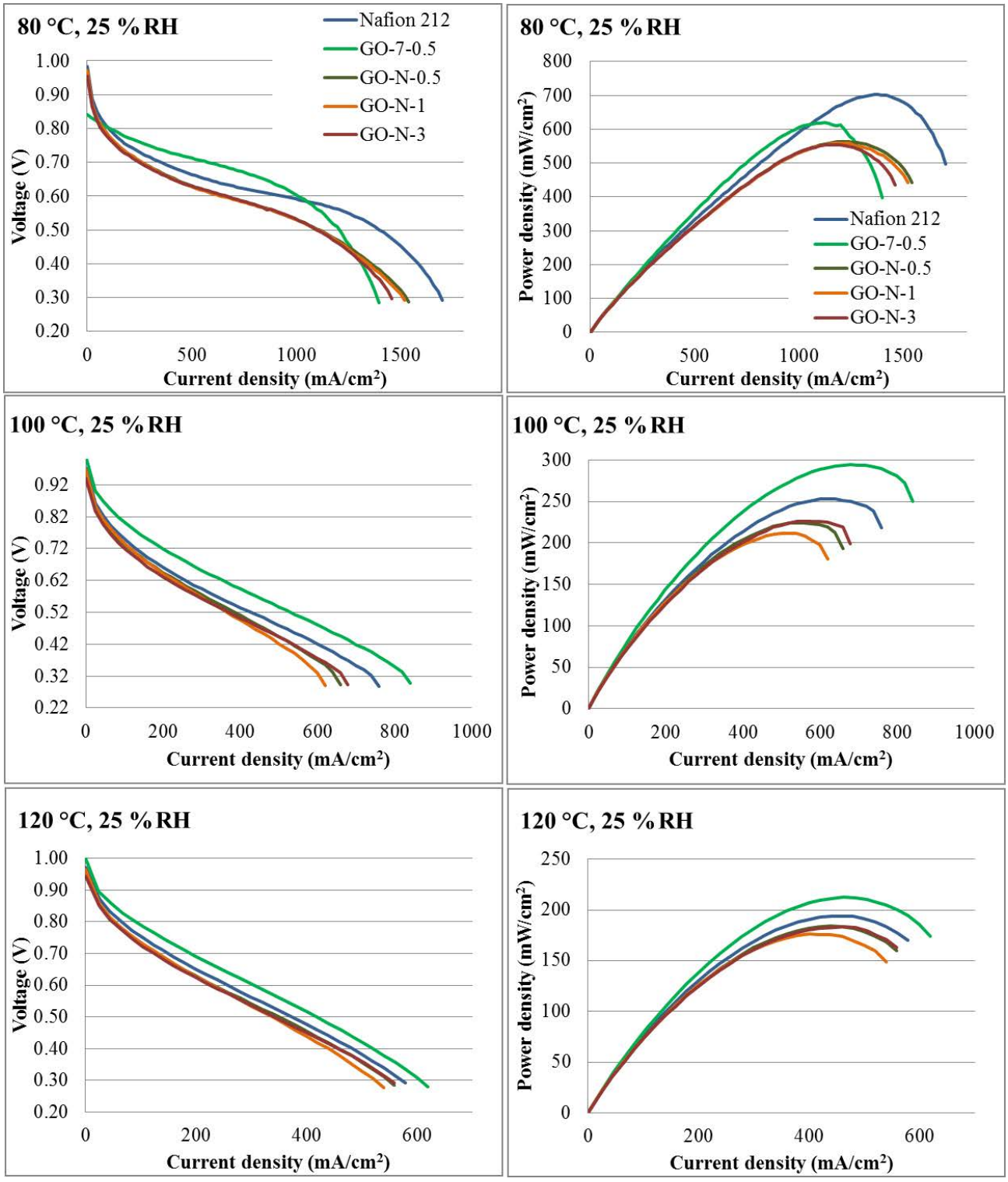

Figure A5-1 Polarisation and power curves for GO-N series membranes, at 25 %RH

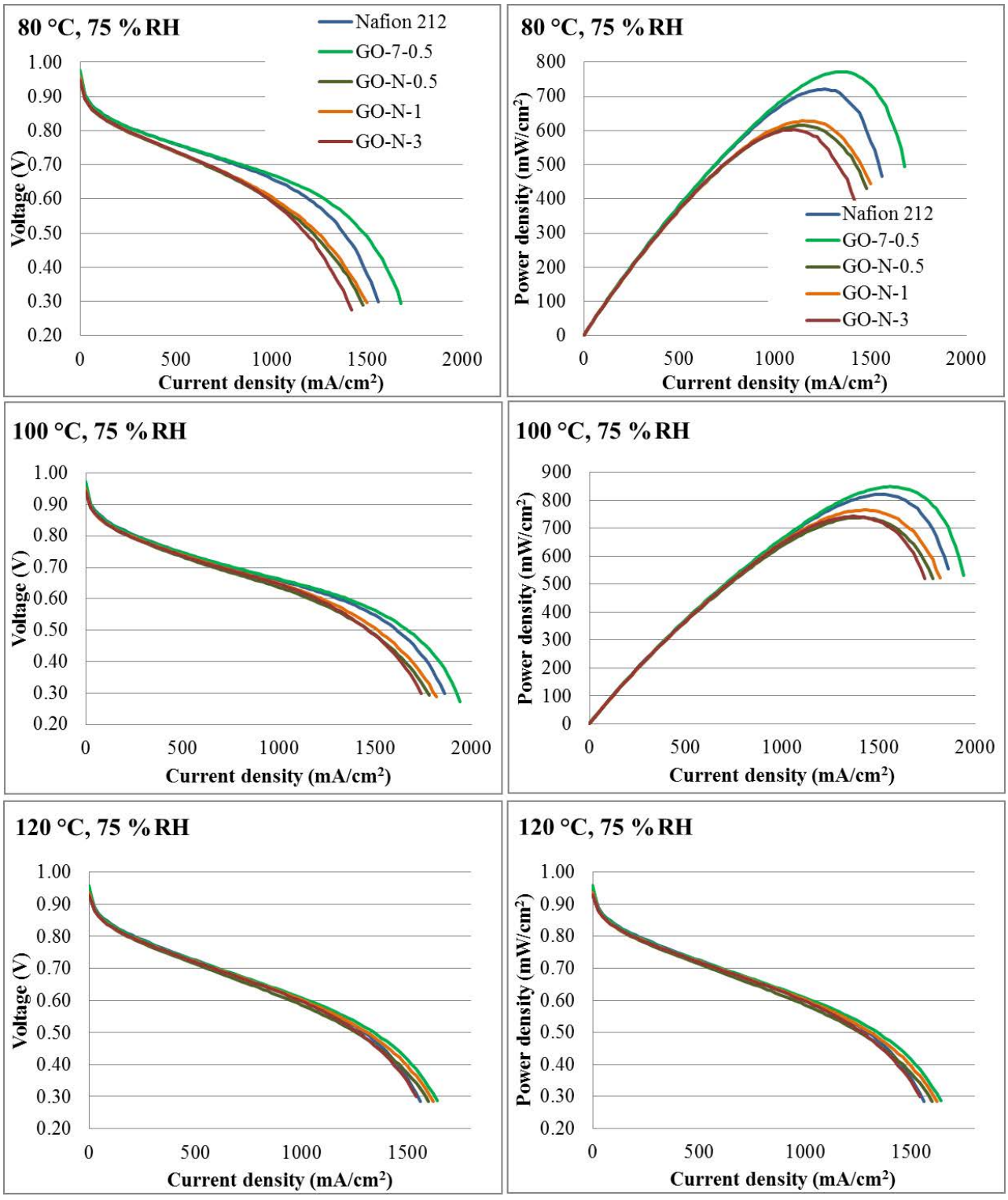

Figure A5-2 Polarisation and power curves for GO-N series membranes, at 75 %RH

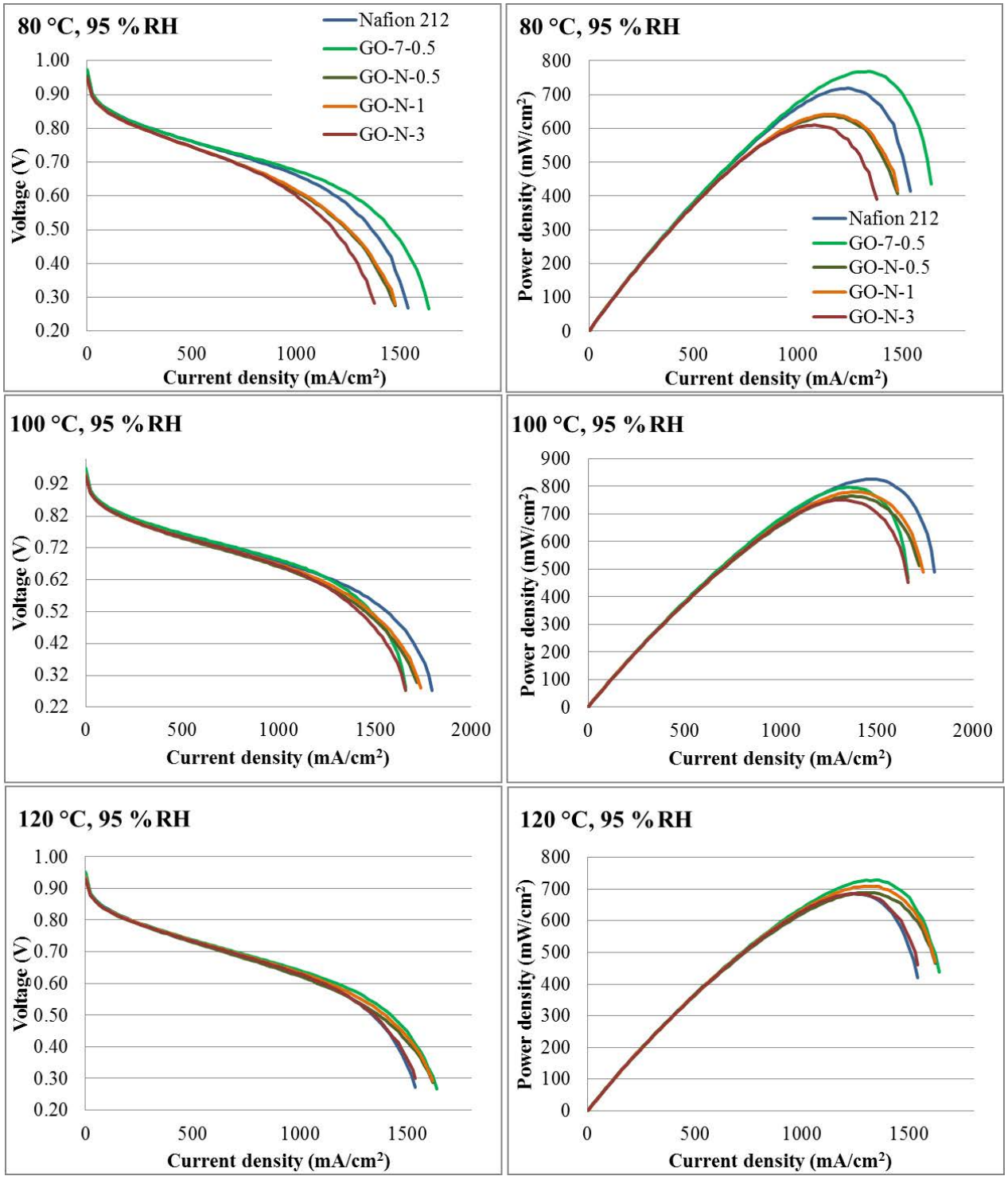

Figure A5-3 Polarisation and power curves for GO-N series membranes, at 95 %RH